Technical University of Crete

School of Production Engineering & Management

Optimal design of smart structures with intelligent control

Ph.D. dissertation

by Georgios K. Tairidis, Dipl. Eng., MSc.

Chania, July 2016

This page was intentionally left blank

Πολυτεχνείο Κρήτης

Σχολή Μηχανικών Παραγωγής & Διοίκησης

Σχεδιασμός και βελτιστοποίηση κατασκευών με ευφυή έλεγχο

Διδακτορική διατριβή

του Γεώργιου Κ. Ταϊρίδη,

Διπλωματούχου Μηχανικού Παραγωγής & Διοίκησης,
κατόχου Μεταπτυχιακού Διπλώματος Ειδίκευσης

Χανιά, Ιούλιος 2016

Technical University of Crete
School of Production Engineering & Management
University Campus
Δ Building
73100, Chania, Greece
Phone: +30 28210 37255 & 37305
info@pem.tuc.gr
http://www.pem.tuc.gr

To the memory of my parents
Kostas and Fotini

Preface

The mediocre teacher tells.
The good teacher explains.
The superior teacher demonstrates.
The great teacher inspires…

William Arthur Ward (1921 – 1994)

This Ph.D dissertation was prepared at the School of Production Engineering & Management of Technical University of Crete as a partial fulfillment of the requirements for the degree of Doctor of Philosophy.

Chania, July 18, 2016

Georgios K. Tairidis

About the author

Georgios K. Tairidis is a Production and Management Engineer with academic, research and working experience. He received the Engineering Diploma from Democritus University of Thrace in 2005 and the Master of Science (MSc) Degree on Production Systems from the Technical University of Crete in 2009. In 2016 Georgios received the degree of Doctor of Philosophy (PhD) from the Technical University of Crete. During his high quality studies Georgios focused mainly on production engineering and intelligent control. As a researcher, he has taken part in several international conferences and he has publications in journals, conference proceedings, as well as contributions in books. He is a member of Technical Chamber of Greece and of Pan-Hellenic Production and Management Engineering Association. His main research interests lie on the fields of mechatronics, control and optimal structural design.

✉ tairidis<at>gmail<dot>com
🔗 https://www.linkedin.com/in/tairidis-georgios-0a32105
Ⓡ https://www.researchgate.net/profile/Georgios_Tairidis

This Ph.D dissertation is approved by:

Advisory Committee

Georgios E. Stavroulakis (Supervisor)

Professor, School of Production Engineering & Management,
Technical University of Crete, Greece

Aristomenis Antoniadis (Co-supervisor)

Professor, School of Production Engineering & Management,
Technical University of Crete, Greece

Antonios Gasteratos (Co-supervisor)

Assoc. Professor, Department of Production Engineering & Management,
Democritus University of Thrace, Greece

Examination Committee

Nikolaos Bilalis

Professor, School of Production Engineering & Management,
Technical University of Crete, Greece

Georgia Foutsitzi

Professor, Department of Accounting and Finance,
Technological Educational Institution of Epirus, Greece

Ioannis Tsompanakis

Assoc. Professor, School of Environmental Engineering,
Technical University of Crete, Greece

Ioannis Marinakis

Asst. Professor, School of Production Engineering & Management,
Technical University of Crete, Greece

Copyright notice

How to cite

If you would like to cite this work, it is recommended to use the following bibtex entry:

@phdthesis{tairidis_2016,
author = "Georgios K. Tairidis",
title = "Optimal design of smart structures with intelligent control",
school = "Technical University of Crete",
year = "2016",
type = "{Ph.D.} dissertation"
address = "Chania",
}

---

[1] For more information please visit: https://creativecommons.org/licenses/by-nc-nd/4.0/

Summary

In the present dissertation different models of smart multilayer composite structures such as beams and plates with sensors and actuators of piezoelectric materials are studied under dynamic external loadings. The discretization of the host structures is made by using the finite element method.

The first purpose of this dissertation is the development of reliable control systems and their connection with numerical integration algorithms for the study of dynamic systems. For the development of the controllers using fuzzy inference tools and artificial neural networks are used.

In the smart structures which are considered here, a significant degree of uncertainty, due to imperfections and errors of both the control mechanisms and the model itself, is always involved. Especially in multilayer structures, several failures, such as delamination between the different layers, fatigue or other damages, may appear.

Thus, the second purpose of the present study is the implementation of suitably defined robust controllers which should be able to function well, despite the existence of failures and errors not only in the controllers' components (sensors, inadequate measurements), but in the mechanical model itself (simplifications of the theory, imperfections, material fatigue).

For the investigation of these phenomena, as well as for the minimization of the errors mentioned above, a generalization of the classical theories in order to include the energy losses in the various layers with adhesives is attempted.

With regard to control, classic monitoring tools often encounter several limitations to the study of such problems. For this reason, the use of intelligent fuzzy and neuro-fuzzy control techniques is suggested. Indeed, to maximize the efficiency of the proposed controllers, their characteristics are fine-tuned using global optimization algorithms.

More specifically, the controllers are first designed and subsequently they are subjected to an optimization process, by using either adaptive neural fuzzy techniques or global optimization.

As a by-product of this work, an exemplary application of the field of micromechanical coordinators for energy harvesting is presented.

Περίληψη

Στην παρούσα διδακτορική διατριβή μελετώνται μοντέλα σύνθετων ευφυών πο-λύφυλλων κατασκευών όπως δοκοί και πλάκες με αισθητήρες και διεγέρτες από πιεζοηλεκτρικά υλικά υπό την επίδραση δυναμικών εξωτερικών φορτίσεων. Η διακριτοποίηση των φορέων γίνεται με τη μέθοδο των πεπερασμένων στοιχείων.

Πρώτος στόχος της διατριβής είναι η ανάπτυξη αξιόπιστων συστημάτων ελέγχου και η σύνδεσή τους με αλγορίθμους αριθμητικής ολοκλήρωσης για τη μελέτη δυ-ναμικών συστημάτων. Για την κατασκευή των ελεγκτών γίνεται χρήση εργαλείων ασαφούς συνεπαγωγής και τεχνητών νευρωνικών δικτύων.

Στις κατασκευές που μελετώνται υπεισέρχεται πάντοτε κάποιος σημαντικός βαθ-μός αβεβαιότητας λόγω ατελειών και σφαλμάτων τόσο των ελεγκτών όσο και του ίδιου του μοντέλου. Ειδικά στις πολυστρωματικές κατασκευές, διάφορες αστοχίες, όπως για παράδειγμα η αποκόλληση μεταξύ των διαφόρων στρωμάτων, κόπωση ή άλλες βλάβες μπορούν να εμφανιστούν και τροποποιούν το μηχανικό μοντέλο κατά τη διάρκεια της ζωής του.

Συνεπώς, δεύτερος στόχος της διατριβής είναι η δημιουργία κατάλληλου εύρω-στου ελεγκτή ο οποίος μπορεί να λειτουργήσει παρά την ύπαρξη ατελειών και σφαλμάτων τόσο στα στοιχεία του ελεγκτή (αισθητήρες, ελλιπείς μετρήσεις) όσο και του ίδιου του μοντέλου (απλοποιήσεις της θεωρίας, ατέλειες, κόπωση υλικού).

Για την μελέτη των φαινομένων αυτών, καθώς και για την ελαχιστοποίηση των σφαλμάτων που προαναφέρθηκαν, επιχειρείται μία γενίκευση των κλασικών θε-ωριών, προκειμένου να συμπεριληφθούν οι απώλειες ενέργειας στα διάφορα στρώματα με τα συγκολλητικά υλικά.

Όσον αφορά στον έλεγχο, τα εργαλεία κλασικού ελέγχου συχνά συναντούν αρ-κετούς περιορισμούς στη μελέτη τέτοιων προβλημάτων. Για το λόγο αυτό προτεί-νεται η χρήση ευφυών ασαφών και νευροασαφών διατάξεων. Μάλιστα για την μεγιστοποίηση της αποδοτικότητας των προτεινόμενων ελεγκτών, τα χαρακτηρι-στικά τους ρυθμίζονται με χρήση αλγορίθμων ολικής βελτιστοποίησης.

Πιο συγκεκριμένα, οι ελεγκτές αρχικά σχεδιάζονται και υπόκεινται σε διαδικασία βελτιστοποίησης τόσο με χρήση νευροασαφών συστημάτων, όσο και εργαλείων ολικής βελτιστοποίησης.

Ως παράπλευρο αποτέλεσμα, παρουσιάζεται κάποια ενδεικτική εφαρμογή από το πεδίο των μικρομηχανικών συντονιστών για την μάστευση ενέργειας.

Contribution to the state of the art

In the literature, a lot of effort has been put on the static and dynamic analysis and control of smart composite structures during the last years.

Several control schemes, either classic or modern ones, have been proposed and tested on structures. However, the use of global optimization for the fine tuning of control parameters seems to lag behind. This is the, let say, gap which this study aspires to cover.

More specifically, fuzzy inference systems are developed for use on smart structures. The initial setting of the control parameters is done based on engineering intuition and data from the literature. The fuzzy rules are of the pendulum-like form, which is proved to be reliable in case of simple collocated controllers with two inputs and one output. Afterwards, the controllers are applied in relatively complicated composite structures such as multilayered beams and plates.

Furthermore, the fuzzy inference system is optimized, either with the use of global optimization techniques, such as genetic algorithms and particle swarm optimization or by using the adaptive neuro-fuzzy inference method.

Subsequently, the robustness of the control is tested for the case of the presence of failures correlated with realistic delamination scenarios.

In other words, the contribution of this dissertation is the incorporation of fuzzy control with global optimization techniques for the modification, i.e. the fine tuning of the control parameters, such as the membership functions and/or the ranges of the fuzzy control variables (inputs/outputs).

This fine tuning is achieved using adaptive neuro-fuzzy inference (ANFIS) techniques, genetic algorithms and particle swarm optimization. The outcome of this procedure is the formulation of powerful and robust control schemes.

The performance of the optimization methods under different conditions, in terms of vibration suppression of smart structures, i.e. beams and plates with piezoelectric sensors and actuators, is studied.

It is noteworthy, that the control is applied not only to simple composite structure models based on the single layer theory, but also to multilayer structures with adhesive layers, which in turn can be used for the modelling of delamination phenomena between the piezoelectric components.

Last but not least, some good effort is put into the related, and in some sense opposite, situation of vibration suppression, namely the energy harvesting, indicating that the optimum positioning of the harvesters can be decided with the same tools, and by all means with respect to the characteristics of the structure.

Publications

For the fulfillment of the present dissertation, 11 papers were published in scientific journals, book chapters and international conferences as follows:

Journals:

1. Tairidis GK, Foutsitzi G, Koutsianitis P, Stavroulakis GE. Fine Tuning of a Fuzzy Controller used for Vibration Suppression of Smart Plates using Genetic Algorithms, Advances in Engineering Software, Elsevier, 2016, doi: 10.1016/j.advengsoft.2016.01.019

2. Koutsianitis P, Tairidis GK, Drosopoulos G, Foutsitzi G, Stavroulakis GE. Effectiveness of Optimized Fuzzy Controllers on Partially Delaminated Piezocomposites, Acta Mechanica, Springer, 2016 (Submitted for publication, under revision)

Book chapters:

3. Tairidis GK, Koutsianitis P, Foutsitzi G, Drosopoulos G and Stavroulakis GE. Delamination and control on multi-layered structures: A review, In: Smart Material Systems and Structures - Modeling and Simulation, Eds. Kuczma M, Schröder J, Stavroulakis G, Szefer G, Springer, 2016 (in press)

4. Koutsianitis P, Drosopoulos G, Tairidis GK, Stavroulakis GE and Foutsitzi G. Optimally tuned fuzzy control for smart, possibly damaged piezocomposites, In: Advances in Mechanics. Theoretical, computational and interdisciplinary issues, Eds. Kleiber M et al. CRC Press, 2016 pp. 301-305

International conferences:

5. Tairidis GK, Papachristou I, Katagas M, Stavroulakis GE. Neuro - fuzzy control of smart structures, 10th HSTAM International Congress on Mechanics, Chania, Greece, 25-27 May 2013

6. Tairidis GK, Foutsitzi G, Tsagkaris A, Stavroulakis G. Fuzzy Control for Vibration Suppression of Smart Plates, CST2014, 12th International Conference on Computational Structures, Naples, Italy, 2-5 September 2014

7. Tairidis GK, Foutsitzi GA, Koutsianitis PI, Stavroulakis GE. Fine Tuning of Fuzzy Controllers for Vibration Suppression of Smart Plates using Particle Swarm Optimization, 8th GRACM International Congress on Computational Mechanics, Volos, Greece, 12-15 July 2015

8. Tairidis GK, Foutsitzi GA, Koutsianitis P, Drosopoulos G, Stavroulakis GE., Design and testing of Fuzzy Controllers on Smart Structures in the Presence of Delamination, Proceedings of the Fourth International Conference on Soft Compu-

ting Technology in Civil, Structural and Environmental Engineering, Y. Tsompanakis, J. Kruis and B.H.V. Topping, (Editors), Civil-Comp Press, Prague, Czech Republic, 1-4 September 2015

9. Tairidis GK, Foutsitzi GA, Koutsianitis P, Stavroulakis GE. Energy harvesting using piezoelectric materials on smart composite structures, Proceedings of the Fifteenth International Conference on Civil, Structural and Environmental Engineering Computing, Prague, Czech Republic, 1-4 September 2015

10. Koutsianitis P, Drosopoulos GA, Tairidis GK, Foutsitzi G, Stavroulakis GE. Optimally tuned fuzzy control for smart, possibly damaged piezocomposites, PCM-CMM-2015 3rd Polish Congress of Mechanics & 21st Computer Methods in Mechanics, Gdansk, Poland, 8-11 September 2015

11. Koutsianitis P, Moutsopoulou A, Drosopoulos GA, Tairidis GK, Foutsitzi G, Stavroulakis GE. Optimal control tuning in smart structures with delaminations, ECCOMAS VII European Congress on Computational Methods in Applied Sciences and Engineering, Eds. Papadrakakis M, Papadopoulos V, Stefanou G, Plevris V, Crete Island, Greece, 5–10 June 2016

Acknowledgements

There are some people who contributed to the completion of this dissertation, whom I really want to acknowledge.

Above any other, I would like to express my sincere gratitude to my advisor Prof. Georgios Stavroulakis for his continuous support during all the stages of my postgraduate studies, from supervising my master thesis to inspiring my Ph.D. study and other related research. I warmly acknowledge his patience, motivation, and vast knowledge. He is a true mentor to me.

I would like to express my very great appreciation to Prof. Aristomenis Antoniadis and Prof. Antonis Gasteratos, members of my advisory committee, for their valuable advice during my Ph.D studies.

Moreover, I am particularly grateful for the assistance and guidance given by Prof. Georgia Foutsitzi, member of my examination committee, during the major part of the research which was taken in the context of this study.

I also gratitude the rest members of the committee, and namely Prof. Nikolaos Bilalis, Prof. Yannis Marinakis and Prof. Yannis Tsompanakis for their insightful comments which motivated me to continue my research.

I deeply thank my colleague and friend Panagiotis Koutsianitis for the endless time we spent together regarding our research activity during the last two years. I would also like to offer my special thanks to Prof. Georgios Drosopoulos, who provided me with very valuable advice during our collaboration and to Dr. Nikos Kaminakis for his very interesting comments. I would also like to extend my thanks to my fraternal friends Antonella Vlassi and Katerina Stavroulaki for their precious assistance.

Last but not the least, I wish to thank my spouse Thalia Stimadoraki for her encouragement and for being a continuous source of support, energy, strength and inspiration to me. I hope to be like her someday.

Table of Contents

List of Figures

List of Tables

List of abbreviations

ADF: Anelastic Displacement Field

ALE: Arbitrary Lagrangian–Eulerian

ANFIS: Adaptive Neuro-Fuzzy Inference System

ANN: Artificial Neural Network

CLPT: Classical Laminated Plate Theory

DE: Differential Evolution

DOF: Degree of Freedom

EA: Evolutionary Algorithm

EP: Evolutionary Programming

ES: Evolutionary Strategies

ESL: Equivalent Single Layer

FEM: Finite Element Method

FIS: Fuzzy Inference System

FRAM: Ferroelectric Random Access Memory

FRP: Fiber Reinforced Polymer

FSDT: First-Order Shear Deformation Theory

GA: Genetic Algorithm

HOLT: High-Order Layerwise Theory

HSDT: Higher-Order Shear Deformation Theory

LLT: Linear Layerwise Theory

LMI: Linear Matrix Inequality

LOM: Largest of Maximum

LQ: Linear-Quadratic

LQG: Linear Quadratic Gaussian

LQR: Linear Quadratic Regulator

LSE: Least-Squares Error Method

MAXGENS: Maximum Number of Generations

MEMS: Microelectromechanical Systems

MF: Membership Function

MIMO: Multiple Inputs – Multiple Outputs

MISO: Multiple Inputs – Single Output

MOM: Mean of Maximum

PID: Proportional Integral Derivative

PMUTATION: Probability of Mutation

POPSIZE: Population Size

PROBOR: Probabilistic Or

PROD: Product

PSO: Particle Swarm Optimization

PVDF: Polyvinylidene Difluoride

PXOVER: Probability of Crossover

PZT: Plumbum (Lead) Zirconate Titanate

RVE: Representative Volume Element

SOM: Smallest of Maximum

TSDT: Third-Order Shear Deformation Laminate Theory

WTAVER: Weighted Average

XFEM: Extended Finite Element Method

1 Introduction

Adaptive smart structures are mainly based on the devastating use of piezoelectric sensors and actuators for analysis and control.

A lot of work has been done on structural analysis and control during the last decades. Nevertheless, the use of optimization tools for the configuration of the involved parameters has not been studied extensively.

The contribution of this dissertation is the incorporation of fuzzy control with global optimization techniques for the modification, i.e. the fine tuning of the control parameters. The outcome is the formulation of powerful and robust control schemes. Moreover, the application of several optimization methods under different conditions is studied.

More specifically, in the present dissertation the formulation and the application of modern control techniques such as fuzzy and neuro-fuzzy control for the vibration suppression on smart structures (beams and plates) with piezoelectric sensors and actuators is considered. The characteristics of the controllers are adjusted (tuned) using neural techniques (ANFIS) and global optimization methods inspired by nature, such as genetic algorithms and particle swarm optimization. The control is applied not only to simple models, but also in multilayer structures with adhesive layers in the presence of delamination at the piezoelectric components. Moreover, some related results applied on energy harvesting are presented.

The proposed methods for control, optimization and energy harvesting are proved to be very efficient and robust as well.

1.1 Motivation

The application of active control techniques in smart structures is an area of intensive research. The need arises from the ever increasing complexity of modern industrial processes, in conjunction with the increasing demands for efficient control schemes.

Piezoelectric materials are smart materials that are well known for their ability to change their shape and produce electric voltage when subjected to mechanical strain. For this reason such materials are used for the construction of sensors and actuators.

Moreover, the piezoelectric materials provide great advantages in terms of control of smart structures, due to their sensitivity to mechanical waves being transferred through the solid body of composite structures.

Thus, smart laminated structures with embedded piezoelectric materials, which are used as sensors or actuators, usually incorporate active control schemes which allow them to react against disturbances. In mechanics we have in mind suppression of mechanical vibrations with possible applications on noise and vibration isolation.

The use of piezoelectric sensors and actuators in smart structures, such as laminated beams and plates, is a very popular and accurate mean for both static and dynamic analyses.

Nevertheless, the results of this work can be transferred (after modification) to other smart structures, using different technologies.

In most cases, instead of three-dimensional models, simplified plane models are studied. In this particular case some assumptions are made in order to solve the problem. For instance, by following simplified theories of technical mechanics, the cross section is considered plane and vertical to the deformed axis. Although the use of three-dimensional models, in general, can provide more accurate results, due to high side-to-thickness ratio, standard 3D finite elements are not adequate for the accurate modeling of plates. Moreover, effective realization of control requires in general small scale dynamical models

Several different, analytical and numerical approaches have been proposed in the past for the investigation of complex, non-linear, heterogeneous structures, like composites. Analytical methods can be more accurate in the description of the micro structure, for relatively simple microscopic patterns and constitutive laws. On the other hand, numerical methods may be used for the simulation of complex microscopic geometries, over a statistically defined representative amount of material.

The major disadvantage of multi-layered composite structures that incorporate piezoelectric actuators and sensors lies to the fact that they can face several nonlinearities, including the presence of damage to the materials, such as delamination and debonding phenomena. Such phenomena are very common in composite materials.

Recently, sophisticated models for the study of severe failure of composite materials have been proposed. According to these efforts, a connection between the size of the microscopic and the macroscopic structure is attempted. This connection is necessary, when localization phenomena, thus unstable failure patterns with softening traction-separation laws which are used for the description of delamination or damage in the micro scale, appear.

Delamination phenomenon leads to changes in the quantities of the structures. More specifically, it is responsible for the weakening and/or ageing of the materials of a

smart structure and modifies in some extend the characteristics of the mechanical system, mainly its stiffness. This fact affects the effectiveness of the control methods proposed. Delamination is modeled here by means of a simplified, interface - interlaminar model. For this reason, robust control schemes are necessary, in order to work with the presence of these deviations.

In general, lack of knowledge of the structure, due to restricted number of measurements or uncertainty about the structural model itself due, say, to damage or general structural degradation, plastification or other sources of nonlinearities, reduce the performance of control. This means that active control methods which are applied to the area of smart structures must take into account model as well as excitation uncertainties and nonlinearities.

Classic mathematical theory of control works well on linear systems, however under many, sometimes unrealistic, restrictions. On the other hand nonlinear controllers, built with smart computational methods, most times can describe well nonlinear structures and/or nonlinear feedback. Again some restrictions appear, as assumptions used for their derivation do not always cover critical applications. This gap is filled by fuzzy, neural and hybrid neuro-fuzzy control methods.

One can say that the core advantage of the classical control tools is summarized in the existence of a strong mathematical framework. From the other hand, in nonlinear control, e.g. fuzzy or neuro-fuzzy control, such framework does not exist. However, this type of control is proved to be more flexible and feasible for systems with presence of nonlinearities.

Fuzzy inference can provide more systematic tools, while artificial neural networks have the ability of training and thus learning. The combination of the core characteristics of these two types of control, can lead to powerful, robust and adaptive neuro-fuzzy controllers.

In the case of fuzzy controllers, the control is based on a set of linguistic rules that combine the membership functions of the variables of the system, using fuzzy inference techniques. Fuzzy controllers in general, are known for their robustness. Also, from the numerical results presented in several publications, it is demonstrated that fuzzy controllers work effectively when applied to different structures either with presence or absence of structural failures such as delamination.

However, the industrial evolution of the last decades has raised dramatically the complexity of systems studied. Thus, plenty of different optimization methods are used in order to design and/or fine tune control schemes. Optimization methods inspired by nature are very popular due to their simplicity in implementation and effectiveness in different problems and situations.

For instance, the optimization process using genetic algorithms present a great distribution of application in a plethora of different fields and, of course, in structural con-

trol. PID control, for example, is one of the most common and powerful control methods in automatic control. In addition, fuzzy and neural control present a large field of applications. However, due to the complexity of modern industrial systems, nonlinearities and other flaws may occur, rendering the controllers less powerful and holding back the control process. Thus, the optimization of the parameters of such controllers is necessary.

1.2 Objectives and approach

Smart composite structures, such as beams and plates with sensors and actuators made of piezoelectric materials are investigated. Two different approaches are considered. Besides the simplified structures which are examined as one body, a layerwise theory which takes into account the existence of adhesive material between layers is also studied. The discretization of the host structures is done within the finite element method.

For the design of composite laminated models of beams and plates which are considered in this dissertation, a generalization of classical technical bending theory to include the energy losses in the layers with adhesive damageable material is necessary.

In order to overcome some of the obstacles mentioned in the previous section, it becomes clear that the main objective of structural control has to be the construction of adaptive and robust controllers which should be able not only to confront the nonlinearities involved, but to keep functioning under different conditions as well.

To achieve this goal, modern non-classical fuzzy and adaptive neuro-fuzzy control tools are used. For the initial configuration of fuzzy controllers in a collocated setting, simple pendulum-like linguistic rules can be used. Besides the rule base, the fuzzy inference system demands the existence of a data base, i.e. a set of membership functions. The definition of these functions can be done based on intuition or with the assistance of algorithms and logical processes.

Moreover, several global optimization methods, such as genetic algorithms can be used for the fine tuning of the control mechanisms.

In fact, genetic optimization is a very powerful tool, which can be used for the optimal design of intelligent fuzzy control mechanisms. Other optimization methods inspired by nature, such as particle swarm optimization or differential evolution can be used as well in order to increase the performance of the control or to optimize the controllers' parameters.

Another option for the construction of robust control schemes is the use of adaptive neuro-fuzzy inference techniques, especially if manual configuration of the control parameters is not possible, due to the non-existence of information about the system. In this case the controllers adjust their parameters automatically, with respect to a set of training data which is obtained from the structural model itself.

The optimized controllers should be capable of functioning even in structures with failures such as delamination, debonding, as well as other nonlinearities.

A related application for energy harvesting is also presented. The procedure utilizes modal analysis tools. Similarly to the appropriate selection of the control points for vibration suppression, suitable positions in order to harvest the maximum amount of energy which produced by the vibrations of the host structure can be selected.

1.3 Dissertation outline

Chapter 1 is an introduction to the present dissertation. The impulse which led to the elaboration of this study, as well as the objectives and the approach which is followed, are presented. In the second chapter, an extensive literature review on layerwise models, structural failures, i.e. delamination, and control mechanisms such as fuzzy, neural and neuro-fuzzy control, is carried out.

In chapter 3, the theory background of structural models is demonstrated. Three different models are considered. A smart beam model with piezoelectric patches, a laminated composite plate model with piezoelectric sensors and actuators based on FSDT theory, and a layerwise plate model accounting for adhesive flexibility. A part of this chapter is also dedicated to the description of the delamination phenomenon and its insertion to the examined layerwise plate. In the last section, a brief presentation of the structural dynamics is done.

In the following chapter 4, the control strategies for the vibration suppression are presented in detail. Namely, theoretical information on fuzzy logic and fuzzy inference systems, on artificial neural networks and their training, as well as on the adaptive neuro-fuzzy inference systems is given. Moreover, the basic formulation of the controllers which used in this dissertation is thoroughly presented. More specifically two fuzzy controllers, which account the mechanical (controller 1) and the coupled electromechanical model, (controller 2), as well as a neuro-fuzzy controller (controller 3) are proposed.

The fifth chapter provides the theoretical framework of the optimization methods which were used for the tuning of the controllers' characteristics, which in turn are genetic algorithms and particle swarm optimization.

Chapter 6 presents the numerical results of the present study. The outcome of fuzzy control on smart plates, either with or without optimization of the control parameters and under various loading and frequency scenarios is demonstrated. The results are verified by comparison with the ones from a tested cantilever beam. Consequently, the robustness of the controllers is proved by testing their ability to operate also in plates under the presence of delamination. Slight, moderate and extensive delamination cases, both in the sensor and the actuator piezoelectric layer, are considered. Finally, an adaptive neuro-fuzzy controller is tested on a cantilever beam and the results are compared to the ones of a classical LQR controller.

An energy harvesting application is considered in chapter 7. The design of the harvester which depends on modal analysis tools is presented, and the results of the energy harvesting for the first three eigenmodes are calculated.

Finally, the conclusions of the dissertation, along with some perspectives for future studies are given in the last chapter 8.

2 Literature review

In literature, several analytical, numerical, and computational methods have been proposed for the investigation of smart structures either with or without the presence of delamination phenomena. For this purpose either two-dimensional, or three-dimensional models have been suggested and presented in detail. Various layerwise models with piezoelectric sensors and actuators are briefly reviewed. In addition, a number of papers on delamination or other failure phenomena is presented.

It is well-known that nonlinearities which are caused either by delamination or other types of damage, or even by the structural model itself, can significantly reduce the performance of any classical control. Thus, suitable control tools are sought. Very powerful control strategies could be either classical tools as H-infinitive control or modern control techniques, e.g. fuzzy, neural and hybrid neuro-fuzzy control. A number of the numerous investigations on the structural control is reviewed in this chapter (Tairidis, et al., 2016b).

2.1   Modelling of smart structures

Smart composite structures with piezoelectric sensors and actuators take advantage of both mechanical, i.e. stiffness, mass and damping, and other properties occurring from the proposed control schemes, e.g. piezoelectric sensors and actuators. Usage of piezoelectricity has a model nature here, and can be replaced by other multiphysics materials, depending on the available technology.

The models used for simplified simulation of smart composite structures may consist of one or more different layers. These separate layers could be the elastic core, the piezoelectric sensors, the piezoelectric actuators, as well as the adhesive material used for the gluing of the components see Figure 1.

Multi-layered structures have the advantage that the several layers could be separated and studied individually. The major disadvantage of such structures lays on the fact that the complexity of the models is dramatically increased.

Smart composite structures with piezoelectric sensor and actuator layers have been extensively studied in the literature. Different models as well as discretization methods have been proposed.

Actuator
Adhesive Layer
Flexible Core
Adhesive Layer
Sensor
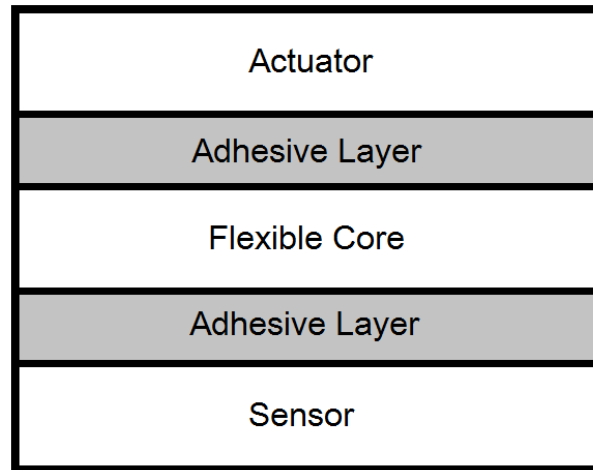
Figure 1: Example of multi-layered smart composite structure

2.1.1   Single layer models

It is well known that the concept of adaptive structures in terms of performance, weight and control, is based on the vast use of distributed sensors and actuators, such as piezoelectric layers. The outcome is hybrid laminated structures, where the let say elastic core is adjoined with surface bonded or embedded sensors and actuators made of piezoelectric materials. These structures which have the capability of sending and actuating, are most commonly referred to as smart structures. The point is that smart structures can be modeled either considering the equivalent single layer (ESL) theory, which deals with the structure as if it was formulated by a single layer, or layerwise theory which studies each layer of the structure separately.

The ESL theories, in turn, can be divided into three major categories which are the classical laminated plate theory (CLPT), the first-order shear deformation theory (FSDT), and the higher-order shear deformation theories (HSDTs).

A simple finite element formulation for a laminated composite plate with piezoelectric layers is presented in (Suleman & Venkayya, 1995). The formulation is based on the classical laminate theory with electromechanical induced actuation, and the finite elements which considered was four-node, bilinear displacement elements based on a Mindlin plate theory. Numerical results of the coupled electromechanical finite element plate model prove the efficiency of the proposed scheme as they are in accordance with experimental data and other formulations suggested in the literature.

In (Reddy, 1999) a theoretical formulation of the displacements and strains of smart plates using the classical laminated plate theory (CLPT) is presented. This theory is based on the Kirchhoff assumption that straight lines which are perpendicular to the midsurface before deformation, are considered inextensible and remain straight and perpendicular to the midsurface after deformation, as well. This theory ignores shear deformation effects and provides reasonable results mainly for thin laminates.

The FSDT which was proposed by Reissner and Mindlin, takes into consideration shear deformation effects by the way of linear variation of in-plane displacements through the thickness.

The effect of transverse shear deformation on the bending of laminated plates is also discussed in (Whitney, 1969). Namely, a theory for laminated plates which includes the effect of transverse shear deformation is presented. Results indicate that shear deformation can be significant for highly anisotropic composites. It is also shown that the proposed theory can accurately predict gross response characteristics, such as plate deflections, buckling loads, *etc.*, of laminated plates.

Moreover, a refined hybrid plate theory for composite laminates with piezoelectric laminae is developed in (Mitchell & Reddy, 1995). The formulation is based on linear piezoelectricity, including the coupling between mechanical deformations and the charge equations of electrostatics. The theory is considered hybrid due to the fact that the mechanical displacement field is studied using an equivalent single-layer theory, while piezoelectrics are modeled using a layerwise discretization.

In (Reddy, 1997), (Reddy, 1999) a generalized third-order shear deformation laminate theory (TSDT), which contains the first-order shear deformation theory (FSDT) as a special case, is used to develop the governing equations of laminated plates with actuating and/or sensing layers.

Another simple first-order shear deformation theory for laminated composite plates is presented in (Thai & Choi, 2013). The core difference of the presented deformation theory to the existing in literature lies to the fact that it takes into account only four unknowns. Moreover, it is very similar to the classical plate theory in many aspects, i.e. in the equations of motion, boundary conditions, *etc*.

2.1.2 Layerwise models

An adhesive interface element for bonding of laminated plates is presented in (Lin & Ko, 1993). More specifically, an isoparametric interface element is used in the analysis of adhesive-bonded structures. The proposed model assumes that stresses dominate in the adhesive layer. The assumptions made for the elastic analysis include small deformations, negligible transverse normal deformation of the plate and overlay, anti-plane stress state for the adhesive and uniform peel and shear stresses along the thickness direction in the adhesive layer. Eight-node isoparametric plate elements made of fiber reinforced composites are used for the formulation of the host structure and patches. The model is based on first order shear deformation theory. The resulting elements can be properly used in solving adhesive-bonded structures problems as it provides realistic assessments of the stress distribution and deformation.

An extended review on the available literature related to the use of piezoelectric sensors and actuators for the disturbance sensing and control of flexible structures has been comprehensively done in the survey (Rao & Sunar, 1994). According to the article, piezoelectric materials can be easily used in order to attain an accurate response

and effective control of smart flexible structures with integrated control schemes. A brief history of piezoelectricity is also included.

Another finite element model for the analysis of smart piezocomposite plates on deflection control is suggested in (Lin, et al., 1996). The proposed model consists of an eight-node isoparametric plate element, an actuator element and an adhesive interface element used for sticking the two separate layers together. The actuator proposed in this investigation relies on first-order shear deformation theory. Some assumptions made include among others that piezoelectric elements are sufficiently thin and perfectly bonded to the structure, the transverse shear strains are uniform through the thickness and the transverse normal strain, as well as the deformations are negligible which means that the linear theory can be used. The results of the analysis indicate that the use of the adhesive material provides flexibility to the structure making possible the solution under any type of boundary conditions and geometry configuration.

A finite-element analysis of strain transfer in an induced strain actuator is presented in (Seshu & Naganathan, 1997). Since the proper selection and application of suitable adhesive bonds between layers play a significant role in maximizing the strain transfer from the actuator layer to the substrate, a detailed finite-element model is necessary in order to model the strain transfer from the actuator to the substrate via an adhesive layer. For this purpose, a two-dimensional Lagrangian finite element has been proposed. The results of the study are compared with those obtained by one-dimensional analytical models in order to show the limitations of the analytical models. In addition, an investigation of different values of the shear lag parameter, which indicates the nature of bonding, is done for extension and bending type actuation. It is also shown that the analytical results are in agreement with the general finite element results obtained by the proposed method.

The formulation of a finite element model of hybrid active–passive vibration damping of multilayer piezoelectric sandwich beams is proposed in (Trindade, et al., 2001). Namely, an electromechanically coupled finite element model is formulated in order to handle active–passive damped multilayer beam structures, and more specifically a viscoelastic core placed between piezoelectric layers which are modeled using the classical laminate theory. The whole system is formulated using classical three-layer sandwich theory, assuming thin faces based on Euler–Bernoulli theory and a Timoshenko thick core. The finite elements are based on Lagrange linear shape functions for the mean and axial displacements and Hermite cubic ones for the transverse deflection. The electric potentials and voltages of the piezoelectric layers are considered as extra degrees of freedom for each layer. An anelastic displacement field (ADF) model is used for the modeling of the viscoelastic core yielding to an augmented state-space system which is capable of time-domain analyses of highly damped beams. In order to improve the efficiency of the proposed method the model is reduced through modal analysis tools.

In (Luo & Tong, 2004) a novel finite element analysis formulation has been considered. Namely, piezoelectric elements with four nodes are used. The adhesive element has finite thickness with shear and peel stiffness and thus gives the insight into the interactive behaviors of the piezoelectric smart plates, which also shows that peel stress is important for the flexible smart plate. This element is placed between two collocated four node plate elements in order to form an adhesively laminated element of the piezoelectric sandwich smart plate. The displacement filed of the laminated element is considered to be continuous and the Reissner–Mindlin plate theory is used. This theory can be accurately applied to a thin or moderately thick host plate with bonded or debonded piezoelectric sensors and actuators. According to this investigation, the shear stresses are highly concentrated near the edges of the piezoelectric actuators. This phenomenon impacts the performance of piezoelectric actuators in smart plates as the assumptions made, may be limited to large piezoelectric patches and thick host plates.

Piezolaminated plates can also be modeled using layerwise mixed finite elements (Garcia Lage, et al., 2004). The finite element model of this work is formulated using a Reissner mixed variational principle. The primary variables of the mixed functional include transverse stresses, transverse electrical displacement, displacement components and electrical potential. Contrary to typical layerwise models, the proposed mixed model ensures the necessary continuity of the primary variables throughout the interface between neighboring layers. Although this approach works well with structures of medium and high thickness, it is rather insufficient for the analysis of thin composite piezoelectric structures, as its performance decreases when the plate becomes thinner. This is due to the fact that its use in the case of highly distorted elements, may lead to locking phenomena, such as the formulation of an over-stiffened structure. However the proposed mixed finite element model is a proper alternative to traditional displacement layerwise finite element models, as it assures the continuity of transverse stresses and electrical displacement and simulates the three-dimensional behavior of plate structures in an accurate way, and at the same time with respect to mechanical and electrical quantities.

An adaptive sandwich piezoelectric composite beam with a foam core is studied in (Plagianakos & Saravanos, 2005). More specifically a coupled high-order layerwise beam model, discretized with finite elements is considered in order to predict the electrostatic response of beams with bonded piezoelectric layers. The stiffness matrix, along with the piezoelectric and the permittivity matrices are formulated from ply to structural level. The results of the work show the capability of the proposed method to capture the local electric and shear stress response of the piezo-composite structure in an efficient and accurate way, including, among others, thick structures and structures with compliant shear layers. The high-order layerwise theory (HOLT) is used in (Plagianakos & Saravanos, 2005) for the calculation of the electrostatic response of thick piezoelectric beams. The numerical results are compared to the ones provided by a linear layerwise theory (LLT). The use of high-order terms both in the elastic, as

well as the electric field of the discrete layers with the form of additional degrees of freedom (DoFs) provide more accurate results for each individual discrete layer of the total structure.

In (Erturk & Tekinalp, 2005) a layerwise approach is used in order to capture the flexibility of the adhesives of a smart piezoelectric plate at delaminated regions. The formulation is done by using the finite element method. Namely, a sort of special finite elements which use both linear Lagrange, as well as conforming Hermite type interpolation functions, are developed and used instead of integration and transfer matrix methods. The adhesive layers are modeled as distributed normal and shear springs. They are also assumed to be very thin, without mass and with linear deformation.

Another, higher-order layerwise laminate theory for the prediction of interlaminar shear stresses in thick composite and sandwich composite plates is presented in (Plagianakos & Saravanos, 2005b). The proposed theory is used for the prediction of the static response of composite structures. The total displacements of each separate layer are given through the thickness of the laminate and include quadratic and cubic polynomial distributions of the in-plane displacements, in addition to linear approximations given by linear layerwise theories. The results of the proposed theory are compared with the ones obtained by a linear layerwise theory which is based on kinematic assumptions with a variable distribution of the transverse displacement through-thickness. The proposed higher-order formulation has two significant benefits compared to linear layerwise theories. The first and very important is that only a small number of different layers is needed in order to model the composite laminate structure which makes the theory efficient. The second, also important advantage of the theory lies to the fact that it provides accurate predictions for the parabolic through-thickness distributions of displacements, strains and stresses both at the interfaces, as well as at the free edges, which makes the theory robust as well.

Another efficient layerwise finite element model for dynamic analysis of laminated hybrid piezoelectric beams is presented in (Kapuria & Alam, 2006). This model consists of a one-dimensional structure which takes into account the electric potential of the piezoelectric components as degrees of freedom. The analysis uses the coupled efficient layerwise (zigzag) theory developed in (Kapuria, et al., 2005). The formulation proposed in (Kapuria & Alam, 2006) can be used for both open and closed circuit boundary conditions which are necessary either for sensory, as well as for active response. The finite element model and the algorithm used for the dynamic analysis have been validated in comparison to the results of hybrid beams solved with analytical Navier-type theory. The finite element model which is used for the analysis is free of shear locking. The comparison between the two theories shows that the proposed layerwise zigzag theory is accurate for both free and forced vibration response of hybrid piezoelectric composites as well as sandwich beams of moderate thickness.

An approach of the use of mixed finite elements for the formulation of layerwise piezoelectric anisotropic plate models is considered in (Carrera & Fagiano, 2007). The finite elements used in this investigation take into account a priori continuous transverse electric displacements. The analysis of the smart structure is performed assuming the unified formulation and the Reissner mixed variational theorem. First, a partial form of the theorem which takes as parameters the displacements, the electric potential and the transverse stresses is considered. Subsequently, a full form of the Reissner mixed variational theorem is considered, which adds the transverse electric displacement as independed variable. The superiority of the latter consideration is shown through examples that demonstrate its effectiveness for the evaluation of interlaminar continuous transverse electric displacement fields. It is also shown that the implemented finite element model can provide very accurate descriptions of both mechanical and electrical fields which makes unified formulation a valuable tool in the hierarchical analysis of smart piezoelectric plates.

The adhesive elements can be formulated in various ways. In (Klug & Sun, 1996) a very efficient analytical model for bonded composite patches to cracked aluminum plates is considered. In this model, the host structure, as well as the composite patches are modeled separately using the Mindlin plate theory. The adhesive layer is formulated with effective springs which are used as joints between the patch and host plate. However, this finite element formulation has the major disadvantage of being applicable to flat elements, which means that it does not consider curvature effects.

It is possible that the size, as well as the thickness of bonded patches can affect the peel stresses, making necessary the optimal design of the adhesive layers in curved surfaces. In (Tong & Sun, 2003) a finite element formulation for developing adhesive elements for conducting quick stress analysis of bonded patch to curved thin-walled structures is presented. The local stiffness matrices for the adhesive elements consist of two shell elements and one pseudo brick element yielding to 8-node, 16-node and 18-node adhesive elements. These elements are assumed to be 2.5D adhesive elements and can be used for the calculation of stresses in the adhesive layer of curved structures. The loading vectors follow the standard finite element analysis procedure. The final elements are suitable to be used as bonded repairs in thin-walled structures.

2.2 Delamination

Delamination is a very common failure for composite materials. In fact, materials of different mechanical properties are bonded and must stay together by following the deformation of the continuum, so that stress concentrations appear.

In laminated composite structures, when delamination occurs, either the sensor and/or the actuator can peel off. The level of abruption could be limited or more extensive. A suitable multilayer formulation of a piezocomposite plate allows us to investigate delamination effects including partial delamination near to reality.

In (Cantwell & Morton, 1991) the impact resistance of fibre-reinforced composite materials is reviewed. As a result, serious concerns regarding this impact are found. Namely, the strain energy capacity of the fibres determines the impact resistance of the whole structure. Moreover, the fibre stacking sequence determines both the elastic energy absorbing capability of the material, along with the failure mode. For decent damage restriction, laminates with abrupt changes in the orientation of the fibres should be avoided.

In laminated materials, such as the ones used in laminated structures, the repeated applied stresses, impact the layers of the structures and can lead them to separate. This phenomenon can form a less tough structure. Prediction of failure in composite laminates can be accomplished using computational methods based on material strength and fracture toughness, as it is presented in (Dávila, et al., 2005).

In (Nikishkov, et al., 2016) a measurement of fracture toughness properties in composite laminates is presented. Namely, the prediction of the matrix failure is accomplished using computational methods based on material strength and fracture toughness. Accurate three-dimensional measurements of crack progression under loading suggest that crack features are strongly related to a mixture of fracture modes. The results obtained suggest that accurate fracture-based predictions of the intralaminar matrix crack propagation should be based on appropriate fracture criteria.

Delamination can also be observed in reinforced concrete structures through the phenomenon of reinforcement corrosion. A review of research literature in this area shows that insufficient theoretical work on corrosion induced concrete delamination has been undertaken, see (Alonso, et al., 1998), or (Maslehuddin, et al., 1990). However, various investigations propose a theoretical framework for the prediction of delamination caused by steel reinforcement corrosion. These methods are based on mechanics and mainly use crack opening in concrete as delamination criterion (Li, et al., 2007).

In (Mahieddine, et al., 2010) a mathematical model for partially delaminated Euler–Bernoulli beams that allows the appearing of delamination anywhere in the structure is presented. It is shown that when the layers become thicker, the axial displacement increases. The results agree with the ones of the exact solution indicating that the proposed method is efficient, as well as that the assumptions made are valid.

In general, the study of delamination or other failure phenomena in structures attracts some interest. For example in (Okafor, et al., 1996) and (Greco, et al., 2015) the effect of delamination on laminated composite beams is examined.

In (Kuo, 1984) a continuous two-dimensional shear spring element was used in order to calculate the stress intensity in smart structures bonded with adhesive materials. The stiffness of the structure is formulated using quadratic quadrilateral isoparametric elements which take into account the continuity of the adhesive layers. The simple two-dimensional model provides an accurate solution in terms of stress intensity,

which makes the proposed formulation a convenient tool for modeling adhesive layers.

In (Okafor, et al., 1996) the prediction of delamination in smart composite piezoelectric beams is examined. The host structure is equipped with built-in piezoelectric sensor and actuator patches, while modal analysis tools and neural networks are employed for the analysis. The results indicate that the proposed techniques provide successful predictions of the delamination size.

In (Erturk & Tekinalp, 2005) the deformation of the adhesive layers in multilayer piezoelectric plates is considered with finite elements. The investigation shows that even if partial delamination between the piezoelectric and non-piezoelectric layers does not affect the maximum deformation significantly, however it affects the local stresses near the delaminated regions of the smart cantilever plate. Another outcome from this investigation is that the more flexible the adhesive layer, the less it deforms when an electric field is applied. It is also notable that the finite elements which are developed in this study are suitable for modeling interlaminar stresses and modeling delamination as well.

Greco et al. propose a novel approach for the prediction of delamination of multi-layered composite beams in (Greco, et al., 2015). To be more specific, a model based on the first-order shear deformable laminated beam theory is considered. In addition, arbitrary Lagrangian–Eulerian formulation is used for the development of moving mesh strategy. The proposed model is capable of avoiding complexities in bi-dimensional structures. A comparison with experimental results indicates that the results of the analysis are valid and that the proposed formulation can be used in more complex structures and/or excitation scenarios.

However, except for delamination, for a given distribution of stresses on a structure, several violations at critical points could be observed. These violations include among others, debonding, penetration, sliding, *etc*.

Some serious work is done regarding debonding in composite structures. For example in (París, et al., 2003) the failure of the matrix in fibrous composite materials is investigated from the micromechanical view. The numerical analysis is performed using the Boundary Element Method, allowing contact between the debonded surfaces of fibre and matrix. The numerical results of the investigation prove that stresses not associated to the macromechanical plane of failure play significant role in the mechanism of failure of fibrous composites in the microscopic scale.

Other works deal with progressive debonding. In (Hsueh, 1995) the criteria for progressive debonding at the fiber/matrix interface with friction along the debonded interface for the case of fiber-reinforced ceramic composites are considered. In (Kushch, et al., 2011) a numerical simulation of progressive debonding in fiber reinforced composite under transverse loading has been performed. Namely, the effect on debonding

progress of local stress redistribution due to interaction between the fibers is studied. The finite element model is developed based on the cohesive-zone model of interface.

In (Caporale, et al., 2006) a micromechanical analysis of interfacial debonding in unidirectional fiber-reinforced composites is performed. Namely, extensive analysis on fiber-matrix debonding phenomena in unidirectional composites with homogeneous, isotropic and linearly elastic constituents is carried out. The failure is given by normal and tangential brittle-elastic springs which are used for the connection between the matrix and the fibers at the interface. The micromechanical analysis which evaluates the first failure loci has been developed using the finite element method.

In (Kumar, et al., 2007) an active vibration control of smart plates with partially debonded multilayered PZT actuators is considered. Namely, a simple modeling scheme for multiple debonding is proposed, which can also idealize multiple delamination in the host laminate. The total influence of the damage of the actuator on the performance of the closed loop control is evaluated. The results of the investigation show that the debonding phenomena in actuators influence both active damping and active stiffening effects.

A multi-scale computational homogenization scheme is proposed in (Drosopoulos, et al., 2014) for the study of debonding in composite materials. A classical unilateral contact law has been incorporated in the microscopic level, for the investigation of the contact between the constitutive materials. By using contact mechanics, non-penetration between the constituent materials of the microscopic structure is taken into account. The influence of microscopic debonding in the macroscopic level of the composite is finally captured.

It is noteworthy that with homogenization techniques, an equivalent anisotropic (e.g. orthotropic) plate can contain the information of the overall possibly damaged microstructure.

2.3   Three-dimensional models

Although the increased complexity, three-dimensional models have been proposed by several investigators due to their higher accuracy in studying delamination phenomena.

For instance, delamination and buckling in three-dimensional composites are examined in (Cox, 1994). Namely, 3D stitched laminates and woven composites containing delamination cracks with some assumptions are considered. A relation for the minimum density of through thickness reinforcement required for the buckling of the delamination layer is given. In this work it is proven that if the length of the delamination crack exceeds a critical length, then buckling will not span the whole delamination. In addition, for normal densities of through-thickness reinforcement, this critical length will rarely exceed the thickness of the delaminated layer.

A stress analysis of multilayered plates, which incorporate induced-strain actuators is presented in (Icardi & Di Sciuva, 1996). Namely, a detailed study of the 3D stress field of multilayered smart plates based on the von Karman strain–displacement relations is developed. The presented third-order zigzag layerwise theory allows for geometrically nonlinear effects. Numerical results indicate that the active control of deflections is rather effective.

Delamination growth in laminated structures is discussed in (Sprenger, et al., 2000). Continuum-based 3D shell elements and a viscoplastic softening model for the simulation of delaminations in composite structures are considered. More specifically, an eight-node brick element with the assumption that its modification is based on natural strain is presented. An inelastic material model with softening, along with a viscoplastic regularization are introduced. Numerical results indicate that 3D shell elements are suitable for the description of the delamination concept.

In (Bruno, et al., 2005) a 3D delamination modeling technique for analyzing mixed mode delamination problems in laminated structures is proposed. The technique, which can be used for very thin adhesive layers, is based on first-order shear deformable plate and interface theories for laminated structures. Delamination phenomena may occur along these interfaces. For the simulation of adhesion and contact effects, Lagrange and other penalty methods are considered. Tests with full 3D finite element models indicate the accuracy and the efficiency of the procedure.

A computational technique for flexural effects in textile reinforced composite shells is presented in (Piezel, et al., 2012). The procedure is used for the in-plane and the out-of-plane behavior of 3D composite shells. The aim of this technique is to analyze the bending effect on the risk for delamination at the interface of 3D woven fabric composites employing shell-like representative volume elements. It is shown that the proposed method is general and can be used for various types of composites.

Finally, 3D delamination in encapsulated silicon devices is discussed in (Ho, et al., 2012). More specifically, an experimental validation using pattern recognition techniques is done for the investigation of delamination characteristics and especially the viability of the cohesive zone. The analysis indicates that a 3D numerical model provides a delamination pattern very close to the one observed through the experiments.

An interesting work on the evaluation of inter-laminar stresses in the adhesive layer of bonded lap shear joints is presented in (Pradhan & Parida, 2013). The non-linear analysis consider three-dimensional finite elements and contact elements in order to avoid penetration phenomena in the area of the delaminated surfaces. The analysis indicate that the use of three-dimensional elements is mandatory due to the existence of 3D state of stress near the delamination region. Moreover, it is shown that the adoption of 3D finite elements diminishes errors that may appear in 2D analyses.

Another 3D finite element analysis of buckling delamination in laminated smart structures is briefly described in (Akbarov, et al., 2014). More specifically, the analysis of a

rectangular plate with an inner rectangular crack under a biaxial compressive force is considered. One critical assumption made in this investigation is that the plate is simply supported at all its lateral sides. A failure criterion is considered for the determination of the critical buckling. Three-dimensional finite elements and the boundary-form perturbation technique are used for the solution of the boundary problem. The results extracted indicate the impact of the topology of the structure and the properties of the materials to the analysis.

In (Liu, et al., 2014) an optical coherence tomography system for the characterization of glass fiber composites is presented. In this work 3D crack surfaces during delamination growth are considered.

A novel three-dimensional computational model is proposed in (Benvenuti, et al., 2016). Namely, an experimentally stable extended finite element model for studying single-lap shear tests in order to simulate delamination in reinforced concrete plates is suggested. The analysis includes regularized three-dimensional elements which can be used for either design or experimental purposes.

Typically, the investigation of delamination phenomenon in smart structures can be based on a simplified model. For further information see (Mistakidis & Stavroulakis, 1998).

2.4   Model uncertainty and control

In general, mathematical theories of control demand the whole information of the studied dynamical system. Even a slight divergence from the nominal values may cause a drastic reduction in the effectiveness of control. This means that, either the system studied must be first reconstructed through the use of some filtering techniques and then controlled, or the adoption of robust controllers, which are insensitive to modification of nominal values, must be considered.

As for vibration control in general, control system can be either active, passive or hybrid i.e. semi active. According to this classification, active control incorporates a set of sensors and actuators in order to apply real-time feedback. From the other hand in passive control there is absolute absence of any kind of feedback, while hybrid systems combine the characteristics of the two distinct types of control.

Piezo-actuator delamination can also affect the performance of active noise and vibration control systems. In (Kim & Jones, 1996) an analytical, as well as an experimental investigation for the identification of the effects of inner and edge delamination phenomena on the performance of surface-mounted piezoelectric actuators on a smart cantilever beam is carried out. From the analysis, it is shown that in case of edge delamination there is an unpropitious effect on the performance of the control system, whereas in case of inner delamination the impact on the performance is negligible.

Vibration control in systems with presence of delamination is studied in (Tylikowski, 2001). More specifically, the effects of piezoactuator delamination on the transfer functions of vibration control systems are considered. The host structure consists of a simply supported laminated piezoelectric beam, which is subjected to excitation by non-symmetric actuator elements. The numerical results indicate the influence of delamination phenomenon on the characteristics of the vibration. In this investigation is shown that the edge delamination has a negative impact to the performance of the piezoelectric actuators. It is also proved that delamination at the edges of the structure decreases the magnitude of transfer functions between the voltage of the actuators and the displacements of the beam.

Active control is also widely used for the vibration suppression of smart structures either with (Kumar, et al., 2007) or without presence of structural failures (Zabihollah, et al., 2007).

For example in (Kumar, et al., 2007) the performance of a linear quadratic Gaussian (LQG) based active vibration control system is tested. The numerical results obtained by the active control simulation suggest that it is necessary to take into account possible failures as uncertainty parameters while designing the controller, in order to make the control system not only effective, but damage-tolerant as well.

The work presented in (Zabihollah, et al., 2007) deals with active vibration suppression of smart beams. The analysis is based on a layerwise theory and an optimal control strategy. The host structure is a smart laminated composite beam, while the actuation and sensing elements are made of piezoceramics. For the design of the control scheme, the state-space representation is considered. Subsequently, a linear quadratic regulator (LQR) controller is designed and tested in order to achieve vibration suppression of the smart beam. The results are compared with those obtained by experiments and show that the controller is accurate and efficient for the reduction of the vibrations of the structure.

An experimental model identification and vibration control of a smart cantilever beam using piezoelectric actuators and sensors is presented in (Nestorovic, et al., 2012). More specifically, the concept of an active vibration control for piezoelectric light weight structures is introduced. The study focuses on structural control with piezoelectric materials as active elements. The efficiency of the proposed model, as well as the control are proven based on experimental verification.

One critical point is that the simulation of smart multi-layered composite structures have to deal with high levels of uncertainty in the proposed models.

In fact, the given parameters that can be measured include the mass and the dimensions of the structure. All the rest parameters need to be computed. Stiffness and damping present a low level of uncertainty. However, serious questions arise for some critical parts of a composite, such as the adhesive materials.

In order to reduce these levels of uncertainty we need to measure the deviation of the nominal terms. This could be done in various ways:

i.   One possibility could be the use of non-mechanical methods, such as for instance interval analysis (Pons, et al., 2008), (Neduncheliyan, et al., 2009). This type of control considers trials and/or combinations within a given interval. This method is known for the simplicity of the output feedback controllers and can demonstrate good closed loop performance, however it is not very accurate due to the assumptions made.

ii.   The other option is to use robust optimal design in order to build robust controllers (Damle, et al., 1994), (Marinova, et al., 2005). For this purpose, a damage parameter is considered, which means that a sustainable way in which the proposed control scheme will continue to work, even with a mismatch of its parameters, is sought.

Thus, the objective is to propose a control model in order to ensure that the structure will remain functional in an optimal way. It is not expected that the structure functions perfectly, but, as a compromise, it remains functional in a satisfactory level. In such cases H-infinitive, fuzzy or adaptive neuro-fuzzy control may be useful.

2.4.1   H-infinitive control

Control usually deals with smooth functions as for instance quadratic functions, linear functions, *etc*. However, when we deal with peculiar features such as eigenmodes or frequency peaks the use of robust control, e.g. H-infinitive control is necessary.

In a few words, an H-infinitive controller takes the response for all the excitations given, it extracts the peak of them and tries to apply the control at this peak. This could be for example the first eigenmode. Once the control is properly applied, the controller moves to the next mode and so on.

For example in (Crassidis, et al., 2000) the control of active damping using the H-infinity control strategy is presented. Namely, two different configurations of the resulting hybrid treatment are considered. The first assumes that active and passive control act separately, while in the second configuration proposed the two different types of control operate together in order to maximize the energy dissipation. The objective of this investigation is the design and the implementation of robust controllers for different control strategies. The robustness of the proposed controller is demonstrated by the comparison between the H-infinitive control scheme and a classical PD controller. Finally, the effectiveness of the H-infinitive scheme in controlling structural vibration is tested.

In (Iorga, et al., 2008) a review of H-infinitive control on smart piezoelectric actuated structures has been done. In this work, the main problems that need to be addressed for the optimal design of robust control laws, which include among others structural modeling techniques, uncertainty modeling, controller order reduction, and robustness validation, are reviewed. The objective of this work is to provide a comprehensive

methodology for the design and the validation of robust H-infinitive controllers for active structures. For this purpose a step-by-step example application for a cantilever piezoelectric actuated smart plate is presented.

In another work (Moutsopoulou, et al., 2014) an active control system for a flexible laminated smart beam with bonded piezoelectric sensors and actuators is developed and studied. The dynamics are formulated using the finite elements method. The theory of robust H- infinitive control is used due to the present of uncertainty in the system. The objective of the control design is to find the optimal control forces in order to reduce the external excitations. The robustness analysis includes the mathematical expression of the uncertainty, the investigation of the robust stability of the system, as well as the confirmation of the robust performance. The numerical simulations verify the effectiveness of the proposed control strategy.

Another investigation on robust active vibration control of smart structures is presented in (Oveisi & Gudarzi, 2012). In this work a comparison between two robust control designing approaches in smart structures is made. The controllers are designed using on the one hand the µ-Synthesis approach and on the other hand the LMI-based design approach based on the augmented plant which consists of the model along with uncertainties. From the results obtained, it is shown that the LMI-based design approach presents higher performance in rejection of random disturbances.

2.4.2 Fuzzy control

The key advantage of classical control theories is the availability of strong mathematical tools for the design of the controllers. However, the fact that a linear feedback is adopted, is considered to be a serious drawback. On the other hand, nonlinear control, e.g. fuzzy control, is more flexible and more suitable to handle nonlinearities. This is due to the fact that the feedback of such controllers is nonlinear and could be of varying intensity in different areas of operation. This is not only expected, but desirable as well, as a nonlinear controller can serve different needs, e.g. slight or more extensive displacements, with the same initial settings.

Specifically for the fuzzy inference systems, the presence of verbal rules can systematize the experience of an advanced user of a system or a process, and can be used for the construction of nonlinear controllers. The control output could be nonlinear and complicated.

An introductory survey of fuzzy control has been conducted in (Sugeno, 1985). The theoretical framework, as well as some industrial and other fuzzy applications are covered. Subsequently, the major advantages and drawbacks of fuzzy control are addressed. The most important features of a controller based on fuzzy logic are, among others, the ability to function under multiple objectives and the adaptiveness to different problems. Another significant advantage of fuzzy control is the robustness. The

major disadvantage seems to be the absence of a complete mathematic framework for the description of such systems.

Fuzzy control offers an efficient interface for the translation of the knowledge of one system into the nonlinearities which are necessary for the control. An introduction to fuzzy control is made in (Driankov, et al., 1996), where all the necessary tools for building robust fuzzy controllers are presented in detail.

A control paradigm for smart structures using fuzzy control is presented in (Mayhan & Washington, 1998). In this study, fuzzy control techniques and smart piezoelectric materials are combined in order to form a robust and adaptive control system. The proposed model is capable of learning and thus of improving its performance over time in presence of uncertainties in the host plant, so as to be adaptive. The robustness is proved by changing the properties of the beam i.e. by adding some extra masses to the host beam.

Fuzzy control is widely used for vibration suppression of smart composite structures as well. In (Cohen, et al., 2002) an active control law for the vibration suppression of smart flexible beams is developed. The control is achieved via collocated pairs of sensors and actuators. The control scheme consists of a closed-loop algorithm based on fuzzy inference. The results of the simulation indicate that the proposed controller can be configured easily and quickly, while the control is effective and robust as well. In this case, the robustness of the controller is examined by altering the dynamic characteristics of the host structure.

A modal control law of cantilever piezoelectric beams using fuzzy logic is presented in (Sharma, et al., 2005). The inputs of the controller are the modal displacements and modal velocities of the modes to be controlled. The performance of the proposed method is proved for the first two modes of the host structure. The results obtained, indicate that the implementation of fuzzy controllers for active vibration control is not only feasible, but effective as well.

In (Tairidis, et al., 2007) and (Tairidis, et al., 2009) the vibration suppression of a smart beam model with embedded piezoelectric sensors and actuators using fuzzy control is considered. Vibration suppression is achieved by using active control. The design of the nonlinear controller is based on pendulum-like fuzzy inference rules. Two different schemes are implemented. First, a collocated controller that takes as input the displacement and the velocity of the free end and gives back the control force to be applied at the same point is considered. The second fuzzy controller consists of two independent fuzzy mechanisms, which can be tuned separately, placed at the middle and at the free end of the cantilever beam. The numerical results which presented indicate that vibration reduction in terms of displacements is accomplished, thus the control is considered to be effective.

Fuzzy logic controllers are also used for active vibration control of smart plates. In (Shirazi, et al., 2011) a simply supported rectangular plate, made from functionally

graded materials, is considered. For the extraction of the equations of motion, classical plate theory is used. The control scheme, which consists of a fuzzy controller, is formulated by considering the conditions of a real physical problem. Numerical results indicate that fuzzy control provides satisfactory suppression of the vibrations of the host structure.

In (Muradova & Stavroulakis, 2013) the vibration control of a smart plate is considered. The model consists of a thin elastic rectangular plate, while the controller is designed using fuzzy inference techniques. In this investigation two different computational procedures are proposed. In the first approach a local controller is considered, while in the second algorithm the controller is distributed. From the numerical results, both methods seem to achieve the desired vibration suppression of the host plate.

A general design method of hedge-algebras-based fuzzy controllers and an application for structural active control is proposed in (Bui, et al., 2015). The method uses inherent order relationships between words instead of using fuzzy sets. Thus the analysis is realized in a word-domain, in order to express the semantics of words. Hedge algebras theory provides an appropriate formal basis to define the fuzziness of vague terms, although the difficulties which come from the high level of abstraction. The definition is achieved by taking advantage of the shape of the fuzzy sets which, in turn, represent the meaning of the variables. Results taken by the simulation, indicate that the proposed method is simple, transparent and efficient in reducing the pick storey drift, as well as the pick absolute acceleration of the structure.

A hybrid control scheme, based on fuzzy techniques, for the suppression of vibrations of a smart von Karman plate is presented in (Muradova & Stavroulakis, 2015). Namely, the suppression of large vibrations of a smart thin elastic rectangular von Kármán plate is studied. The considered nonlinear problem is spatially discretized by means of the time spectral method. As for the time integration, the implicit Newmark-β iterative method is employed. The nonlinear controllers are designed, considering the fuzzy inference techniques. The numerical results presented indicate the efficiency of control.

Moreover, it is shown that the characteristics of fuzzy controllers can be easily tuned by using global optimization methods, such as genetic algorithms (Lu, et al., 2003) particle swarm optimization (Marinaki, et al., 2011), (Marinaki, et al., 2011b), *etc*.

For example in (Lu, et al., 2003) a genetic algorithm is used for the design of fuzzy controllers for smart structures. The effectiveness of the proposed optimization algorithm is demonstrated by testing on a cantilever piezoelectric beam.

Another example of the use of genetic algorithms for the optimal tuning of control is studied in (Mahmoodabadi & Jahanshahi, 2016). Namely, a multi-objective algorithm for the optimization of the characteristics of controllers for fourth order nonlinear systems is presented. The results demonstrates that the proposed methodology can be effectively applied for the optimization of control of nonlinear systems.

In (Marinaki, et al., 2011) the particle swarm optimization (PSO) method is used for the fine tuning of fuzzy controllers. More specifically, three different variants of the Particle Swarm Optimization are tested, namely, the simple Particle Swarm Optimization, the inertia Particle Swarm Optimization and the Constriction Particle Swarm Optimization. From the numerical results the effectiveness of the proposed methods is shown.

Moreover, in (Marinaki, et al., 2011b) a multi-objective particle swarm optimization algorithm for the optimization of a fuzzy controller used for the vibration suppression of a smart beam. The mathematical formulation of the beam model is based on the Timoshenko beam theory. The sensors and the actuators are formulated considering the linear theory of piezoelectricity. The proposed PSO method takes into account a combination of continuous and discrete variables. In the present investigation, the break points of the membership functions of the fuzzy variables are optimized.

Another multi-objective particle swarm optimization algorithm for the optimum design of fuzzy controllers for nonlinear systems is presented in (Mahmoodabadi, et al., 2016). More specifically, a multi-objective particle swarm optimization algorithm is used in order to obtain the Pareto frontiers of the different commensurable and conflicting objective functions which are used for the optimum design of fuzzy controllers. In order to illustrate the equitable solutions, the Lorenz dominance method is used. The comparison of the obtained results with those in the literature demonstrates the efficiency of the proposed method.

For the optimal design and/or the fine tuning of fuzzy controllers other methods can be used as well. In (Marinaki, et al., 2015) a new multi-objective differential evolution (DE) algorithm is proposed and tested on smart beams. More specifically a mixed-variable differential evolution method is used for the optimal design of a fuzzy controller. The results obtained show the efficiency of the proposed method, as significant vibration suppression in terms of both displacement and velocity is achieved.

It is worth mentioning that global optimization methods, such as genetic algorithms, can be used for the optimal placement of piezoelectric elements on smart structures.

One approach for the optimal placement of piezoelectric sensors and actuators for vibration control of a composite plate using genetic algorithms is presented in (Han & Lee, 1999). More specifically, genetic algorithms have been used to find efficient locations of piezoelectric sensors and actuators with consideration of controllability, observability and spillover prevention. In the proposed scheme, some modifications of genetic algorithms have been suggested to improve searching efficiency.

In another study (Nestorovic, et al., 2015), a multi-objective genetic algorithm for the optimal placement of piezoelectric actuators and sensors on a smart beam and a smart plate is considered.

Among the plethora of applications covered by fuzzy control, the use of such controllers in structures with presence of delamination has been also investigated. Fuzzy control is also applicable in structures with failures either for the deterioration of vibrations or the detection of possible damages.

In (Sawyer & Rao, 2000) a methodology for the identification of damage in structures is proposed. In this investigation, fuzzy techniques combined with continuum damage mechanics are used to recognize both the location and the extent of the failure. The suggested methodology is a new approach which monitors static and dynamic responses and can be used for the damage detection of various civil structures. The numerical examples presented in this paper indicate that the performance of fuzzy systems are vigorous under conditions of noise or high uncertainty. See also the related paper (Hadjigeorgiou, et al., 2006).

Finally, in (Latha & Senthilkumar, 2009) a fuzzy rule based model for the prediction of delamination in drilling of glass fiber reinforced plastic composites has been introduced. The results of the analysis are verified with experimental ones, indicating the efficiency of the proposed method.

2.4.3 Neural and neuro-fuzzy control

An artificial neural network is a machine learning system with inputs and outputs based on biological neural networks. The learning process is based on a set of paradigms i.e. available learning examples and can be either supervised or unsupervised. Neural networks are widely used in control. This is due to the fact that they are very powerful in solving nonlinear control problems of high complexity.

Neural networks can be used for self-learning control systems. In (Nguyen & Didrow, 1990) it is shown that a nonlinear control problem can be addressed using neural networks. The proposed method demonstrates that neural controllers can be used in solving complex control problems where analytical methods may fail. The characteristics of the network can be the outcome of a self-learning procedure. The controller is trained using the error back-propagation method. At each step the network starts from an initial state and terminates at a final state, while the objective of the whole process is the minimization of an error function between the measured and the desired values.

Artificial neural networks provide better solutions to some problems due to their capability of parallelism and learning. More specifically, the use of neural networks in control is considered as a natural step in the evolution of control methodology. A short review on neural networks for control systems is done in (Antsaklis, 1990). This work deals among others with the mathematical framework of the neural networks, the learning process, the system modeling, *etc*.

A novel methodology for on-line structural damage detection and identification using neural networks is presented in (Tsou & Shen, 1994). The presence of damage can be identified considering the changes in the dynamic properties of the structure. A back propagation three-layered neural network is used for the recognition of the location

and the severity of the failure. The proposed network is tested on a spring-mass damper system with three degrees of freedom for the identification of both single and multiple damages. The results show that the use of neural networks is feasible with some limitations. The proposed network is capable of recognizing the locations and the severity of failures for either single or multiple damages. The training process is easy and suitable for implementation using parallel processors. In addition, the procedure takes place at the design stage, which makes the neural network suitable for online structural health monitoring in real-time.

Adaptive neural controllers are also widely used. In (Youn, et al., 2000) a neuro-adaptive scheme for the vibration control of composite beams subject to sudden delamination is implemented within the MATLAB®-SIMULINK environment. Namely, the variations in natural frequencies and the characteristics of the actuators according to delaminations in the bonding layer are investigated. Numerical simulations using neural controllers at delaminated piezoelectric actuators have been performed for the vibration control of the composite structure. The results obtained indicate that the proposed control scheme is robust and efficient.

In (Abdeljaber, et al., 2016) a methodology for active vibration control of flexible cantilever plates using piezoelectric materials and artificial neural networks is proposed. A smart controller based on neural networks is designed in order to control the amount of voltage applied to the piezoelectric patches of the plates. The training procedure is based on predictions of the future response of the host structure. The trained controller is tested for different types of dynamic loadings. The results suggest that the proposed control scheme is robust and efficient. Namely, the proposed neurocontroller provide a significant suppression of the accelerations of the cantilever plate under several types of excitations.

Hybrid approaches incorporate the best characteristics of neural networks and other methods. For example the combination of artificial neural networks and fuzzy logic provides powerful and effective neuro-fuzzy controllers. This amalgamation is possible due to the similarities between the two techniques, as they both are capable of handling extended nonlinearities and in the same time they both allow interpolative reasoning.

Neural networks and fuzzy logic in intelligent control are examined in (Berenji, 1990). In this investigation, the core characteristics of fuzzy, as well as neural network controllers are presented, along with the available tools for the unification of their capabilities in order to design hybrid neuro-fuzzy controllers. The proposed hybrid schemes are compared with individual neural and fuzzy controllers through several examples. The models presented in this work are capable of modeling nonlinear control systems.

Thus, the usage of adaptive fuzzy controllers could be a more systematic approach. The adaption can be achieved by embedding the fuzzy controller into a suitable network architecture using neural network training techniques.

A well-established implementation of the adaptive neuro-fuzzy system is the adaptive neuro fuzzy inference system (ANFIS) of MATLAB®, as presented in (Stavroulakis, et al., 2011). The procedure followed, may be summarized in a number of steps as follows. Firstly, a detailed mechanical model of the total system is constructed. Subsequently, the dynamics of the system are calculated and saved. These data are used for the optimization and training of the neuro-fuzzy controller by using the ANFIS procedure. The resulting controller can be used for the control of the total system. The numerical results indicate the efficiency of the proposed control scheme for the vibration suppression on a cantilever beam under sinusoidal and ramp-type excitations. The control is not only efficient, but smooth as well.

Adaptive neuro fuzzy inference system can be used for structural damage identification as well. In (Hakim & Razak, 2013), techniques based on neural networks and on the ANFIS method in order to identify possible damages in a steel girder bridge dynamic model are developed. The data used for training obtained from modal analysis of the structure. The numerical results obtained from the analysis indicate that the ANFIS, which is trained using the hybrid learning algorithm, presents very accurate results and can be used for the identification of a failure in a bridge girder, as well as for the severity of the damage. Moreover, the results of the ANFIS model are more accurate compared to those occurred from a back-propagation neural network, indicating that the use of neuro-fuzzy techniques for the prediction of delamination is feasible.

Finally, a neural fuzzy analysis of delaminated composites using shearography imaging is presented in (Nyongesa, et al., 2001). In this paper, a combination of the neural networks classification and the fuzzy inference is used for the construction of an automated system for the identification of damage in laminated composite structures using shearograms. From the analysis is concluded that the use of a neural network, when combined with a fuzzy decision-making system, is very efficient for the classification of the shearograph images and thus for the damage detection in laminates.

2.5   Conclusions

Modern computational mechanics' tools allow us to accurately model structures and their degradation along service. Therefore, model uncertainty can be estimated in most cases. This is outlined with the example of study smart multilayered structures with uncertainties due to the presence of adhesive materials.

Classical control suffers from degradation in its efficiency in the presence of nominal structure's uncertainty. Besides classical robust control theory, which has many limitations, we are able to build and test efficient soft controllers, i.e. controllers that can work in various modes. A thorough comparison between the two approaches, as well as study of various test cases in more complicated structures, like shells, is still missing from the literature.

The main areas of contribution of the present dissertation to the state of the art can be concluded to the following: the estimate of structural modification due to delamination which is based on nonlinear computational methods and the testing of fuzzy and adaptive, i.e. optimized, fuzzy controllers on the modified structure to demonstrate robustness.

3 Structural models

In the present dissertation, in order to check the robustness of the proposed control schemes, three different models are used. The core characteristic of the proposed models is the coupling of the mechanical with electric field which is implemented through the use of piezoelectric sensors and actuators.

The first one consists of a smart beam with surface bonded piezoelectric sensor and actuator layers. The model is based on Timoshenko theory and on induced strain actuation theory. Next, the finite element formulations for the smart beam have been performed. It is worth to mention that this model, besides control, is also used for an energy harvesting application.

In order to analyse thicker laminated composite plates, a coupled electromechanical model has been developed based on first order shear deformation theory, incorporating both the displacement and the electric potentials as the state variable in the formulation. It should be noted that, compared to the uncoupled (induced strain) models, the coupled electromechanical models provide more consistent representation of both the sensor and actuator response of the piezoelectric materials.

Both previous models are based on equivalent single layer (ESL) theory, where layers in the structure are assumed to be one equivalent single layer. However, layerwise theories (in which separate degrees of freedom are defined within each layer) simulate more accurately the mechanical behaviour of laminated composite structures with relatively large thickness, which consists of various plies with different material properties and/or stacking sequences. Furthermore, it provides the ability to model discontinuities in the displacement field, hence enabling study of the delamination of the layers at some points.

On the other hand, the research on the area of smart structures has been mostly dealing with composite thin-walled structures, in which the adhesive material between the structural elements and the piezoelectric sensors and actuators must be taken into account, since the adhesive material layer affects the dynamic behaviour of the structure.

Therefore, a layerwise model that considers the adhesive layer flexibility is used to describe the electromechanical behaviour of a three-layered composite plate containing piezoelectric sensors and actuators and adhesive layers between them.

However, before we move to the models, a simple reference to piezoelectric materials and their properties is appropriate.

3.1   Piezoelectricity and piezoelectric materials

Piezoelectricity or piezoelectric effect was discovered in 1880 by French physicists Jacques and Pierre Curie (Curie & Curie, 1880). It is based on the ability of certain solid materials, mainly crystals (Figure 2) and certain ceramics, to produce an electric voltage in response to an applied mechanical stress. Etymologically, the word piezoelectricity is of Greek origin and means electricity obtaining from pressure. It is derived from the Greek word piezo (πιέζω), which means to press, and electron (ήλεκτρον), which stands for amber.

Figure 2: Piezoelectric crystal (http://leafcutterjohn.com/?p=1548)

There are two forms of the piezoelectric effect, which are the direct and the reverse effect. In the first case an electric voltage occurs when an external pressure is applied to the piezoelectric material. In the reverse effect, a mechanical strain results from an applied electric field. It is notable that materials which exhibit the direct effect, also exhibit the reverse piezoelectric effect and vice versa.

Generally, the piezoelectric effect is anisotropic, i.e. occurs in materials with a crystal structure without a center of symmetry. At some ceramic materials, below a critical temperature, known as the Curie temperature, electric dipoles with random orientation are generated within the crystal, which macroscopically are zero. During the polarization process, in the presence of a strong electric field, these dipoles tend to align

leading macroscopically to an electric dipole. After the cooling process and the removal of the polarizing field, the electric dipoles cannot return to their original positions and the material becomes permanently piezoelectric, with the ability to convert mechanical energy into electrical energy and vice versa. This status is lost only when the temperature exceeds the Curie temperature, or when the transducer is subjected to a very strong electric field.

The most important international standards for piezoelectricity are the following:

- ANSI-IEEE 176 (1987) (Standard on piezoelectricity)
- IEC 302 (1969) (Standard definitions and methods of measurement for piezoelectric vibrators operating over the frequency range up to 30MHz)
- IEC 444 (1973) (Basic method for the measurement of resonance frequency and resistance of quartz crystal units by zero-phase technique in a pi-network)
- IEEE 177 (1976) (Standard definitions and methods of measurement for piezoelectric vibrators)

Materials with piezoelectric properties are, among others, the Quartz crystal (SiO_2), the Rochelle or Seignette salt (Potassium Sodium Tartrate), the Ammonium Dihydrogen Phosphate ($NH_4H_2PO_4$), the Lithium Sulphate (Li_2SO_4), the Tourmaline, the polymer PVDF (Polyvinylidene Difluoride ($CH_2CF_2)_n$) and the ceramic PZT (Lead Zirconate Titanate).

The PZT or Lead Zirconate Titanate is a ceramic material and its molecular formula is given as $PbZr_xTi_{1-x}O_3$ for $0 < x < 1$ which means that x is defined into the interval (0, 1). It was developed by the physicists Gen Shirane, Etsuro Sawaguchi and Yutaka Takagi at Tokyo Institute of Technology in 1951 (Shirane, et al., 1951).

Among the most popular piezoelectric materials are the PVDF and the PZT. Especially for use in structural control, one of the most suitable material for the construction of the sensors and actuators devices is PZT.

This is due to the fact that the PZT material is also pyroelectric, which means that it is capable of producing an electric voltage in case of change of its temperature, as well as ferroelectric, i.e. it has a spontaneous electric polarization (electric dipoles) that can be reversed by the application of an external electric field.

Moreover, the PZT is characterized by its high dielectric constant which is near the morphotropic phase boundary when $x \approx 0.52$ i.e. when the molecular formula is given as $PbZr_{0.52}Ti_{0.48}O_3$. Due to this fact, the Lead Zirconate Titanate is considered to be one of the most important and useful electroceramic materials which is used for the construction of sensors, actuators, ultrasonic converters, ceramic capacitors, ferroelectric random access memory (FRAM) circuits, *etc*.

In control system applications with piezoelectric materials, the objective is the reduction of bending phenomena. The process is extremely simple. The electric stimulation in which the material is subjected, is translated into bending moments. These moments are used as control forces to the system. Some examples of different shapes of electrodes with respectively piezoelectric loads are shown in Figure 3.
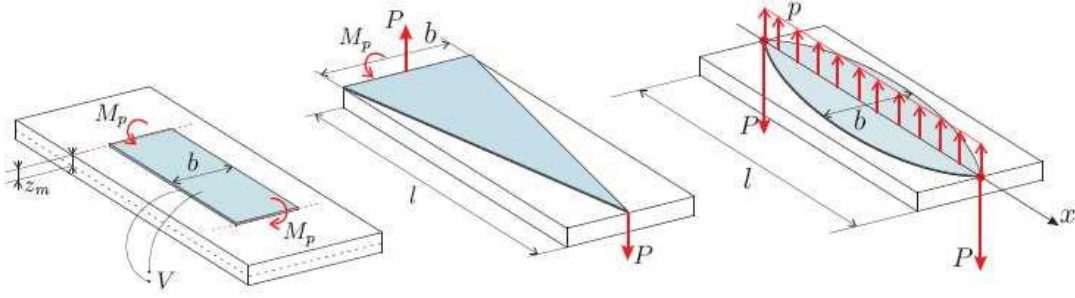
Figure 3: Examples of piezoelectric electrodes: rectangular, triangular and parabolic (Preumont, 2006)

The rectangular electrode of Figure 3(a) is equivalent to a pair of bending moments M_P applied to its ends. The triangular electrode of Figure 3(b) is equivalent to a pair of forces P and a bending moment M_P. If the beam is supported at the left end, the loads arise from the support reaction and the unique power remaining, i.e. the loading at the right end. Finally, a parabolic electrode, such as that of Figure 3(c), is equivalent to a uniformly distributed load p and a pair of forces P at the two ends. In each case the piezoelectric loads are self-balanced (Preumont, 2006).

3.2 Piezoelectric constitutive equations

For the formulation of the constitutive equations of a smart piezoelectric structure several assumptions must be made. Firstly, both mechanical and electrical forces in the piezoelectric materials are considered to be balanced at any given time instance due to the existence of oscillations. As a result, the piezoelectric equations can be decoupled, which means that finally, a quasi-static approximation is used in the analysis. It is also assumed that in case of fast oscillating piezoelectrics the temperature variation is negligible, i.e. the pyroelectric effect is not taken into account in the analysis.

Under these assumptions, the linear piezoelectric constitutive equations coupling the elastic and the electric field can be expressed as the direct and converse piezoelectric effect equations. These equations are given in simple matrix form as:

$$\{D\} = [e]\{\varepsilon\} + [\xi]\{E\} \tag{1}$$

$$\{\sigma\} = [c]\{\varepsilon\} - [e]^T\{E\} \tag{2}$$

where $\{D\}$ is the electric displacement vector, $[e]$ is the piezoelectric stress constant matrix, $\{\varepsilon\}$ is the strain vector, $[\xi]$ is the dielectric constant matrix at constant mechanical strain, $\{E\}$ is the electric field vector, $\{\sigma\}$ is the stress vector and $[c]$ is the plane-stress reduced elastic matrix for a constant electric field. However, for piezoelectric laminate structures that are used in this dissertation, it is sufficient to use the simplified form of the formulation.

Indeed, for a piezoelectric laminated[2] plate that consists of a number of layers (including the piezoelectric layers) and each layer possesses a plane of material symmetrically parallel to the x-y plane the constitutive equations of the kth layer can be derived by the 3D equations (1)-(2) by assuming plane stress approximation (Reddy, 2004), (Elshafei & Alraiess, 2013).

$$
\begin{Bmatrix} D_1 \\ D_2 \\ D_3 \end{Bmatrix}_k = \begin{bmatrix} 0 & 0 & 0 & e'_{15} & 0 \\ 0 & 0 & e'_{24} & 0 & 0 \\ e'_{31} & e'_{32} & 0 & 0 & 0 \end{bmatrix}_k \begin{Bmatrix} \varepsilon_{11} \\ \varepsilon_{22} \\ \varepsilon_{23} \\ \varepsilon_{13} \\ \varepsilon_{12} \end{Bmatrix}_k + \begin{bmatrix} \xi'_{11} & 0 & 0 \\ 0 & \xi'_{22} & 0 \\ 0 & 0 & \xi'_{33} \end{bmatrix}_k \begin{Bmatrix} E_1 \\ E_2 \\ E_3 \end{Bmatrix}_k \tag{3}
$$

$$
\begin{Bmatrix} \sigma_{11} \\ \sigma_{22} \\ \sigma_{23} \\ \sigma_{13} \\ \sigma_{12} \end{Bmatrix}_k = \begin{bmatrix} Q_{11} & Q_{12} & 0 & 0 & 0 \\ Q_{12} & Q_{22} & 0 & 0 & 0 \\ 0 & 0 & Q_{44} & 0 & 0 \\ 0 & 0 & 0 & Q_{55} & 0 \\ 0 & 0 & 0 & 0 & Q_{66} \end{bmatrix}_k \begin{Bmatrix} \varepsilon_{11} \\ \varepsilon_{22} \\ \varepsilon_{23} \\ \varepsilon_{13} \\ \varepsilon_{12} \end{Bmatrix}_k - \begin{bmatrix} 0 & 0 & e'_{31} \\ 0 & 0 & e'_{32} \\ 0 & e'_{24} & 0 \\ e'_{15} & 0 & 0 \\ 0 & 0 & 0 \end{bmatrix}_k \begin{Bmatrix} E_1 \\ E_2 \\ E_3 \end{Bmatrix}_k \tag{4}
$$

where

$$
e'_{31} = e_{31} - \frac{c_{13}}{c_{33}} e_{33}, \ e'_{32} = e_{32} - \frac{c_{23}}{c_{33}} e_{33}, \ e'_{24} = e_{24}, \ e'_{15} = e_{15},
$$

$$
\xi'_{11} = \xi_{11}, \ \xi'_{22} = \xi_{22} \ \xi'_{33} = \xi_{33} + \frac{e_{33}^2}{c_{33}}
$$

The elastic coefficients c_{ij} of the reduced matrix c (see Equation (2)) can be found for example in (Reddy, 2004). The reduced stiffness coefficients Q_{ij} in the material axes of the layer are related to the engineering constants as follows (Reddy, 2004):

Case I. Isotropic plate.

$$
Q_{11} = Q_{22} = \frac{E}{1-v^2}, \ Q_{12} = \frac{vE}{1-v^2}, \ Q_{44} = Q_{55} = Q_{66} = G
$$

where E, v and G are the isotropic material properties.

Case II. Orthotropic plate.

$$
Q_{11} = \frac{E_1}{1-v_{12}v_{21}}, \ Q_{12} = \frac{v_{12}E_2}{1-v_{12}v_{21}}, \ Q_{22} = \frac{E_2}{1-v_{12}v_{21}}, \ Q_{44} = G_{23}, \ Q_{55} = G_{13}, \ Q_{66} = G_{12}
$$

The electric field components are related to the electrostatic potential ϕ by the equation (IEEE Standard 1978):

---

[2] A laminate is formed from several layers bonded together to act as a single layer material; the bond between two layers is assumed to be perfect, so that the displacements remain continuous across the bond (see (Reddy, 2004))

$$E_i = -\varphi_{,i} \tag{5}$$

The constitutive equations for layer k in the global axes of coordinates read (Reddy, 2004):

$$\begin{Bmatrix} D_x \\ D_y \\ D_z \end{Bmatrix}_k = \begin{bmatrix} 0 & 0 & \overline{e}_{14} & \overline{e}_{15} & 0 \\ 0 & 0 & \overline{e}_{24} & \overline{e}_{25} & 0 \\ \overline{e}_{31} & \overline{e}_{32} & 0 & 0 & \overline{e}_{36} \end{bmatrix}_k \begin{Bmatrix} \varepsilon_{xx} \\ \varepsilon_{yy} \\ \gamma_{yz} \\ \gamma_{xz} \\ \gamma_{xy} \end{Bmatrix}_k + \begin{bmatrix} \overline{\xi}_{11} & \overline{\xi}_{12} & 0 \\ \overline{\xi}_{12} & \overline{\xi}_{22} & 0 \\ 0 & 0 & \overline{\xi}_{33} \end{bmatrix}_k \begin{Bmatrix} E_x \\ E_y \\ E_z \end{Bmatrix}_k \tag{6}$$

$$\begin{Bmatrix} \sigma_{xx} \\ \sigma_{yy} \\ \sigma_{yz} \\ \sigma_{xz} \\ \sigma_{xy} \end{Bmatrix}_k = \begin{bmatrix} \overline{Q}_{11} & \overline{Q}_{12} & 0 & 0 & \overline{Q}_{16} \\ \overline{Q}_{21} & \overline{Q}_{22} & 0 & 0 & \overline{Q}_{26} \\ 0 & 0 & \overline{Q}_{44} & \overline{Q}_{45} & 0 \\ 0 & 0 & \overline{Q}_{45} & \overline{Q}_{55} & 0 \\ \overline{Q}_{16} & \overline{Q}_{26} & 0 & 0 & \overline{Q}_{66} \end{bmatrix}_k \begin{Bmatrix} \varepsilon_{xx} \\ \varepsilon_{yy} \\ \gamma_{yz} \\ \gamma_{xz} \\ \gamma_{xy} \end{Bmatrix}_k - \begin{bmatrix} 0 & 0 & \overline{e}_{31} \\ 0 & 0 & \overline{e}_{32} \\ \overline{e}_{14} & \overline{e}_{24} & 0 \\ \overline{e}_{15} & \overline{e}_{25} & 0 \\ 0 & 0 & \overline{e}_{36} \end{bmatrix}_k \begin{Bmatrix} E_x \\ E_y \\ E_z \end{Bmatrix}_k \tag{7}$$

where $\overline{Q}_{ij}$ and $\overline{e}_{ij}$ are the transformed reduced stiffness coefficients, and piezoelectric modules, respectively (Reddy, 2004).

In order to derive the constitutive equations for one–dimensional beam, additional assumptions are used: (i) the width in the y direction is stress free and the plane stress assumption is used. Therefore, it is possible to set $\sigma_{yy} = \sigma_{yz} = \sigma_{xy} = \gamma_{yz} = \gamma_{xy} = 0$, and $\varepsilon_{yy} \neq 0$ in equation (7). (ii) The polarization axis z is aligned with the thickness direction of the beam, thus only D_z in equation *(6)* is taken into consideration. (iii) By introducing E_z applied across the actuator thickness and the other components of the electric fields are zeros. (iv) The coefficients e_{15} and ξ_{11} are neglected.

Therefore the constitutive relations equations (6) and (7) are reduced to:

$$\sigma_x = \tilde{Q}_{11}\varepsilon_x - \tilde{e}_{31}E_z, \qquad \tau_{xz} = \tilde{Q}_{55}\gamma_{xz}, \qquad D_z = \tilde{e}_{31}\varepsilon_x + \tilde{\xi}_{33}E_z \tag{8}$$

where the coefficients in relations (8) are given by:

Case I. Isotropic beam.

$$\tilde{Q}_{11} = E, \quad \tilde{Q}_{55} = G$$

Case II. Orthotropic beam.

$$\tilde{Q}_{11} = \overline{Q}_{11} - \frac{\overline{Q}_{12}\overline{Q}_{12}}{\overline{Q}_{22}}, \quad , \quad \tilde{Q}_{55} = \overline{Q}_{55}$$

and the piezoelectric constants are given by:

$$\tilde{e}_{31} = \overline{e}_{31} - \frac{\overline{Q}_{12}}{\overline{Q}_{22}}\overline{e}_{32}, \quad \tilde{\xi}_{33} = \overline{\xi}_{33} - \frac{\overline{e}_{32}\overline{e}_{32}}{\overline{Q}_{22}}$$

In smart structures, there are several issues that need to be addressed such as the modelling, placement of actuators and sensors, and controller design. The modelling of smart structures does not just involve the modelling of flexible structures, but also includes the modelling of the smart materials used as actuators and sensors. For piezoelectric laminate structures, the derivations of equations of motion involve the modelling of forces or moments generated by the bonded piezoelectric actuators.

3.3 Beam model

A smart composite beam with bonded piezoelectric sensors and actuators, is considered. Namely, the model consists of a slender uniform elastic beam with rectangular cross-section having length L, width b and thickness h. A pair of piezoelectric layers with thickness h_S and h_A is symmetrically attached at the top and the bottom surfaces of the beam serving as sensors and actuators, as shown in Figure 4. In the simplified beam model, the piezoelectric sensors and actuators are used for the measurements and application of control forces, respectively.
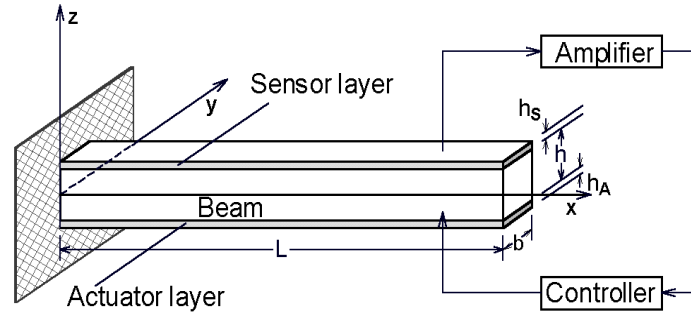
Figure 4: Schematic representation of the smart beam

The longitudinal and thickness axes are along x- and z-directions. The xy-plane is chosen to be the plane which is the midplane of the beam. In developing this model, the piezoelectric patch is assumed to be perfectly bonded to the structure with zero glue thickness. This implies that the displacements remain continuous across the bond.

It is assumed that the geometrical parameters of the beam permit the use the Timoshenko beam approximation. The displacement field equations for the beam at any point through the thickness are presented by:

$$u_x(x,y,z,t)= z\psi(x,t), \qquad u_y(x,y,z,t)=0, \qquad u_z(x,y,z,t)=w(x,t) \qquad (9)$$

where t denotes time; w denotes the transverse displacements of the beam's mid-plane, and ψ is the rotation of normal to the x-axis about the y-axis. Assuming a small deformation, the strain-displacement relation can be expressed as:

$$\varepsilon_x = z\frac{\partial \psi}{\partial x}, \qquad \gamma_{xz} = \psi + \frac{\partial w}{\partial x} \qquad (10)$$

It is noted that in Euler-Bernoulli theory the rotation ψ is the negative of the beam slope: $\psi = -\partial w / \partial x$, and so the transverse shear deformation γ_{xz} is equals to zero.

The stress-strain relations for the smart beam are given by the constitutive equations (8), which are rewritten here for convenience:

$$\sigma_x = \tilde{Q}_{11}\varepsilon_x - \tilde{e}_{31}E_z, \qquad \tau_{xz} = \tilde{Q}_{55}\gamma_{xz}, \qquad D_z = \tilde{e}_{31}\varepsilon_x + \tilde{\xi}_{33}E_z \tag{8}$$

The elastic core beam is assumed to be insulated and is obtained by annulling the piezoelectric constants. The electric field intensity E_z can be expressed as:

$$E_z = \frac{V}{h_p} \tag{11}$$

where V is the applied voltage across the thickness direction of the actuator and h_P is the thickness of the actuator layer.

3.3.1   Sensor Equation

In the case that the piezoelectric patch acts as a sensor, the sensor equation can be derived from the third equation of the electro-elastic relation of a piezoelectric material (Equation (8)₃). Only strains produced by the host beam, act on the piezoelectric patch, thus the output charge from the sensor is given by:

$$q(t) = \frac{1}{2}\left\{ \left(\int_{S_{ef}} D_z dS \right)_{z=h/2} + \left(\int_{S_{ef}} D_z dS \right)_{z=h/2+h_p} \right\} \tag{12}$$

where S_{ef} is the effective surface electrode of the patch. The effective surface electrode of the patch is the portion of the patch that is covered by electrodes on both sides. The electric charge generated due to the external mechanical disturbance will be detected only if the charge is collected through the effective surface electrode. In this work, it is assumed that the entire piezoelectric patch serves as effective surface electrode. Using the direct piezoelectric equation (Equation (8)₃) and taking into account that no electric field applied to the sensor layer, we get

$$q(t) = \int_{S_{ef}} \tilde{e}_{31}\varepsilon_x dS = \int_{S_{ef}} \tilde{e}_{31}\left(\frac{h+h_p}{2} \right)\frac{\partial \psi}{\partial x} dS \tag{13}$$

The current on the surface of the patch can be calculated by differentiating the charge with respect to time.

$$i(t) = \frac{dq(t)}{dt} \tag{14}$$

The current is converted into open-circuit voltage output by:

$$V(t) = G_s i(t) \tag{15}$$

where G_s is the gain of the current amplifier.

3.3.2 Equations of motion for the beam

The equations of motion for the beam with surface bonded piezoelectric patches, are derived by the Hamilton's principle:

$$\int_0^T (\delta T - \delta U + \delta W)dt = 0 \tag{16}$$

The total strain energy U and the kinetic energy T are calculated using the expressions:

$$U = \frac{1}{2}\int_0^L\int_A [\sigma_x \varepsilon_x + \tau_{xz}\gamma_{xz} - E_z D_z]dAdx, \quad T = \frac{1}{2}\int_0^L\int_A \rho[\dot{u}_x^2 + \dot{u}_z^2]dAdx \tag{17}$$

where dA is the area of cross-section of the beam.

If the only loading consists of moments induced by piezoelectric actuators and since the structure has no bending-twisting couple then δW is given as:

$$\delta W = b\int_0^L M^A \delta\left(\frac{\partial \psi}{\partial x}\right)dx \tag{18}$$

where M^A is the moment per unit length induced by the actuator and expressed as:

$$M^A = \int_{-h/2-h_A}^{-h/2} z\sigma_x^A dz = \int_{-h/2-h_A}^{-h/2} zQ_{11}d_{31}E_z^A dz \tag{19}$$

and

$$E_z^A = \frac{V_A}{h_A} \tag{20}$$

3.3.3 Finite element formulation

Two-node finite elements with two mechanical degrees of freedom, w and ψ, per node are used (see Figure 5). Using standard discretization techniques,

$$\{u\} = \{w, \psi\}^T = [N]\{X\} = \left[[N_w]\ [N_\psi]\right]^T \{X\} \tag{21}$$

where $\{X\} = \{w_1, \psi_1, w_2, \psi_2\}^T$ and $[N_w]$, $[N_\psi]$ are Lagrange linear shape functions.
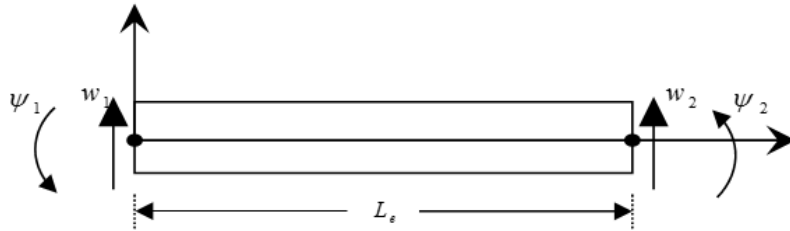
Figure 5: Finite element modeling using standard techniques

From Hamilton's Principle (Equation (16)) and collecting the common coefficients and

the contribution of all finite elements, the total stiffness $[K_{uu}]$ and mass $[M]$ matrices of the beam are derived similarly to Ref. (Hadjigeorgiou, et al., 2006), while the generalized displacement $\{X(t)\}$ is provided by the following equations:

$$[M]\{\ddot{X}\}+[K_{uu}]\{X\}=\{F_m\}+\{F_{el}\} \tag{22}$$

where $\{F_m\}$ is the global mechanical force and $\{F_{el}\}=-[K_{u\phi}]V$ is the electrical force vector due to the actuation.

This latter Equation (22) represents the dynamic equations of motion for a mechanical structure including piezoelectric stiffness.

Similar models can be used in various applications including, among others, the design of smart piezocomposite structures (Hadjigeorgiou, et al., 2006), (Stavroulakis, et al., 2005), in structural control as can be found in review articles (Irschik, 2002), (Song, et al., 2006) or energy harvesting applications as considered, among others, in (Cook-Chennault, et al., 2008), (Sodano, et al., 2004), (Priya & Inman, 2009), (Tairidis, et al., 2015c).

3.4 Laminated composite plate model with piezoelectric sensors and actuators based on FSDT

One of the most widely used theories for plate analysis is the Mindlin-Reissner theory. An extension of this theory to laminate structures is the first-order shear deformation theory for laminated composite plates (FSDT) which is known simply as Mindlin theory. In this section, we present a smart composite laminated plate model using the FSDT theory.

A laminated plate with integrated piezoelectric sensors/actuators, as shown in Figure 6, is considered.
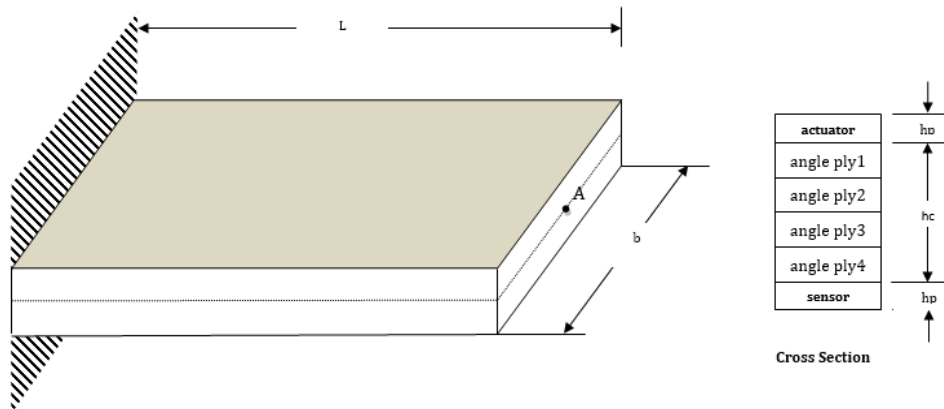
Figure 6: Layerwise plate model with adhesive material

The length, width and thickness of the whole structure are denoted by L, b and h_c, respectively. Two piezoelectric layers of thickness h_p are symmetrically bonded perfectly on the top and bottom surface of the host composite plate. The top layer acts like an actuator and the bottom one as a sensor. The poling direction of the piezoelectric

actuator is assumed to be along the z-axis. The stress–strain relationships, accounting for transverse shear deformation and piezoelectric effect, are given by Equations (6) and (7).

3.4.1 Strain and electric fields

The FSDT theory is very common for the analysis of laminated plates. It is a displacement based theory, i.e. it depends on the displacement field according the following equations:

$$u(x, y, z) = u_0(x, y) + z\theta_x(x, y) \tag{23}$$

$$v(x, y, z) = v_0(x, y) + z\theta_y(x, y) \tag{24}$$

$$w(x, y, z) = w_0(x, y) \tag{25}$$

where (u, v, w) denote the displacements of a single point (x, y, z) in the laminate, (u_0, v_0, w_0) are the displacements of a midplane point and (θ_x, θ_y) are the rotations of the transverse normal about the y and x axes, respectively. Note that the form of the displacement field of Equations (23)-(25) allows reduction of the 3D problem to one of studying the deformation of the reference plane $z = 0$ (or midplane). Once the midplane displacements and rotations are known, the displacements at any arbitrary point (x, y, z) in the 3D continuum can be determined using Equations (23)-(25).

The bending strain ε_b and the shear strain ε_s are given as:

$$\varepsilon_b = \begin{Bmatrix} \dfrac{\partial u}{\partial x} \\[2mm] \dfrac{\partial v}{\partial y} \\[2mm] \dfrac{\partial u}{\partial y} + \dfrac{\partial v}{\partial x} \end{Bmatrix} \quad \text{and} \quad \varepsilon_s = \begin{Bmatrix} \dfrac{\partial w}{\partial x} + \theta_x \\[2mm] \dfrac{\partial w}{\partial y} + \theta_y \end{Bmatrix} \tag{26}$$

The electric field E in the pth piezoelectric layer is expressed as:

$$\{E\}_P = \{E_x^P, E_y^P, E_z^P\} = -[B_\phi]_P \phi^P = -\begin{bmatrix} 0 & 0 & \dfrac{1}{h_p} \end{bmatrix}^T \phi^P(x, t) \tag{27}$$

where h_p is the thickness and ϕ^P is the electrical voltage of the pth piezoelectric layer, respectively.

3.4.2 Variational form of the equations of motion

In order to derive the equations of motion for the laminated composite plate with surface bonded sensor and actuator layers, Hamilton's principle is used:

$$\int_0^T (\delta T - \delta U + \delta W) dt = 0 \tag{28}$$

The kinetic energy T, the potential energy U and the total work done due to virtual displacements δu are given as follows:

$$\delta T = -\int_V \rho\{\ddot{u}\}^T\{\delta u\}\,dV \qquad \delta U = \int_V \left(\{\sigma\}^T\{\delta\varepsilon\} - \{D\}^T\{\delta E\}\right)dV$$

$$\delta W = \{\delta u\}^T\{F_c\} + \int_S \{\delta u\}^T\{f_S\}\,dS + \int_V \{\delta u\}^T\{f_V\}\,dV - \int_{S_p}\{\delta E\}^T\{q\}\,dS \tag{29}$$

where $\{F_c\}$ is the concentrated force vector, $\{f_S\}$ is the surface force vector, $\{f_V\}$ is the body force vector, $\{q\}$ is the surface charge vector, S is the surface area where external force is acting, and S_p is the surface area of piezoelectric layer where applied electric charge is acting.

Substituting relations (29) in Hamilton's principle (28), we obtain:

$$\int_0^T \left\{\int_V \left(\{\ddot{u}\}^T\{\delta u\} + \{\sigma\}^T\{\delta\varepsilon\} - \{D\}^T\{\delta E\} - \{\delta u\}^T\{f_V\}\right)dV\right.$$
$$\left. - \{\delta u\}^T\{F_c\} - \int_S\{\delta u\}^T\{f_S\}\,dS + \int_{S_p}\{\delta E\}^T\{q\}\,dS\right\}dt = 0 \tag{30}$$

Equation (30) is a good starting point for finite element approximations using independent variables $\{u\}$ and ϕ^p.

3.4.3 Finite element formulation

For the discretization of the composite plate the finite element method is used. Namely, four-node rectangular bilinear isoparametric elements with five degrees of freedom per node, i.e. $\{u_0, v_0, w_0, \theta_x, \theta_y\}$, are used. The first three degrees of freedom of each node correspond to the displacements in directions x, y and z respectively, while the last two the rotations around the axes x and y.

Next we use the notations:

$$\{u\} = \{u, v, w\}^T, \quad \{\bar{u}\} = \{u_0, v_0, w_0, \theta_x, \theta_y\}^T$$

where $\{\bar{u}\}$ are the nodal degrees of freedom. Using theses relations, the kinematic relations (23)-(25) can be written as:

$$\{u\} = [L_Z]\{\bar{u}\} \tag{31}$$

where:

$$[L_Z] = \begin{bmatrix} 1 & 0 & 0 & -z & 0 \\ 0 & 1 & 0 & 0 & -z \\ 0 & 0 & 1 & 0 & 0 \end{bmatrix} \tag{32}$$

Next, the displacement field is approximated by:

$$\{\bar{u}(x,y,t)\} = [L_Z][N]\{d_e\} \tag{33}$$

where $[N]$ is the matrix of shape functions and $\{d_e\}$ is the vector of nodal variables given by:

$$[N] = [[N_1][N_2][N_3][N_4]] \quad [N_j] = N_j I_5, \ j = 1,2,3,4$$

$$\{d_e\} = \left\{ \{d_1\}^T, \{d_2\}^T, \{d_3\}^T, \{d_4\}^T \right\}^T \tag{34}$$

$$\{d_j\} = \{u_j, v_j, w_j, \theta_{xj}, \theta_{yj}\}^T, \ j = 1,2,3,4$$

where I_5 is a 5×5 identity matrix and N_j, $j = 1,2,3,4$ are the bilinear shape functions

$$N_j(\xi,\eta) = \frac{1}{4}(1+\xi_j\xi)(1+\eta_j\eta), \quad j = 1,2,3,4$$

Substituting equation (33) in the strain-stress relations (26), we obtain:

$$\{\bar{\varepsilon}(x,y,t)\} = \{\varepsilon_b, \varepsilon_s\}^T = [B]_e \{d_e\} \tag{35}$$

where $[B]_e$ is the derivative operator between the corresponding strain and the generalized nodal displacements.

Substituting (31)-(35) into the variational principle (30) and allowing arbitrary variations of $\{d_e\}$ and $\{\phi\}$, the governing equations of an element can be written as:

$$[M]_e \{\ddot{d}_e\} + [K_{uu}]_e \{d_e\} + [K_{u\phi}]_e \{\phi\}_e = \{F_{(m)}\}_e$$

$$[K_{\phi u}]_e^T \{d_e\} - [K_{\phi\phi}]_e \{\phi\}_e = \{F_{(q)}\}_e \tag{36}$$

where the element mass matrix $[M]_e$, the element elastic stiffness matrix $[K_{uu}]_e$ and the element mechanical load vector $\{F_m\}_e$ are given by:

$$[M]_e = \sum_{k=1}^{nplies} \int_{-1}^{1}\int_{-1}^{1} \rho_k [N]^T \left[\int_{z_k}^{z_{k+1}} [L_Z]^T [L_Z] dz \right] [N] |J| d\xi d\eta$$

$$[K_{uu}]_e = \sum_{k=1}^{nplies} \int_{-1}^{1}\int_{-1}^{1} \left[\int_{z_k}^{z_{k+1}} [B]^T [\bar{Q}]_k [B] dz \right] |J| d\xi d\eta$$

$$\{F_m\}_e = \int_{V_e} [N]^T \{f_V\}_e dV + \int_{S_e} [N]^T \{f_S\}_e dS + [N]^T \{F_c\}_e$$

At the pth piezoelectric layer, the electromechanical coupling matrix and the permittivity matrix are given by:

$$\left[K_{u\phi} \right]_e = \int_{V_p} [B]^T [\overline{e}][B_\phi] dV = \left[K_{\phi u} \right]_e^T$$

$$\left[K_{\phi\phi} \right]_e = \int_{V_p} \left[B_\phi \right]^T \left[\overline{\xi} \right]_k \left[B_\phi \right] dV$$

The global equations can be obtained by assembling the elemental equations (36) as:

$$[M]\{\ddot{d}\} + [K_{uu}]\{d\} + \left[K_{u\phi} \right]\{\phi\} = \{F_m\}$$

$$\left[K_{\phi u} \right]\{d\} + \left[K_{\phi\phi} \right]\{\phi\} = \left\{ F_q \right\} \tag{37}$$

where $\{d\}$ and $\{\phi\}$ are the global mechanical and electrical DoFs vectors, $[M]$ is the global mass matrix, $[K_{uu}]$, $\left[K_{u\phi} \right] = \left[K_{u\phi} \right]^T$ and $\left[K_{\phi\phi} \right]$ are the global mechanical stiffness, mechanical–electrical coupling stiffness and dielectric stiffness matrices respectively. $\{F_m\}$ and $\left\{ F_q \right\}$ are the respective global mechanical and electrical loads vectors.

Next we assume that the electrical DoFs vector in Equation (37) can be divided into the actuating and sensing DoFs, $\{\phi\}_e = \{\phi_a, \phi_s\}^T$, where the subscripts 'a' and 's' denote the actuating and sensing capabilities. Hence, considering open-circuit electrodes, and in that case $\left\{ F_q \right\} = \{0\}$, the non-specified potential differences in Equation (37) can be statically condensed and the equations of motion and charge equilibrium become:

$$[M]\{\ddot{d}\} + [K_{uu}]\{d\} = \{F_m\} - \left[K_{u\phi} \right]_a \{\phi\}_a$$

$$\{\phi\}_s = -\left[K_{\phi\phi} \right]_s^{-1} \left[K_{\phi u} \right]_s \{d\} \tag{38}$$

where $\left[K_{uu}^* \right] = \left[K_{uu} \right] - \left[K_{u\phi} \right]_s \left[K_{\phi\phi} \right]_s^{-1} \left[K_{\phi u} \right]_s$.

Equations (38) can be used in smart structures applications such as vibration control, static or dynamic shape control, *etc.*

3.5 A layerwise approach to piezo-electric plates accounting for adhesive flexibility

The models presented in previous sections are based on equivalent single layer theories. A more accurate and efficient plate model for investigating the dynamics of composite smart structures is presented in this section based on a layerwise theory taking into account adhesive layer flexibility.

The layerwise theories which are used to simulate the dynamic behavior of composite smart structures are very important because they give a more accurate modeling of the dynamic behavior of structures of large thickness that are made of several plies

with different properties and / or stacking sequence. Furthermore, these theories provide the possibility to study problems of delamination of the layers in some regions.

Most research on the area deals with composite structures that are flexible and thin (thin-walled structures). In these cases, models that take into account the adhesive layer are very important, since this layer is not so thin compared to the piezoelectric ones and thus can affect the mechanical behavior of the structure, with direct consequences on the control process.

A laminated composite plate bonded with piezoelectric sensor and actuator layers and adhesive layers between them is considered as shown in Figure 7. The length, width and thickness of the whole plate are denoted by L, b and h, respectively. As it becomes evident in the following subsections, the theory is able to handle plates with an arbitrary number of actuators, sensors, and elastic layers, including the adhesive layers between them.
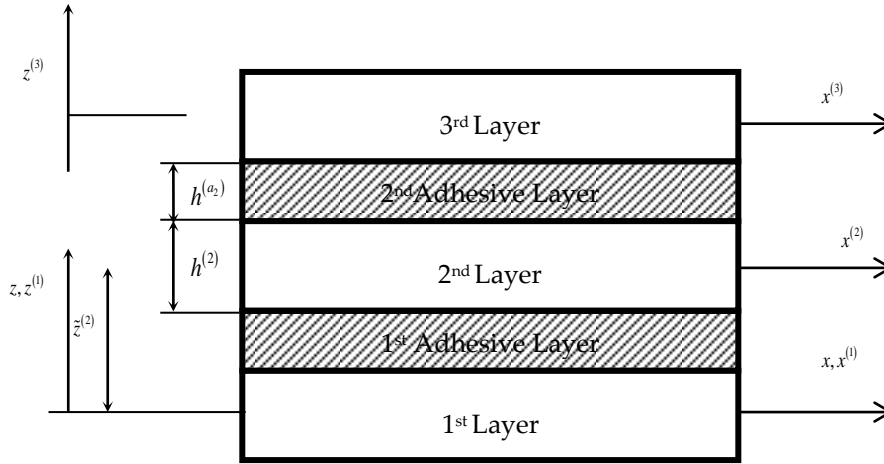
Figure 7: A three-layered composite plate with adhesive materials

3.5.1 Piezoelectric constitutive equations

For simplicity of the notation, all the non-adhesive layers will be considered as piezoelectric layers. Elastic layers are then obtained by making their piezoelectric constants vanish. The linear constitutive equations coupling the elastic and the electric fields in a piezoelectric medium are expressed as:

$$\left\{\sigma^{(i)}\right\} = \left[Q^{(i)}\right]\left\{\varepsilon^{(i)}\right\} - \left[e^{(i)}\right]^{T}\left\{E^{(i)}\right\} \tag{39}$$

$$\left\{D^{(i)}\right\} = \left[e^{(i)}\right]\left\{\varepsilon^{(i)}\right\} + \left[\xi^{(i)}\right]\left\{E^{(i)}\right\} \tag{40}$$

where $\left\{\sigma^{(i)}\right\}$ is the stress tensor, $\left\{\varepsilon^{(i)}\right\}$ is the strain tensor, $\left\{D^{(i)}\right\}$ is the electric displacement, $\left\{E^{(i)}\right\}$ is the electric field, $\left[Q^{(i)}\right]$ is the elastic stiffness matrix, $\left[e^{(i)}\right]$ is the piezoelectric matrix, $\left[\xi^{(i)}\right]$ is the permittivity matrix of the ith layer and the superscript T denotes the transpose of a matrix. Equation (39) describes the inverse piezoelectric effect and Equation (40) describes the direct piezoelectric effect.

Next, we assume that the piezoelectric material exhibits orthorhombic 2mm symmetry. Making use of the plane strain approximation and separating the bending and shear related variables, Equations (39) and (40) become:

$$\left\{\sigma_b^{(i)}\right\} = \left[Q_b^{(i)}\right]\left\{\varepsilon_b^{(i)}\right\} - \left[e_b^{(i)}\right]^T\left\{E^{(i)}\right\},$$

$$\left\{\sigma_s^{(i)}\right\} = \left[Q_s^{(i)}\right]\left\{\varepsilon_s^{(i)}\right\} - \left[e_s^{(i)}\right]^T\left\{E^{(i)}\right\},$$

(41)

$$\left\{D^{(i)}\right\} = \left[e_b^{(i)}\right]\left\{\varepsilon_b^{(i)}\right\} + \left[e_s^{(i)}\right]\left\{\varepsilon_s^{(i)}\right\} + \left[\xi^{(i)}\right]\left\{E^{(i)}\right\},$$

(42)

where $\left\{\sigma_b^{(i)}\right\} = \left\{\sigma_{xx}^{(i)}, \sigma_{yy}^{(i)}, \tau_{xy}^{(i)}\right\}^T$, $\left\{\sigma_s^{(i)}\right\} = \left\{\tau_{yz}^{(i)}, \tau_{xz}^{(i)}\right\}^T$ and:

$$\left[Q_b^{(i)}\right] = \begin{bmatrix} Q_{11}^{(i)} & Q_{12}^{(i)} & 0 \\ Q_{21}^{(i)} & Q_{22}^{(i)} & 0 \\ 0 & 0 & Q_{66}^{(i)} \end{bmatrix} \qquad \left[Q_s^{(i)}\right] = \begin{bmatrix} Q_{44}^{(i)} & 0 \\ 0 & Q_{55}^{(i)} \end{bmatrix}$$

(43)

$$\left[e_b^{(i)}\right] = \begin{bmatrix} 0 & 0 & 0 \\ 0 & 0 & 0 \\ e_{31}^{(i)} & e_{32}^{(i)} & 0 \end{bmatrix} \quad \left[e_s^{(i)}\right] = \begin{bmatrix} 0 & e_{15}^{(i)} \\ e_{24}^{(i)} & 0 \\ 0 & 0 \end{bmatrix} \quad \left[\xi^{(i)}\right] = \begin{bmatrix} \xi_{11}^{(i)} & 0 & 0 \\ 0 & \xi_{22}^{(i)} & 0 \\ 0 & 0 & \xi_{33}^{(i)} \end{bmatrix}$$

In Equations (43), $Q_{kl}^{(i)}$ are the reduced elastic constants, $e_{kl}^{(i)}$ are the reduced piezoelectric constants and $\xi_{kk}^{(i)}$ are the reduced permittivity constants of the ith layer. The detailed expressions for these constants can be obtained from (Reddy, 1999). In Equations (41) and (42), a layer can be either a piezoelectric or an elastic one. In the latter case, material constants $e_{kl}^{(i)}$ and $\xi_{kk}^{(i)}$ should be zero.

3.5.2 Displacement-strain relation

The kinematic assumption is based on a first order shear theory of small strains. Assuming that the mid-planes of the individual layers are parallel to each other and employing a common coordinate system (x, y, z) given in Figure 7, the displacements of the non-adhesive layers can be written as:

$$u_1^{(i)}(x, y, z, t) = u^{(i)}(x, y, t) - \left(z - \tilde{z}^{(i)}\right)\theta_x^{(i)}(x, y, t),$$

$$u_2^{(i)}(x, y, z, t) = v^{(i)}(x, y, t) - \left(z - \tilde{z}^{(i)}\right)\theta_y^{(i)}(x, y, t),$$

(44)

$$u_3^{(i)}(x, y, z, t) = w^{(i)}(x, y, t),$$

where $u^{(i)}, v^{(i)}$ and $w^{(i)}$ are the mid-plane deformations of the ith layer, $\theta_x^{(i)}$ and $\theta_y^{(i)}$ are rotation angles of the normal to the mid-plane about the y and x axes, respectively and $\tilde{z}^{(i)}$ is the thickness of the mid-plane of the ith layer.

The bending and shear strains of the ith layer can be written as:

$$\left\{\varepsilon_b^{(i)}\right\} = \left\{\varepsilon_{0b}^{(i)}\right\} + \left(z - \tilde{z}^{(i)}\right)\left\{\kappa^{(i)}\right\}, \qquad \left\{\varepsilon_s^{(i)}\right\} = \left\{\varepsilon_{0s}^{(i)}\right\} \tag{45}$$

where

$$\left\{\varepsilon_b^{(i)}\right\} = \left\{\varepsilon_{xx}^{(i)}, \varepsilon_{yy}^{(i)}, \gamma_{xy}^{(i)}\right\}^T, \quad \left\{\varepsilon_s^{(i)}\right\} = \left\{\gamma_{yz}^{(i)}, \gamma_{xz}^{(i)}\right\}^T, \quad \left\{\varepsilon_{0b}^{(i)}\right\} = \left\{\frac{\partial u^{(i)}}{\partial x}, \frac{\partial v^{(i)}}{\partial y}, \frac{\partial u^{(i)}}{\partial y} + \frac{\partial v^{(i)}}{\partial x}\right\}^T,$$

$$\left\{\kappa^{(i)}\right\} = \left\{-\frac{\partial \theta_x^{(i)}}{\partial x}, -\frac{\partial \theta_y^{(i)}}{\partial y}, -\left(\frac{\partial \theta_x^{(i)}}{\partial y} + \frac{\partial \theta_y^{(i)}}{\partial x}\right)\right\}^T, \quad \left\{\varepsilon_{0s}^{(i)}\right\} = \left\{\frac{\partial w^{(i)}}{\partial y} - \theta_y^{(i)}, \frac{\partial w^{(i)}}{\partial x} - \theta_x^{(i)}\right\}^T \tag{46}$$

3.5.3 Electric field-electric voltage relations

A constant transverse electrical field is assumed for the piezoelectric layers and the remaining in-plane components are supposed to vanish. Consequently, the electric field intensity can be expressed as:

$$\left\{E^{(i)}\right\} = -\left[B_E^{(i)}\right]\phi^{(i)} \tag{47}$$

where $\left[B_E^{(i)}\right] = \left\{0, 0, -\dfrac{1}{h^{(i)}}\right\}^T$ and $h^{(i)}$, $\phi^{(i)}$ are the thickness and the electric voltage of the

i-th piezoelectric layer.

3.5.4 The adhesive layer

The adhesive layers between the host plate and the piezoelectric layers are assumed to be very thin, and their deformation is linear. Only transverse normal stress $\sigma_z^{(a)}$ and strains $\varepsilon_z^{(a)}$, and in-plane shear stress $\tau_{yz}^{(a)}, \tau_{xz}^{(a)}$ and strains $\gamma_{yz}^{(a)}, \gamma_{xz}^{(a)}$ are taken into account. The in-plane stretching of the adhesive layer is neglected, since its stiffness in that direction is quite small.

The linear deformations of the adhesive layers are written in terms of the deformations of the adjacent structural layers as follows (see Figure 8).

$$u_1^{(a_i)} = u_1^{(i),t} + \left(u_1^{(i+1),b} - u_1^{(i),t}\right)\frac{z - z^{(i),t}}{h^{(a_i)}}$$

$$u_2^{(a_i)} = u_2^{(i),t} + \left(u_2^{(i+1),b} - u_2^{(i),t}\right)\frac{z - z^{(i),t}}{h^{(a_i)}} \tag{48}$$

$$u_3^{(a_i)} = u_3^{(i),t} + \left(u_3^{(i+1),b} - u_3^{(i),t}\right)\frac{z - z^{(i),t}}{h^{(a_i)}}$$

where superscripts 't' and 'b' refer to the top or bottom surface of the related layer. For example,

$$u_1^{(i),t} = u^{(i)} - \theta_x^{(i)}\frac{h^{(i)}}{2}, \quad u_1^{(i+1),b} = u^{(i+1)} + \theta_x^{(i+1)}\frac{h^{(i+1)}}{2} \text{ and } z^{(i),t} = \tilde{z}^{(i)} + \frac{h^{(i)}}{2}$$

In addition, since transverse displacement is independent from the vertical coordinate:

$$u_3^{(i),t} = u_3^{(i),b} = w^{(i)}.$$

Then Equations *(48)* can be rewritten into the following compact form:

$$\left\{ \overline{u}^{(a_i)} \right\} = \left[R_t^{(a_i)}(z) \right] \left\{ \overline{u}^{(i+1)} \right\} + \left[R_b^{(a_i)}(z) \right] \left\{ \overline{u}^{(i)} \right\} \tag{49}$$

where $\left\{ \overline{u}^{(i)} \right\} = \left\{ u^{(i)}, v^{(i)}, w^{(i)}, \theta_x^{(i)}, \theta_y^{(i)} \right\}^T$ is the generalized displacement vector,

$$\left[R_t^{(a_i)}(z) \right] = \begin{bmatrix} Z & 0 & 0 & \dfrac{h^{(i+1)}}{2}Z & 0 \\[2mm] 0 & Z & 0 & 0 & \dfrac{h^{(i+1)}}{2}Z \\[2mm] 0 & 0 & Z & 0 & 0 \end{bmatrix}, \left[R_b^{(a_i)}(z) \right] = \begin{bmatrix} 1-Z & 0 & 0 & -\dfrac{h^{(i)}}{2}Z & 0 \\[2mm] 0 & 1-Z & 0 & 0 & -\dfrac{h^{(i)}}{2}Z \\[2mm] 0 & 0 & 1-Z & 0 & 0 \end{bmatrix}$$

and $Z \equiv \dfrac{1}{h^{(a_i)}} \left(z - \tilde{z}^{(i)} - \dfrac{h^{(i)}}{2} \right).$

Using these displacements and taking into account that the adhesive layer is much thinner than the adherents, the shear and peel strains of the adhesive layers can be written as (Erturk & Tekinalp, 2005):

$$\varepsilon_{zz}^{(a_i)} = \frac{w^{(i+1)} - w^{(i)}}{h^{(a_i)}},$$

$$\gamma_{yz}^{(a_i)} = \frac{1}{h^{(a_i)}} \left[v^{(i+1)} - v^{(i)} + \frac{h^{(i)}}{2}\theta_y^{(i)} + \frac{h^{(i+1)}}{2}\theta_y^{(i+1)} \right], \tag{50}$$

$$\gamma_{xz}^{(a_i)} = \frac{1}{h^{(a_i)}} \left[u^{(i+1)} - u^{(i)} + \frac{h^{(i)}}{2}\theta_x^{(i)} + \frac{h^{(i+1)}}{2}\theta_x^{(i+1)} \right]$$

Equations (50) can be written into the following compact form:

$$\left\{ \varepsilon^{(a_i)} \right\} = \left[L_t^{(a_i)}(z) \right] \left\{ \overline{u}^{(i+1)} \right\} + \left[L_b^{(a_i)}(z) \right] \left\{ \overline{u}^{(i)} \right\} \tag{51}$$

where $\left\{ \varepsilon^{(a_i)} \right\} = \left\{ \varepsilon_{zz}^{(a_i)}, \gamma_{yz}^{(a_i)}, \gamma_{xz}^{(a_i)} \right\}^T$ and:

$$\left[L_t^{(a_i)}(z)\right] = \frac{1}{h^{(a_i)}} \begin{bmatrix} 0 & 0 & 1 & 0 & 0 \\ 0 & 1 & 0 & 0 & \dfrac{h^{(i+1)}}{2} \\ 1 & 0 & 0 & \dfrac{h^{(i+1)}}{2} & 0 \end{bmatrix}, \qquad \left[L_b^{(a_i)}(z)\right] = \frac{1}{h^{(a_i)}} \begin{bmatrix} 0 & 0 & -1 & 0 & 0 \\ 0 & -1 & 0 & 0 & \dfrac{h^{(i)}}{2} \\ -1 & 0 & 0 & \dfrac{h^{(i)}}{2} & 0 \end{bmatrix}$$

The peel and shear stresses in the adhesive layer can be written as:

$$\left\{\sigma^{(a_i)}\right\} = \left[Q^{(a_i)}\right]\left\{\varepsilon^{(a_i)}\right\} \tag{52}$$

or in the more detailed form:

$$\begin{Bmatrix} \sigma_{zz}^{(a_i)} \\ \tau_{yz}^{(a_i)} \\ \tau_{xz}^{(a_i)} \end{Bmatrix} = \begin{bmatrix} E^{(a_i)} & 0 & 0 \\ 0 & G^{(a_i)} & 0 \\ 0 & 0 & G^{(a_i)} \end{bmatrix} \begin{Bmatrix} \varepsilon_{zz}^{(a_i)} \\ \gamma_{yz}^{(a_i)} \\ \gamma_{xz}^{(a_i)} \end{Bmatrix} \tag{53}$$

where $E^{(a_i)}$, $G^{(a_i)}$ are the elastic and shear moduli of the adhesive layer a_i.
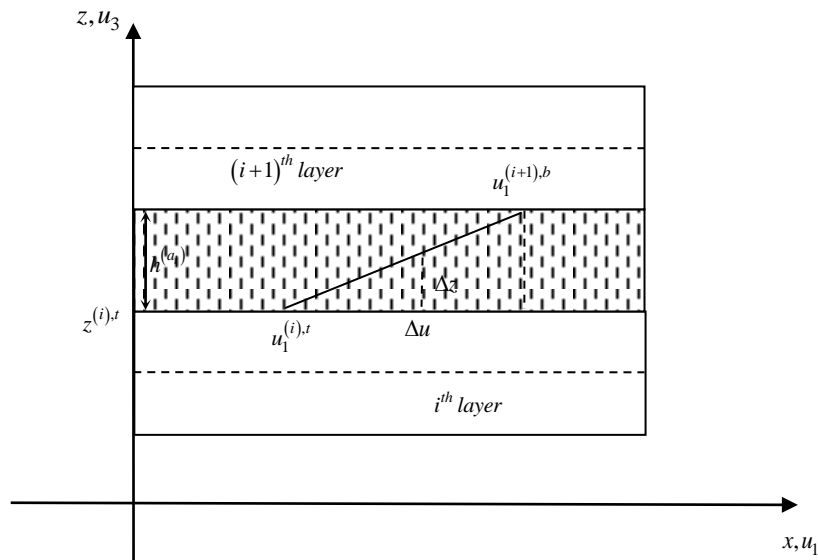
Figure 8: The displacement field of the adhesive layer

3.5.5   Finite Element Formulation

Hamilton's variational principle is used to derive the equations of the plate, i.e.

$$\int_0^T \left(\delta T - \delta U + \delta W\right) dt = 0 \tag{54}$$

where T is the total kinetic energy, U is the total strain energy and W is the work done by the loads.

The total kinetic energy and the total strain energy of the system is the sum of the corresponding energies of the individual layers.

The kinetic energy of the ith layer and the kinetic energy of the a_i adhesive layer, respectively, are given by:

$$T^{(i)} = \frac{1}{2} \int_{V^{(i)}} \{\ddot{u}^{(i)}\}^T \left[I^{(i)}(z) \right] \{\ddot{u}^{(i)}\} dV \ , \ T^{(a_i)} = \frac{1}{2} \int_{V^{(a_i)}} \{\dot{u}^{(a_i)}\}^T \left[I^{(a_i)}(z) \right] \{\dot{u}^{(a_i)}\} dV \tag{55}$$

where:

$$\left[I^{(i)}(z) \right] = \rho^{(i)} \begin{bmatrix} 1 & 0 & 0 & -\left(z - \tilde{z}^{(i)}\right) & 0 \\ 0 & 1 & 0 & 0 & -\left(z - \tilde{z}^{(i)}\right) \\ 0 & 0 & 1 & 0 & 0 \\ -\left(z - \tilde{z}^{(i)}\right) & 0 & 0 & \left(z - \tilde{z}^{(i)}\right)^2 & 0 \\ 0 & -\left(z - \tilde{z}^{(i)}\right) & 0 & 0 & \left(z - \tilde{z}^{(i)}\right)^2 \end{bmatrix}, \left[I^{(a_i)}(z) \right] = \rho^{(a_i)} I_3 ,$$

I_3 is the 3x3 identity matrix, $u^{(a_i)} = \{u_1^{(a_i)}, u_2^{(a_i)}, u_3^{(a_i)}\}^T$ and $V^{(i)}$, $V^{(a_i)}$ are the volumes of the ith layer and a_i adhesive layer, respectively.

The strain energy for the ith layer is given by:

$$U^{(i)} = \frac{1}{2} \int_{V^{(i)}} \left(\{\varepsilon^{(i)}\}^T \{\sigma^{(i)}\} \right) dV = \frac{1}{2} \int_{V^{(i)}} \left(\{\bar{\varepsilon}^{(i)}\}^T \left[\mathcal{D}^{(i)}(z) \right] \{\bar{\varepsilon}^{(i)}\} - \{\bar{\varepsilon}^{(i)}\}^T \left[\mathcal{E}^{(i)}(z) \right] \{E^{(i)}\} \right) dV \tag{56}$$

where:

$$\{\bar{\varepsilon}^{(i)}\} = \left\{ \{\varepsilon_{0b}^{(i)}\}^T, \{\kappa^{(i)}\}^T, \{\varepsilon_{0s}^{(i)}\}^T \right\}^T \tag{57}$$

and:

$$\left[\mathcal{D}^{(i)}(z) \right] = \begin{bmatrix} \left[Q_b^{(i)} \right] & \left(z - \tilde{z}^{(i)}\right)\left[Q_b^{(i)} \right] & 0 \\ \left(z - \tilde{z}^{(i)}\right)\left[Q_b^{(i)} \right] & \left(z - \tilde{z}^{(i)}\right)^2\left[Q_b^{(i)} \right] & 0 \\ 0 & 0 & \left[Q_s^{(i)} \right] \end{bmatrix} \left[\mathcal{E}^{(i)}(z) \right] = \begin{bmatrix} \left[e_b^{(i)} \right]^T \\ \left(z - \tilde{z}^{(i)}\right)\left[e_b^{(i)} \right]^T \\ \left[e_s^{(i)} \right]^T \end{bmatrix} \tag{58}$$

The strain energy for the a_i adhesive layer is given by:

$$U^{(a_i)} = \frac{1}{2} \int_{V^{(i)}} \left(\{\varepsilon^{(a_i)}\}^T \{\sigma^{(a_i)}\} \right) = \frac{1}{2} \int_{V^{(a_i)}} \left(\{\varepsilon^{(a_i)}\}^T \left[Q^{(a_i)} \right] \{\varepsilon^{(a_i)}\} \right) dV \tag{59}$$

The total work is the sum of the work done by the electrical forces $W_E^{(i)}$ and the work done by the mechanical forces $W^{(i)}$, where:

$$W_E^{(i)} = \frac{1}{2} \int_{V^{(i)}} \{E^{(i)}\}^T \left[D^{(i)} \right] dV = \frac{1}{2} \int_{V^{(i)}} \left\{ \{E^{(i)}\}^T \left[\xi^{(i)} \right] \{E^{(i)}\} + \{\bar{\varepsilon}^{(i)}\}^T \left[\mathcal{E}^{(i)} \right] \{E^{(i)}\} \right\} dV \tag{60}$$

$$W^{(i)} = \{\bar{u}^{(i)}\}^T \{F_c^{(i)}\} + \int_{S^{(i)}} \{\bar{u}^{(i)}\}^T \{f_s^{(i)}\} dS + \int_{V^{(i)}} \{\bar{u}^{(i)}\}^T \{f_v^{(i)}\} dV - \int_{S^{(i)}} \{E^{(i)}\}^T \{q^{(i)}\} dS \tag{61}$$

In Equation *(61)*, $\{F_c^{(i)}\}$ denotes the concentrated forces, $\{f_s^{(i)}\}$ and $\{f_v^{(i)}\}$ denote the surface and volume force vectors, respectively and $\{q^{(i)}\}$ denotes the surface charge vector.

From the Hamilton's principle given in Equation (54), a finite element model has been developed for the three layered adhesively bonded plate. The elements are rectangular and have four nodes in each layer. Thus, a finite element for a three-layered plate has $4 \times 3 = 12$ nodes with five degrees of freedom at each node.

The generalized displacement vector $\{\bar{u}^{(i)}\}$ is interpolated as:

$$\{\bar{u}^{(i)}(x,y,t)\} = [H]\{d_e^{(i)}\} \tag{62}$$

where $[H]$ is the interpolation matrix and $\{d_e^{(i)}\}$ is the nodal variable vector given by:

$$[H] = [[H_1][H_2][H_3][H_4]], \quad [H_j] = H_j I_5, \quad j = 1,2,3,4 \tag{63}$$

$$\{d_e^{(i)}\} = \left\{\{d_1^{(i)}\}^T, \{d_2^{(i)}\}^T, \{d_3^{(i)}\}^T, \{d_4^{(i)}\}^T\right\}^T, \quad \{d_j^{(i)}\} = \{u_j^{(i)}, v_j^{(i)}, w_j^{(i)}, \theta_{xj}^{(i)}, \theta_{yj}^{(i)}\}^T, \quad j = 1,2,3,4$$

H_j, $j = 1,2,3,4$ are bilinear isoparametric shape functions and I_5 is the unit matrix.

Substituting Equation (62) into (57), gives:

$$\{\bar{\varepsilon}^{(i)}(x,y,t)\} = [B]\{d_e^{(i)}\} \tag{64}$$

where $[B] = [[B_1][B_2][B_3][B_4]]$,

$$[B_j] = \begin{bmatrix} \partial_x & 0 & 0 & 0 & 0 \\ 0 & \partial_y & 0 & 0 & 0 \\ \partial_y & \partial_x & 0 & 0 & 0 \\ 0 & 0 & 0 & -\partial_x & 0 \\ 0 & 0 & 0 & 0 & -\partial_y \\ 0 & 0 & 0 & -\partial_y & -\partial_x \\ 0 & 0 & \partial_y & 0 & -1 \\ 0 & 0 & \partial_x & -1 & 0 \end{bmatrix} H_j$$

and $\partial_x = \partial/\partial x$, $\partial_y = \partial/\partial y$.

Applying Hamilton's Principle Equation (54), the Equations (65) for each element can be obtained:

$$[M_e]\{\ddot{d}_e\} + [K_{e(uu)}]\{d_e\} + [K_{e(u\phi)}]\{\phi_e\} = \{F_{e(m)}\}$$
$$[K_{e(\phi u)}]\{d_e\} + [K_{e(\phi\phi)}]\{\phi_e\} = \{F_{e(q)}\} \tag{65}$$

where $\{d_e\} = \left\{\{d_e^{(1)}\}^T, \{d_e^{(2)}\}^T, \{d_e^{(3)}\}^T\right\}^T$, $\{\phi_e\} = \{\phi_e^{(1)}, \phi_e^{(2)}, \phi_e^{(3)}\}^T$,

$$
[M_e] = \begin{bmatrix} \left[M_e^{(1)} \right] + \left[M_{e(bb)}^{(a_1)} \right] & \left[M_{e(bt)}^{(a_1)} \right] & 0 \\ \left[M_{e(tb)}^{(a_1)} \right] & \left[M_e^{(2)} \right] + \left[M_{e(tt)}^{(a_1)} \right] + \left[M_{e(bb)}^{(a_2)} \right] & \left[M_{e(bt)}^{(a_2)} \right] \\ 0 & \left[M_{e(tb)}^{(a_2)} \right] & \left[M_e^{(3)} \right] + \left[M_{e(tt)}^{(a_2)} \right] \end{bmatrix} \tag{66}
$$

$$
\left[K_{e(uu)} \right] = \begin{bmatrix} \left[K_e^{(1)} \right] + \left[K_{e(bb)}^{(a_1)} \right] & \left[K_{e(bt)}^{(a_1)} \right] & 0 \\ \left[K_{e(tb)}^{(a_1)} \right] & \left[K_e^{(2)} \right] + \left[K_{e(tt)}^{(a_1)} \right] + \left[K_{e(bb)}^{(a_2)} \right] & \left[K_{e(bt)}^{(a_2)} \right] \\ 0 & \left[K_{e(tb)}^{(a_2)} \right] & \left[K_e^{(3)} \right] + \left[K_{e(tt)}^{(a_2)} \right] \end{bmatrix} \tag{67}
$$

$$
\left[K_{e(u\phi)} \right] = \begin{bmatrix} \left[K_{e(u\phi)}^{(1)} \right] & 0 & 0 \\ 0 & \left[K_{e(u\phi)}^{(2)} \right] & 0 \\ 0 & 0 & \left[K_{e(u\phi)}^{(3)} \right] \end{bmatrix} , \left[K_{e(\phi\phi)} \right] = \begin{bmatrix} \left[K_{e(\phi\phi)}^{(1)} \right] & 0 & 0 \\ 0 & \left[K_{e(\phi\phi)}^{(2)} \right] & 0 \\ 0 & 0 & \left[K_{e(\phi\phi)}^{(3)} \right] \end{bmatrix} \tag{68}
$$

$$
\left[K_{e(\phi u)} \right] = \left[K_{e(u\phi)} \right]^T , \left\{ F_{e(q)} \right\} = \left\{ \left\{ F_{e(q)}^{(1)} \right\}^T \left\{ F_{e(q)}^{(2)} \right\}^T \left\{ F_{e(q)}^{(3)} \right\}^T \right\}^T ,
$$

$$
\left\{ F_{e(m)} \right\} = \left\{ \left\{ F_{e(m)}^{(1)} \right\}^T \left\{ F_{e(m)}^{(2)} \right\}^T \left\{ F_{e(m)}^{(3)} \right\}^T \right\}^T \tag{69}
$$

Detailed expressions of the submatrices appearing in Equations *(64)-(69)* are given be-low:

Element mass and stiffness matrices of the ith layer:

$$
\left[M_e^{(i)} \right] = \int_{V^{(i)}} [H]^T \left[I^{(i)}(z) \right] [H] dV \qquad \left[K_e^{(i)} \right] = \int_{V^{(i)}} [B]^T \left[\mathcal{D}^{(i)}(z) \right] [B] dV
$$

Element mass and stiffness matrices of the adhesive layer *a$_i$*:

$$
\left[M_{e(bb)}^{(a_i)} \right] = \int_{V^{(a_i)}} [H]^T \left[R_b^{(a_i)} \right]^T \left[I^{(a_i)} \right] \left[R_b^{(a_i)} \right] [H] dV \quad \left[M_{e(bt)}^{(a_i)} \right] = \int_{V^{(a_i)}} [H]^T \left[R_b^{(a_i)} \right]^T \left[I^{(a_i)} \right] \left[R_t^{(a_i)} \right] [H] dV
$$

$$
\left[M_{e(tb)}^{(a_i)} \right] = \int_{V^{(a_i)}} [H]^T \left[R_t^{(a_i)} \right]^T \left[I^{(a_i)} \right] \left[R_b^{(a_i)} \right] [H] dV \quad \left[M_{e(tt)}^{(a_i)} \right] = \int_{V^{(a_i)}} [H]^T \left[R_t^{(a_i)} \right]^T \left[I^{(a_i)} \right] \left[R_t^{(a_i)} \right] [H] dV
$$

$$
\left[K_{e(bb)}^{(a_i)} \right] = \int_{V^{(a_i)}} [H]^T \left[L_b^{(a_i)} \right]^T \left[Q^{(a_i)} \right] \left[L_b^{(a_i)} \right] [H] dV \quad \left[K_{e(bt)}^{(a_i)} \right] = \int_{V^{(a_i)}} [H]^T \left[L_b^{(a_i)} \right]^T \left[Q^{(a_i)} \right] \left[L_t^{(a_i)} \right] [H] dV
$$

$$
\left[K_{e(tb)}^{(a_i)} \right] = \int_{V^{(a_i)}} [H]^T \left[L_t^{(a_i)} \right]^T \left[Q^{(a_i)} \right] \left[L_b^{(a_i)} \right] [H] dV \quad \left[K_{e(tt)}^{(a_i)} \right] = \int_{V^{(a_i)}} [H]^T \left[L_t^{(a_i)} \right]^T \left[Q^{(a_i)} \right] \left[L_t^{(a_i)} \right] [H] dV
$$

Element matrices related to the external mechanical excitation:

$$
\left\{ F_{e(m)}^{(i)} \right\} = \int_{V^{(i)}} [H]^T \left\{ f_v^{(i)} \right\} dV + [H]^T \left\{ F_c^{(i)} \right\} + \int_{S^{(i)}} [H]^T \left\{ f_s^{(i)} \right\} dS
$$

Element matrices related to the electrical excitation:

$$\left\{ F_{e(q)}^{(i)} \right\} = \int\limits_{S^{(i)}} \left[B_E^{(i)} \right]^T \left\{ q^{(i)} \right\} dS$$

Element piezoelectric coupling matrix and element dielectric stiffness matrix of the ith layer:

$$\left[K_{e(u\phi)}^{(i)} \right] = \int\limits_{V^{(i)}} \left[B \right]^T \left[\mathcal{E}^{(i)}(z) \right] \left[B_E^{(i)} \right] dV \ , \quad \left[K_{e(\phi\phi)}^{(i)} \right] = \int\limits_{V^{(i)}} \left[B_E^{(i)} \right]^T \left[\xi^{(i)}(z) \right] \left[B_E^{(i)} \right] dV \ ,$$

We note here that special care is needed in the numerical integration of $\left[K_e^{(i)} \right]$. The element stiffness matrix can be considered to be composed of a bending stiffness part $\left[K_{e(b)}^{(i)} \right]$ and a transverse shear stiffness part $\left[K_{e(s)}^{(i)} \right]$. Exact, or full integration is then used for computing $\left[K_{e(b)}^{(i)} \right]$, but reduced integration (one order lower) is used for evaluating $\left[K_{e(s)}^{(i)} \right]$.

Following the routine of the assembly procedure, the global equations for the smart composite plate can be obtained.

3.6   Delamination

Delamination is one of the most common failures for composite materials, i.e. the ones used in laminated composite structures. This is due to the fact that the repeated applied stresses impact the layers of the structures and can lead to separation. It is notable that in smart structures, in case of delamination, either the sensor and/or the actuator can peel off in a limited or a more extensive grade.

Moreover, this phenomenon leads to changes in the morphology and the characteristics of the mechanical system of the structure, mainly its stiffness, as it is responsible for the weakening or the ageing of the materials.

The purpose of this section is the insertion of a non-linear delamination law, in the existing composite piezoelectric finite element model of a plate. The finite element model, with the non-linear delamination law, includes the possibility of applying both mechanical and electrical load and the possibility of simulating static and dynamic problems.

3.6.1   Description of the delamination model

For the simulation of delamination, the following non-linear stress-strain law is used:
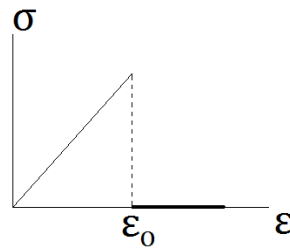
Figure 9: Delamination law

The above law leads to appropriate modification of the existing stiffness matrix of the structure in order to take into account the differences in the behavior before and after the delamination (Mistakidis & Stavroulakis, 1998).

For each finite element of the adhesive layer subjected to delamination, the element average strain ε_{zz} is calculated as follows:

$$\varepsilon_{zz}^{(a_i)} = \frac{w^{(i+1)} - w^{(i)}}{h^{(a_i)}} \tag{70}$$

where w is the vertical displacement of layers, whose behavior in delamination is investigated, and h^a is the thickness of the adhesive layer. If the strain is less than ε_o, no delamination appears in the element. Otherwise, delamination takes place. The delamination can occur between the lower-middle and the middle-upper plate layer.

3.6.2   Numerical simulations of delamination

For the implementation of the non-linear delamination law, the Newton-Raphson incremental-iterative procedure has been used, as follows:

Incremental step

   Load enforcement

      Start iterations

      -Loop to the whole of elements

      -Calculate the mean strain of each element

      -Compare with ε_o

      -Appropriate estimation of the tangential stiffness matrix

      -Estimation of the internal force vector

      -Solving equilibrium equations and finding incremental

           and global displacements

      -Error control and continuation iteration

           or continue the incremental step

It is worth noting that the existing composite piezoelectric model of the plate, fully facilitate the above iterative process of finding the tangential stiffness of the structure, by appropriately changing members from the initial stiffness matrix.

Therefore we have the following four cases:

a) No delamination
b) Delamination between lower-middle layers
c) Delamination between middle-upper layers
d) Delamination between both lower-middle and middle-upper layers

The numerical scheme is applied to a composite plate with dimensions 100x100 mm, fixed on the left side. Each element consists of 12 nodes: 4 nodes belong to the lower layer, 4 nodes to the middle and 4 nodes to the upper layer. Every node has 5 degrees of freedom (three translational and two rotational). Therefore, the structure has 363 nodes and 1815 degrees of freedom.
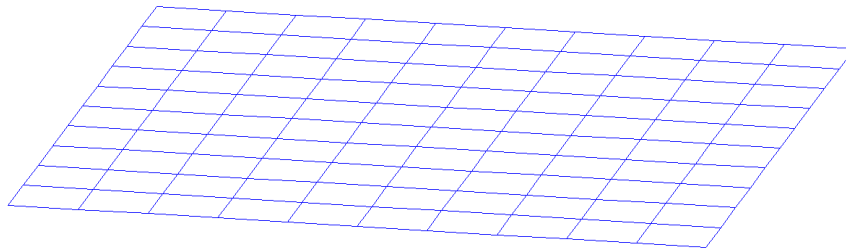
Figure 10: Mesh of the structure

In the structure, a nodal mechanical load is applied to the right side, on the upper piezoelectric layer. First, a force mechanical load is used and a force control procedure is followed. However, for the improved monitoring of the phenomenon of delamination, a displacement mechanical load is then used (displacement control).

At the first example a small mechanical load is applied to the structure. According to the results, no delamination appears and the behavior of the material is linear, as shown by the shape of the displacement of the structure and the load-displacement diagram (see Figure 11 and Figure 12).
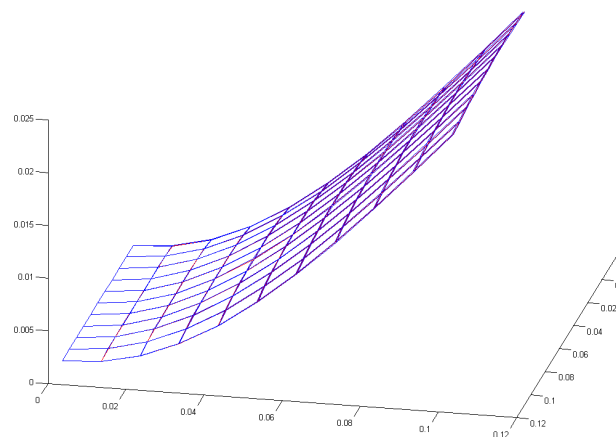
Figure 11: Displacement of the structure, when no delamination appears
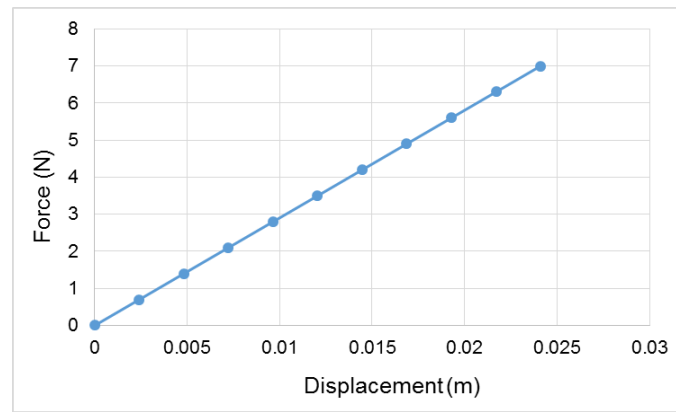
Figure 12: Force – displacement diagram for the structure, when no delamination appears

When the mechanical load is increased, the behavior of the structure changes thus, delamination and non-linear behavior appear. According to the shape of the displacement which is shown in Figure 13, the delamination occurs across the upper layer, which at the end of the analysis operates completely independently of the underlying layers. As a result, large displacements occur in this layer. The change of the slope of the load-displacement diagram, which is nonlinear, expresses the phenomenon of delamination, which is accompanied by a decrease in the stiffness of the system (see Figure 14).
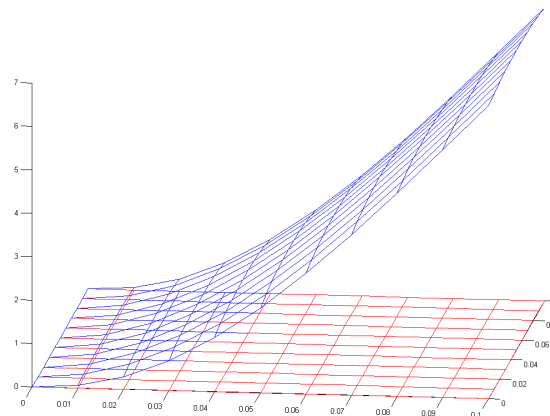
Figure 13: Displacement of the structure, when delamination in the whole middle-upper layer interface appears
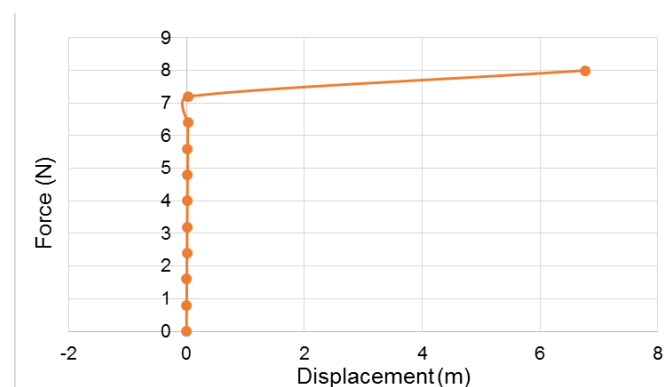

Figure 14: Force – displacement diagram for the structure with delamination (load control)

As already mentioned above, the delamination in the last example happens simultaneously to all elements of the interface (Fremond, 2002). The gradual appearance of delamination only to certain parts of the interface, cannot be illustrated by a force mechanical load (load control), due to the numerical instability which is introduced by the iterative Newton-Raphson procedure up to the point of failure. Consequently, the softening behavior cannot be depicted by the load control procedure (Mistakidis & Stavroulakis, 1998).

For this reason, the code has been changed, so that the applied mechanical force is a displacement control. As seen from Figure 15 and Figure 16, it is possible then to display gradual delamination. At the same time, the load-displacement diagram shows a softening branch similar to the stress-strain diagram.
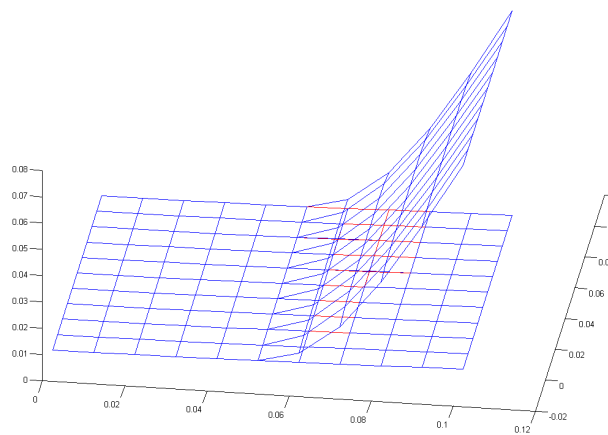
Figure 15: Displacement of the structure, when partial delamination in the whole middle-upper layer interface appears
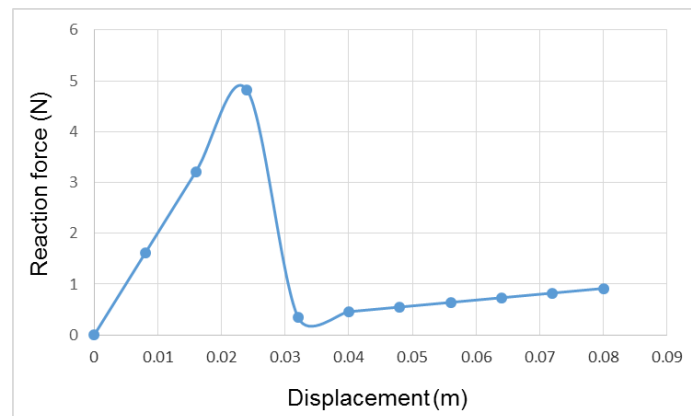
Figure 16: Force – displacement diagram for the structure with delamination (displacement control)

Further information on delamination modelling can be found in (Wriggers, et al., 1998), (Drosopoulos, et al., 2014).

3.7   Structural dynamics

As already noted in the previous sections, the derived set of the equations of motion of the dynamic system, is of the form:

$$M \cdot \ddot{u} + C \cdot \dot{u} + K \cdot u = P + Z \tag{71}$$

where M is the mass matrix, C is the damping matrix, K is the stiffness matrix, P is the loading vector, Z is the control force vector, and with u, $\dot{u}$ and $\ddot{u}$ are denoted the displacement, the velocity and the acceleration respectively.

The damping matrix C is given in the sense of Rayleigh assumption by:

$$C = 0.01 \cdot (M + K) \tag{72}$$

Finally, the external loading P is given by:

$$P = P_0 \cdot sin(\omega \cdot t) \tag{73}$$

where P_0 and ω are the excitation's amplitude and frequency respectively.

For the integration of the differential equations of motion (1), the Houbolt numerical integration method was chosen. Houbolt factors were set to:

$$\beta = 0.25, \ \gamma = 0.5 \tag{74}$$

The integration time was set to 3 seconds, while the time step Δt was chosen equal to 0.01 seconds.

Integration constants are given as:

$$c_1 = \frac{1}{\beta \cdot (\Delta t)^2}, \ c_2 = \frac{1}{\beta \cdot \Delta t}, c_3 = \frac{1}{2\beta}, \ c_4 = \frac{\gamma}{\beta \cdot \Delta t}, c_5 = \frac{\gamma}{\beta}, c_6 = \Delta t \left(\frac{\gamma}{2\beta} - 1 \right) \tag{75}$$

The controller returns a control force $Z(t)$ in each time-step (t) of the integration, taking as inputs the displacement u and the velocity $\dot{u}$. The total force, that is the control force plus the external loading, give the next step's ($t + \Delta t$) values of displacement and velocity.

Houbolt integration algorithm pseudocode can be written as follows:

Step 1: Initialization of variables

$u, \dot{u}, \ddot{u}, F_m, M, C, K, \beta, \gamma, c_1, c_2, c_4, c_5, c_6$

Step 2: Calculation of intermediate matrix F^*: $K^* = K + c_1 M + c_4 C$

Inversion of matrix K^*: $F^* = (K^*)^T$

Start of loop for t_0 to t_f

Step 3: Calculation of intermediate matrix P^*

Calculation of difference of loadings: $dF_m = F_m(t+1) - F_m(t)$

Calculation of difference of control force z

Aggregation to the quantity dF_m: $dF_m = dF_m + z$

Calculation of matrix P^* using mass matrix M and damping matrix C of the system:

$P^*=dF_m+M[c_2\dot{u}(t)+c_3\ddot{u}(t)]+C[c_5\dot{u}(t)+c_6\ddot{u}(t)]$

Step 4: Calculation of response step du

$$du=F^*P^*$$

Step 5: Solution for the next step $(t+\Delta t)$

Calculation of acceleration: $\ddot{u}(t+1)=\ddot{u}(t)+c_1du-c_2\dot{u}(t)-c_3\ddot{u}(t)$

Calculation of velocity: $\dot{u}(t+1)=\dot{u}(t)+c_4du-c_5\dot{u}(t)-c_6\ddot{u}(t)$

Calculation of displacement: $u(t+1)=u(t)+du$

end for

end

This page was intentionally left blank

4 Fuzzy and neuro-fuzzy control strategies

As mentioned in previous chapters, vibration suppression on smart structures can be achieved using active control. It was also said that classical mathematical control tools usually provide satisfactory results for linear feedback laws under given assumptions.

However, the design of nonlinear controllers based on fuzzy inference systems and/or artificial neural networks, or even hybrid neuro-fuzzy controllers can provide satisfactory results when the system is partially known.

In this chapter, the main tools of the proposed control strategy, which was applied for the reduction of the oscillations in the smart structures presented above, are presented.

4.1 Fuzzy logic

Fuzzy inference systems are a part of the fuzzy theory with applicability to control. The recurring systems can be used for the control of various processes, from many scientific fields that may vary. The whole idea is based on a quite modern science of reasoning which in turn is called fuzzy logic.

Operators use common sense to solve complex problems. Fuzzy logic is a set of mathematical principles that is used to represent an experienced operators' knowledge to a computer system.

In essence, fuzziness is not a part of the logic. In fact, a set of logical expressions is used to describe the fuzziness that exists in most systems. The representation is based on the membership level of the involved parameters that interact with each other through a set of verbal rules.

According to Boolean logic, concepts and variables are divided in a loose manner. For instance, if we divide men in groups according to their height, setting the limit of 1.80 m as the minimum height for the tall ones, someone with 1.79 m height is considered short, while a man of 1.81 m height is considered tall.

Fuzzy logic is based on the principle that all parameters or concepts of a system does not have a single meaning, but are subjected to ratings. Distance, speed, temperature,

height, weight, service, *etc.* can be described using scales. For example, George is very tall. Service is below average, and so on.

In other words fuzzy logic reflects how people think, avoiding generalization errors verbalizing variables and simulating the human sense. In that meaning, it does not face things in a black and white scale, but includes many intermediate states (grey scale) see Figure 17. This property leads to the construction of smart control systems.
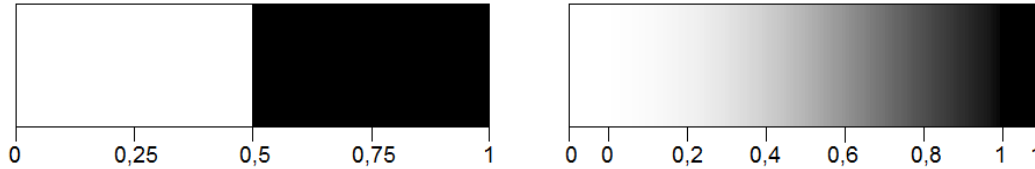

Figure 17: Boolean vs fuzzy logic

The forefather of Fuzzy Logic was the probability theory, according to which each parameter could belong in a set with a percentage from 0 to 1.

For example we can say that if someone has a height of 1.81 m. is tall with probability 1, very tall with probability 0.8 and short with probability 0.

However, the father of fuzzy logic, as we know it today, is L. Zadeh, who in 1965 in his article entitled "Fuzzy sets" introduced the concept of fuzzy sets using the mathematical tools of the probability theory, introducing a totally new logic which was based in verbal terms which he called "fuzzy logic" (Zadeh, 1965).

4.1.1 Fuzzy sets

In crisp sets, a space element is considered part of the set under examination when taking the value 1. In other case, the element takes the value 0 and is not considered part of the set. In fuzzy sets this is not true. Each space element can receive its value from a range of values and be part of the under examination set with this value which depicts the participation (membership) rate of the element in the set. The higher the value is, the greater the participation of the element is in the set. This function is called membership function while the set is called fuzzy set.

Therefore, in order for an element to belong in a fuzzy set, full participation is not required like in the crisp sets. The dipole 0 or 1 of crisp sets is replaced by a range of values between [0, 1]. Additionally, every element of the space may simultaneously participate in more than one fuzzy sets with different degree of membership.

Fuzzy sets accept all the operators (union, intersection, complement) and all the properties (distributivity, associativity, commutativity) of crisp sets. The only exception is the law of the excluded middle (see Figure 18). Because of the overlap that can be present in fuzzy sets, this principle differentiates from that of crisp sets as follows:

$$A \cup \bar{A} \neq X \text{ and } A \cap \bar{A} \neq \emptyset \tag{76}$$
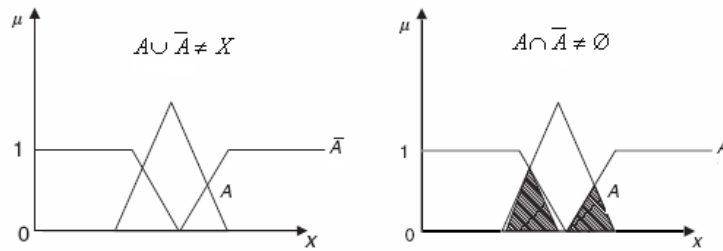
Figure 18: The law of the excluded middle

Fuzzy sets can be classified according to membership functions as shown in Figure 19 as follows:

a) Normal fuzzy sets (at least one membership function reaches 1)
b) Subnormal fuzzy sets (no membership function reaches 1)
c) Convex fuzzy sets
d) Non-convex fuzzy sets
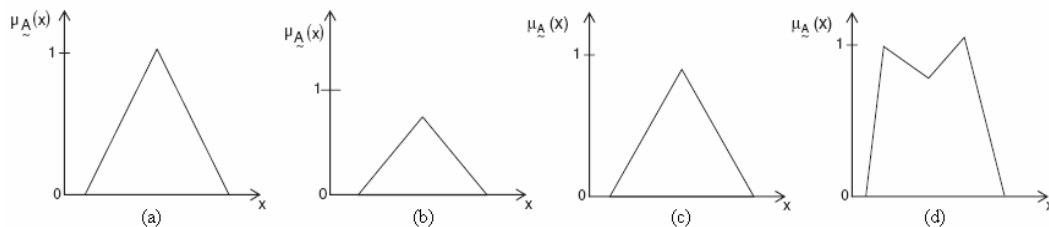
Figure 19: Various types of fuzzy sets

4.1.2   Membership functions

The degree of fuzziness of a fuzzy set is defined by its membership functions. The representation of these functions can be done either numerically or graphically.

The graphical representations include various forms, each with its own restrictions. The membership functions can have any parameterized form, either symmetric or asymmetric. The most popular forms include among others:

a) Triangular membership functions
b) Trapezoidal membership functions
c) Bell membership functions
d) Gaussian membership functions
e) Sigmoid membership functions
f) Polynomial membership functions

A graphical representation of a membership function in comparison with a crisp set is shown in Figure 20.
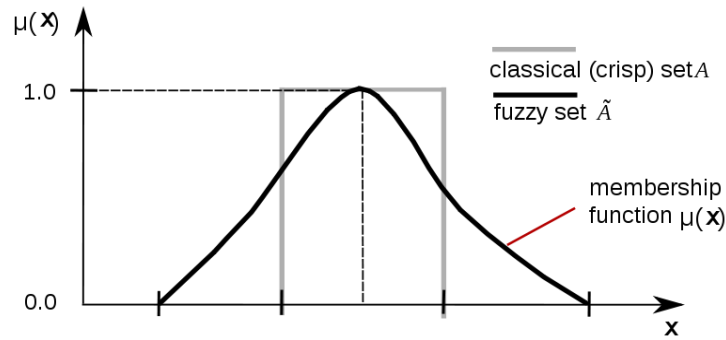
Figure 20: A fuzzy membership function in comparison to a crisp set
(https://commons.wikimedia.org/wiki/File:Fuzzy_crisp.svg)

4.1.3 Fuzzification

Fuzzification is among the most important processes in the fuzzy theory. In particular, it is the process of converting an explicit numerical quantity into a fuzzy one, which is represented by the membership functions. The process is based on the recognition of the uncertainty which exist in explicit quantities

On practical applications it is possible for errors to occur with a consequent reduction of data accuracy. This reduction of precision can also be represented by the membership functions.

The definition or fine tuning of the membership functions can be done either intuitively or by using algorithms and logical processes. The most popular methods include among others:

- Intuition
- Inference
- Rank ordering
- Angular fuzzy sets
- Neural networks
- Genetic algorithms
- Inductive reasoning

4.1.4 Defuzzification

With the term defuzzification is denoted the conversion process of the fuzzy outputs into explicit values. This process is necessary as the value of outputs must be accurate, especially when the fuzzy system is used as a controller, where the fuzzy outputs are not useful for further processing. For the defuzzification of fuzzy output functions, the following methods can be used:

1. Maximum membership principle

2. Centroid

3. Bisector

4. Middle or mean of maximum (MOM)

5. Smallest of maximum (SOM)

6. Largest of maximum (LOM)

7. Centre of sums

8. Centre of largest area

9. Weighted average (WTAVER)

The choice of the appropriate defuzzification method is often a subjective process and depends on the data and/or the requirements of each problem.

Two different methods can give completely different results. It is also possible the results of two or more methods to be identical. For example if the final surface is triangular, the result of methods SOM, MOM and LOM will be identical (the top of the triangle).

In the applications of Mamdani-type fuzzy control which were implemented in this dissertation, the MOM, centroid and bisector methods were used for the defuzzification of the fuzzy outputs (see Figure 21).
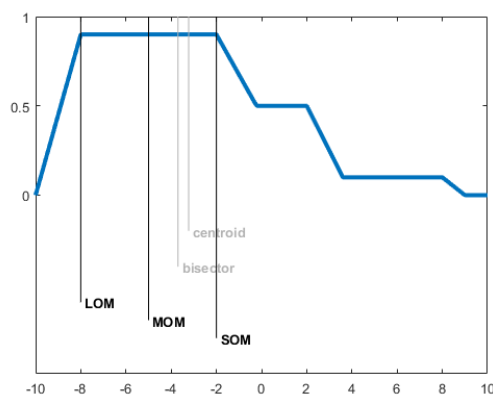
Figure 21: An example of defuzzification methods
(http://www.mathworks.com/help/examples/fuzzy_featured/defuzzdm_04.png)

The defuzzification with the method of middle of maxima or MOM method is calculated by taking the average membership rate (average) of output data located in the edge of the area with the largest value (the maximum).

According to the centroid method, for the conversion of the final surface of the output to a single point, the center of gravity is calculated and then its projection point on the x axis is taken. The derived value is the defuzzified value.

Another method for the defuzzification of the output can be the calculation of the bisector of the surface and taking its projection on the x axis, as before. The bisector

method usually produces relatively similar results to the ones produced with the centroid method, if the surface is relatively uniform. These methods are shown graphically in Figure 21.

On the other hand, the calculation of outputs in Sugeno-type controllers is not based on membership functions of fuzzy sets, but on linear functions, due to the nature of their outputs.

This means that a different way of calculation of outputs should be used. In this case, the weighted average method can be useful. This method is a variation of the ordinary arithmetic mean, as for the calculation of the average uses weights, which in turn change the contribution of the involved outputs. Thus, the calculation of outputs is based on linear functions of the type:

$$z_0 = \frac{\sum_{i=1}^{n} a_i C_i}{\sum_{i=1}^{n} a_i} \tag{77}$$

where α_i are the trigger points of membership functions and C_i the individual values of the outputs.

It is worth mentioning that weighted average is not exactly a defuzzification method, in the context which this term is met in the Mamdani-type controllers, but it is usually called like that due to the fact that it is used for the calculation of the final outputs.

4.1.5 Fuzzy inference systems

Fuzzy inference systems or FIS are also known as fuzzy rule – based systems or fuzzy models.

The rules of verbal variables can be formed by deterministic statements (e.g. velocity = high), condition statements (e.g. IF grade $\geq$ 8.5 THEN excellent) or statements without condition (e.g. GO TO). The properties of the set of the rules is the fullness, consistency, continuity and interaction.

A fuzzy system is usually described with more than one rules. The process of summarizing the rules for obtaining an overall conclusion is called aggregation. In the case where the individual rules are associated with the AND operator, the determination of the aggregation is done by the conjugation of the rules system taking the intersection of the individual rules. If the individual rules are associated with the OR operator, the determination of the aggregation is done by the disjunction of the rules system, calculating the union of the individual rules. The methods of conjugation and disjunction are also known as methods of minimum (min) and maximum (max), respectively.

A fuzzy inference system consists of the following elements:

- Rule base (IF – THEN rules)
- Data base (set of membership functions)
- Decision – making unit (inference process)
- Fuzzification interface
- Defuzzification interface

The operation of the inference system goes as follows. The explicit inputs are converted into fuzzy via fuzzification. Then the set of rules is drafted, which together with the data, forms the knowledge data base. Subsequently, the decision is made by implication, and the fuzzy output arises. Finally this value is defuzzified. This process is depicted in Figure 22.
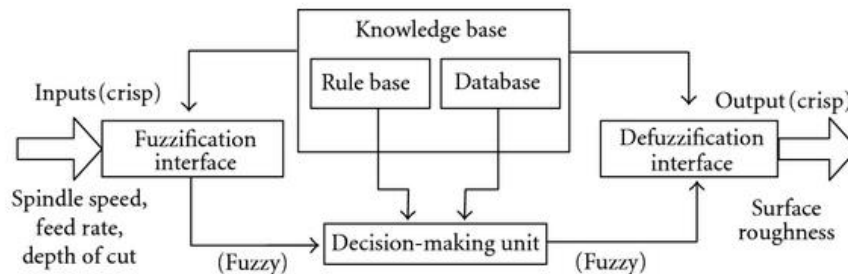

Figure 22: The structure of a fuzzy inference system taken from a machining application (http://www.hindawi.com/journals/acisc/2011/183764/)

4.1.6 Fuzzy inference methods

The two main methods of fuzzy inference are the Mamdani method and the Sugeno method. Other known methods are the Inference of Larsen and the Tsukamoto method. For the investigations considered in the present dissertation, two Mamdani-type fuzzy controllers and one Sugeno-type neuro-fuzzy controller were developed.

The first method, which is the most widespread, was introduced by Mamdani and Assilian in 1975 (Mamdani & Assilian, 1975). Ten years later Takagi and Sugeno introduced the second method, which is known as Takagi - Sugeno method (Takagi & Sugeno, 1985). These two methods have several common characteristics. Their main difference lies in the type of membership functions of their outputs. In Mamdani method, the membership functions are fuzzy sets. Instead, in the Sugeno method the outputs are either linear functions or constant values.

The main advantages of each of the two methods of fuzzy inference are summarized as follows:

The Mamdani method:

It is an intuitive method, which is widely accepted and it adapts well to real problems. It is a relatively simple method which works well even in complex models, without sacrificing accuracy.

The basic steps of the implementation process of the Mamdani method are:

1. Fuzzification of inputs using the membership functions

2. Definition of verbal rules of fuzzy system

3. Evaluation of the rules

4. Calculation of system outputs

5. Defuzzification

The Sugeno method:

It is a computationally accurate method, which works very effectively in combination with linear techniques. It also works effectively in combination with optimization techniques. Moreover, the Sugeno method presents a guaranteed continuous output surface and it is susceptible to mathematical analysis.

Likewise to the Mamdani method, the steps for the Sugeno inference are:

1. Fuzzification of input variables (clustering)

2. Determination of system rules

3. Evaluation of system rules

4. Calculation of outputs

In the Sugeno controllers fuzziness of inputs and their categorization (clustering) in membership functions is similar to that followed by Mamdani-type controllers. The same applies to the rules governing the fuzzy system.

However, the major advantage of Sugeno-type controllers is the fact that they can be trained using adaptive neuro-fuzzy inference (ANFIS) techniques, as it will be described in the following section.

4.2 Artificial neural networks

Machine learning is a scientific field that includes adaptive methods, which in turn allow computers to be trained based on experience, examples and proportionality. A core characteristic of these methods lies to the fact that learning abilities improve the performance of a machine learning system over time.

An artificial neural network (ANN) is an approach of machine learning which attempts to simulate the function of the human central nervous system, i.e. of the biological neural networks. It is about a network of interconnected calculating nodes (artificial neurons) which are algorithms of computational intelligence.

4.2.1 What is a neural network

A biological neural network is a model of logical thinking which is based on the human brain. Our cerebrum consists of a 10 billion neural cells network and these cells have 60 trillion connections that are called synapses.

The cell (soma) is the structural element of a neural network. Each cell has a simple structure, however the combination of a huge number of cells provides incredible computational power, allowing the rapid processing of stimuli by the human brain.

In a neural network, besides the body (soma) of the cell there is also the axon, the synapses and the dendrites (see Figure 23).
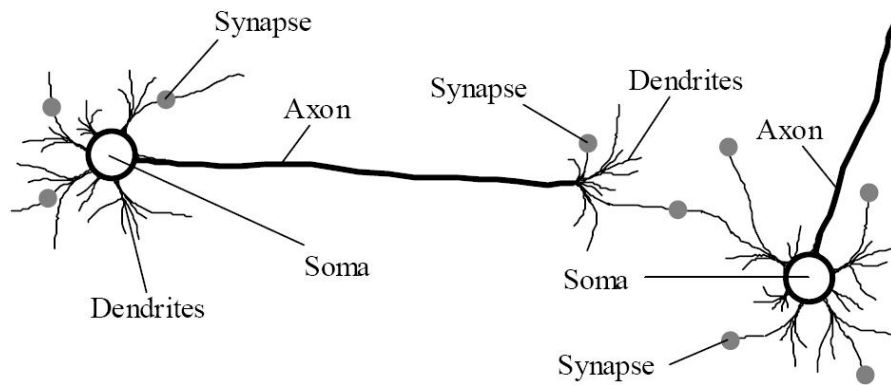
Figure 23: Biological neural network

Any given neuron of a biological neural network is able to respond only to a certain subset of stimuli which are within its receptive field, i.e. its sensory space. This property of the networks is called tuning. This core characteristic of biological neural networks has inspired the design and formulation of artificial neural networks.

Thus, the comparative advantage of an artificial neural network is the fact that it is also open to training. This process, known as learning, trains the network in order to be capable of better solving several problems. This is done through a repeated process where the parameters of the network are self-adjusted.

Once trained, the network receives inputs from the environment (stimuli) processes them and provides an output (decision), which is sent either to the environment or to the next neuron until the final processing is made.

If the training is done properly, the network will be able to solve even problems for which it has not been trained for. This means that it should be able to produce outputs even for inputs that it ignores, which in turn is the objective. This property is called generalization.

The first artificial neural network was designed by McCulloch and Pitts in 1942 (McCulloch & Pitts, 1942). This was one of the first studies of computer systems that relied on the functioning of the human brain. In 1957, Rosenblatt introduced the concept of the neuron Perceptron (Rosenblatt, 1957). In 1986 Rumelhart, Hinton and Williams suggested the backward propagation method of errors, known simply as back-propagation method (Rumelhart, et al., 1986).

Neural networks are used in a wide range of applications from different sciences. Some of these are systems control, pattern recognition, stock market control, equipment maintenance, various robotics applications, *etc*.

The main advantages of such networks over other heuristic methods are among others, their ability to solve highly complex problems, their tolerance to the existence of noise, as well as the fact that they do not require previous knowledge of the model.

This latter feature makes neural networks particularly useful in systems where experimental measurements exist, but there is lack of information about the model. In this case, these experimental measurements can be used for training and control of the network.

4.2.2 The concept of artificial neuron

Artificial neurons are the structural elements of artificial neural networks. In fact they are nodes which take inputs and produce outputs. The inputs can be received from other neurons or directly from the environment. Similarly, the output is sent either to the external environment or is used as input to other network neurons.

Artificial neurons consist of the following five elements (the index i indicates the i-th input element or synaptic weight)

1. A set of inputs, x_i

2. A set of synaptic weights, w_i

3. A bias, θ

4. An activation function, f

5. The output of the neuron, y or O
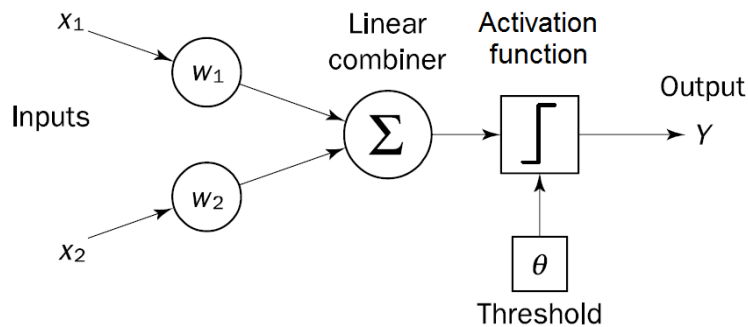
Figure 24: A typical neuron

Generally, there are three different types of neurons: the input neurons, the output neurons and the hidden neurons.

Input neurons are not responsible for calculations. Their role is to import the inputs of the network to the intermediate (hidden) neurons where the calculations take place.

The role of output neurons is to export the final results (outputs) of the neural network of the intermediate levels in the environment.

The hidden neurons are responsible for the calculations. Each input is multiplied by the corresponding synaptic weight. The sum of the products of these multiplications is being calculated and then inserted in the activation function, which is calculated at each node. The value of the function is the output of the hidden neuron for the given inputs.

By nature, neurons located in the so-called hidden layers have the ability to "hide" their desired output. For this reason, no information from the interaction between inputs and outputs can be extracted. Moreover, there is no obvious way to know which could be the desired values of the outputs of hidden neurons.

Artificial neural networks used for educational or commercial purposes usually include three or four levels. This means that there will be one or two hidden layers respectively. Each layer contains from 10 to 1000 neurons.

4.2.3 Calculation of outputs

A neuron with n inputs $x_1,...,x_n$ where every synapsis has a synaptic weight $w_1,..., w_n$ is considered.

The input x_0 is always 1 and the synaptic weight x_0 is the threshold for the activation of the neuron.

The output y_k of every neuron is calculated by the following equation:

$$y_k = f\left(\sum_{i=0}^{n} x_{ki} \cdot w_{ki}\right) \tag{78}$$

where x_{ki} and w_{ki} are the i-th input and weight of the neuron k, respectively, n is the number of neurons and f is the activation function.

A neuron is positively activated when:

$$\sum_{i=0}^{n} w_i x_i \geq w_0 \tag{79}$$

The weight $w_0 = \theta$ is called threshold. If θ is equal to zero, then the input is disregarded.

The activation of the neurons of an artificial neural network can be done using several activation functions.

4.2.4 Activation functions

The activation function could be any of the following functions:

- step function

- sign function

- linear function

- non-linear function

A step activation function is of the form:

$$f(x) = \begin{cases} 1, & x \geq 0 \\ 0, & x < 0 \end{cases} \tag{80}$$

A sign function can be used as activation function and is given as:

$$f(x) = \begin{cases} +1, & x \geq 0 \\ -1, & x < 0 \end{cases} \tag{81}$$

The linear activation function is given by:

$$f(x) = a \cdot x \tag{82}$$

where α is any given constant

The non-linear activation function could be any non-linear function. When, for example, the activation function is a sigmoid function, it is given by the formula:

$$f(x) = \frac{1}{1 + e^x} \tag{83}$$

The schematic representation of the above activation functions is shown in Figure 25.
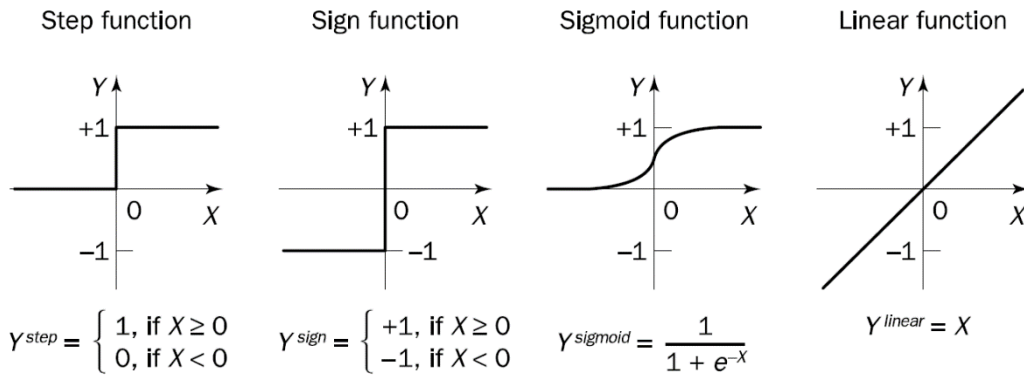
Figure 25: Graphic representation of the most common activation functions

4.2.5   The perceptron

The perceptron is a simple neural network which was invented by Frank Rosenblatt in the 1957 (Rosenblatt, 1957). It is a feed-forward neural network which is based on the idea of the simple neuron. Alternatively, in the literature can be also found as linear classifier.

The model consists of a linear combiner and a limiter that produces the values of the outputs. The purpose of the perceptron is the classification of the inputs x_1, x_2,..., x_n, into two categories e.g. A_1 and A_2.

A multilayer perceptron with two hidden layers is shown in Figure 26.
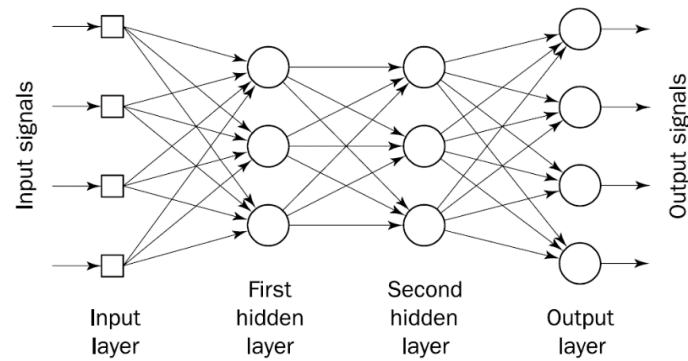
Figure 26: A multilayer perceptron with four layers

4.2.6 Training of neural networks

The objective of the training procedure is to find the appropriate weights of the synapses, for which the network will be able to produce the desired values of the outputs for given inputs.

There are several ways of learning, and thus training of artificial neural networks, which can be classified into two major categories: supervised learning and unsupervised learning.

4.2.6.1 Supervised learning

Supervised learning is the process that combines the existence of an external trainer and the total amount of the available information for the model. This category includes the back-propagation method of errors, the perceptron method, the stochastic learning, *etc*.

In supervised learning the supervisor have to decide on a number of issues such as:

- the examples (experimental data) that will be used for training
- the progress of the training process
- the termination of the training

4.2.6.2 The perceptron training method

The training of a perceptron is a classic case of supervised training. The training is done through an iterative process by making small adjustments to the synaptic weights so as to reduce the difference between the current and the desired output of each neuron. The initial weights are randomly selected, usually between the range [-0.5, 0.5], and then updated until the outputs approximate the training examples.

The training error is given by:

$$e(p) = Y_d(p) - Y(p) \tag{84}$$

where *p=1,…,n* is the number of iterations (training examples), $Y(p)$ is the actual output and $Y_d(p)$ is the desired output of the system.

The error determines the success of the training procedure. If the training error *is* $e(p) > 0$, the value of the actual output $Y(p)$ should be increased. If the training error *is* $e(p) < 0$, the value of the actual output $Y(p)$ should be reduced.

The learning rule, i.e. the calculation of the synaptic weights w, is provided by:

$$w_i(p + 1) = w_i(p) + a \cdot x_i(p) \cdot e(p) \tag{85}$$

where α represents the learning rate and is a positive constant less than unity.

4.2.6.3 Perceptron training algorithm

Step 1: Initialization

Set random values for the initial weights w_1, w_2,…, w_n and for bias θ from the range [-0.5, 0.5].

If the error e(p) is positive, increase the value of the output

If the error e(p) is negative, reduce the value of the output

Step 2: Activation

Activate the neuron by applying inputs $x_1(p)$, $x_2(p)$,…, $x_n(p)$ and the desired output $Y_d(p)$.

Calculate the actual output at the first iteration p=1 using the output equation:

$$Y(p) = f(\sum_{i=0}^{N} x_i(p) \cdot w_i(p) - \theta) \tag{86}$$

where N is the number of inputs and f is the activation function (e.g. the step function).

Step 3: Calculation of the synaptic weights

Update the values of the weights according to the relation:

$$w_i(p + 1) = w_i(p) + \Delta w_i(p) \tag{87}$$

where $\Delta w_i(p)$ is the correction of the weight in iteration p and is given by the delta rule as:

$$\Delta w_i(p) = a \cdot x_i(p) \cdot e(p)$$

Step 4: Iterations

Increase the number of iterations by 1:

$$p = p + 1$$

Go to step 2 and repeat the procedure until the desired convergence is achieved.

4.2.6.4 Back-propagation method of errors

The back-propagation method of errors is a common training method for multilayer neural networks, that is, networks with many layers. Quite often, it is used in combination with other methods such as the steepest descend algorithm.

The method calculates the derivative of the error function considering all the network weights. The calculated derivative is fed to the optimization method, which in turn uses it to update the weights in order to minimize the error.
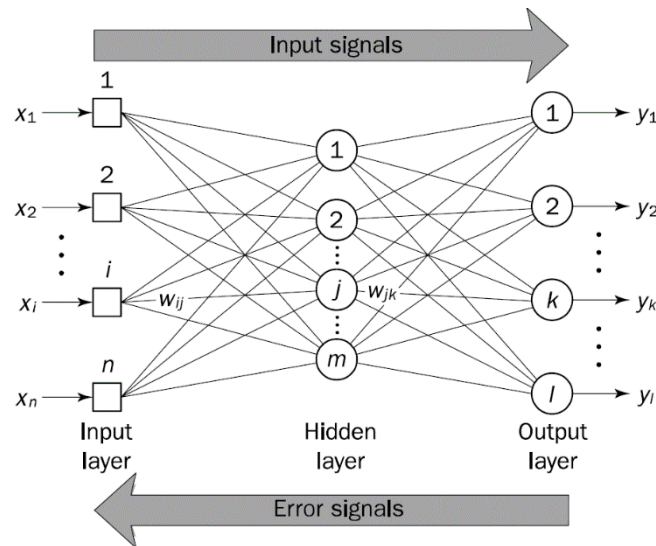
Figure 27: Backpropagation process

This method requires knowledge of the desired outputs for every input, in order to calculate the derivative of the error. Another requirement of this method is the differentiability of the activation function which is used by the neurons.

The training process is similar to that of a perceptron. More specifically, a training data set is selected, the outputs are calculated and if an error exist, the weights are adjusted to minimize this error.

4.2.6.5 The back-propagation training algorithm

<u>Step 1: Initialiazation</u>

Set random values for the initial weights w_1, w_2,…, w_n and the bias θ evenly distributed in a narrow range $\left(-\dfrac{2.4}{F_i}, \dfrac{2.4}{F_i}\right)$.

where F_i is the total number of neuron inputs.

The initialization of the weights is done for each neuron.

<u>Step 2: Activation</u>

Activate the neuron by applying inputs $x_1(p)$, $x_2(p)$,…, $x_n(p)$ and the desired outputs $Y_{d,1}(p)$, $Y_{d,2}(p)$,…, $Y_{d,n}(p)$. On the first iteration p=1:

a) Calculate the actual outputs of the neurons of the hidden layer using the output calculation equation:

$$y_j(p) = f(\sum_{i=0}^{N} x_i(p) \cdot w_{ij}(p) - \theta_j) \tag{88}$$

where N is the number of inputs of the neuron j at the hidden layer and f is the activation function (e.g. sigmoid function)

b) Calculate the actual outputs of the neurons of the output layer using the output calculation equation:

$$y_k(p) = f(\sum_{j=0}^{M} x_j(p) \cdot w_{jk}(p) - \theta_k) \tag{89}$$

where M is the number of inputs of the neuron k at the output layer.

Step 3: Calculation of the synaptic weights

Update the values of the weights in the network propagating the error backwards, i.e. from the output neurons towards the neurons of the hidden layer.

a) Calculate the derivative of the error for the neurons of the output layer using the relation:

$$\delta_k(p) = y_k(p) \cdot [1 - y_k(p)] \cdot e_k(p) \tag{90}$$

where $e_k(p) = y_{d,k}(p) - y_k(p)$

Calculate the correction of the weight:

$$\Delta w_{jk}(p) = a \cdot y_j(p) \cdot \delta_k(p) \tag{91}$$

Update the weights on the output neurons:

$$w_{jk}(p + 1) = w_{jk}(p) \cdot \Delta w_{jk}(p) \tag{92}$$

b) Calculate the derivative of the error for the neurons of the hidden layer using the following equation:

$$\delta_j(p) = y_j(p) \cdot [1 - y_j(p)] \cdot \sum_{k=1}^{L} \delta_k(p) \cdot w_{jk}(p) \tag{93}$$

where L is the number of the neurons of the hidden layer

Calculate the correction of the weight:

$$\Delta w_{ij}(p) = a \cdot x_i(p) \cdot \delta_j(p) \tag{94}$$

Update the weights on the output neurons:

$$w_{ij}(p + 1) = w_{ij}(p) \cdot \Delta w_{ij}(p) \tag{95}$$

<u>Step 4: Iterations</u>

Increase the number of iterations by 1:

$$p = p + 1$$

Go to step 2 and iterate the process until the error tolerance criterion is met.

4.2.7 Unsupervised training

The unsupervised training of an artificial neural network tends to follow the neurobiological organization of the human brain. This type of training is very fast and therefore can be used in real-time applications.

The training is done by self-organized algorithms, which train the network based only on local information without requiring the existence of a supervisor.

During the training, the neural network receives an amount of training data, finds similarities or important features of these data and learns to classify them into categories.

Some of the most popular methods of unsupervised training are, among others, the Hebb training algorithm, the competitive learning (Kohonen networks), *etc*. However, the presentation of these methods does not fall within the scope of this dissertation.

4.3 Adaptive neuro – fuzzy inference systems (ANFIS)

Simple fuzzy systems are very popular in several scientific fields, such as control, robotics, *etc*. The basic structure of these systems relies on membership functions for inputs and outputs, as well as a set of verbal rules in order to establish the decision-making system as described in section 4.1. Membership functions should be chosen by experience or arbitrarily and the structure of the rules should be predetermined and based on user's interpretation of the model.

Such systems are very efficient when applied to control. However, there are some critical limitations, such as the absence of a systematic framework or method of transforming human experience into a set of if-then rules, and/or the lack of an intact methodology for the fine tuning of the parameters of fuzzy controllers, and especially of membership functions.

Moreover, the application of fuzzy inference techniques to systems for which a set of input/output data already exist, is quite common. Structural control is only one example. In many industrial applications, the model is more or less known, or a collection of measurements could be easily obtained.

Actually, it is rather often that when the control mechanism is built, the designer or the engineer cannot decide the form and the other characteristics of the membership functions, or the coherence of the rules just considering the available data. In this case, adaptive fuzzy systems can solve the problem.

4.3.1 What is ANFIS

ANFIS is one of the most popular adaptive fuzzy systems, if not the most popular. A thoroughly study of the adaptivity of fuzzy systems, especially in control, as well as their stability properties can be found in classical monographies as "Adaptive fuzzy systems and control: Design and stability analysis" (Wang, 1994).

The forerunner of adaptive network-based fuzzy systems was a fuzzy system which was modeled using generalized neural networks (GNN) and a Kalman filter algorithm to minimize the squared error (Jang, 1991). In this approach, a fuzzy inference system with parameters that could be updated was built. From the simulation results was extracted that the proposed fuzzy system is able to fine-tune its parameters (e.g. the membership functions of inputs), as well as to incorporate prior knowledge about the original system.

The architecture of ANFIS is based on a fuzzy inference system which in turn is implemented inside the framework of adaptive neural networks and introduced by Jyh-Shing R. Jang at University of California in 1993. (Jang, 1993).

ANFIS consists of fuzzy rules which, in contrast to classical fuzzy systems, are local mappings instead of global ones (Jang & Sun, 1995). These mappings facilitate the minimal disturbance principle, which states that the adaptation should not only reduce the output error for the current training pattern but also minimize disturbance to response already learned (Widrow & Lehr, 1990). This is particularly important if an online learning process is considered. Comparisons with neural network approaches can be found in (Jang, 1993).

The process which should be followed in order to create a fuzzy inference system is usually called fuzzy modeling. On the other hand, neuro-fuzzy modeling refers to the way of applying various learning techniques developed in the neural network literature to fuzzy inference systems. Back-propagation neural networks are mostly used for the identification of the parameters of an adaptive fuzzy inference system.

The learning procedure could be hybrid, i.e. the proposed control model can construct an input-output mapping based on both human knowledge, just like in fuzzy systems, and appropriate input/output data pairs. However, even if human expertise is unavailable, it is still possible to set up the initial parameters intuitively and generate the fuzzy rules using a learning process in order to approximate a desired performance.

This means that, rather than choosing the parameters of the controller (membership functions, rules, *etc*.) arbitrarily, an automated process can provide tailor-made membership functions for the fuzzy variables (inputs and outputs) based on the available system's data. Moreover a set of rules, or other parameters of the control can also be considered, and the most important; the controller can be trained in order to be robust, i.e. capable of functioning under different conditions.

It is a common fact that fuzzy control is by far the most successful application of the fuzzy theory. However, due to the adaptive capability that ANFIS technique provides, fuzzy control becomes even more powerful, to the extent that it could be able to replace neural networks in control systems.

4.3.2 What is the ANFIS routine of MATLAB®

In this case the acronym ANFIS is derived from adaptive neuro-fuzzy inference system and it can be used in MATLAB® as part of the fuzzy logic toolbox. Namely, it is a training routine for Sugeno-type fuzzy inference systems.

With ANFIS, a fuzzy inference system can be constructed, just using a given input/output data set. The parameters of the system can be adjusted using either a back propagation algorithm alone or in combination with an algorithm based on the least squares method. This tuning allows fuzzy systems to learn from the same data they are modeling. The learning method works similarly to that of neural networks.
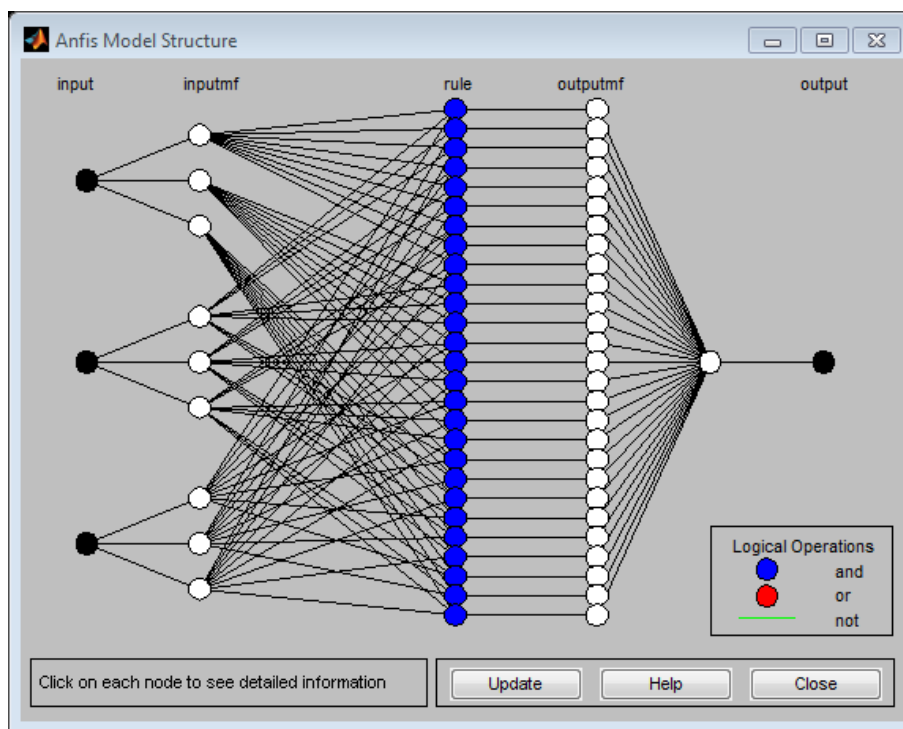

Figure 28: An ANFIS model structure in MATLAB®

The modeling approach is similar to many system identification techniques. First, a parameterized model is considered and then a set of data for training is collected and applied. The parameters of the fuzzy system will be adjusted automatically using these data until an error criterion is met.

It is essential that the training data (data for learning) are carefully chosen. This means that in general as for simple models, the more the data the better the approximation; however for noisy systems or when the collected data are not representative of the system, model validation might be helpful.

This validation can be achieved using another data set (data for testing). In general, model validation is the process by which inputs on which the system was not trained, are presented to the trained model, to check the accuracy of the prediction. This is necessary because after a certain point in the training process, the model may overfit the training data. The testing data also allow the designer to check the generalization capability (robustness) of the resulting fuzzy inference system.

4.3.3   Training of adaptive neuro-fuzzy inference systems through MATLAB®

The first step is the collection of a set of training data with the desired input/output data of the system to be modeled. These data must be an array with the data arranged as column vectors, and the output data in the last column. The data for training could be loaded either from a file or from the MATLAB® workspace.

4.3.3.1   Initialization of the system parameters

The initial fuzzy inference system parameters could be parameterized manually or, if there is no preference or experience on how they should look like, ANFIS can initialize the parameters automatically. This means that the model structure can be loaded either by a previously saved Sugeno-type fuzzy inference system structure or generated by choosing one of the following partitioning techniques.

Grid partition, which generates a single-output Sugeno-type fuzzy inference system by using grid partitioning on the data or subtractive clustering, which generates an initial model for ANFIS training by first applying subtractive clustering on the data.

A typical grid partition in a two-dimensional input space is one of the most common options when designing a fuzzy controller, especially if the desired number of the clusters is known. This method usually takes into account only certain of the parameters of the controller, such as the input variables. This partition strategy works perfect for a small amount of membership functions for each input (Jang & Sun, 1995).

However, when a moderately large number of inputs exists, grid partition method encounters serious problems. For instance, a fuzzy model with 10 inputs and two membership functions on each input would result in $2^{10} = 1024$ fuzzy if-then rules, which is prohibitively large. This problem, usually referred to as the curse of dimensionality and can be alleviated by other partition strategies such as tree partition and scatter partition which both overcome the problem of the exponential increase in the number of fuzzy rules by covering only a subset of the input space, which in turn needs to be carefully selected by the designer.

Subtractive clustering, on the other hand, is the suitable option if the designer of the controller does not have a clear idea of how many clusters there should be at each input for a given set of data (Chiu, 1994). It is a fast, one-pass algorithm for estimating the number of clusters and the cluster centers in a set of data. These estimates can be used to initialize iterative optimization-based clustering methods and model identification methods like ANFIS.

4.3.4 The training process through ANFIS

After loading the training data and generating the initial FIS structure, the training process can be procced. As mentioned above, there are two optimization methods available; the backpropagation and the hybrid method, which is a combination of least-squares error method (LSE) and backpropagation. Both of these methods are used in order to train the membership function parameters to emulate the available training data.
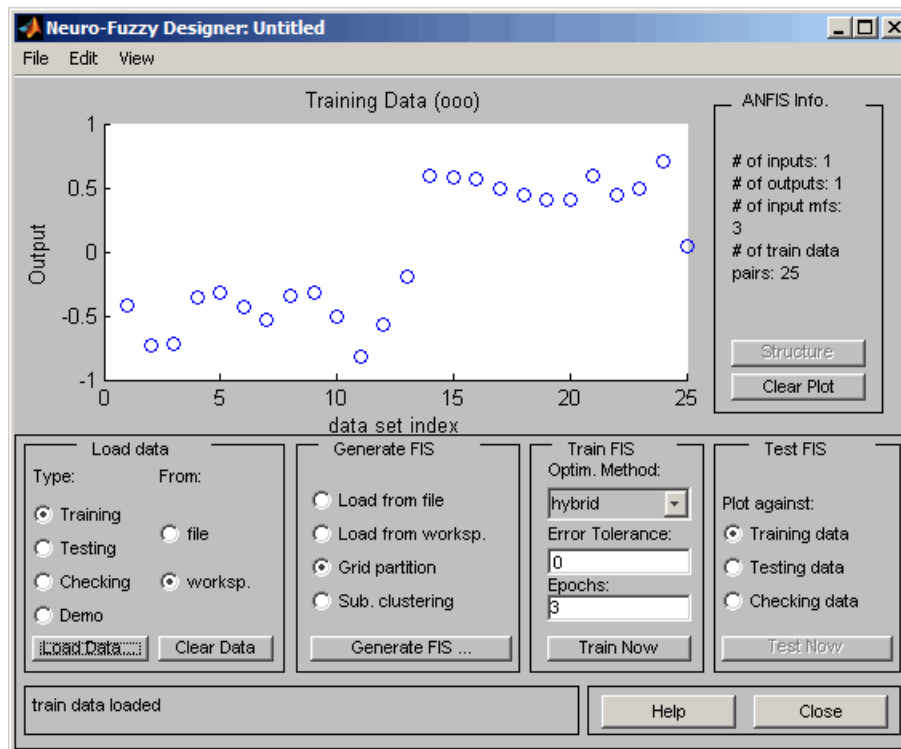

Figure 29: An example of training through ANFIS of MATLAB®

The backpropagation method is a gradient descent method which is presented thoroughly in subsubsection 4.2.6.4. Least squares method is a standard approach in regression analysis which is used for the computation of an approximate solution in overdetermined systems, i.e., systems of equations with more equations than unknowns. The term least squares suggests that the overall solution minimizes the sum of the squares of the computational errors of every single equation.

The hybrid method is based on backpropagation for the calculation of the parameters associated with the input membership functions, and least squares method for the estimation of the parameters related to the output membership functions. It is found that the use of least-squares method for the calculation of outputs of each local mapping is very important. It is notable that without using LSE, the learning time would be ten times longer (Jang, 1993).

The number of training epochs and the error tolerance are the stopping criteria for training and are both set by the designer of the model. The training process stops whenever one of the above criteria is met, i.e. when the maximum epoch number is

reached or the training error goal is achieved. If the impact of the training error to the results is unknown, error tolerance should be set to zero.

To make the training process more accurate, the results of each iteration are used as the initial conditions for the next epoch. The training error, which occurs in the output, decreases, at least locally, throughout the learning process. This means that, the more the initial membership functions approach the optimal ones, the easier it will be for the training algorithm to converge. Human knowledge or expertise about the target system can be of great assistance in setting up these initial parameters of the fuzzy inference system.

4.4 Linear quadratic regulator (LQR)

The core aspect of optimal control is the creation of controllers capable of operating a dynamic system at minimum cost. Linear optimal control is a special sort of optimal control. More specifically, linear control refers to the case where system dynamics are described by a set of linear differential equations (see Equations (22) and (96)) and the cost is described by a quadratic function (see Equation (97)). These methods that achieve linear optimal control are known as Linear-Quadratic (LQ) methods and the control problem is termed LQ problem.

One of the most fundamental optimal control problems is the so-called linear quadratic Gaussian (LQG) control problem. The solution could be provided by the linear quadratic regulator (LQR) which is one of the most powerful tools of optimal control.

The equations of motion are given in Equation (22), however they are rewritten here for convenience.

$$[M]\{\ddot{X}\}+[K_{uu}]\{X\}=\{F_m\}+\{F_{el}\} \tag{22}$$

The state space representation of these equations is given by:

$$\begin{aligned} \dot{x} &= Ax + Bu \\ y &= Cx + Du \end{aligned} \tag{96}$$

where x is the state vector, u is the control vector and y are the available measurements

For the construction of the LQR controller the following quadratic cost function should be minimized:

$$J = \frac{1}{2}\int_0^\infty (x^T Q x + u^T R u)dt \tag{97}$$

The main design parameters Q and R represent the weights on the different states and the control respectively, while J represents the weighted sum of the energy of the state and control. Matrix Q must be symmetric semi-positive definite and R is required to be symmetric positive definite for problems of optimal control.

Assuming a full state feedback, the control law is given by:

$$U = -K_{LQR}x \tag{98}$$

where $K_{LQR}x = R^{-1}B^T P$ is the constant control gain.

The constant matrix P is a solution of the Riccati Equation:

$$A^T P + PA + Q - PBR^{-1}B^T P = 0 \tag{99}$$

The closed loop system is given by:

$$\dot{x} = (A - K_{LQR})x + F_m \tag{100}$$

A significant advantage of the LQR formulation of a problem is the guaranteed linearity of the control law, which in turn leads to facile analysis and implementation. Another advantage of this type of control is its behavior in disturbance rejection and tracking. Finally, the gain and the phase margins indicate good stability.

However, for the implementation of LQR, a complete knowledge of the whole state space for each time step of the analysis is necessary. If only a limited number of measurements is available and/or any measurement errors are present, the effectiveness of control significantly deteriorates. In this case, first the system is reconstructed by the available measurements using a filtering technique (e.g. a Kalman filter, and then the optimal control problem is based on the new estimated system.

An outline of the basic theory of the linear quadratic regulator, as well as techniques of controller reduction and implementation, along with useful information on how to use LQR effectively for the design of control systems can be found in (Anderson & Moore, 1989).

4.5 The controllers

For the investigations that are held in the present dissertation, three different intelligent controllers are built. More specifically, two Mamdani-type fuzzy controllers, one for the mechanical and one for the electrical model of the structure, as well as one Sugeno-type neuro-fuzzy controller are implemented and tested. The basic characteristics of these controllers are shown below.

4.5.1 Fuzzy controller for the mechanical model (Controller 1)

The fuzzy inference system shown in Figure 30 is developed within MALAB using the fuzzy toolbox. The control scheme consists of a Mamdani-type controller of two inputs and one output. Controller 1 takes as inputs displacement and velocity from the mechanical model and returns the control force.

The membership functions of the fuzzy variables which were used for the construction of controller 1 are of triangular and trapezoidal form, both for inputs and output as shown in Figure 31, Figure 32 and Figure 33 for the displacement, the velocity and the control force respectively.
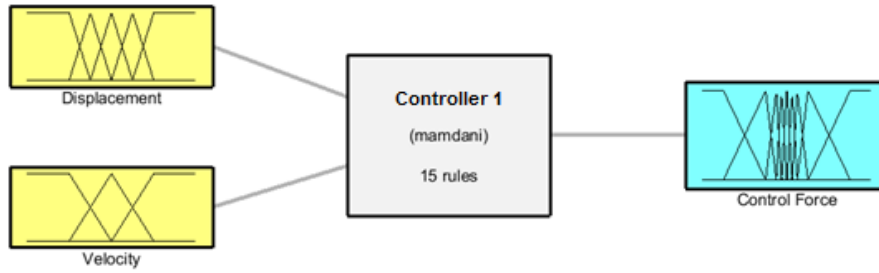
Figure 30: Mamdani fuzzy inference system of controller 1

The inference system involves a decision making system which is based on the combination of the membership functions with use of logical operations. Namely, the decision (output) is computed through a set of if-then rules, thus the recurring system is a rule-based system. For the implementation of the present fuzzy controller, a set of 15 rules is used as shown in Table 1. All rules have weights equal to unity and are connected using the AND operator. The graphic representation of the linguistic rules is shown in Figure 34.

The implication method is set to `minimum` and the aggregation one is set to `maximum`. The `mom` (Mean of Maximum), the `bisector`, as well as the `centroid` method are chosen as defuzzification methods in several investigations of the present study.

Table 1: Fuzzy rules (e.g. if displacement is far up and velocity is up then the control force is max)

| Displacement / Velocity	Far up	Close up	Equilibrium	Close down	Far down
Up	Max	Med+	Low+	Null	Low-
Null	Med+	Low+	Null	Low-	Med-
Down	High+	Null	Low+	Med-	Min
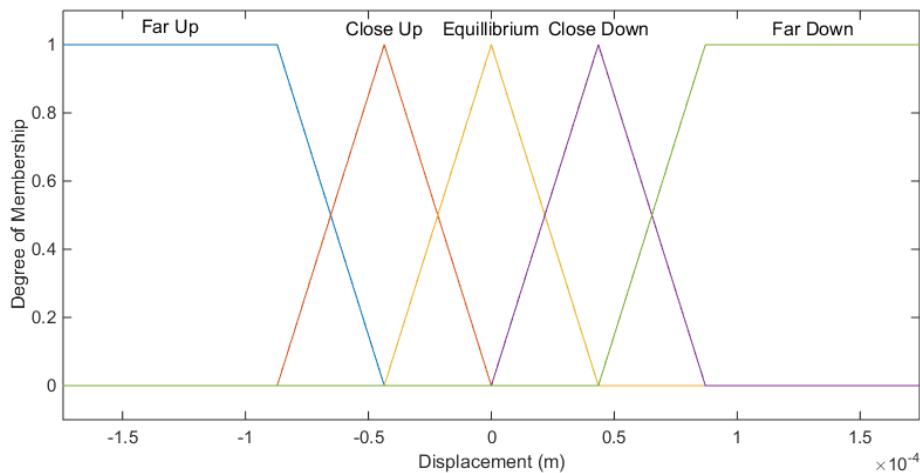
Figure 31: Membership function of displacement (input 1)
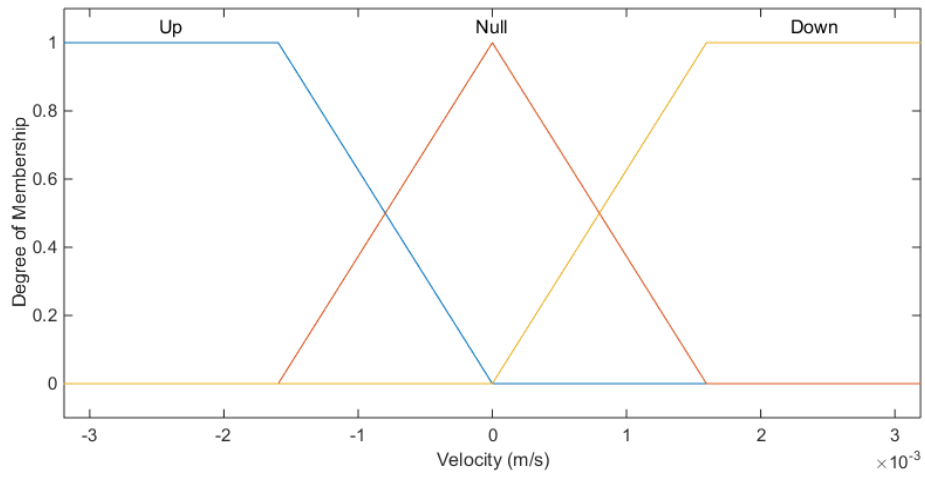
Figure 32: Membership function of velocity (input 2)
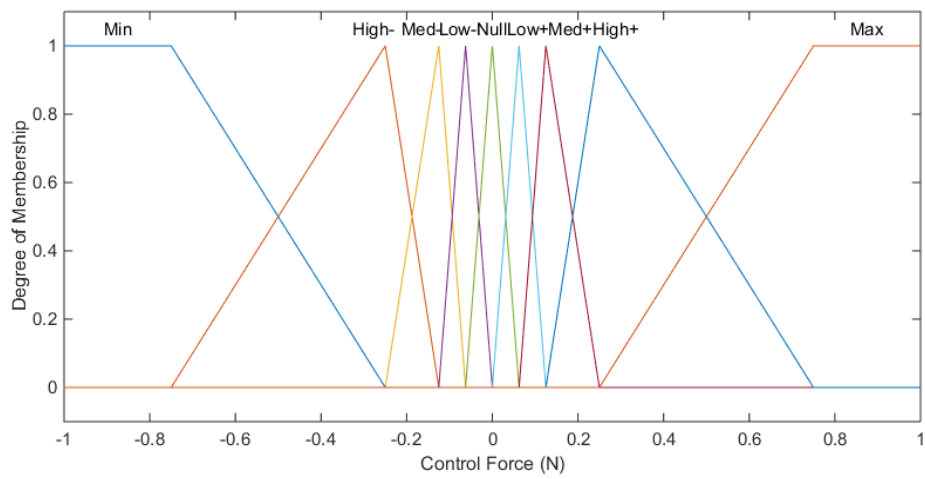

*Figure 33: Membership function of control force (output)*
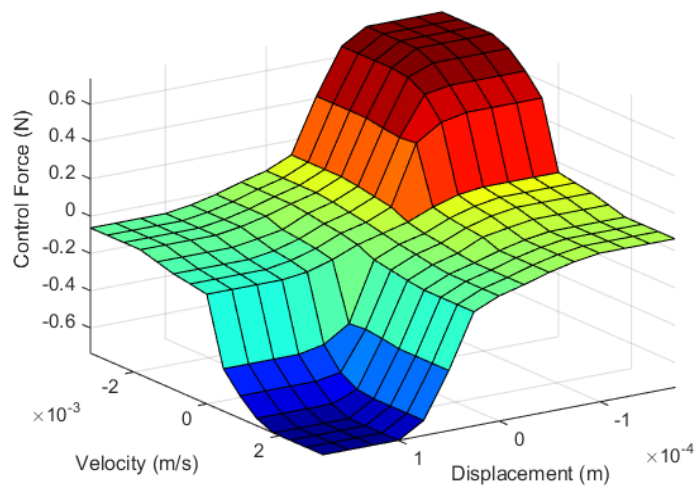
Figure 34: Graphic representation of the fuzzy rules of controller 1

4.5.2   Fuzzy controller for the coupled electromechanical model (Controller 2)

The controller 2 which is set taking into account the electromechanical model, is also Mamdani-type and consists of two inputs and one output, exactly as the one of the mechanical system. The main difference lies into the fact that this controller takes as inputs, not the displacement and the velocity, but the electric potential and the electric current, while returns as output not a control force, but an electric signal which can be used for control. Controller 2 is shown in Figure 35 below.
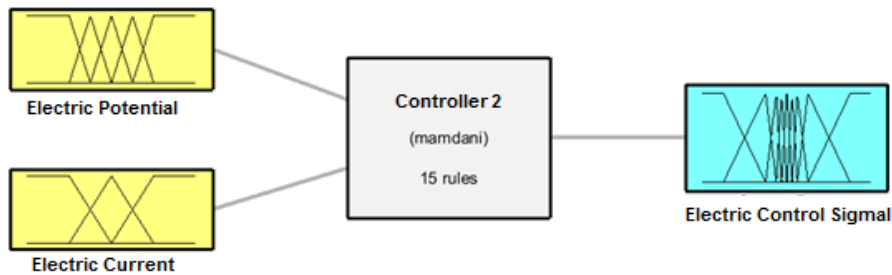

Figure 35: Mamdani fuzzy inference system of controller 2

The membership functions of the variables of controller 2 are again of triangular and trapezoidal form, for both inputs, i.e. the electric potential and the electric current, as well as for the output, that is, the control signal (see Figure 36, Figure 37 and Figure 38).

It is worth mentioning that the range of the output, i.e. of the control signal of the actuator, is set to [-200, 200] as the piezoelectric materials used for the analysis can produce voltage which is up to 200 Volts.

The set of rules is written similarly to the rules of controller1 and is shown in Table 2 and in Figure 39. Again, all rules have weights equal to unity and are connected using the AND operator.

Table 2: Fuzzy inference rules for the electrical system (e.g. if Electric potential is far positive and electric current is positive then the electric control signal is max)

| Electric potential ⟍ Electric current	Far Positive	Close Positive	Equilibrium	Close Negative	Far Negative
Positive	Max	Med+	Low+	Null	Low-
Null	Med+	Low+	Null	Low-	Med-
Negative	High+	Null	Low+	Med-	Min
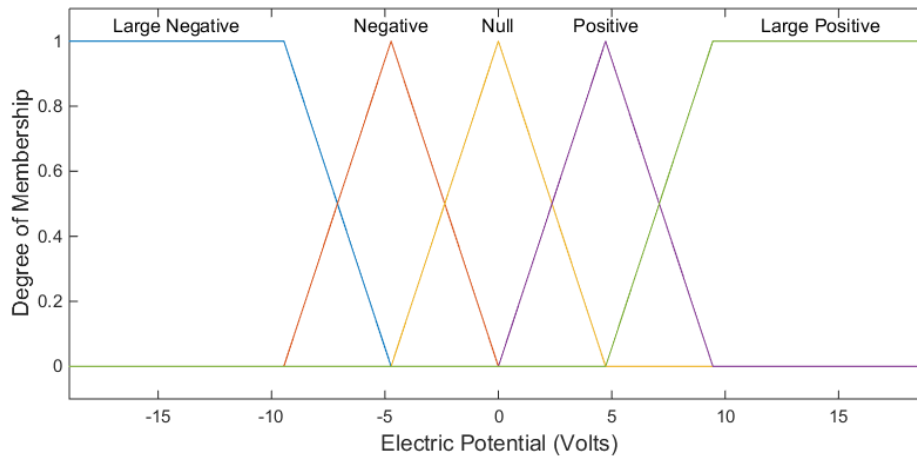
*Figure 36: Membership function of the electric potential (input 1)*
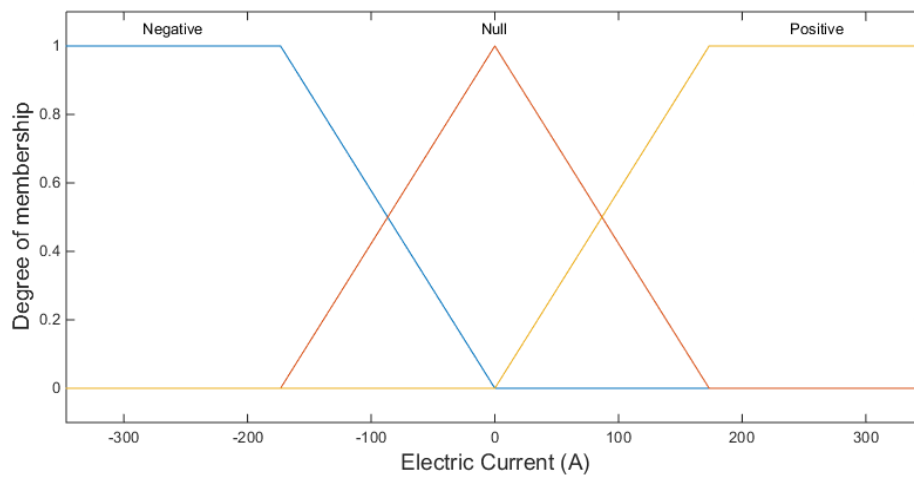
*Figure 37: Membership function of the electric current (input 2)*
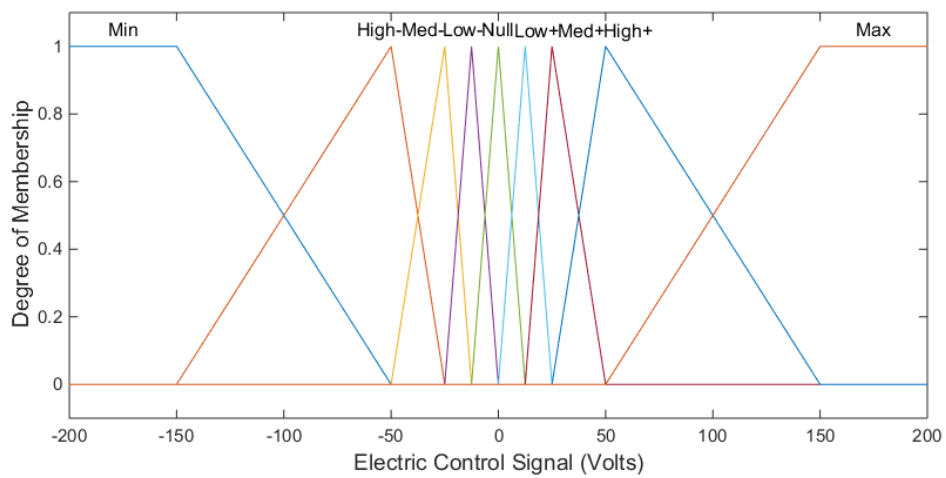
*Figure 38: Membership function of the electric control signal (output)*
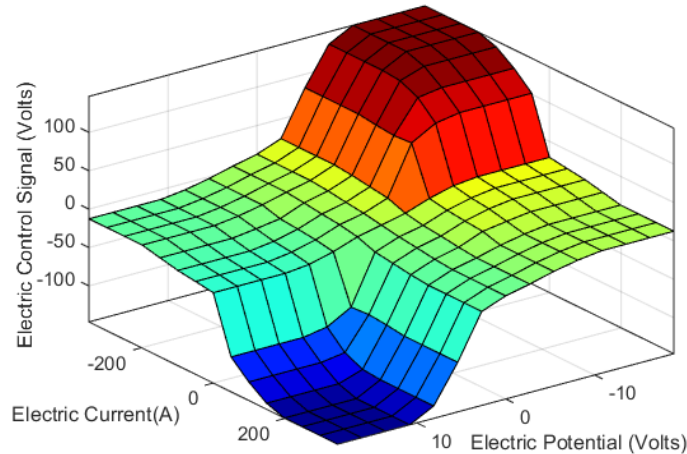
Figure 39: Graphic representation of the fuzzy rules of controller 2

4.5.3   Neuro-fuzzy controller (Controller 3)

In contrast to Mamdani-type fuzzy controllers, the adaptive neuro-fuzzy control schemes that are presented here are based on Sugeno-type controllers. Again the system takes two inputs (displacement and velocity) and returns one output (control force), thus is a multiple inputs – single output (MISO) control device. The overview of the Sugeno controller is shown in the following Figure 40.

As mentioned above, controllers of this type, use the same forms of membership functions exactly as the mamdani-type ones, regarding inputs. However, the output, in this case, can be only linear (i.e. of the form: $y = ax + b$) or constant.
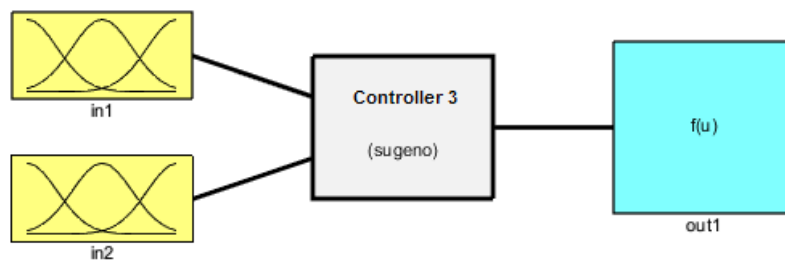
Figure 40: Sugeno fuzzy inference system of controller 3

Optimization of the controllers is achieved via a training process within the adaptive neuro - fuzzy inference system (ANFIS) package of MATLAB®. As mentioned in subsection 4.1.6, only Sugeno-type controllers are eligible for training with ANFIS.

The characteristics of the fuzzy system in this case are tuned using artificial neural networks. More specifically, a well-chosen set of training data is used in order to adjust the system parameters. For the compilation of these data, the model is first simulated without any control mechanism attached, in order to collect the necessary vibration data. Subsequently, these data are used for the training of the Sugeno controller.

Once loading the data to the ANFIS editor of MATLAB®, the initial fuzzy inference system can be generated either using grid partitioning on the data with the `Grid partition` option, if the form and the number of the membership functions is known, or, otherwise, if there is no such information, subtractive clustering (`Sub. clustering` option) may be used (see subsection 4.3.3).

The procedure of the computation of the clusters of the inputs of this controller via the subtractive clustering method through the ANFIS editor is shown in Figure 41.
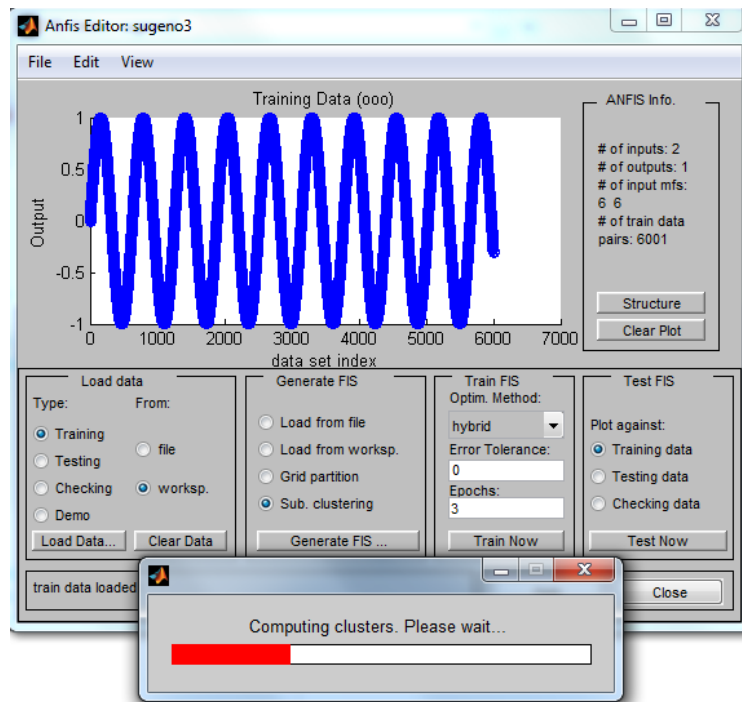
Figure 41: Computing of the clusters of the Sugeno controller using subtractive clustering

The resulting form of the membership functions (clusters) of the inputs i.e. the displacement (in1) and the velocity (out2), after the initialization process are shown in Figure 42 and Figure 43 respectively. Namely, four clusters of Gaussian form for each input occurred from the subtractive clustering process.
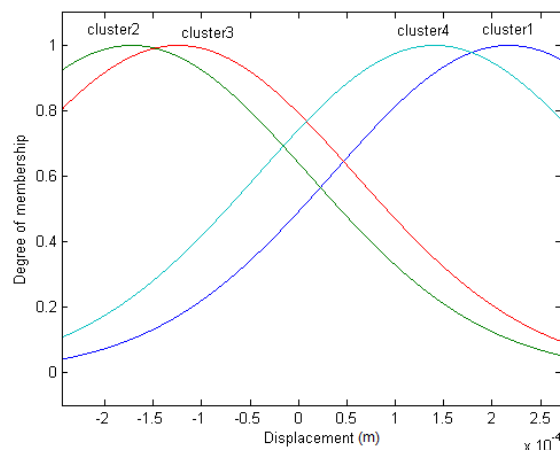
Figure 42: Membership function of the displacement
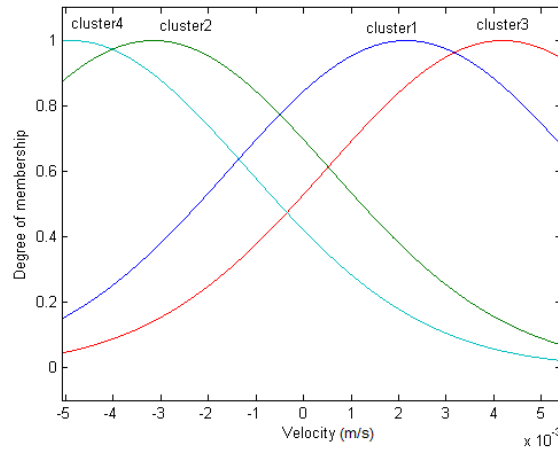
Figure 43: Membership function of the velocity

The output variable, i.e. the control force (out1), can take either constant values or linear functions taking values within the range [-1 1].

The verbal rules which describe the emerging system are given in Table 3:

Table 3: Fuzzy rules of the ANFIS controller (e.g. if Displacement is in cluster 1 and velocityis in cluster 1 then the control force is out1)

Displacement \ Velocity	Cluster 1	Cluster 2	Cluster 3	Cluster 4
Cluster 1	Out1	-	-	-
Cluster 2	-	Out2	-	-
Cluster 3	-	-	Out3	
Cluster 4	-	-	-	Out4

For the structure of rules in ANFIS see Figure 44. The visualization of the rules is shown in Figure 45.
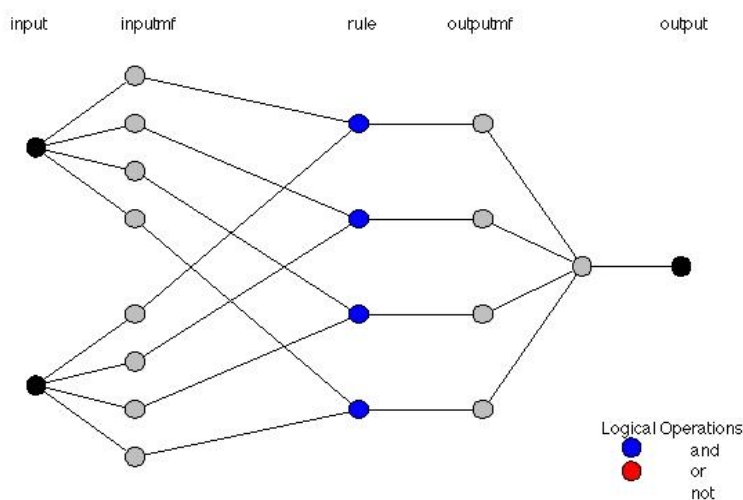
Figure 44: The structure of rules in ANFIS
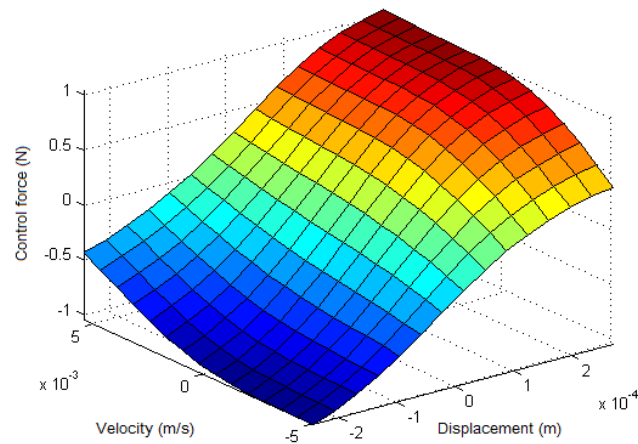
Figure 45: Graphic representation of the fuzzy rules of controller 3

The "and" method has been set to `prod` (product), while the "or" method has been set to `probor` (probabilistic or). The implication and the aggregation method have been set to `min` and `max` respectively. As defuzzification method the weighted average (`wtaver`) method is chosen.

It is worth mentioning that the characteristics of this controller (membership functions, rules, *etc.*) came through a training process, unlike the ones of fuzzy controllers which have been set based on experience.

This page was intentionally left blank

5 Optimization methods

Initially, the parameters of the fuzzy controllers which were used for vibration suppression of smart structures, where chosen from the literature and applied to the control strategy directly or were fine-tuned using the trial and error method.

The fuzzy controller described in 4.5.1, was tested in different smart structures (Tairidis, et al., 2009), (Tairidis, et al., 2014), (Tairidis, et al., 2007), providing very satisfactory results for vibration reduction in terms of displacement. However, the suppression of velocity was not good and the results concerning the acceleration were totally disappointing.

Due to this situation, the need of optimization of some of the parameters of the fuzzy controller arose. This fine tuning is a really demanding process, thus a simple, effective and well known procedure had to be chosen.

Classic optimization methods such as gradient descent can be proved quite unreliable due to the fact that the range of the parameters of the optimization could considerably vary. Moreover, classic optimization tools are quite sensitive to local optima.

Thus, among the plethora of optimization methods and algorithms, genetic algorithms as well as the particle swarm optimization method were selected due to their simplicity and smooth behavior in such problems.

These algorithms were used in order to optimize some parameters of the fuzzy controllers, such as the membership functions and the ranges of the fuzzy variables (inputs/outputs).

5.1 Genetic algorithms (GAs)

A genetic algorithm is a nature inspired method which in turn is based on the natural selection process. Namely, it simulates biological evolution. A major advantage of the method is that is suitable for both constrained and unconstrained optimization problems. The difference between genetic algorithms and other optimization methods based on derivatives, is that it creates a population of possible solutions (members) instead of a single individual solution. Thus, the optimum is being approached by the best member of the whole population at each iteration.

It is a stochastic process, which means that the population of solutions is produced and modified in each iteration at some extend in a random manner. As the generations pass by, the population is following an evolutionary course in order to approach the optimal solution.

5.1.1 The history of genetic algorithms

Evolutionary algorithms (EAs) are optimization methods, whose operation is based on imitation of the natural evolution process. These algorithms appear in three different forms, each one following a distinct path, but at the same time having strong interactions between them: genetic algorithms (GAs), evolutionary programming (EP) and evolution strategies (ES).

The first appearance of genetic algorithms dates to the early 1950s, when several scientists from the biology field decided to use computers in their attempt to simulate complex biological systems. However, their systematic development, which led to the form in which they are known today, was conducted in the early 1970s by John Holland and his colleagues at the University of Michigan (Holland, 1975)

The idea of natural selection, which is the base of evolutionary algorithms, is described by Michalewicz using the following example, which refers specifically to the genetic algorithms (Michalewicz, 1996):

"Let us take rabbits as an example: at any given time there is a population of rabbits. Some of them are faster and smarter than other rabbits. These faster, smarter rabbits are less likely to be eaten by foxes, and therefore more of them survive to do what rabbit do best: make more rabbits. Of course, some of the slower, dumber rabbits will survive just because they are lucky. This surviving population of rabbits starts breeding. The breeding results in a good mixture of rabbit genetic material: some slow rabbits breed with fast rabbits, some fast with fast, some smart rabbits with dumb rabbits and so on. And on top of that, throws in a 'wild hare' every once in a while by mutating some of the rabbit genetic material. The resulting baby rabbits will (on average) be faster and smarter than these in the original population because more faster, smarter parents survived the foxes. (It is a good thing that the foxes are undergoing similar process - otherwise the rabbits might become too fast and smart for the foxes to catch any of them). A genetic algorithm follows a step by step procedure that closely matches the story of the rabbits".

5.1.2 How genetic algorithms work

Evolutionary algorithms are mainly based in imitating the evolution process, as well as the heredity process in living organisms. It was therefore expected to borrow the terminology of biology for many processes similar to the corresponding biological ones (Goldberg, 1989).

For example genetic algorithms are using terminology borrowed from the field of genetics. They refer to individuals or genotypes within a population. Any individual or genotype consists of chromosomes. In genetic algorithms we usually refer to individuals with only one single chromosome. Chromosomes, in turn, are composed of genes that are arranged in a linear sequence. Each gene affects the inheritance of one or more

characteristics. Genes affecting specific features of the individual are situated in respectively specific positions of the chromosome called loci. Each distinctive trait of the individual (such as hair color, eye shape, height, *etc.*) can be displayed in various forms, depending on the corresponding influencing gene. These alternative forms, which a gene may obtain, are called alleles.

Many organisms have more than one chromosomes in each one of their cells. The total sum of genetic material, i.e. the total amount of chromosomes, is called genome of the organism. The term genotype refers to a specific set of genes of the genome. Finally, after the fetal development of the organism, the genotype gives its position to the phenotype, that is, the physical and mental characteristics, such as eye color, height, brain size, intelligence, *etc*. Therefore, the genotype is referred to coding procedure of the external characteristics, while the phenotype is referred to the inherent characteristics of the organism. Natural selection directly affects the phenotype, due to the interaction between the external characteristics of the organism and the environment. However, the influence of natural selection in the genotype, is done indirectly through the survival of the best adapted individuals (Goldberg, 1989).

Chromosomes, unlike the genes, are not permanent structures. They can be fragmented and their parts can be then combined in a different way, thus forming new sets of genes. The basic operations which take place in organisms are the reproduction and mutation.

During the reproduction process, two members of the organism can exchange genetic material in order to create offspring. The procedure is as follows: first, the chromosomes are divided in several parts. Then, the parts of the one chromosome are combined with the parts of the other. This process is called crossover. In each parent, the genes are shared between chromosome pairs in order to form the gamete, which is a simple chromosome, and then the gametes of both parents mate and create a complete set of chromosomes (chromosomes in pairs) to their offspring. Offspring which are produced get some of the characteristics not only of their parents, but even of past generations as well.

Mutation is an error in the reproduction of the genetic material during the process of mitosis (cell division and proliferation). If this error takes place during the replication stage, which is following the crossover, then the modified chromosome can be passed to the next generation. This procedure occurs very infrequently and is caused either by genetic or by environmental factors.

The basic scope of genetic algorithms is to maintain the population in the form of encoded information, along with the evolution of this population over time. The evolution of the members of the population is based on the principles of natural selection (survival of the fittest) and on the recombination of genetic material into the population. The evolving population samples the exploration space, accumulating information regarding the areas of good and poor quality solutions and forms optimal performance solutions for each specific problem, by exchanging information parts.

5.1.3   Genetic algorithms and optimization

Regarding the optimization of systems, first of all, the modeling of the system should be created. The model is a simplified representation of the system. The mapping is performed using a finite number of parameters of the independent design variables. These variables could either be in binary format (classical genetic algorithms), or in an integer or a real number format (hybrid evolutionary algorithms). When in binary form, each independent design variable is a gene and consists of a binary digit (0 or 1) or a series of bits (e.g. 1101010).

Each row, consisting of the encoded genes, is the chromosome. When the independent design variables take specific values in the chromosome, then we have a candidate solution. The coding of a particular system in the form of a chromosome is the genotype, while the system that is produced if this genotype is applied to the system model is the phenotype, which is the one that is finally evaluated.

The fitness function value, which controls how strong a chromosome is, depends on the value of the objective function for the given chromosome. The strongest chromosomes are selected and combined with other strong chromosomes in order to create offspring, while the rest are gradually removed from the population. Fitness function optimization corresponds to the adjustment of each individual in the environment during the process of natural selection.

Crossover is implemented by exchanging genetic material between two haploid parents, i.e. between the chromosomes of two solutions of the same generation. In its simplest form, the two chromosomes are cut in the same random point and the first part of the first chromosome is joined to the second part of the second and vice versa, thereby resulting in two new solutions (two offspring). The mutation is performed by changing a gene's value in a randomly selected position of the chromosome.

The new value is obtained from the alleles (the different values that a gene can take) of that specific gene. Therefore, if the coding is done with binary numbers, then if the value of the selected item is 0 it is converted to 1, while if it has a value of 1 is converted to 0.

The selection operator actuates the exploration in areas with greater potential, in terms of objective function.

The mutation and crossover operators explore the space of solutions, while the selection operator exploits the information that exists in the population. The first operators tend to increase differentiation among individuals within populations, while the selection operator tends to decrease it, leading to a greater uniformity of individuals with high value of the objective function. A balance adjustment between the two conflicting functions (exploration - exploitation) is performed by the mechanism of selection. The term which expresses the prevalence of exploitation at the expense of exploration property is called "selective pressure". Increasing the selective pressure, which

is achieved by changing variable q, leads to increasing convergence speed of the algorithm, although sometimes it also increases the possibility of being trapped in a local optimum (Michalewicz, 1996).

The optimization process is as follows: initially, a randomly generated number of P solutions, coded in the form of strings (usually binary), which represent the natural chromosomes is created. The concept of population gives to genetic algorithms unique features, such as the ability of using many candidate solutions, that is, a large population of candidate solutions, simultaneously.

After the creation of the initial population, each member of the population is decoded in a candidate solution of the problem, while a "fitness" value is given to this solution, through a quality function which gives a measure of the quality of each solution. Then, pairs of members of the population are selected in order to reproduce and form offspring (new solutions). The choice of pairs is probabilistic, so that the probability of each solution is proportional to its "suitability". This ensures that high-quality solutions will be chosen many times and will become the "parents" for many new solutions, while low-quality solutions will contribute less to the new population, since the probability of not being selected to reproduce is higher. (Holland, 1975). Popular selection methods are among others the tournament selection, the roulette-wheel selection the truncation selection, *etc*. In practice, tournament selection, is used more often, due to the fact that it is fast and easy to implement, it have a constant selection pressure and presents less stochastic noise than other methods. (Blickle & Thiele, 1996). In this method, in order to select a new member of the intermediate population, q members (q≥1) of the population are selected, with uniform probability. Usually q=2 or q=3. Within those q members the best are selected for the intermediate population. This process is repeated until the number of individuals of the intermediate population is completed.

When the two solutions (parents) are selected, their strings are combined again in order to produce a solution-offspring, using operators which simulate respective genetic mechanisms. The basic genetic operators used, are crossover and mutation. Crossover recombines parents' strings in order to produce an offspring which inherits characteristics of both parents. The crossover operator, although being the basic exploration mechanism for new solutions, in fact it is not able to produce information that is not already present in the population. This need is covered by mutation. With this operator it is possible to introduce new information to the new offspring. Mutation is accomplished by randomly changing values of the new offspring. Generally, mutation is considered as a minor, but useful operator, which gives a non-zero probability for checking and evaluating every possible solution. The two most known types of mutation are the random uniform mutation and the random non-uniform mutation.

When M new solutions are produced, these are considered as the new generation and completely replace their "parents" in order for the development to proceed. Many generations are needed until the population converges to the optimal solution or to a

close to the optimal one. The number of generations required increases proportionally to the difficulty of the optimization problem.

The general steps of a genetic algorithm are given below:

Step 1: Time **t=0**

Initialization of the population of P solutions (t=0)
Evaluation of the population of the solutions

Step 2: Time **t=t+1**

Selection of new population of solutions P(t+1) from the old P(t)
Application of operators to the new population
Evaluation of the new population
Return to Step 2[3]

A simple genetic algorithm in the form of pseudocode can be written as follows:

generation=0
Initialize
Evaluate
KeepBest

do generation = 1, MAXGENS
Select
Crossover
Mutate
Report
Evaluate
Elitist

enddo

The above functions, which are denoted with bold letters, can be described as follows:

Initialize: generates the initial population, giving random values, with uniform probability and within the limits of each independent design variable, to the genes of each chromosome of the population.

Evaluate: calculates the fitness function of each chromosome. It is worth noting that the fitness function differs depending upon the problem.

KeepBest: keeps the best individual of each generation (chromosome and its fitness function).

Select: selects intermediate population chromosomes.

---

[3] Step 2 is repeated until the stop criterion is met, so that the algorithm gives an optimal solution which satisfies all the involving constraints.

Crossover: selects the pairs to apply the crossover. Scans all individuals within the population. Each one is selected as a candidate for the crossover with probability pxover. Once the pair is completed, Xover is called.

Xover: performs a single-point crossover between two individuals of the selected chromosome pair. The intersection point is selected with uniform probability.

Mutate: genes are selected (with uniform probability) within the total population and the total set of the genes of each chromosome, in order to be mutated. The new value for each gene is resulting with uniform probability within the definition space of the relevant design variable.

Report: calculates population statistics in each generation and exports them to the output file.

Elitist: if the best individual of the current generation is worse than the previous generation's best, the latter replaces the worst individual of the current generation.

5.1.4   Selection of the control parameters

The Control Parameters of a genetic algorithm are the following:

- Number of variables (NVARS)

- Number of chromosomes (POPSIZE)

- Number of generations (MAXGENS)

- Crossover Probability (PXOVER)

- Mutation Probability (PMUTATION)

- Selection Operator (q)

Control parameter values should be selected carefully, as they play particularly important role in the performance of the genetic algorithm. This means that in order to find the appropriate values for each problem one may use the trial and error method.

Generally, in order to choose the values of these parameters one should have in mind the following:

The larger the number of chromosomes i.e. the population size (POPSIZE), the greater the amount of the variations shown in the initial population. However, this increase the computational cost, as more fitness function calculations are necessary. The size of the population depends on the problem. A good population includes a diverse selection of possible structural units, resulting in a better exploration. If the population loses its diversity, then the algorithm has premature convergence and the exploration is limited. In complex optimization problems, with large chromosome size, a larger population size is required. The range of the population size proposed in literature is between 25 and 200 chromosomes.

The number of generations (MAXGENS) is the termination criterion of the genetic algorithm and it depends on its convergence. This parameter's value usually ranges from 5 to 100 generations, depending on the problem.

The crossover probability (PXOVER) refers to the crossover process as follows: once the two chromosomes to be crossed are selected, a random number is chosen from the range [0-1]. If that number is less than the crossover probability PXOVER then crossover takes place. Usually the probability is selected within the range from 0.5 to 1.

The mutation probability (PMUTATION) determines the probability that a gene of a chromosome has to change from 0 to 1 or vice versa. The mutation restores part of the variety of genetic material which has been destroyed by the selection procedures and crossover. While selection and crossover tend to homogenize the population based on the principle of survival of the strongest, the mutation restores some of the genes that have been eliminated in the process and that they may be necessary in order to avoid being trapped in local solutions. In practice, it has been found that mutation probability typically ranges from 0.001 to 0.15.

As mentioned above, the selection operator (q) is the parameter that adjusts the "selective pressure", which reflects the predominance of exploitation at the expense of exploration property. It should be carefully selected in order to avoid local optima (Michalewicz, 1996).

The performance of a genetic algorithm can be improved in several ways if the results at the initial stage are not satisfactory. One way is by varying the values of the parameters mentioned above. This trial and error method can be time consuming, however it has the ability of increasing the performance of the algorithm. If the change of the parameters has no effect, one may needs to change the encoding. Note that in some applications binary (discrete) encoding is required, whereas in other problems real (continuous) encoding provide better results.

5.1.5   Genetic algorithms with constraints

The optimization problems can be distinguished, according to several criteria, in different categories, as for example: problems with or without constraints, static or dynamic optimization problems, optimal or non-optimal control problems and so on.

Generally, an optimization problem is based in the finding of a vector that correspondingly minimizes or maximizes the objective function $f(x)$ of the problem. Additionally, in case of a problem with constraints, it should also satisfy the constraints of the problem.

$$min_x f(x) \text{ or } max_x f(x) \tag{101}$$

where $x = [x_1, x_2, \dots, x_n]$ are the design variables.

subject to:

$$g_i(x) \leq 0, \; where \; i = 1,2,3, \dots, m \tag{102}$$

$$i_j(x) = 0, \quad where \ j = 1,2,3,\dots,p \tag{103}$$

The vector x represents the decision variables, the function $f(x)$ the objective function, the functions $g_i(x)$ the inequality constraints and the functions $i_j(x)$ the equality constraints.

5.1.6 Penalty functions

In the general case of non-convex solution space with non-linear constraints, most proposed methods for evolutionary algorithms, are based on the principle of penalty functions. A penalty method can transform a problem with constraints to a problem without constraints in two ways. The first one uses the aggregated form:

$$eval(x) = \begin{cases} f(x), if \ x \ is \ feasible \\ f(x) + penalty(x), otherwise \end{cases} \tag{104}$$

where the *penalty(x)* stands for the penalty function and *f* the feasible space solution. If there are no violations, the *penalty(x)* will be null; otherwise it will obtain a positive value. The function *eval(x)* becomes the main objective function of the problem.

The second way uses the dot product form:

$$eval(x) = \begin{cases} f(x), if \ x \ is \ feasible \\ f(x) \cdot penalty(x), otherwise \end{cases} \tag{105}$$

In most methods, several penalty functions are being used, one for each constraint of the problem. Each function measures the degree of non-satisfaction of the restriction and adds some amount to the objective function (penalty). If there are no violations, *penalty(x)* will be unity; otherwise it will be greater than one.

5.2 Particle swarm optimization (PSO)

Particle swarm optimization (PSO) algorithm is a very popular global optimization algorithm which has been introduced by Kennedy and Eberhart (Kennedy & Eberhart, 1995).

It is a population based optimization algorithm and a totally stochastic technique that simulates the movement of particles i.e. the flying motion of a flock of birds, of a swarm of insects, *etc*. In similar manner, the "flock" or "swarm" of possible solutions "flies" towards the optimum solution.

More specifically, this optimization algorithm takes into account the natural movement of the individuals (particles) of the population (swarm) towards the search of food and is very adaptive to the global, as well as the local exploration ability of the swarm.

Particle swarm optimization is widely used in various applications of different scientific sectors, as it is considered to be one of the most promising algorithms inspired by

nature. It also has the advantage of being very simple and easy to implement and presents significant adaptiveness in many different problems, especially in those using continuous values. The PSO method can also be used for the optimization of the characteristics of fuzzy controllers (Tairidis, et al., 2015), (Marinaki, et al., 2011), (Marinaki, et al., 2011b). An extensive literature review of particle swarm optimization method can be found in (Banks, et al., 2007), (Banks, et al., 2008).

5.2.1   The implementation of the algorithm

Similarly to the genetic algorithms, initially, a population of particles is created, most times randomly. Each particle has a certain position x_{ij} in the space of solutions and is moving with a specific velocity u_{ij}, where $i = 1,2,3, \dots, m$ and $j = 1,2,3, \dots, n$. Note that m is the population size and n is the number of iterations.

The position of the particles is given as:

$$x_{ij}(t + 1) = x_{ij}(t) + u_{ij}(t + 1)$$

(106)

The velocity denotes the change of the position at each iteration and is given by:

$$u_{ij}(t + 1) = u_{ij}(t) + c_1 r_1 \left(p_{best\ ij} - x_{ij}(t) \right) + c_2 r_2 \left(g_{best\ j} - x_{ij}(t) \right)$$

(107)

where $c_1 = c_2 = 2$ are constants of acceleration that can control exploration, i.e. they indicate how far a particle can travel, r_1 and r_2 are random values in the interval [0, 1], $p_{best\ ij}$ is the optimal position of a single particle (personal best) and $g_{best\ j}$ is the optimal position of the whole swarm at every iteration (global best).

In the case of minimization problems, the personal best of each particle at every iteration is given as:

$$p_{best\ ij} = \begin{cases} x_{ij}(t + 1), & if\ \ f\left(x_{ij}(t + 1) \right) < f\left(x_{ij}(t) \right) \\ p_{best\ ij}, & elsewhere \end{cases}$$

(108)

In this case, the global best of the swarm at every iteration should be:

$$g_{best\ j} = min\{f\left(p_{best\ 1j} \right), f\left(p_{best\ 2j} \right), \dots, f\left(p_{best\ nj} \right)\}$$

(109)

where n is the number of iterations.

The optimum solution results from the iterative process and is returned after the completion of the total number of iterations.

5.2.2   Variations of the PSO method

In order to increase the efficiency of the PSO algorithm by increasing its exploration capability, avoiding local optima, several variations of the original method were proposed.

5.2.2.1 Inertia PSO

A method which introduces an inertial weight, also known as inertia PSO, was introduced by Shi and Eberhart in (Shi & Eberhart, 1998).

In this algorithm the velocity at each iteration is calculated by:

$$u_{ij}(t+1) = w\, u_{ij}(t) + c_1 r_1 \left(p_{best\ ij} - x_{ij}(t)\right) + c_2 r_2 \left(g_{best\ j} - x_{ij}(t)\right) \quad (110)$$

The inertia weight w is given by:

$$w = w_{max} - \frac{w_{max} - w_{min}}{max\_iteration}\, t \qquad (111)$$

where usually $w_{max} = 0.99$, $w_{min} = 0.01$ have been chosen from the literature.

It is notable that the choice of the inertial weight is very important, as it affects the convergence of the algorithm.

In structural design optimization (Perez & Behdinan, 2007) through the analysis of the eigenvalues of the structure the following stability conditions derived for the inertia PSO parameters:

$$c_1 r_1 + c_2 r_2 > 0$$

$$\frac{(c_1 r_1 + c_2 r_2)}{2} - w < 1 \qquad (112)$$

$$w < 1$$

From the above, the upper limit for $(c_1 r_1 + c_2 r_2)$ is $(c_1 r_1 + c_2 r_2) < 4$. Moreover, knowing that the random variables r_1 and r_2 lie in the interval [0, 1], the cognitive parameter c_1 and the social parameter c_2 should be:

$$0 < c_1 + c_2 < 4 \qquad (113)$$

It is worth mentioning that even if conditions (113) are satisfied, only the convergence of the algorithm to a stable equilibrium point is guaranteed. This does not indicate that the algorithm has reached the global optimum.

5.2.2.2 Constriction PSO

Another successful variation, known as constriction PSO was introduced by Clerc and Kennedy (Clerc & Kennedy, 2002). In this algorithm a constriction factor χ is used in order to restrict the velocity of the particles so as to improve the convergence of the algorithm. In this case the velocity of the particles of the swarm is given by:

$$u_{ij}(t+1) = \chi \left(u_{ij}(t) + c_1 r_1 \left(p_{best\ ij} - x_{ij}(t)\right) + c_2 r_2 \left(g_{best\ j} - x_{ij}(t)\right)\right) \quad (114)$$

Constriction factor χ is given as:

$$\chi = \frac{2}{\left|2 - c - \sqrt{c^2 - 4c}\right|} \tag{115}$$

where the constant c is given as:

$$c = c_1 + c_2, \quad c > 4$$

In case of constriction PSO, the values of these constants are proposed from the litera-ture to be selected as: $c_1 = c_2 = 2.05$.

6 Numerical results

In this chapter, several control schemes are applied on smart composites structures for the suppression of vibrations in terms of displacement, velocity and acceleration. More specifically smart beams and plates based on single layer, as well as on layerwise theories are considered. The analytical description of the models has been presented in chapter 3.

Regarding control, fuzzy and adaptive neuro-fuzzy controllers are implemented and tested (see section 4.5).

Moreover, the initial characteristics of the control are modified using ANFIS (see section 4.3) and global optimization tools (see chapter 5) for the improvement of the obtained results. In other words, the fuzzy control incorporates global optimization techniques such as genetic algorithms and particle swarm optimization. The effectiveness and the robustness of the proposed control schemes is shown.

Furthermore, the robustness of control is investigated under several delamination cases between the piezoelectric components.

6.1 Fuzzy control of smart plates

In this investigation, the structure consists of a composite plate (see section 3.4). The length of each side of the plate is 0.8m, the elastic modulus is $150 \times 10^9 \text{N/m}^2$, the shear modulus is $7.1 \times 10^9 \text{N/m}^2$ and the density of the material is 1600kg/m^3.

The model consists of four composite layers and two outer piezoceramic layers. The stacking sequence the composite is antisymmetric angle-ply ([-45° /45°/-45°/45°]).

The plate is made of T300/976 graphite-epoxy composite and the piezoceramic is PZT G1195N. The material properties of the structure are given in detail in Table 4. For further details see (Lam, et al., 1997).

The proposed plate model is shown in Figure 46. The structure is discretized using the finite element method. Namely, it is divided into 144 (12x12) quadratic finite elements, yielding to a system of 169 nodes with 825 degrees of freedom.

The plate is fixed at the left end. The fixed nodes are denoted by the bold line at the left side of the structure (see Figure 47).

Table 4: Material properties of the composite plate with piezoelectric sensors and actuators

Property	Graphite/epoxy	Piezoceramic
E_1 (GPa)	150	63
$E_2 = E_3$ (GPa)	9.0	63
G_{12} (GPa)	7.1	24.2
$G_{23} = G_{13}$ (GPa)	2.5	24.2
$\nu_{12} = \nu_{13} = \nu_{23}$	0.3	0.3
ϱ (kg/m³)	1600	7600
$d_{13} = d_{23}$ (m/V)	-	$254 \cdot 10^{-12}$
$d_{42} = d_{51}$ (m/V)	-	$584 \cdot 10^{-12}$
Ply thickness (mm)	0.25	0.1
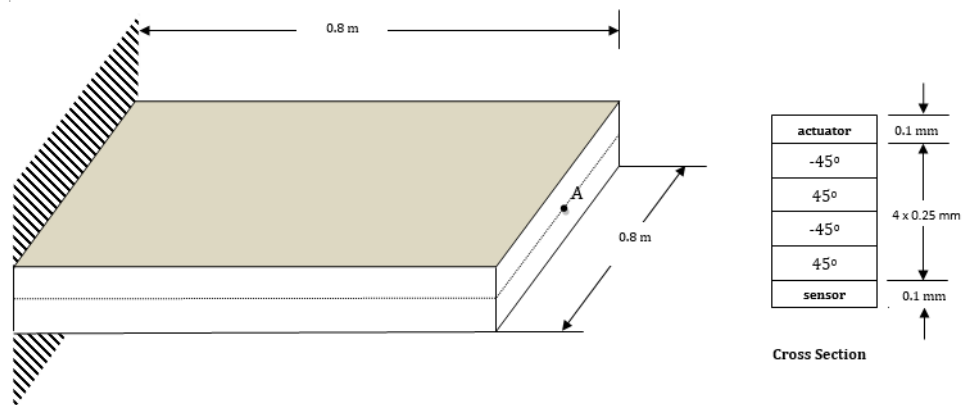
Figure 46: The simplified plate model
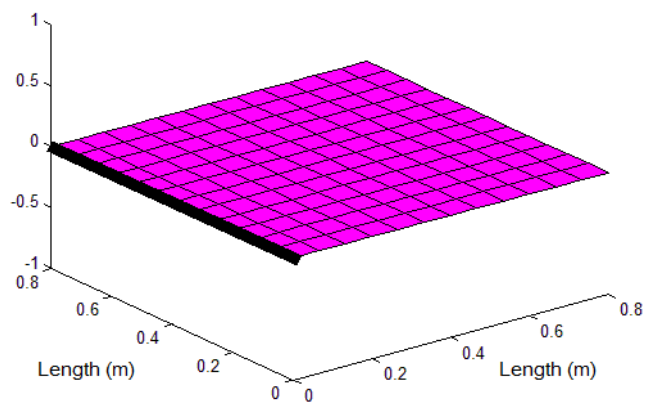
Figure 47: The discretized plate model (mesh)

6.1.1 Results without optimization of the controller's parameters

Two different loading scenarios are examined (Tairidis, et al., 2014). The first one include a three-point loading at the unsupported end of the plate, while the second scenario consider a five point loading applied to the free end of the host structure.

The fuzzy controller which is used for the vibration suppression is the one described in subsection 4.5.1 (controller 1).

6.1.1.1 Three-point loading scenario

In this first scenario, a sinusoidal loading was applied to three nodes. These nodes correspond to the upper corner, the middle point and the lower corner of the free side of the plate respectively, as shown in Figure 48(a). With blue arrow in Figure 48(b) is shown the position (node) of the control mechanism (collocated sensor and actuator).

The loading that is applied to each node is given by:

$$P = \frac{1}{3} sin(20t) \ (N) \tag{116}$$
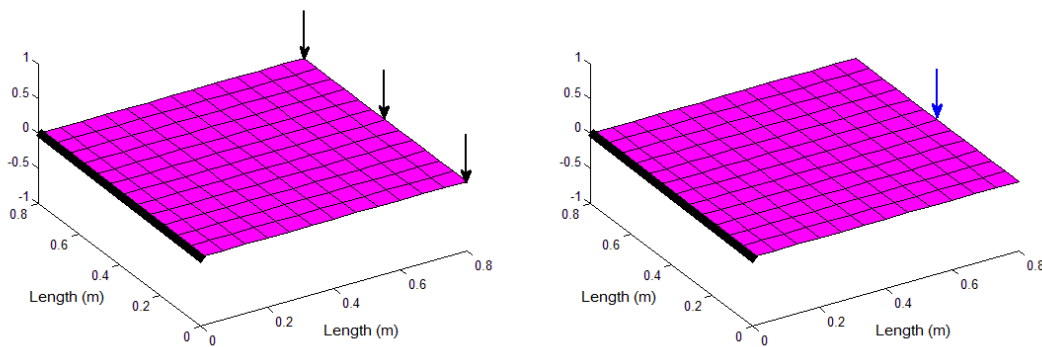
Figure 48: a. The loading points (black arrows) and b. the control node (blue arrow) for the three point loading scenario

In the following Figure 49, the transverse displacement, the velocity and the acceleration respectively, as well as the excitation and the control force at the control point (see Figure 48(b)), are shown.

With blue colour is denoted each quantity before the application of the control, while with red colour is the same value after the application of controller 1. In the last diagram with blue colour is denoted system's excitation, with red the control force, while with black colour is shown the control force rate. The results are also presented numerically in Table 5.
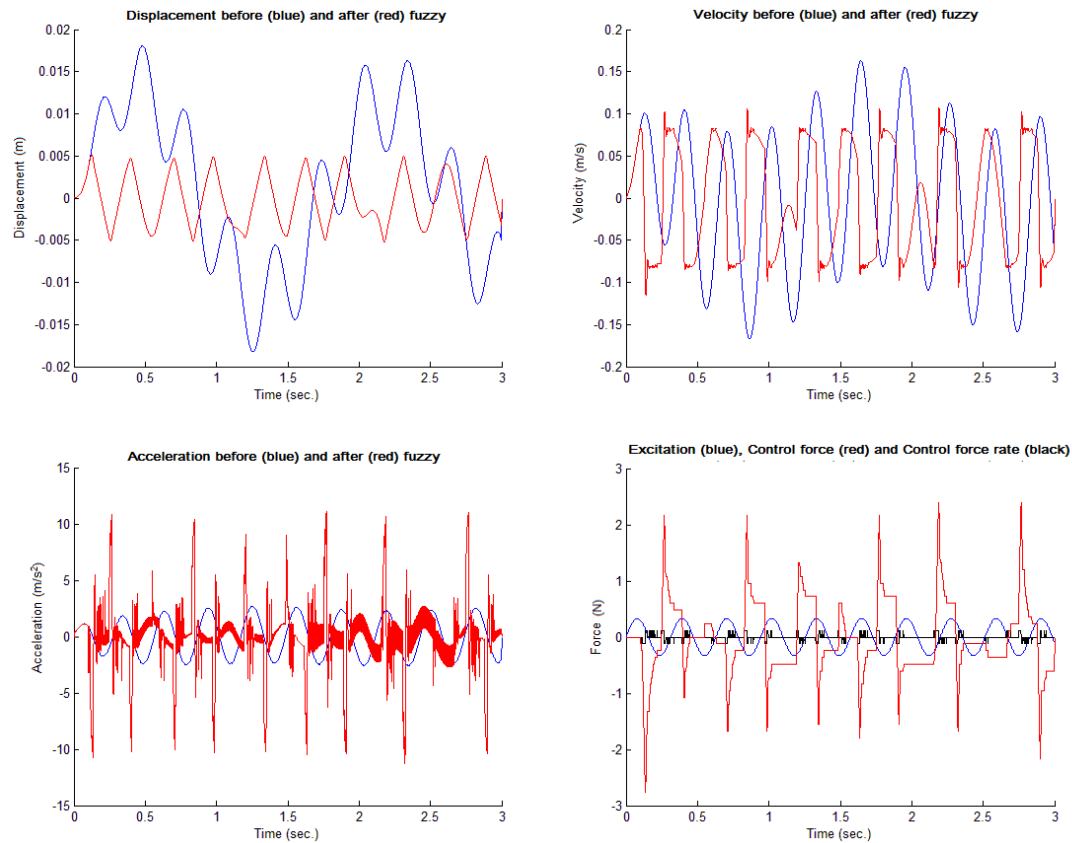
Figure 49: Displacement, velocity, acceleration and forces at the middle point of the free end (see Figure 48a) for three point loading

Table 5: Numerical results for the three-point loading scenario at the middle point of the free end (see Figure 48a)

Three point loading scenario	Max u (m)	Max $\dot{u}$ (m/s)
Uncontrolled	0.0198	0.1957
Controller 1	0.0058	0.1347
Percentage of reduction	71%	31%

From the results of Table 5, one can observe that the control strategy applied to this scenario is very efficient in terms of displacement (71% oscillation reduction) and velocity (31% reduction). Moreover, as shown in Figure 49, this kind of control is not only effective, but smooth as well. On the other hand, the results in terms of acceleration are very disappointing and a burden for the material and/or the sensors and actuators. Namely, an increase of the order of 167% in the oscillations in terms of the second derivative of displacement is derived.

6.1.1.2   Five-point loading scenario

In this case the external loading is applied to five different points across the free side of the plate, opposite to the fixed one, as shown in Figure 50(a). In Figure 50(b) is shown the position of control.
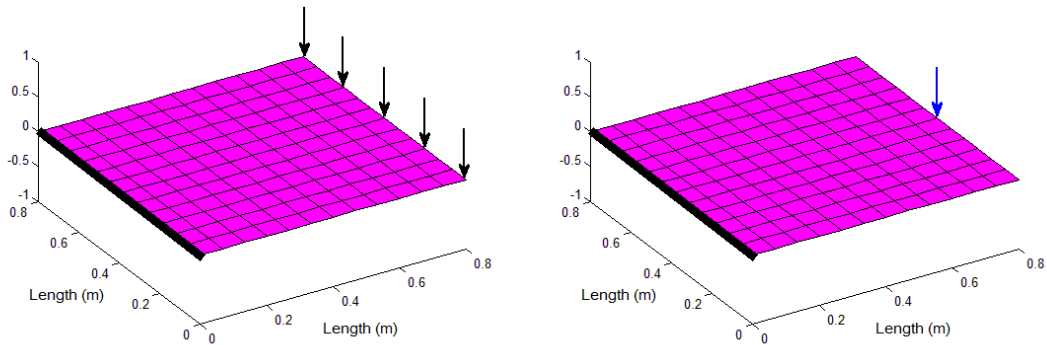

Figure 50: a. The loading points (black arrows) and b. the control node (blue arrow) for the five point loading scenario

The loading which is applied to each node in this particular case is given as:

$$P = \frac{1}{5} sin(20t) \text{ (N)} \tag{117}$$
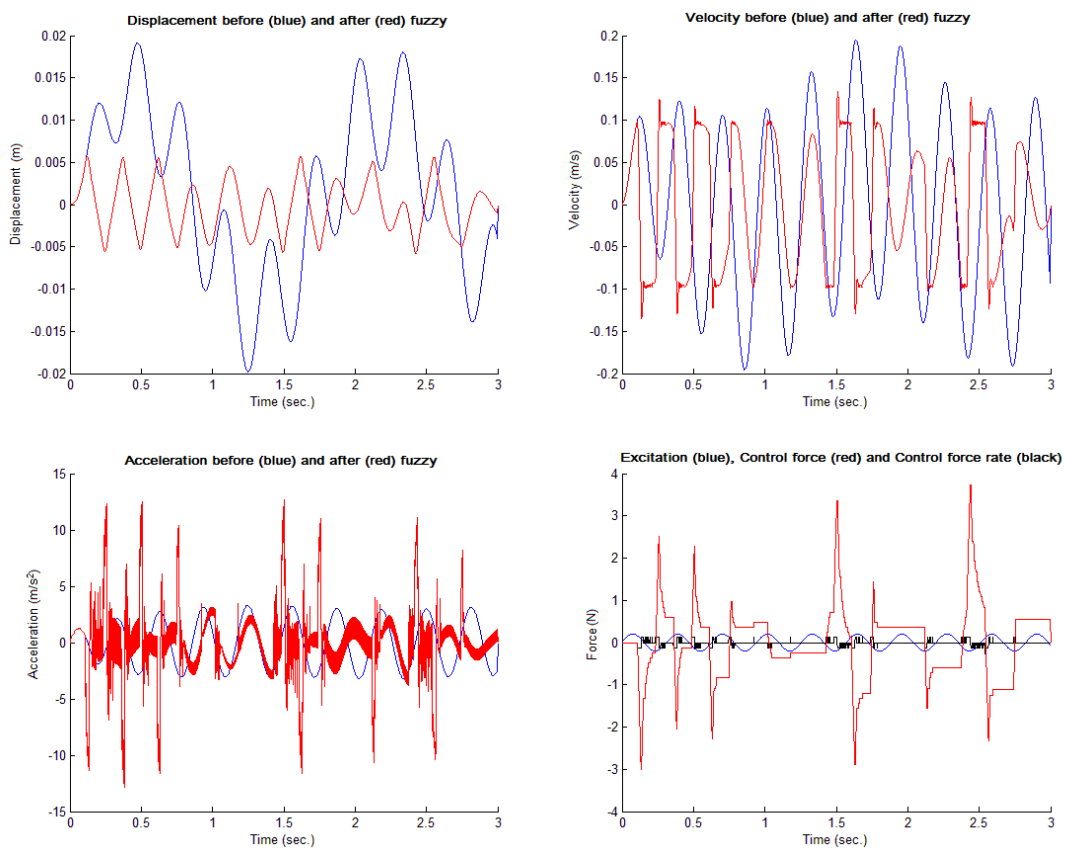
Figure 51: Displacement, velocity, acceleration and forces at the middle point of Figure 50a for five point loading

Table 6: Numerical results for the five-point loading scenario at the middle point of Figure 50a

Five point loading scenario	Max u (m)	Max $\dot{u}$ (m/s)
Uncontrolled	0.0182	0.1668
Controller 1	0.0052	0.115
Percentage of reduction	71%	31%

As seen from Figure 51 and

 Table 6, the oscillation reduction with this scenario is also very efficient. Again the displacement field is reduced by 71% and velocity by 31%. One can easily observe that these results are very similar to the ones of the previous scenario.

6.1.1.3   Comparison with a tested cantilever beam results

In order to check the robustness of the proposed control scheme, a comparison with the results of the same controller (Tairidis, et al., 2007), (Tairidis, et al., 2009), tested on a beam model is presented. The beam (see section 3.3) is made of the same material, i.e. of T300/976 graphite-epoxy composite with elasticity modulus E = 150 Gpa and density ϱ = 1600 kg/m³. The structure has a total length of 0.8 m and a square cross-section with dimensions 0.02×0.02 m.

The beam is discretized using four finite elements resulting in a model with eight degrees of freedom (see section 3.3 and section 6.3). The excitation is again of sinusoidal form, it is applied to the free end of the cantilever and it is given by:

$$P = 1 \cdot sin(20t) \ (N) \tag{118}$$

In the following figures the results of the cantilever beam described above are presented. In Figure 52, the displacement field, the velocity and the acceleration of the cantilever, as well as the forces of the system (loading and control force) are shown. The numerical results are presented in detail in Table 7. Prior to the evaluation of the results of the beam model, one may assert that they are comparable to the ones of the plate model, due to the similarity of the excitations as well as the structures themselves, i.e. material properties, dimensions, *etc*.

Table 7: Numerical results for the cantilever beam

| Beam results	Max u (m)	Max $\dot{u}$ (m/s)
Uncontrolled	$1.19 \cdot 10^{-5}$	$1.73 \cdot 10^{-4}$
Controller 1	$3.25 \cdot 10^{-6}$	$1.00 \cdot 10^{-4}$
Percentage of reduction	72.71%	42.15%
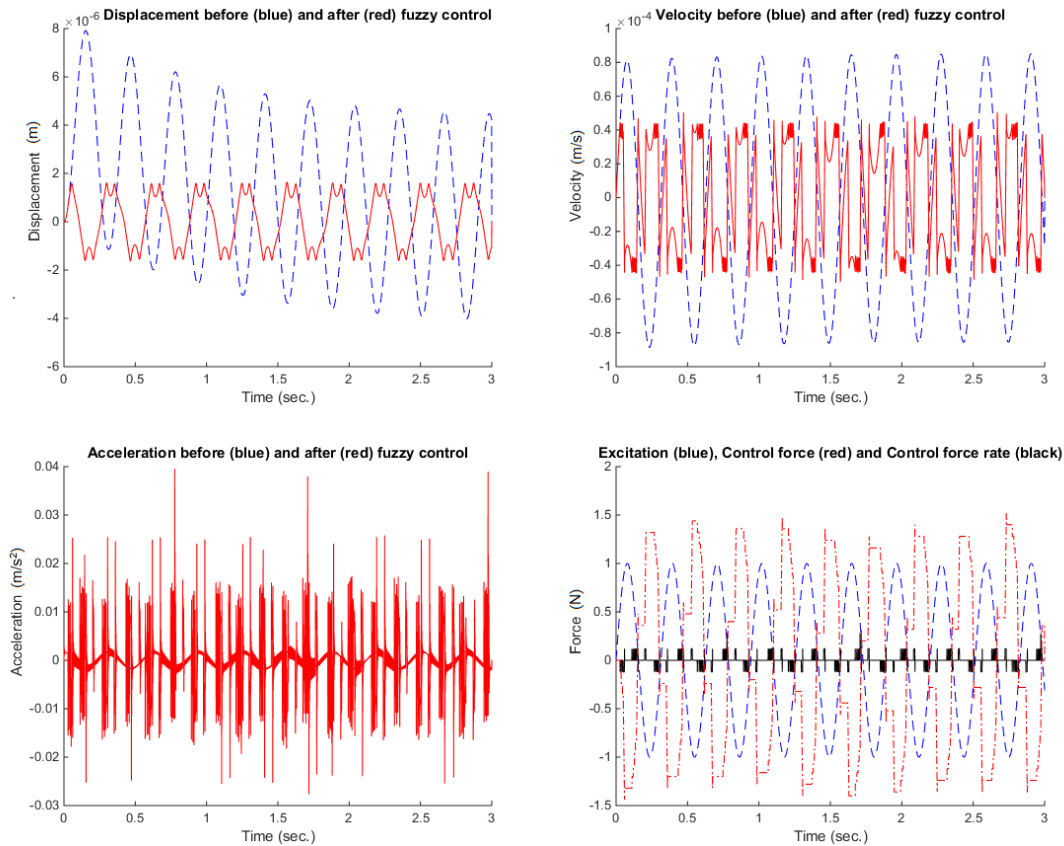
Figure 52: Displacement (m), velocity (m/s), acceleration (m/s²) and forces (N) of the beam model

Indeed, from the results of Table 7, one can conclude that the control strategy is very efficient for the beam model as well, especially in terms of displacement (72.71% reduction) and velocity (42.15% reduction). By comparison with the results of the plate model which were presented in the previous subsubsections, it is stated that the suppression of beam is slightly better in terms of displacement (72.71% instead of 71%) and velocity (42.15% instead of 31%). However, the results regarding acceleration are totally unacceptable, as an increase of almost 1400% occurs (instead of 167% for the plate, which is also unsatisfactory).

Form the results above it becomes clear, that a fine tuning of the parameters of the fuzzy controller is mandatory.

6.1.2   Optimization of fuzzy control with genetic algorithms

In this investigation, the simplified plate using fuzzy control is again considered. However, instead of the manually tuned controller 1, an optimized one was used for vibration suppression. A genetic algorithm is used for the optimization (Tairidis, et al., 2016). The objective function consists of the percentage of oscillation reduction in terms of displacement as given in equation (119).

The design variables are the possible positions of the points a, b, c and a, b, c, d that define the membership functions, of both inputs and output, for triangular and trapezoidal functions respectively, as shown in the Figure 53 below.
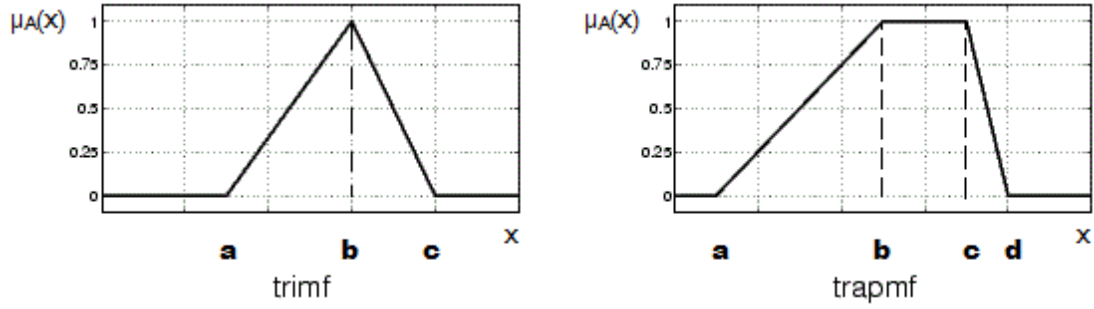
Figure 53: Plot points of triangular (a, b, c) and trapezoidal (a, b, c, d) membership function

More specifically, the objective is to maximize the following function that gives the percentage of the oscillation reduction, thus to minimize the oscillation of the structure in terms of displacement, subject to linear inequality constraints as follow.

Maximize:

$$\text{percentage(u)} = \frac{(\text{max\_displ before control}) - (\text{max\_displ after control})}{\text{max\_displ before control}} \cdot 100 \quad (119)$$

subject to:

$$x(i) < x(i+1) \tag{120}$$

$$x(j) < x(j+1) \tag{121}$$

$$x(k) < x(k+1) \tag{122}$$

where:

$$max\_displ\ before\ control = max(u\ before\ control) + |min(u\ before\ control)| \quad (123)$$

$$\text{max\_displ after control} = \text{max(u after control)} + |\text{min(u after control)}| \quad (124)$$

$$\min(u) < x(i) < max(u), i = 1, \dots, 4 \tag{125}$$

$$\min(\dot{u}) < x(j) < max(\dot{u}), j = 1, \ 2 \tag{126}$$

$$-P_0 < x(k) < P_0, \ k = 1, \dots, 8 \tag{127}$$

The membership functions are discretized in i, j or k points for each variable, i.e. the displacement, the velocity and the control force respectively, as shown in Figure 54. In order to retain the symmetry of the membership functions, the zero point is kept constant at the center of the design variables x(i), x(j) and x(k) of the horizontal axis, respectively.
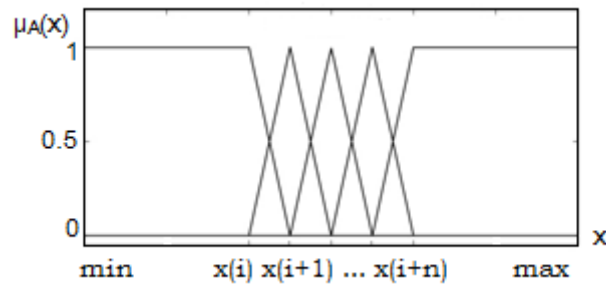
Figure 54: Discretization of membership function for optimization

For instance, in the case of the fuzzy input of displacement, which has five membership functions, the design variables are x(1) and x(2) to the left of zero (fixed point), as well as x(3) and x(4) to the right of this point. This means that in this case there are four design variables for the optimization problem. Similarly, in case of velocity, there are only two design variables, while for the optimization of the membership functions of the control force a set of eight design parameters is needed.

The genetic algorithm used for this investigation has been built within MATLAB® as part of the optimization toolbox. The parameters of the algorithm are chosen after a number of trials, taking into account the size and the special characteristics of the problem.

Finally, the `population size` is set to 20 members, that is, 20 different possible solutions. The `maximum number of generations`, which denote the number of total iterations, is set to 50. A `stopping criterion` is set in order to terminate the process after 20 generations without any improvement of the results, even if the maximum number of iteration have not been reached. The creation function for the `initial population` is chosen to be the `feasible population function`. The `tolerance` of the algorithm is set to 10^{-6} and the `penalty factor` to 100. For the modification of the population through generations `tournament selection` method is chosen. As for the main operators of the genetic algorithm, `intermediate crossover` with probability of 0.8 and `adaptive feasible mutation` are used.

During the optimization of the membership functions of the controller 1 two different scenarios are implemented. The first one concerns the optimization of the inputs only while in the second scenario the inputs, as well, the output are optimized.

The loading and the control for all applications considered in this subsection were applied to the middle of the free end of the structure as denoted by the blue arrow in Figure 55.

In all cases, a sinusoidal loading is applied, which is given by:

$$P = 1 \cdot sin(20t) \ (N) \tag{128}$$
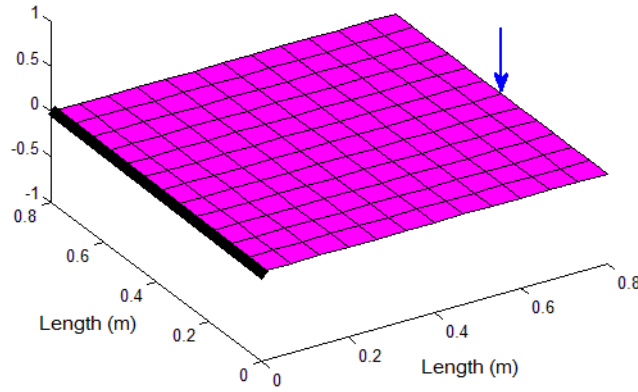
Figure 55: Loading and control point at the middle of the free end

6.1.2.1 Optimization of inputs

In the first scenario only the membership functions of the fuzzy inputs are optimized. The optimized controller 1 has the membership functions shown in Figure 56 and Figure 57 for the displacement and the velocity respectively. The membership function of the output (control force) is not modified (see Figure 33).
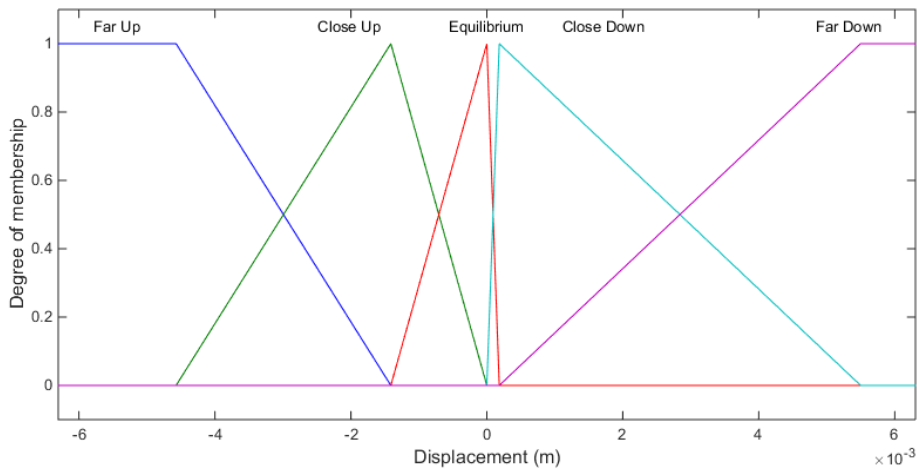

*Figure 56: Optimized membership function of displacement (optimization of inputs of controller 1)*
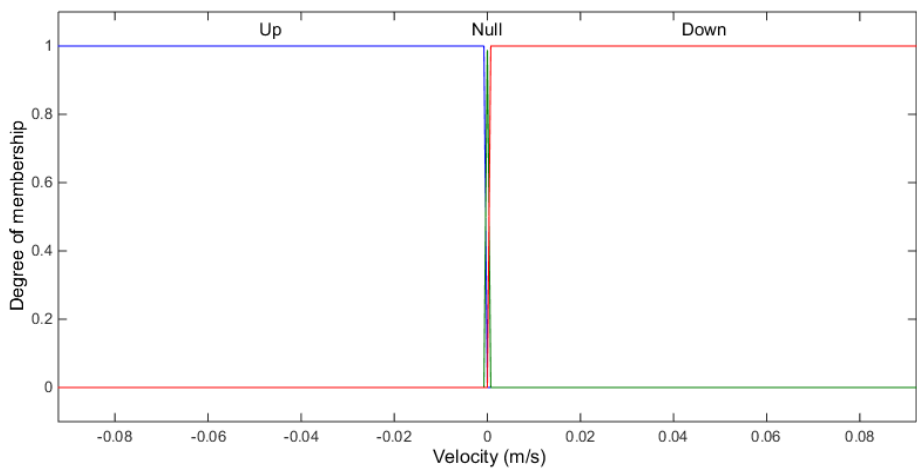
Figure 57: Optimized membership function of velocity (optimization of inputs of controller 1)

In Figure 58, the transverse displacement, the velocity, the acceleration and the forces respectively, at the control point shown in Figure 55, are presented. With blue colour is denoted each quantity before the application of any control, while with red colour is the same quantity after the application of the fuzzy optimized controller described above. As for the forces, with blue colour is denoted system's excitation, with red the control force and with black the control force rate.
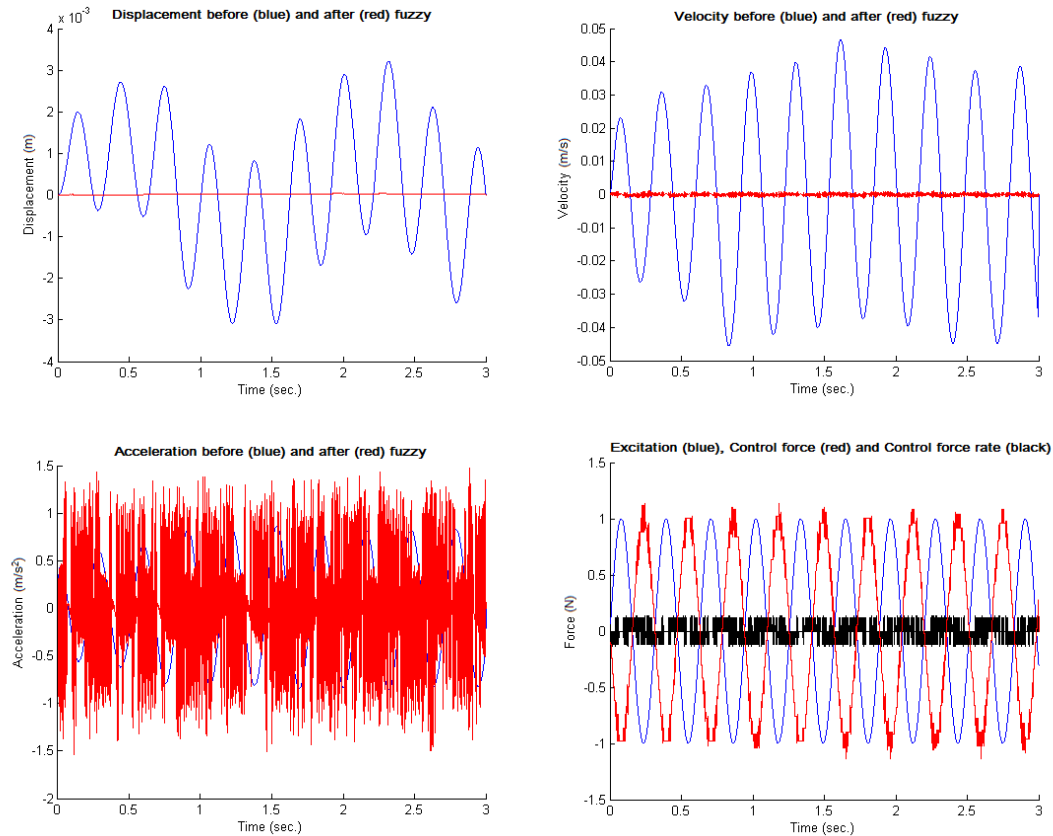

Figure 58: Displacement, velocity, acceleration and forces of the system with the optimized inputs of controller 1

Table 8: Numerical results for optimized membership functions of inputs of controller 1

Optimization of inputs	Max u (m)	Max $\dot{u}$ (m/s)	Max $\ddot{u}$ (m/s²)
Uncontrolled	0.0063	0.0921	1.7128
Optimized MFs of inputs of controller 1	4.25·10-5	0.0022	3.0063
Percentage of reduction	99.33%	97.61%	-75.52%

From the results of Table 8, one can observe that the optimized controller gives excellent results in terms of displacement, that is, an impressive 99.33% reduction. As for velocity the reduction is also very high at 97.61%. Moreover, as shown in Figure 58, this kind of control is not only effective, but smooth as well in both terms. However,

the results concerning the acceleration are very poor, as the oscillations in terms of acceleration, not only had not improved, but increased by 72.52%. At the same time, the qualitative characteristics of the second derivative of displacement are inadequate as well.

6.1.2.2   Optimization of inputs and output

Analyzing the results of the previous subsubsection, one can observe that the optimization of inputs provides very satisfactory oscillation reduction of displacement and velocity. But there is another problem to be solved, namely the oscillation of the acceleration. Again, the genetic algorithm is called, this time to optimize the membership functions of the inputs, as well as of the output.

The genetic algorithm provided the membership functions shown in Figure 59, Figure 60 and Figure 61 for the displacement, the velocity and the control force respectively.
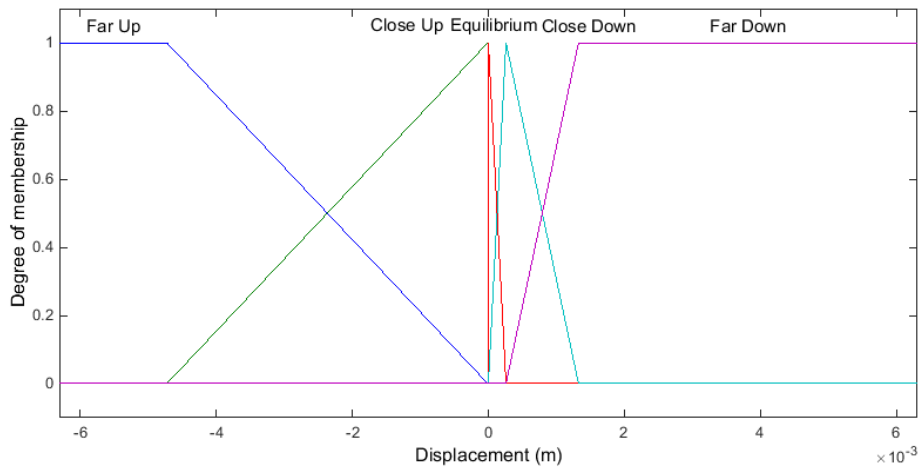

Figure 59: Optimized membership function of displacement (optimization of inputs and output of controller 1)
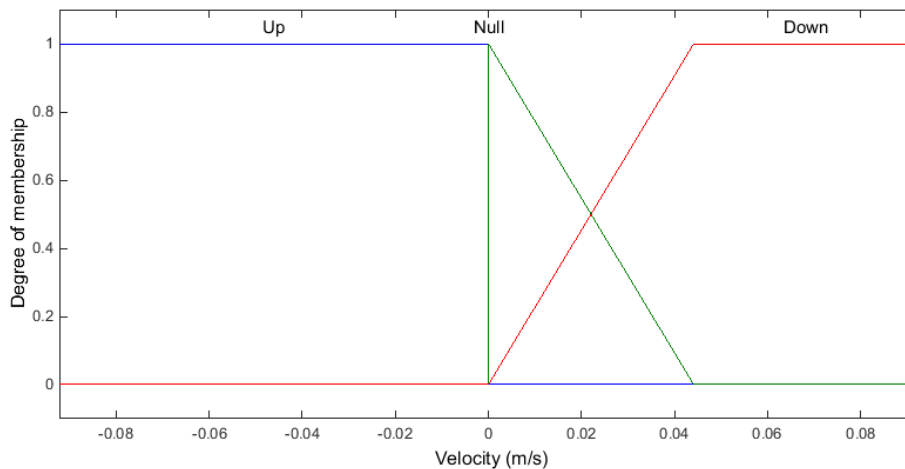

Figure 60: Optimized membership function of velocity (optimization of inputs and output of controller 1)
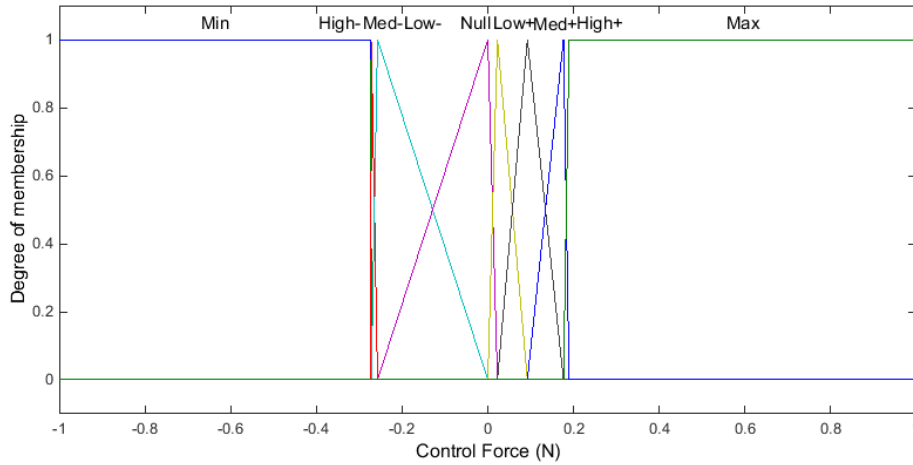
Figure 61: Optimized membership function of control force (optimization of inputs and output of controller 1)

The results which occurred for the displacement, the velocity and the acceleration, along with the loadings, are shown in Figure 62. The total vibration suppression which achieved is presented, in numerical terms, in Table 9.
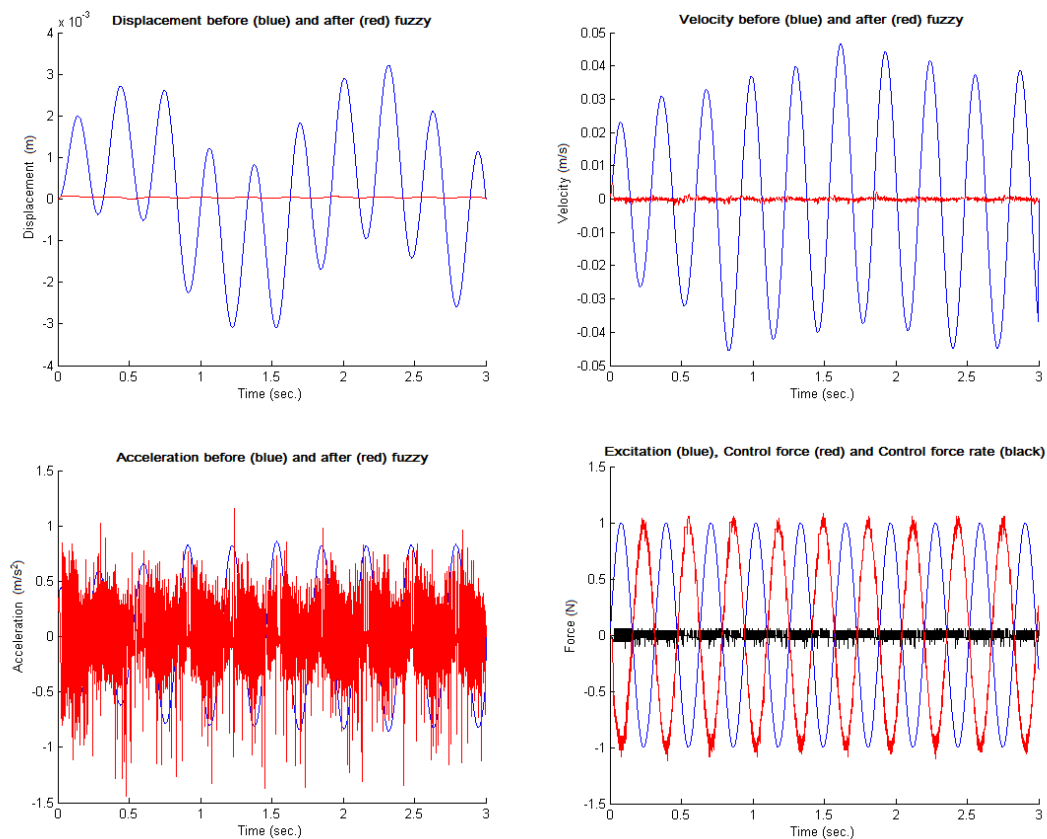

Figure 62: Displacement, velocity, acceleration and forces of the system with the optimized inputs and output of controller 1

Table 9: Numerical results for optimized membership functions of inputs and output of controller 1

Optimization of inputs and output	Max u (m)	Max $\dot{u}$ (m/s)	Max $\ddot{u}$ (m/s²)
Uncontrolled	0.0063	0.0921	1.7128
Optimized MFs of inputs and output of controller 1	7.75·10-5	0.0066	2.5982
Percentage of reduction	98.77%	92.84%	-51.69%

The oscillation reduction in this scenario is again efficient in terms of displacement. Namely the displacement field is reduced significantly by 98.77% and velocity by 92.84%. One can observe that the qualitative characteristics of the results are quite similar to the ones of the previous scenario. Thus, the problem with the acceleration remains. However, a slightly improvement is apparent, as the oscillations were increased this time by 51.69%. The graphic representation of acceleration was again non smooth, but better than in previous case. It is obvious that in this case, velocity reduction is sort of sacrificed, in order for the results concerning acceleration to be improved.

6.1.3   Further fine tuning of the fuzzy controller utilizing different defuzzification techniques

In order to achieve better and/or smoother results for the acceleration, a different fine tuning scheme, relying on the trial and error method is considered. Namely, different types of defuzzification methods are tested. This case is based on the results described in subsubsection 6.1.2.1. In this investigation, best results are given with use of the bisector and the centroid method and are presented below.

6.1.3.1   The bisector method

As mentioned in subsection 4.1.4, the bisector is the vertical line that divides a surface into two parts of equal area. Depending on the surface, it is quite common that the bisector and the centroid line coincide. The results concerning the displacement, velocity and acceleration at the given control point (see Figure 55) are shown in Figure 63. The vibration suppression achieved is presented in the following Table 10:

Table 10: Numerical results for the controller with the bisector method

| Bisector method	Max u (m)	Max $\dot{u}$ (m/s)	Max $\ddot{u}$ (m/s²)
Uncontrolled	0.0063	0.0921	1.7128
Optimized MFs of inputs of controller 1	2.12·10-5	9.07·10-4	1.2194
Percentage of reduction	99.66%	99.02%	28.81%
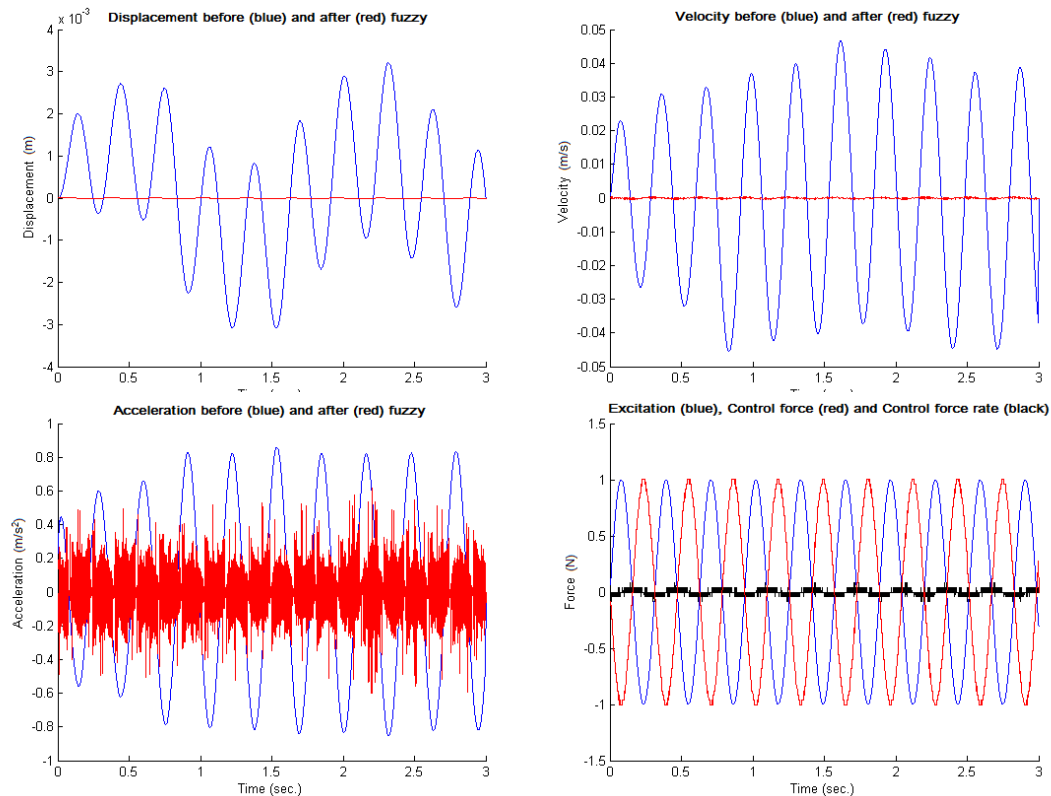
Figure 63: Displacement, velocity, acceleration and forces of the system with the bisector method

From the results given in Table 10, one can observe that along with the impressive reduction of both displacement and velocity, for the first time there is a significant reduction of the oscillations by 28.81% in terms of acceleration as well. It seems that the change of the defuziffication method was beneficiary.

However, the problem with the qualitative characteristics of the acceleration remains, therefore, further improvement is sought.

6.1.3.2   The centroid method

As seen from the results above, the oscillation reduction which achieved using the bisector as defuzzification method, was very satisfactory. However, in order to improve further the results for the acceleration, the centroid method is tested.

In this method (see subsection 4.1.4), the defuzzification process returns the center of the area that exists under the curve of the membership functions that participate in the result. If this area is of equal density, this method gives the point along the x axis at which the shape would balance, that is the center of gravity of the surface. The results for the displacement, velocity and acceleration at the control point (see Figure 55) are shown in Figure 64. The vibration suppression achieved, is presented in Table 11.

From these results one can observe that along with the impressive reduction of both displacement and velocity by 99.86% and 99.64% respectively, significant reduction is achieved also in terms of acceleration by 74.05%. A slight problem which lies in the qualitative characteristics of the oscillatory acceleration remains, but nonetheless, one

can clearly observe that the use of the centroid method for defuzzification, provides a significant reduction of oscillation in every field, including acceleration.
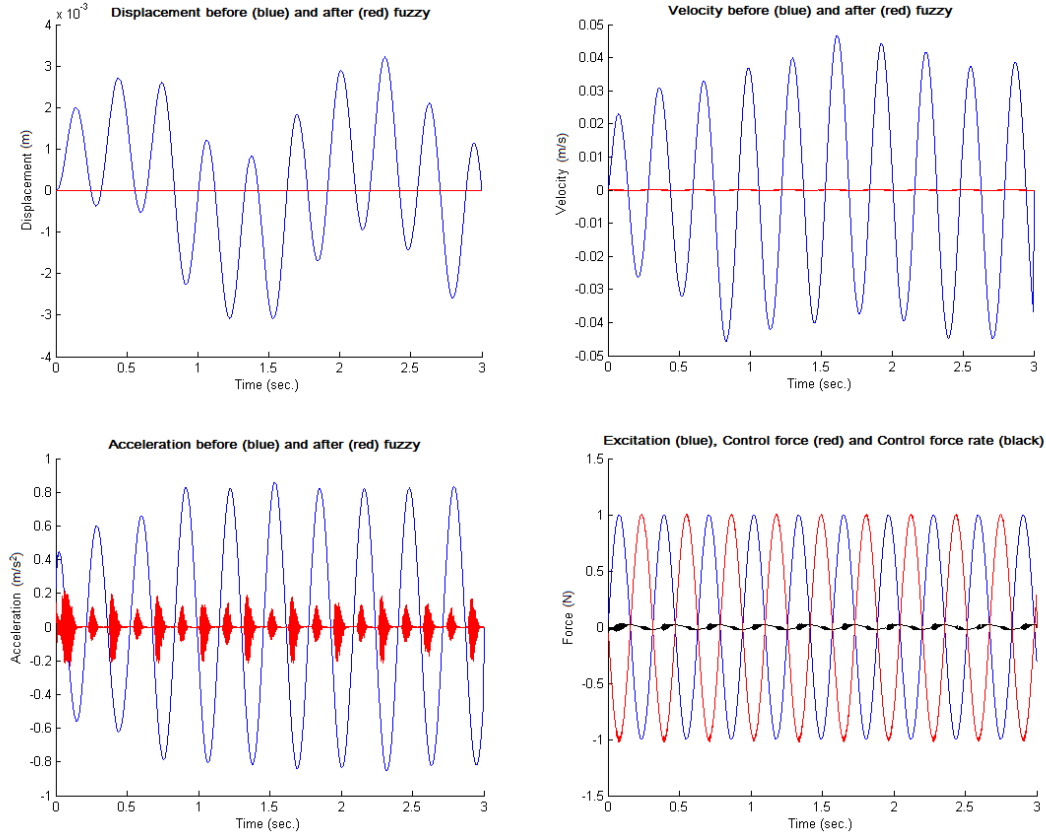

Figure 64: Displacement, velocity, acceleration and forces of the system with the centroid method

Table 11: Numerical results for the controller with the centroid method

Centroid method	Max u (m)	Max $\dot{u}$ (m/s)	Max $\ddot{u}$ (m/s²)
Uncontrolled	0.0063	0.0921	1.7128
Optimized MFs of inputs of controller 1	0.0880	$3.32 \cdot 10^{-4}$	0.4446
Percentage of reduction	99.86%	99.64%	74.05%

6.1.4   Comparison with the results of controller 1 prior optimization

The optimized and fine-tuned mamdani-type fuzzy controller tested in subsection 6.1.2 (Tairidis, et al., 2016) is quite comparable with the one tested in subsection 6.1.1 (Tairidis, et al., 2014). The plate model has exactly the same characteristics in both cases and the same external loading is considered. Namely, an excitation, again of sinusoidal form is chosen and applied to the middle of the free end of the plate (see Figure 55).

This excitation is given by:

$$P = 1 \cdot sin(20t) \ \ (\text{N}) \qquad\qquad (129)$$

Thus, a comparison is not only feasible, but desirable as well. In the following figures this comparison is presented. Namely, the displacement, the velocity and the acceleration field, along with the excitation and the control force of the two models are shown.

From the results below, one can observe that after the optimization of the characteristics of the controller, the oscillation reduction achieved is significantly greater. Namely, a reduction by 99.86% instead of 68.78% for displacements, 99.64% instead of 32.87% for velocities and 74.05% instead of -244.69% for accelerations is observed. At the same time, the results were smoother as well.

It is also notable that the control forces needed in order to obtain this reduction were significantly lower. More specifically, the total width of the control force for the case of the non-optimized controller is 4,88 N, which is more than two times the total width of the excitation which is 2.00 N, as shown in Figure 68. In fact, the optimized controller produces a control force that is equal to the excitation, which is more reasonable and desirable.
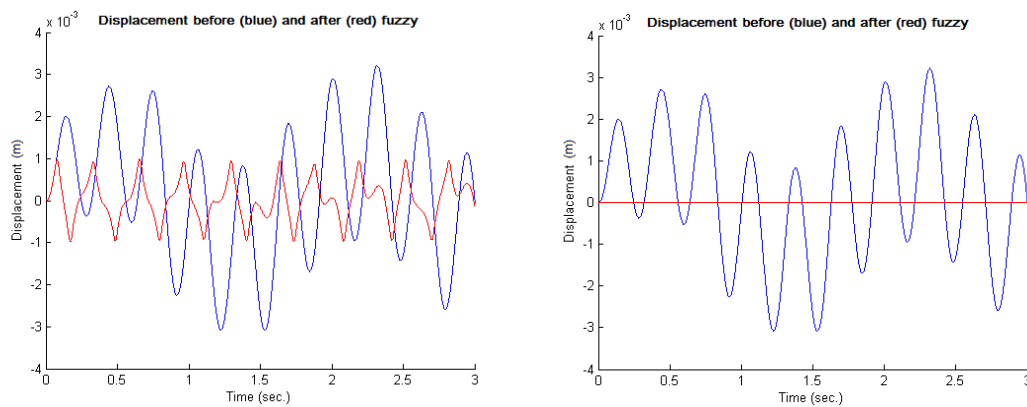

*Figure 65: Displacement of the plate before and after the optimization of control*
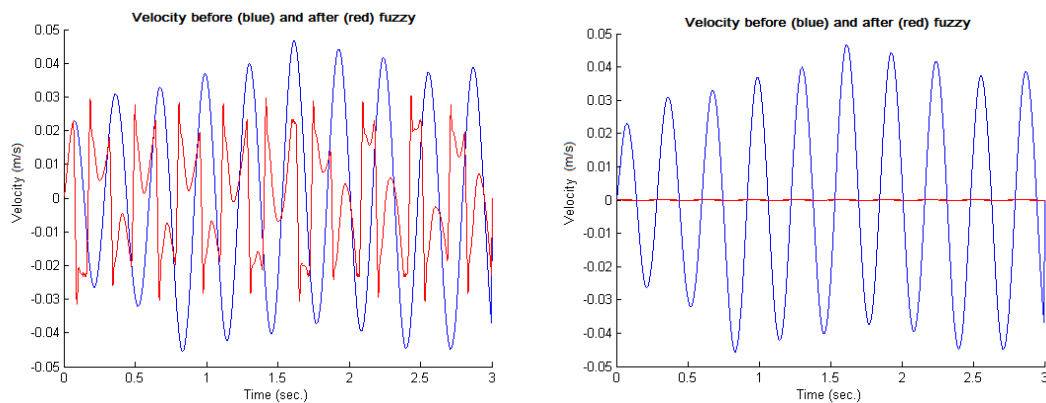
Figure 66: Velocity of the plate before and after the optimization of control
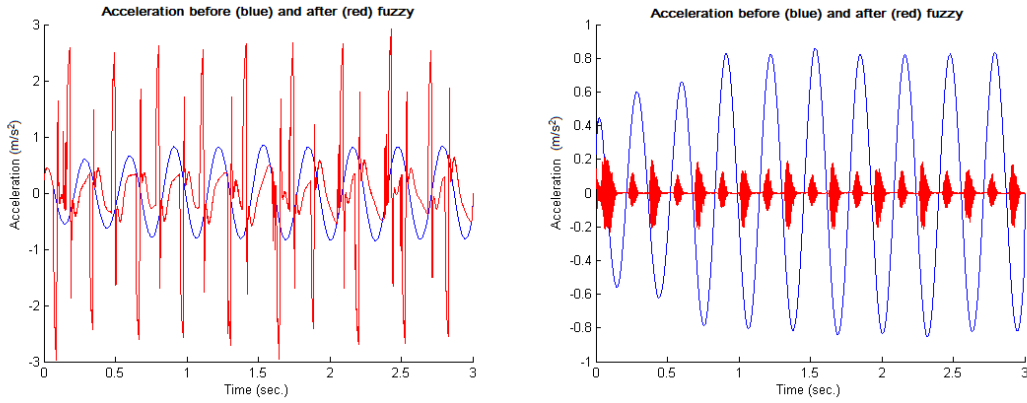
*Figure 67: Acceleration of the plate before and after the optimization of control*
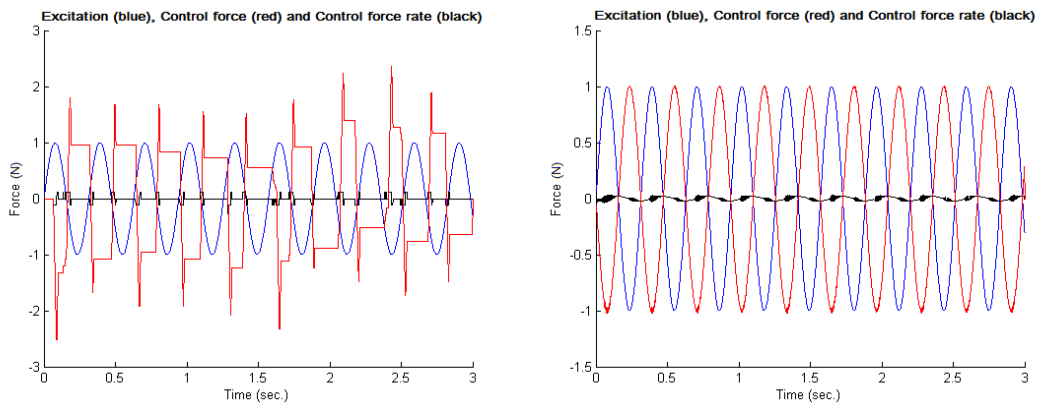
Figure 68: Excitation and control force of the plate before and after the optimization of control

6.1.5   Investigation for various excitation frequencies

In order to test the functionality of the optimized controller proposed in subsection 6.1.2 a further investigation checking the oscillation reduction achieved under different external loading conditions is carried out. For this purpose, sinusoidal loadings of the form $P = P_o \cdot sin(\omega t)$, for various frequencies ω, are considered. In the investigations of this subsection, the optimized and fine-tuned controller of subsubsection 6.1.3.2 is used. The loadings are applied at the middle point of the free end of the plate as mentioned above (see Figure 55).

Firstly, the frequency is set equal to 15 rad/sec, thus an external loading of the following form is considered:

$$P = 1 \cdot sin(15t) \ \ (\text{N}) \tag{130}$$

The application of the optimized fuzzy controller 1 at the given smart plate, is shown in Figure 69. The vibration suppression achieved is presented in the

Table 12.
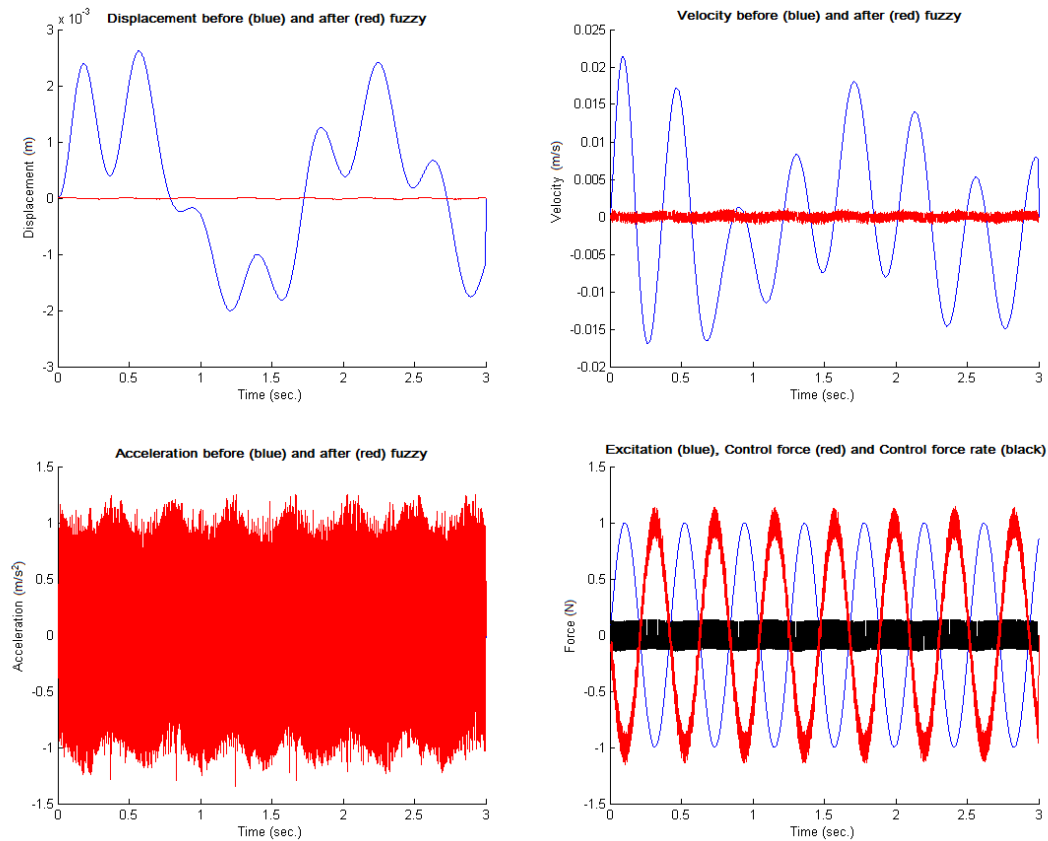
Figure 69: Displacement, velocity, acceleration and forces of the system under a loading with frequency 15 rad/sec.

Table 12: Numerical results for the controller with the centroid method and loading of freq. 15 rad/sec

ω = 15 rad/sec.	Max u (m)	Max $\dot{u}$ (m/s)	Max $\ddot{u}$ (m/s²)
Uncontrolled	0.0046	0.0383	0.7054
Optimized MFs of inputs of controller 1	$2.57 \cdot 10^{-5}$	0.0021	2.5963
Percentage of reduction	99.44%	94.41%	-268.07%

One can easily observe that even if a high reduction of oscillations is achieved in terms of displacement and velocity, however the acceleration is augmented by more than 268%. This is definitely unacceptable. As for the control force, only a slight augmentation to the width, 2.29 N instead of the optimum 2.00 N of excitation, is observed.

In another investigation, the frequency is set equal to 25 rad/sec, thus an external loading of the following form is considered:

$$P = 1 \cdot sin(25t) \ \text{(N)} \tag{131}$$

The results of the simulation of the smart plate are shown in Figure 70. The vibration suppression achieved is presented in the

Table 13 below:
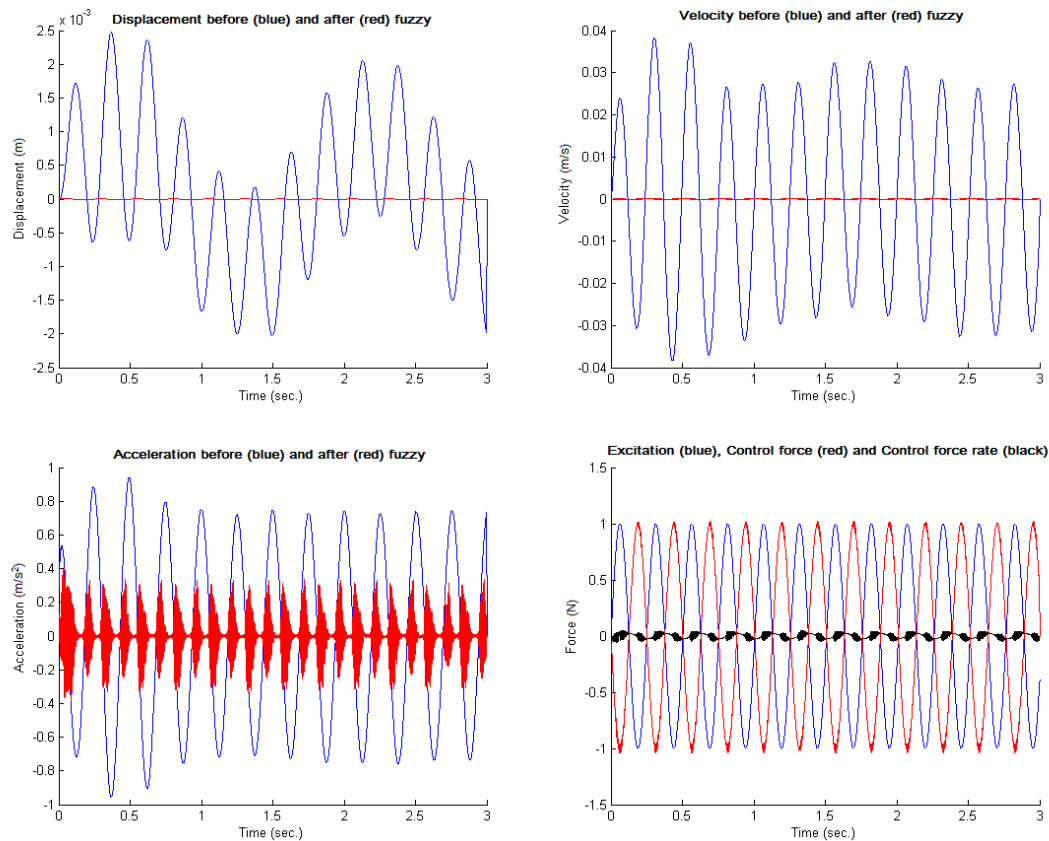
Figure 70: Displacement, velocity, acceleration and forces of the system under a loading with frequency 25 rad/sec.

Table 13: Numerical results for the controller with the centroid method and loading of freq. 25 rad/sec

ω = 25 rad/sec.	Max u (m)	Max $\dot{u}$ (m/s)	Max $\ddot{u}$ (m/s²)
Uncontrolled	0.0045	0.0767	1.9004
Optimized MFs of inputs of controller 1	$8.51 \cdot 10^{-6}$	$4.61 \cdot 10^{-4}$	0.7809
Percentage of reduction	99.81%	99.40%	58.91%

From the results of the present simulation, one can observe that a significant reduction of the oscillations of the displacement (99.81%), velocity (99.4%) and acceleration (58.91%) is achieved. Again, the results regarding acceleration are not smooth enough.

The width of the control force equals 2.06 N, which is very close to the let say optimum 2.00 N of excitation.

In the ultimate investigation, the frequency is set at 30 rad/sec, i.e. the external loading is of the following form:

$$P = 1 \cdot sin(30t) \ \ (\text{N}) \tag{132}$$

The oscillation suppression achieved in terms of displacement, velocity and acceleration is presented in Figure 71 and Table 14.

One can observe that a significant reduction of the oscillations of displacement (99.78%), velocity (99.46%) and acceleration (76.92%) is achieved. This is the best result regarding acceleration which is achieved with the maximum suppression, near 100% of displacement and velocity fields.

The width of the control force in this case equals to 2.03 N, which is even most close to the optimum width 2.00 N of excitation.
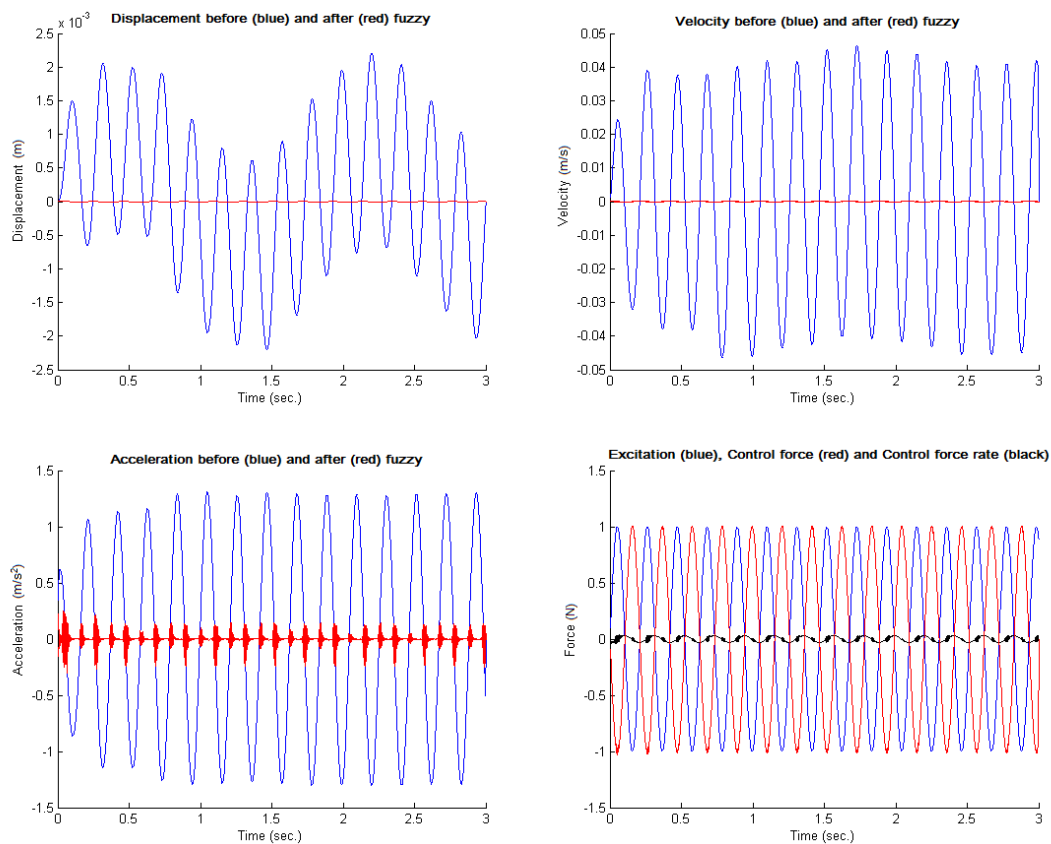
Figure 71: Displacement, velocity, acceleration and forces of the system under a loading with frequency 30 rad/sec.

Table 14: Numerical results for the controller with the centroid method and loading of freq. 30 rad/sec

ω = 30 rad/sec.	Max u (m)	Max $\dot{u}$ (m/s)	Max $\ddot{u}$ (m/s²)
Uncontrolled	0.0044	0.0928	2.6116
Optimized MFs of inputs of controller 1	$9.51 \cdot 10^{-6}$	$4.97 \cdot 10^{-4}$	0.6028
Percentage of reduction	99.78%	99.46%	76.92%

6.1.6   Optimization of fuzzy control with particle swarm optimization

In the present investigation, the controller's parameters were fine-tuned using the inertia particle swarm optimization method (Tairidis, et al., 2015).

The optimization algorithm which is used here is included in the optimization toolbox package of MATLAB®. The parameters of the algorithm are chosen with the trial and error method, taking into account the size of the problem, the computational cost and the desired accuracy.

Namely, the inertia range is set to [0.1, 1.1], the maximum number of iterations to 50, the self-adjustment and the social-adjustment parameters of the algorithm to 1.49, the stall iteration limit is set to 10 iterations and the swarm size is chosen to be 4 particles.

The characteristics of the algorithm, such as the inertia range and the cognitive, as well as the social parameter are chosen based on criteria for PSO stability given in literature. For further information see section 5.2, (Perez & Behdinan, 2007), (Marinaki, et al., 2011), (Marinaki, et al., 2011b).

The main objective of the control, is the minimization of the oscillations of the structure, or in other words the maximization of the percentage of the vibration reduction. Thus, the problem can be considered a problem of maximization of the quotient of the ratio of the difference between the maximum displacement before and after control, to the maximum displacement before control.

The design variables x_1, x_2 and x_3 of the algorithm are coefficients which adjust the range of the membership functions of the three fuzzy variables (two inputs and one output) of the fuzzy controller.

The initial controller's ranges were set to [-0.0077, 0.0077] for the displacement and to [-0.1209, 0.1209] for the velocity respectively. The values 0.0077 and 0.1209 were the maximum displacement and the maximum velocity respectively and were calculated by solving the dynamic system without control. The initial ranges for the force were set to [-1, 1]. However, we shared it to three different points (nodes), that is, the range of the membership function of the output, i.e. the control force, changed to [-1/3, 1/3].

The tuning of these ranges is the object of the investigation. The idea is to find the ranges of fuzzy inputs that maximize the vibration reduction. The design variables take values between 0 and 1, thus the range can be a percentage of the maximum values mentioned above. The optimization results (coefficients) are multiplied with the initial ranges yielding the new tuned ranges.

Particle swarm optimization has the advantage that needs lower computational power compared to other methods, like genetic optimization. On the contrary, it is more sensitive to local optima. In the present problem, strong local optima and/or non-convexity does not exist, making the use of this method suitable. Moreover, due to the simplicity of the optimization problem only a small number of iterations along with a

small size of swarm is needed. However, the results are very satisfactory as it will be shown below.

As mentioned above, the loading is applied to three nodes. These nodes correspond to the upper corner, the middle point and the lower corner of the free side of the plate respectively, as shown in Figure 72(a). The position of control is shown with blue arrow in Figure 72(b).
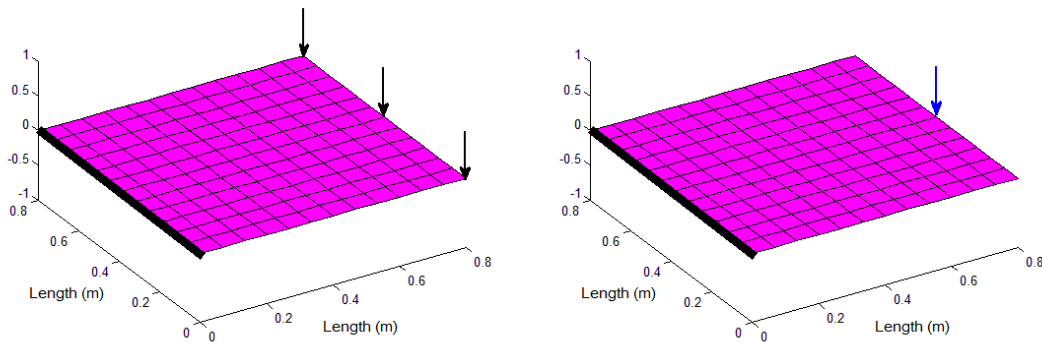

Figure 72: a. The loading nodes (black arrows) and b. the control node (blue arrow)

The loading that is applied to each node is given by:

$$P = \frac{1}{3} \cdot sin(20t) \ \ (N) \tag{133}$$

It is already shown that the vibration suppression of the smart plate before the optimization of the controller's parameters (Tairidis, et al., 2014) was 71% for displacements and 31% for velocities. On the other hand the acceleration field increased by 167% (see subsection 6.1.1).

One can observe that even if the reduction of displacement and velocity is not negligible, the appearance of so high accelerations is a burden for the structure and the piezoelectric devices, since they lead to material fatigue and discomfort problems. Thus, the optimization of the controller's parameters is quite necessary.

In order to achieve this goal, two different cases were considered. The first one deals with the optimization of the ranges of the membership functions of inputs and output, while in the second case the tuning of solely the inputs' ranges is performed.

6.1.6.1 Tuning of the ranges of fuzzy inputs and output

In this tuning scenario, we try to optimize the parameters of the inputs and of the output of the fuzzy inference system. This means that the ranges of the membership functions of displacement and velocity, as well as of the control force have changed. The particle swarm optimization algorithm returns the new ranges as follows. As for the two inputs of the controller, the new ranges occurred as a percentage of 34.04% of the maximum displacement and 25.51% of the maximum velocity respectively. The range for the output variable derived to be at the 95.93% of the maximum force width.

The recurring membership functions, which occurred through the optimization process, are shown in the following figures.
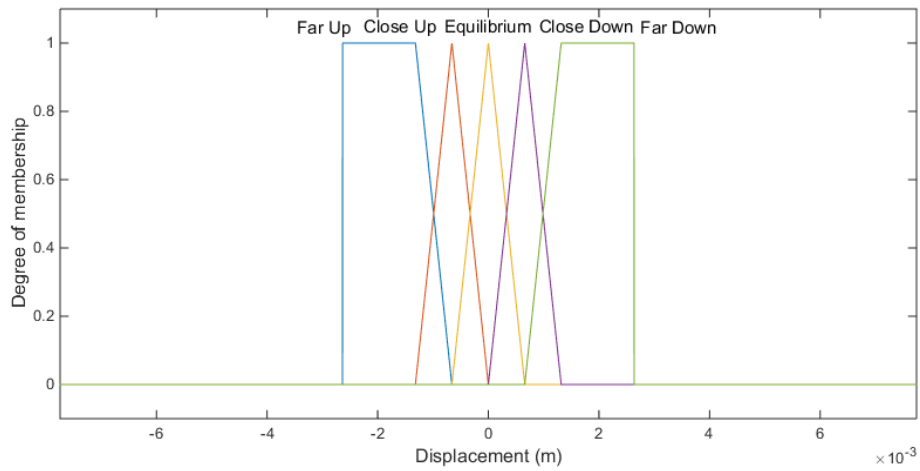

Figure 73: Membership functions of displacement (input 1) after optimization of inputs and output
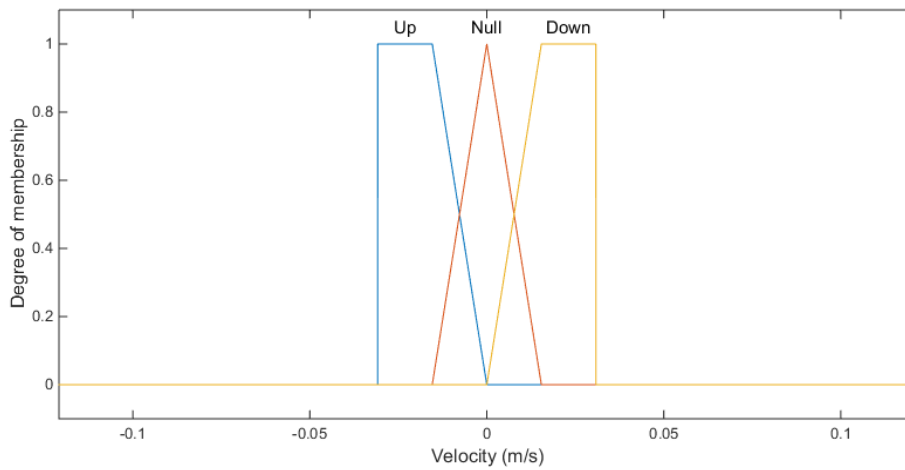

Figure 74: Membership functions of velocity (input 2) after optimization of inputs and output
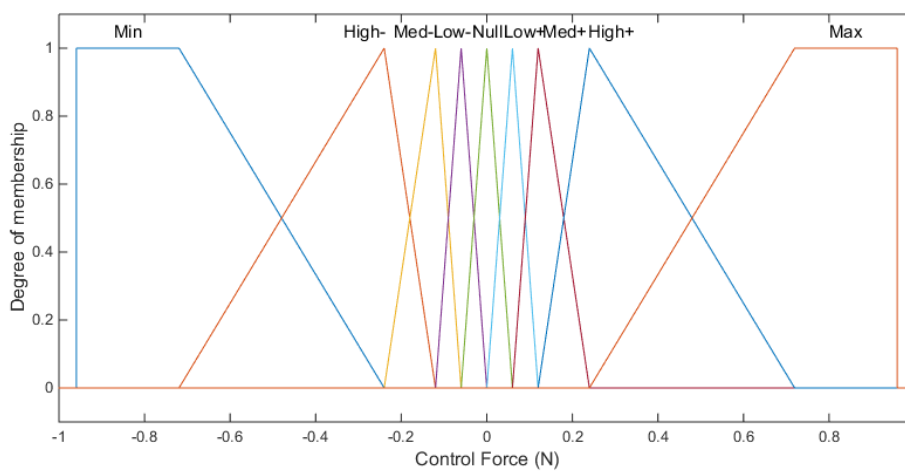

Figure 75: Membership functions of control force (output) after optimization of inputs and output

The new optimized fuzzy controller reduced oscillations by 90.59% for displacement. The velocity reduced by 79.78%, while acceleration was again increased by 115.72%. This increase of the acceleration is a serious problem that demands further tuning of the fuzzy controller. Schematically, these numerical results are shown in Figure 76. Another deficiency is that the control force is high.
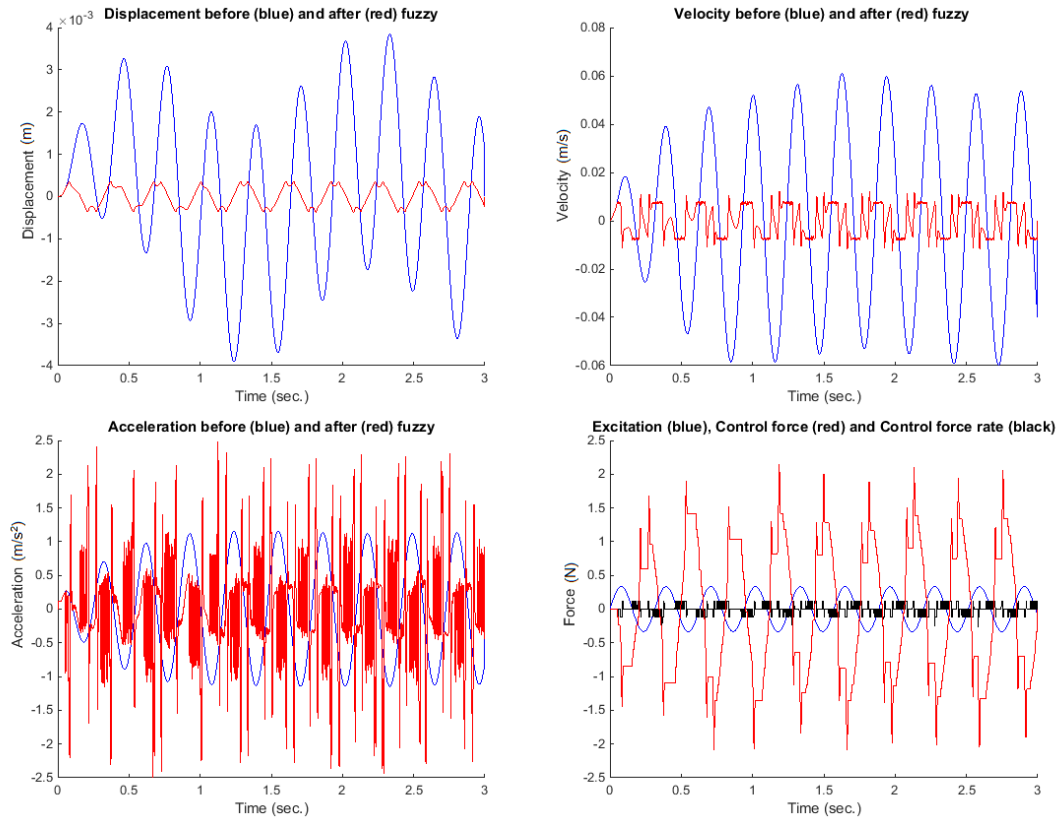

Figure 76: Displacement, velocity, acceleration and forces at the middle of the free end of the structure after optimization of inputs and output

6.1.6.2 Tuning of the ranges of the fuzzy inputs only

From the previous tuning scenario, one can easily observe that the range of the membership functions of the output, practically, remain unchanged, or if we want to be precise, changes slightly (only by 4%). Namely, the value of maximum control force that came from the optimization process was 0.96 instead of 1. For this reason and in order to simplify more the optimization problem, only the ranges of the fuzzy inputs are tuned. Thus, the recurring optimization problem has only two design variables, that is, the range of each input of the fuzzy system; the displacement and the velocity.

From the optimization process, the particle swarm algorithm provided the new ranges for the two inputs of the controllers as a percentage of 69% of the maximum displacement and 5.5% of the maximum velocity, which are quite different from the ones of the previous scenario. The membership function of the output remained, as said, unchanged. The membership functions that occurred, are shown in the following figures.
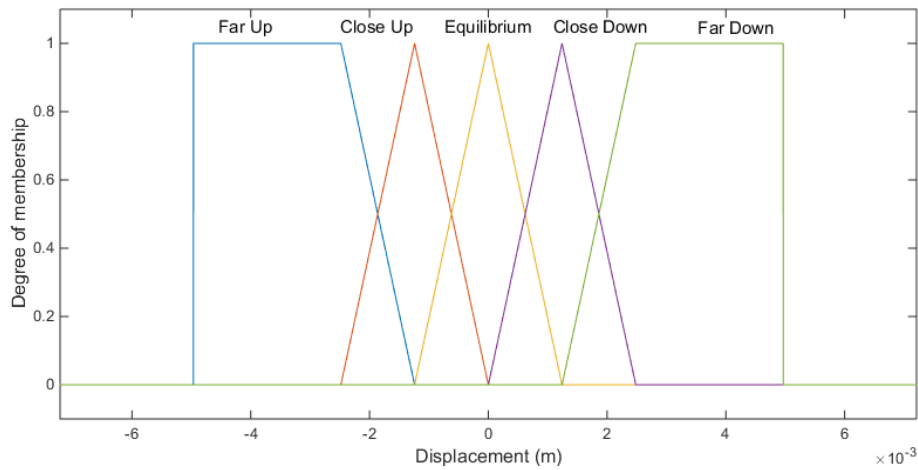
Figure 77: Membership functions of displacement (input 1) after optimization of inputs
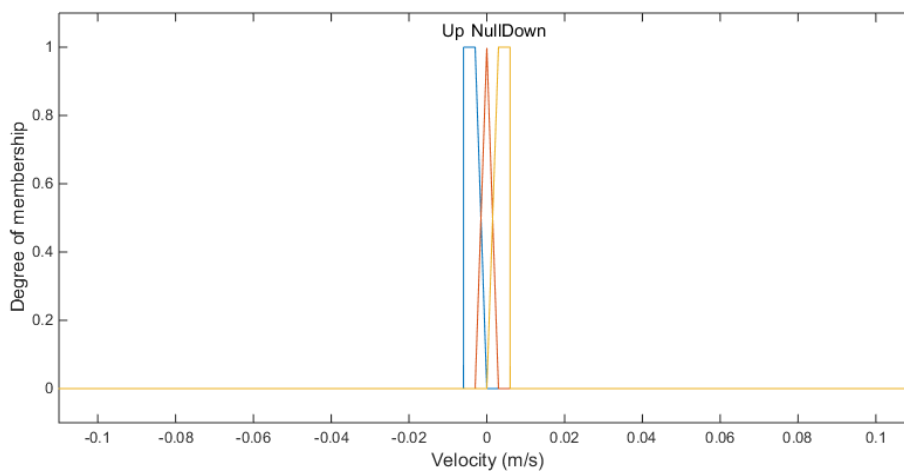
Figure 78: Membership functions of velocity (input 2) after optimization of inputs
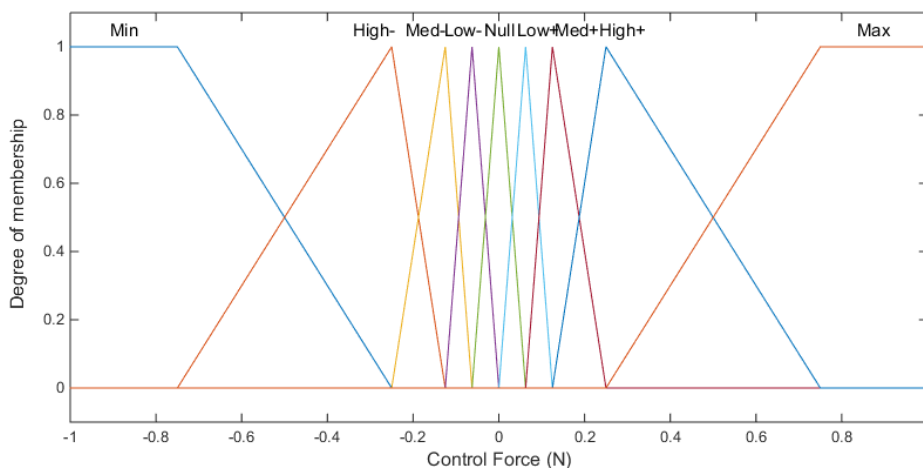
Figure 79: Membership functions of control force (output) after optimization of inputs

The control with these tuned ranges is proved very efficient in terms of displacement and velocity. The reduction of the displacement was 96.35%, while velocity reduced by 96.64%. The acceleration again increased, but only by 6.10%, which is much better than the 167% that appeared before the tuning and the 115.72% that occurred in the

previous scenario. This means that the controller's performance was improved, how-ever, further refinement is possible. The results are shown schematically in Figure 80.
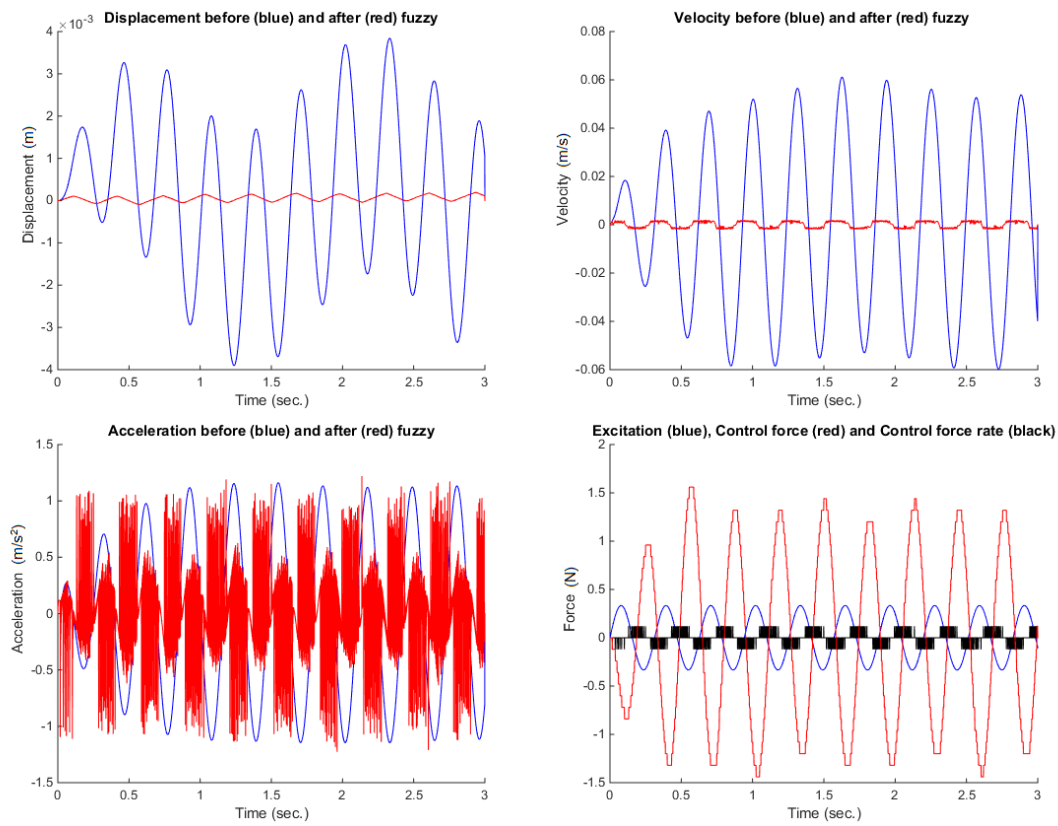
Figure 80: Displacement, velocity, acceleration and forces at the middle of the free end of the structure after optimization of inputs only

6.1.6.3   Further tuning by changing the defuzzification method

As one can easily observe from the results in the previous subsubsection, the reduction of displacement and velocity is very sufficient and smooth as well. As for the acceler-ation, even if the results have improved significantly, they remain rough. For this pur-pose some further fine tuning is done by changing the defuzzification methods. The best results produced by the centroid method.

In this case, both displacement, velocity, and acceleration filed reduced significantly. These results as shown schematically in Figure 81. Namely, the displacement reduced by 99.35%, the velocity by 98.98% and acceleration by 95.89%. Moreover, even if the control force needed for the suppression is obviously higher than the external force, its form is smooth enough as it is shown in the figure below.

As shown in the latter case, the vibration suppression achieved by the tuned controller is exceedingly satisfactory, for both displacement and velocity and even for accelera-tion. The results were very smooth as well.
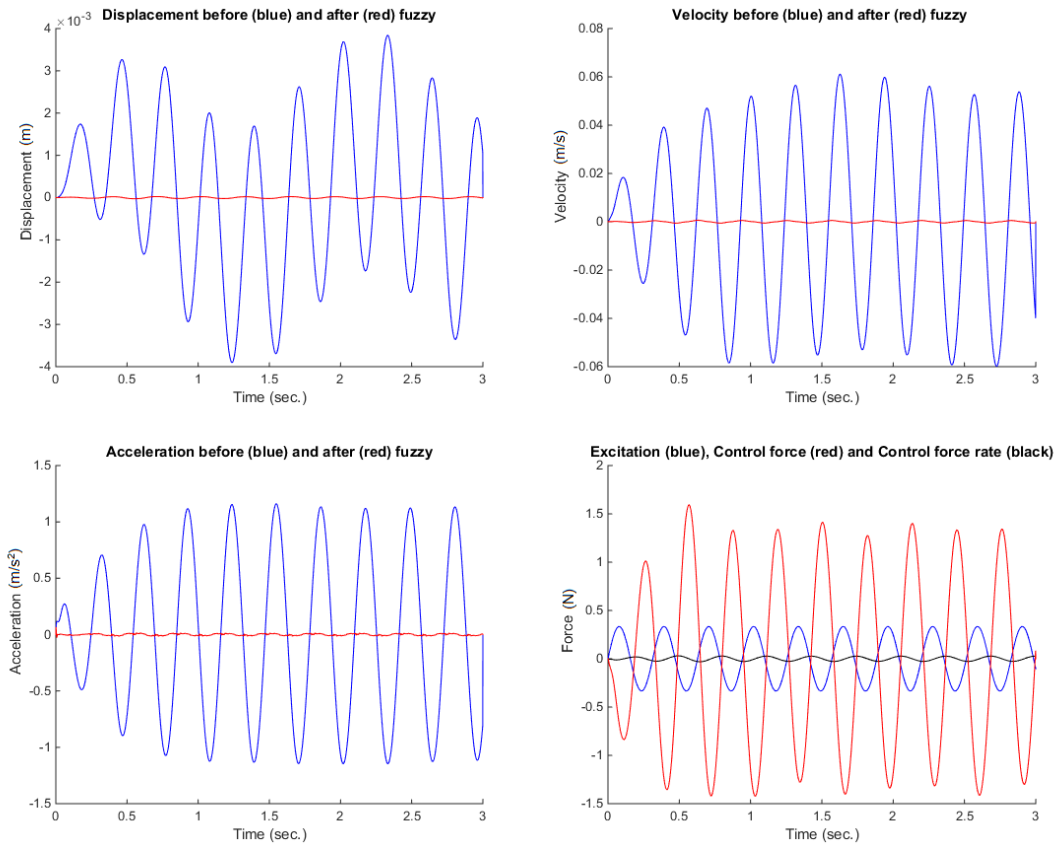
Figure 81: Displacement, velocity, acceleration and forces at the middle of the free end of the structure after optimization of inputs and selecting centroid method

6.2   Fuzzy control of smart plates in the presence of delamination

In this section, fuzzy control of smart plates under delamination conditions is examined (Tairidis, et al., 2015b), (Koutsianitis, et al., 2015), (Koutsianitis, et al., 2016), (Koutsianitis, et al., 2016b). In order to be able to describe delamination phenomena, one may consider a layerwise model with adhesive material, as the one described in section 3.5.

The plate model considered for this investigation is shown in Figure 7. The material properties of the composite structure are given in the following Table 15. Further information can be obtained from (Han & Lee, 1998).

The stacking sequence of the plate is [0/±45/90]. The dimensions of the structure are 100mm × 100mm × 1.3mm. 10 × 10 isoparametric elements are used for the analysis and realistic boundary conditions (RBC) are chosen, yielding to a system of 100 elements. Each finite element consists of 12 nodes and every node has 5 degrees of freedom (three translational and two rotational). Therefore, the structure has 363 nodes and 1815 degrees of freedom. The mesh of the structure is shown in the following Figure 82.

Table 15: Material properties of the composite plate with piezoelectrics and adhesive material

Property	Graphite/epoxy	Adhesive	Piezoceramic
E_1 (GPa)	130	1.78	59
E_2 (GPa)	9.6	1.78	59
G_{12} (GPa)	4.8	-	-
G_{23} (GPa)	3.2	-	-
ν_{12}	0.31	0.3	0.34
ϱ (kg/m³)	1570	1050	7400
$d_{31} = d_{32}$ (m/V)	-	-	$-260 \cdot 10^{-12}$
Ply thickness (mm)	0.1	0.05	0.2
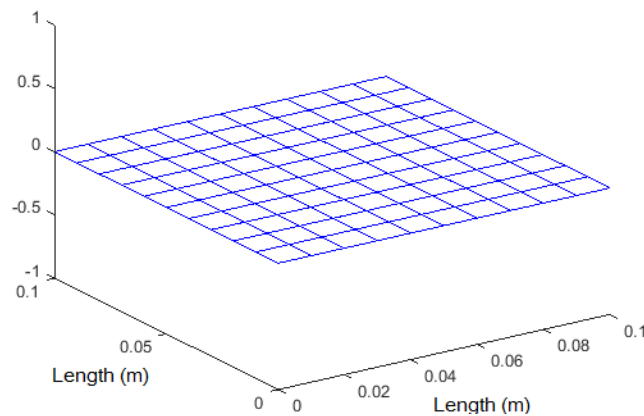
Figure 82: Plate discretized with finite elements

Figure 83 presents the three layers of the structure. Note that the upper layer is used as actuator, the middle layer represents the elastic core of the beam (graphite/epoxy), while the lower layer is used as sensor. One can observe that the numbering of nodes starts from the lower layer and is continuing to the other two.

It is also worth mentioning that the use of RBC is fundamental for the accurate prediction of the parameters of the closed loop system. This is due to the fact that piezoelectric components are able to actuate more effectively. In this context, fuzzy control is used for the vibration suppression of the multilayered plate both before and after the appearance of delamination. The main objective is the construction of robust controllers, which could be able to keep functioning under failure conditions, even if they are initially set without considering such phenomena.
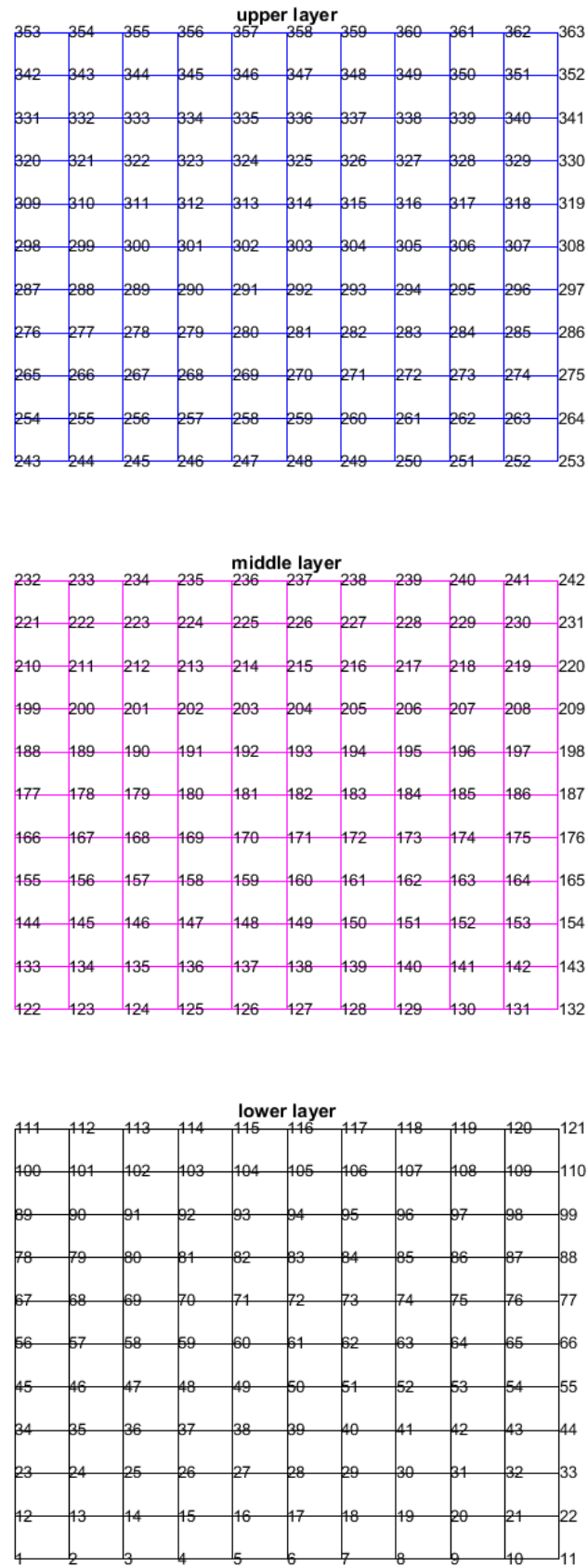
Figure 83: Numbering of nodes for the three layers of the structure

We have tested two settings for the control structure, the so-called mechanical and electromechanical models as presented in subsections 4.5.1 and 4.5.2 respectively. In the mechanical model measurements are taken directly from the nodes of the structure and control forces are applied directly to the same nodes (collocated configuration). This setting is more suitable for the experimental environment. On the other hand, in the electromechanical model the measurements are taken and the control forces are applied on the piezoelectric layers and through them, related to the mechanical quantities of the composite structure.

In the first case, the measurements (data) for the inputs of the fuzzy control (controller 1) are received from a single node of the lower layer, and namely, from the node which is located at the center of the free end of the structure. The control force is applied perpendicularly to the plate (in the direction of z-axis), and more specifically, to the node 308 (see Figure 83), which is the node at the central point of the free end of the upper piezoelectric layer which is used as actuator as shown in Figure 84.
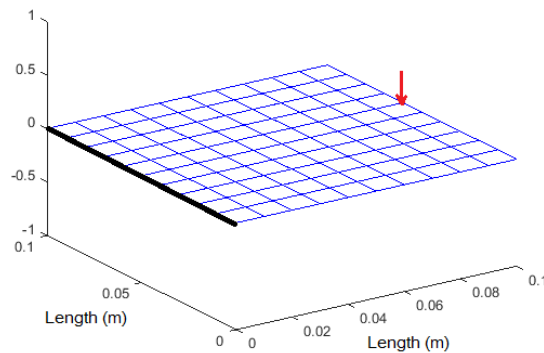
Figure 84: Application of control in the mechanical model

On the other hand, the mode of functioning of the coupled electromechanical model is completely different. In that case, the measurements for the inputs of the control (controller 2) are again taken form an element of the lower piezoelectric layer (see sub-subsection 6.2.2.2), however, the electric control signal (voltage) is transferred to the upper layer which acts like an actuator. The control forces are not perpendicular to the plate's surface, but are applied through the piezoelectric phenomenon at the piezoelectric layer in the direction of x and y axes as shown in Figure 85. These forces produce bending moments which are acting to the whole structure.
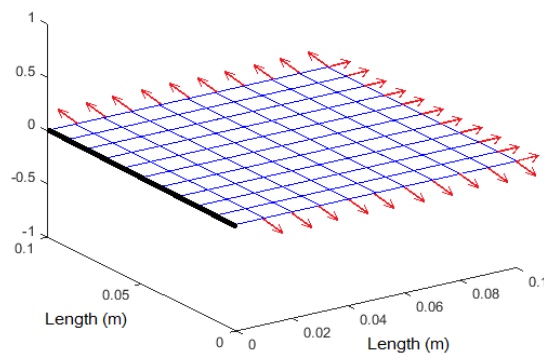
Figure 85: Application of control in the coupled electro-mechanical model

It is noteworthy that these forces are transferred to the edge nodes that remain glued. This means that in case of delamination at one node, the forces of this node are transferred to the closest glued node.

Another major difference between the two models, lies to the way that measurements are received from the sensor patch. In the mechanical model, as seen above, the measurements are taken from a single node. In the coupled electromechanical model, the inputs of the control are taken from a certain element of the sensor patch. Obviously, in case of delamination of this element, the control stops functioning.

The delamination of the piezoelectric patch may occur either to the upper, or the lower layer, which means that either the sensor or the actuator can peel off. The results for both cases are presented below.

6.2.1   Delamination of the sensor layer

Firstly, the behavior of the controller, which was initially designed for the control of non-delaminated composite structures, is tested for delaminated plates with different delamination rates of the lower layer, i.e. of the sensor (Tairidis, et al., 2015b).

For this investigation the mechanical model is considered, that is, controller 1 is used. Due to the presence of delamination, the controller takes different data for inputs and output. The investigations were carried out for 10%, 50% and 90% delamination levels of the interface (glue) material.

The measurements are taken from node 66 of the lower layer, that is, at the center of the free end of the structure (see Figure 83 and Figure 84). The external loading is applied to five nodes of the middle layer and more specifically to nodes 132, 154, 187, 220 and 242 (see Figure 83) and is of the form:

$$P = \frac{1}{5} \cdot sin(20t) \ \ (\text{N}) \tag{134}$$

6.2.1.1   10% delamination of the sensor

In the first case, the composite plate presents 10% loss of the piezoelectric material as shown in Figure 86. The displacement, velocity, acceleration and the forces before (blue line) and after (red line) control are shown in Figure 87.

From the diagrams, one can observe that a significant suppression in terms of displacement, velocity and acceleration is achieved. This means that the behavior of the structure and the operation of the controller are very satisfactory.
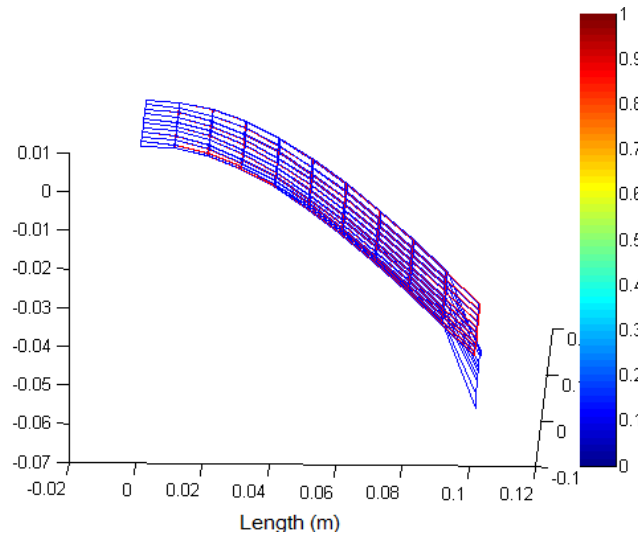
Figure 86: Plate with 10% delamination
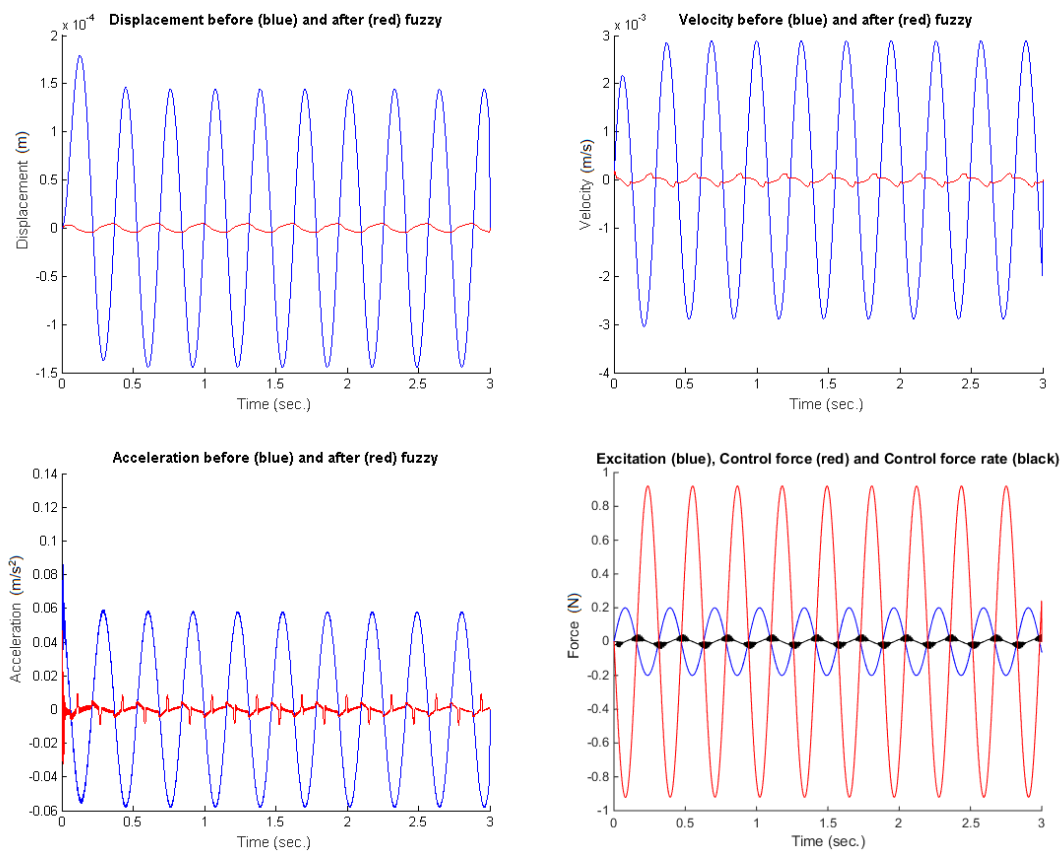
Figure 87: Displacement, velocity, acceleration and forces with 10% delamination

6.2.1.2   50% delamination of the sensor

Consequently, a model with delamination equal to the 50% of the piezoelectric material of the sensor is studied (see Figure 88). The displacement, velocity, acceleration and the forces before (blue line) and after (red line) control are shown in Figure 89.
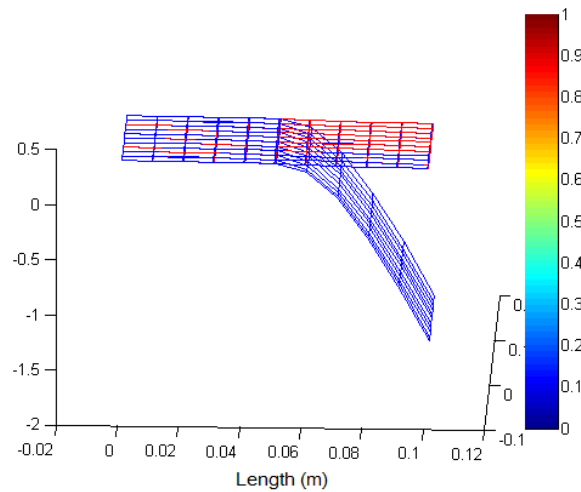
Figure 88: Plate with 50% delamination
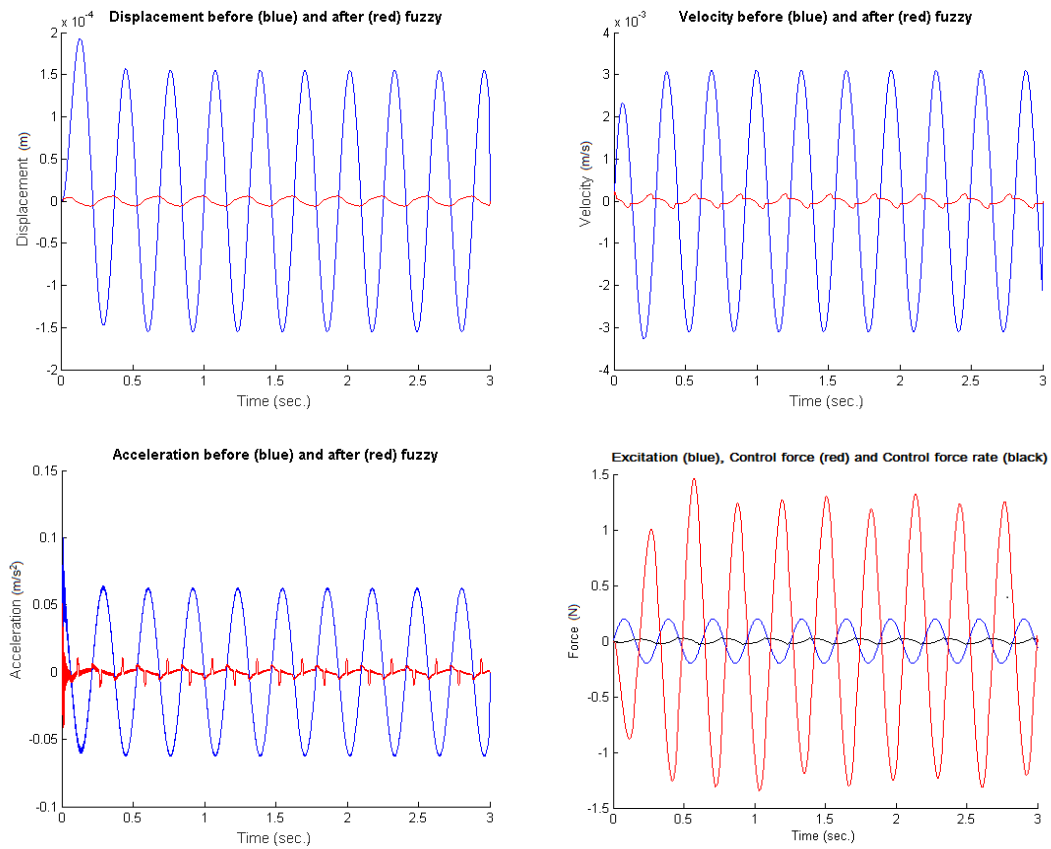
Figure 89: Displacement, velocity, acceleration and forces with 50% delamination

The vibration suppression in terms of displacement, velocity and acceleration is again satisfactory. A small increase in the amplitude of the displacement, velocity and acceleration before control appears due to the modification of stiffness. However, the controller continues functioning well, as in the case of the model with 10% delamination.

6.2.1.3 90% delamination of the sensor

Finally, a study was conducted with 90% delamination of material (see Figure 90). The
results are shown in Figure 91.
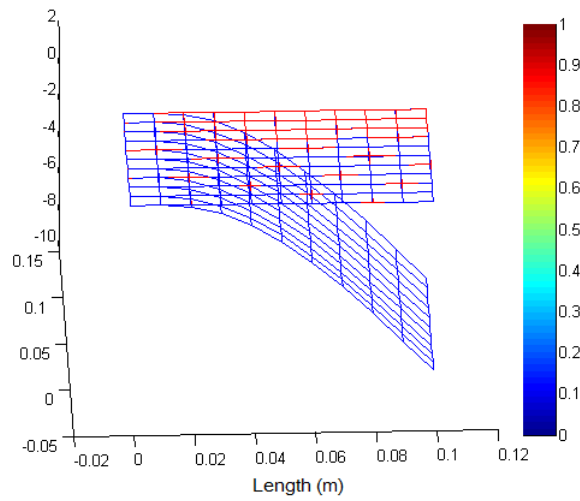
Figure 90: Plate with 90% delamination
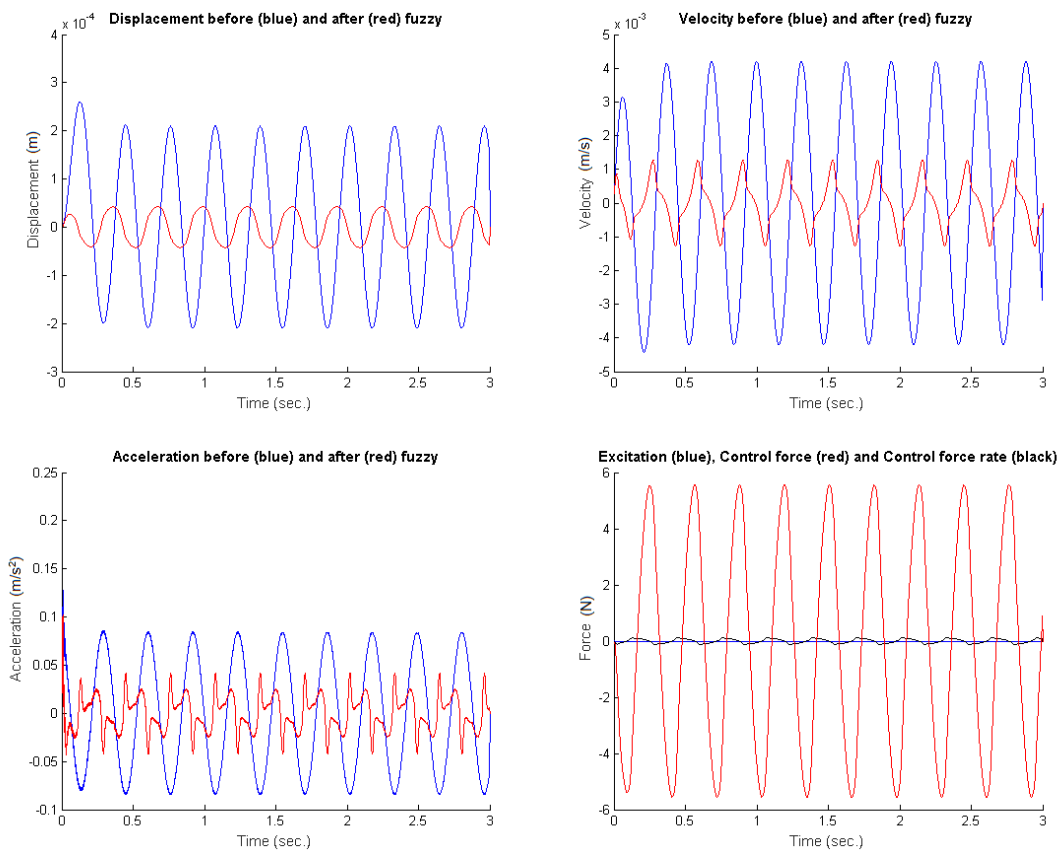
Figure 91: Displacement, velocity, acceleration and forces with 90% delamination

In this latter case of extensive delamination of the piezoelectric layer, some useful con-
clusions are made, not only for the functionality of control, but for the behavior of the
structure as well. It is obvious that the control gives worst results compared to the
previous cases, however it provides quite satisfactory vibration suppression in terms

of displacement, velocity and even acceleration, at the cost of a much larger control force. As for the structure, one can observe that the amplitude of displacement, velocity and acceleration are increased. This is due to the fact that the structural dynamics of the plate have changed.

In this case, the presence of delamination on the sensor layer may have affected the performance of the controller, but not to the extent that the controller has not a decent effect on the structure.

It is notable that the results above were obtained from the fuzzy controller 1 without use of any optimization method for fine tuning.

It is also worth mentioning that in case of delamination of the sensor layer, and especially of the element where the measurements are taken, the control does not function at all when the coupled electromechanical model is considered.

6.2.2   Delamination of the actuator layer

For the study of delamination of the actuator level, a different strategy is considered. For this investigation both the mechanical, as well as the electromechanical model are considered. In the first case controller 1 is used, while in the second scenario controller 2 is called.

An external loading of sinusoidal form is applied to five nodes of the free end of the structure as shown in Figure 92.
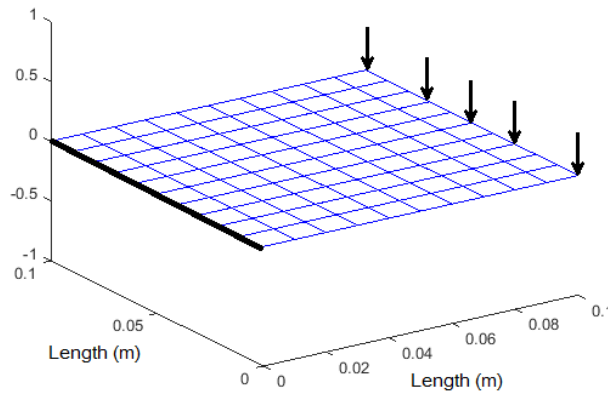
Figure 92: Nodes of application of loading

The loading at each node is of the form:

$$P = \frac{1}{5} \cdot sin(20t) \ \ (N) \tag{135}$$

6.2.2.1   Results for the mechanical model

In this investigation, the efficiency of the proposed control scheme (controller 1) is examined for different grades of delamination of the actuator layer. First, the scenario of the absence of delamination is considered. The case of 50% delamination is following.

6.2.2.1.1   Delamination of 0% of the actuator for the mechanical model

The results for the non-delaminated structure are shown in Figure 93 and Table 16. With blue color is denoted the vibration before the application of control, while with red color is shown the response of the structure after the application of the fuzzy controller.
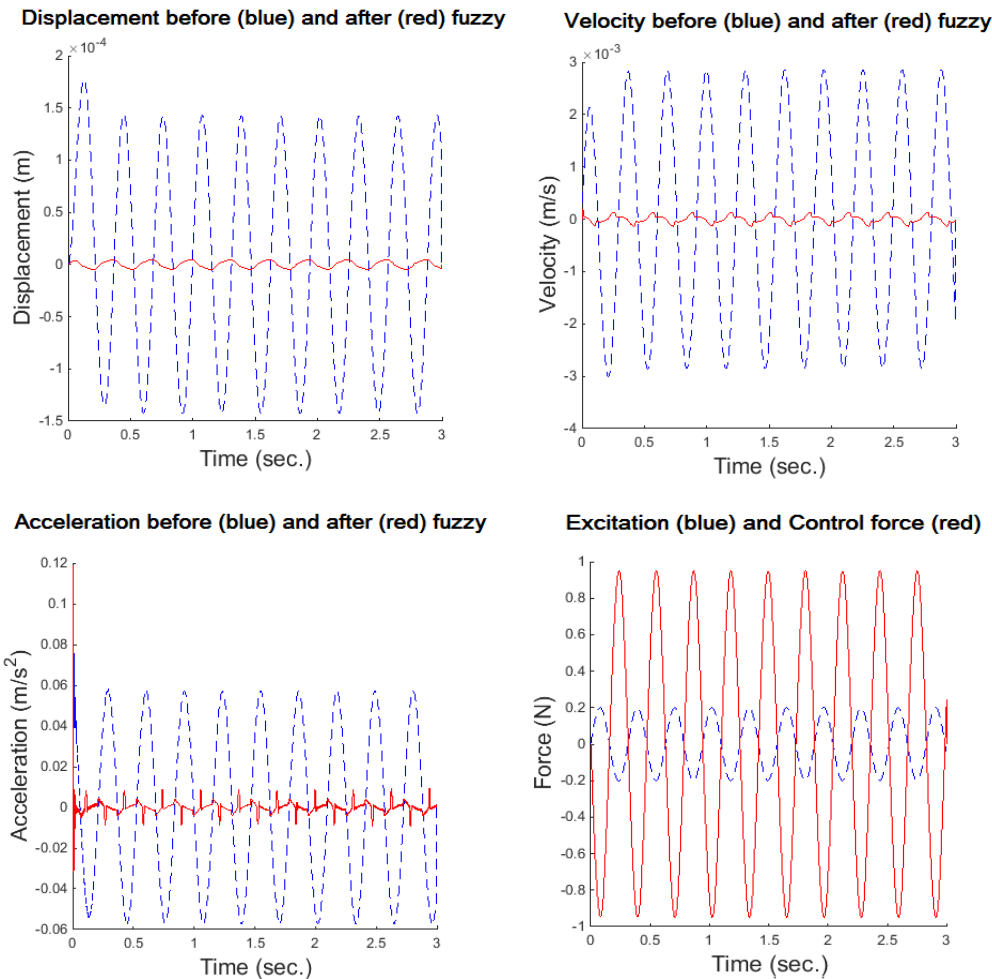
Figure 93: Displacement, velocity, acceleration and forces for the case with no delamination of the actuator (mechanical model)

From Figure 93, it is clear that a significant suppression in terms of displacement, velocity and acceleration is achieved. Namely, a reduction in vibrations of the order of 97.14%, 94.53% and 87.02% respectively is observed. Considering these results, one may state that the control is very efficient. In paragraph 6.2.2.1.2 the case of 50% delamination is presented. As seen from Figure 94 the failure starts from the free end and extends to the inner area of the structure.

6.2.2.1.2   Delamination of 50% of the actuator for the mechanical model

In this paragraph, the case where the failure extends to the half piezoelectric layer, that is, the 50% of the actuator (see Figure 94) is studied. As seen from the results below (Figure 95 and Table 16), the control scheme remains efficient, that is, significant vibration suppression is achieved for displacements, velocities and accelerations.
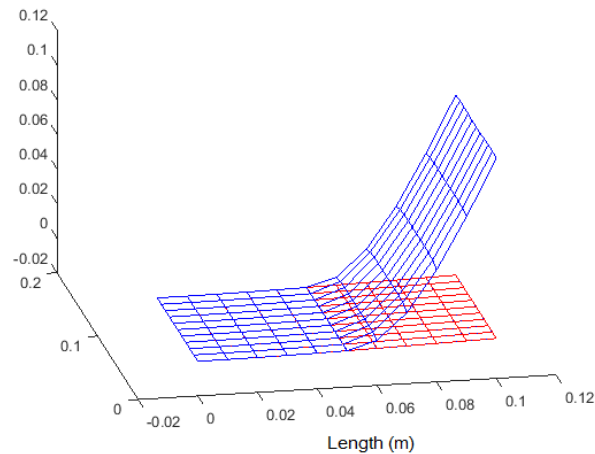
Figure 94: Discretized plate with 50% delamination
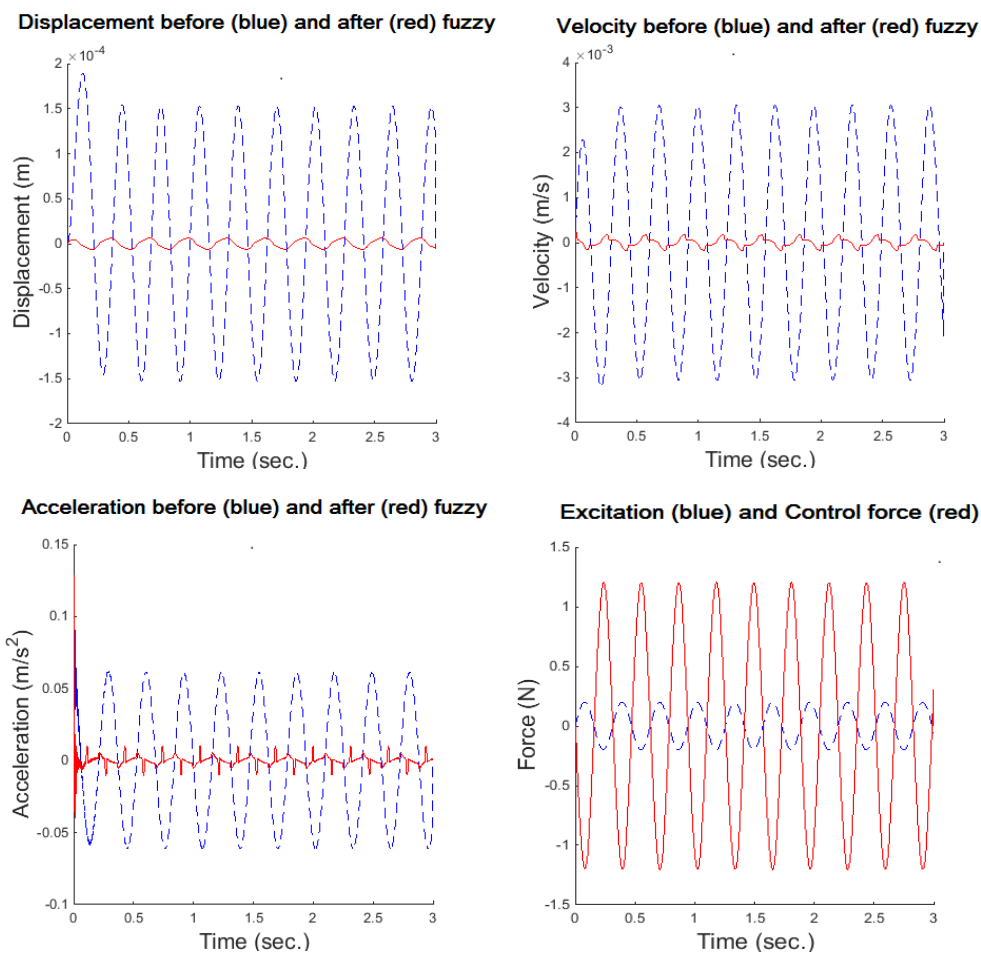
Figure 95: Displacement, velocity, acceleration and forces for the case of 50% delamination of the actuator (mechanical model)

Note that blue color is used for the oscillations prior the application of control, while with red are denoted the vibrations after the application of fuzzy control. In the last part of Figure 95, with blue color is given the external loading, while with red is shown the control force.

From the results of Figure 95, one may also observe a slight change also to the vibrations of the structure prior the application of control. This modification stemmed from the alteration of the structures characteristics, i.e. the stiffness, due to the presence of delamination.

It is worth mentioning that delamination cases of the 10% and 90% of the actuator patch for the mechanical model were also studied. As for the structure, a further alteration of its characteristics is observed, in case of extensive delamination. However, such phenomena attracts interest, as loadings capable of causing failures of this extent actually exist. The results of these cases are presented in detail in (Koutsianitis, et al., 2016b).

The results for the two different cases of the mechanical model which are presented in this dissertation are summarized in Table 16.

Table 16: Numerical results for delamination of actuator (mechanical model)

	Delamination 0%	Delamination 50%
Reduction of displacement	97.14%	96.48%
Reduction of velocity	94.53%	93.35%
Reduction of acceleration[4]	87.02%	82.23%

6.2.2.2   Results for the coupled electromechanical model

In the present subsubsection, fuzzy control which takes into account the coupled electromechanical model (see subsection 4.5.2) is tested. The main purpose is again to design a controller which continue to function effectively, even in presence of partial delamination (Koutsianitis, et al., 2016b). As mentioned in section 6.2, in the case of the electromechanical model, the control forces act in the direction of axes x and y producing bending moments which are acting to the whole structure as shown in Figure 85. It is also stated that the measurements are received from an element of the sensor patch, instead of a single node.

Thus, the element which will serve as sensor needs to be properly chosen. The selection is made from a genetic algorithm. The objective is the maximum reduction of vibrations in terms of displacement and acceleration, while the optimization problem is considered unconstrained. The design variable is one, which is the position of the sensor element. The recurring problem is as follows:

Maximize:

$$percentage = 0.4 \cdot percentage(u) + 0.6 \cdot percentage(\ddot{u}) \qquad (136)$$

---

[4] Note that for the calculation of the suppression in terms of acceleration after the application of the control, the initial large peak of the amplitude which occur in Figure 93 and Figure 95 is not considered.

As mentioned above, the problem is not subject to any constraints. The `population size` is set to 25 members, that is, 25 different possible solutions. The `maximum number of generations`, is set to 50.

The `initial population` was chosen by a stochastic process. As for the `selection`, the `Tournament Selection` method was used, with the parameter q for the selection set to 2 members of the population.

For the genetic operators of crossover and mutation, `the random crossover B` and the `random non-uniform mutation` were chosen with possibilities of 0.8 and 0.1 respectively.

The element occurred from the process is the element 84 as shown in Figure 96.
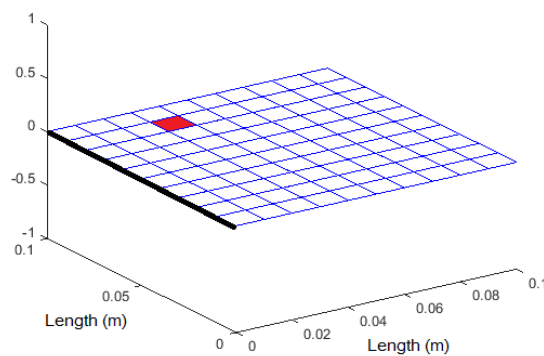
Figure 96: The element 84 which is used as sensor

Subsequently, the fuzzy controller which is presented in section 4.5.2 (controller 2) is tested on the model without the presence of delamination. For the fine tuning of its parameters, a suitably genetic algorithm is applied. After this process, the optimized controller is tested for three cases of delamination of the actuator layer.

6.2.2.2.1 Fuzzy control on the non-delaminated coupled electromechanical model

In this paragraph, a structure without delamination of piezoelectric layers is investigated. In contrast to the results of the mechanical model, one can observe that the oscillation reduction in this case is not so satisfactory. This comes as a result of the conversion of the displacement and velocity, in electrical potential and electric current respectively and the indirect transfer of the information on the mechanical model through the sensor and actuator.

With blue color is denoted the vibration prior the application of fuzzy control, while the red color is used for the response after the application of the control. Similarly, in the last section of Figure 97 with blue and red color are denoted the external loading and the control force respectively.
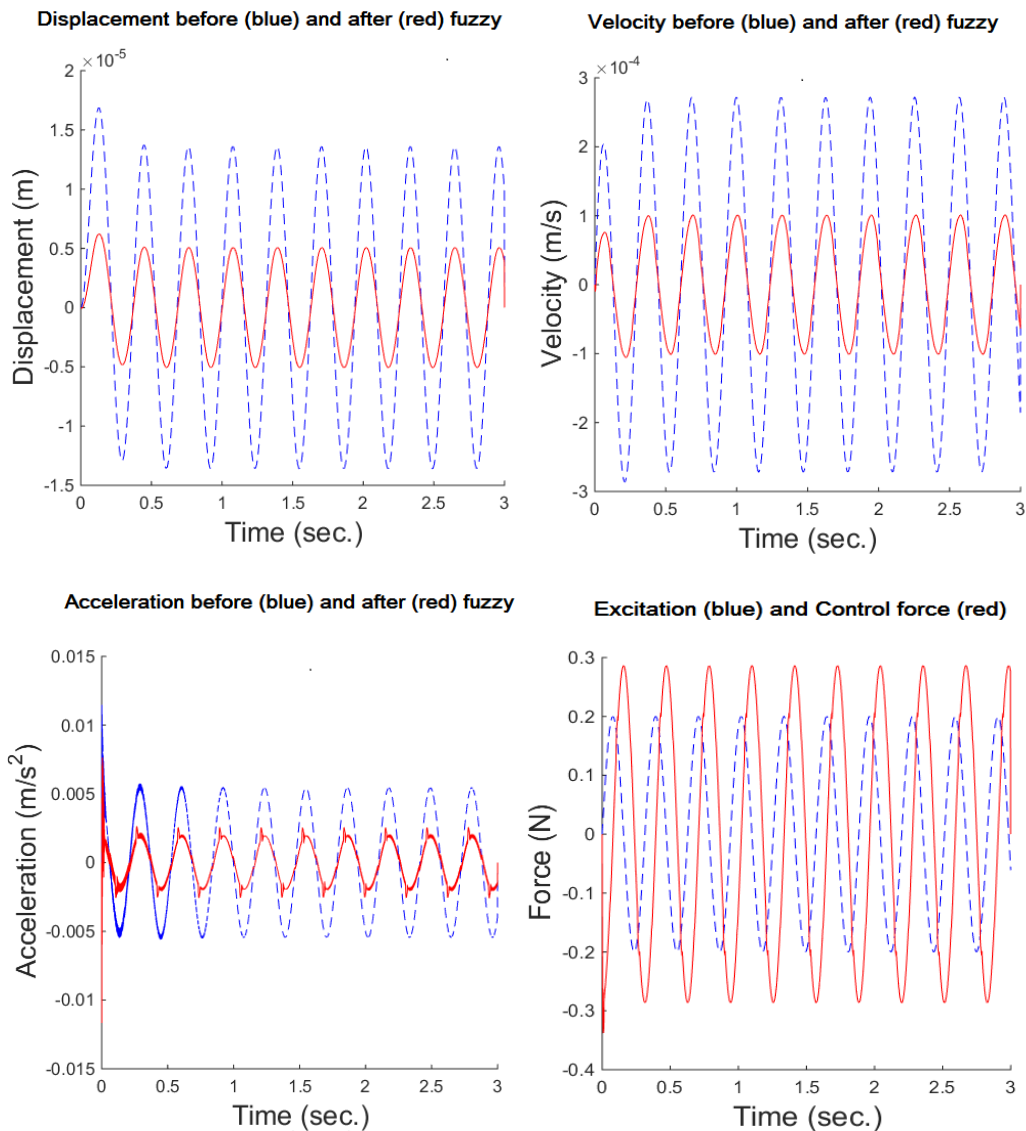
Figure 97: Displacement, velocity, acceleration and forces for the system without delamination (coupled electromechanical model)

From the results shown in Figure 97 and Table 17, a satisfactory decrease of the oscillations in terms of displacement and velocity is achieved. One disadvantage is that the form of the acceleration is little rough, which makes the control quite unsatisfactory.

6.2.2.2.2   Optimization of fuzzy control (controller 2) with genetic algorithms

In order to improve the results obtained from controller 2, a fine tuning of its parameters is made. The main purpose of the optimization process is the reduction of the displacement field and the improvement of the rough character of the acceleration diagram. For this purpose, a genetic algorithm is implemented and used in order to fine-tune the membership functions of the fuzzy variables.

The genetic algorithm which is used in this paragraph is based on the algorithm proposed by Zbigniew Michalewicz (Michalewicz, 1996) and is programmed in the MATLAB® environment. The membership functions of the electric potential and the electric current were discretized in i, j or k points for each variable as shown in Figure

98. Due to symmetry reasons the zero point has been kept constant at the center of the functions as in the previous case (see subsubsection 6.1.2).
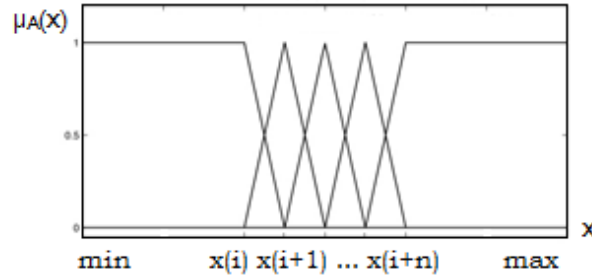
Figure 98: Discretization of membership functions for optimization of categories

In this case the optimization problem consists of the maximization of the objective function which is the percentage of oscillation reduction not only in terms of displacement, but in terms of acceleration as well, as given in Equation (137). The problem is subject to linear inequality constraints which are given in (138). It is noted that the maximum reduction is translated in minimum oscillations of the structure.

Maximize:

$$percentage = 0.4 \cdot percentage(u) + 0.6 \cdot percentage(\ddot{u}) \tag{137}$$

Subject to:

$$x(i) < x(i+1) \, if \, el.\, potential \geq 0$$

$$x(i) > x(i+1) \, if \, el.\, potential < 0$$

$$x(j) < x(j+1) \, if \, el.\, current \geq 0 \tag{138}$$

$$x(j) > x(j+1) \, if \, el.\, current < 0$$

where:

$$percentage(u) = \frac{(\text{max}\_displ\_before\_control) - (\text{max}\_displ\_after\_control)}{\text{max}\_displ\_before\_control}$$

$$percentage(\ddot{u}) = \frac{(\text{max}\_acc\_before\_control) - (\text{max}\_acc\_after\_control)}{\text{max}\_acc\_before\_control}$$

$$\text{max}\_displ\_before\_control = \max(u \, before \, control) + |\min(u \, before \, control)|$$

$$\text{max}\_displ\_after\_control = \max(u \, after \, control) + |\min(u \, after \, control)|$$

$$\text{max}\_acc\_before\_control = \max(\ddot{u} \, before \, control) + |\min(\ddot{u} \, before \, control)|$$

$$\text{max}\_acc\_after\_control = \max(\ddot{u} \, after \, control) + |\min(\ddot{u} \, after \, control)|$$

$$0 < x(i) < 1, i = 1, \dots, 4$$

$$0 < x(j) < 1, j = 1,2$$

At this investigation, the `population size` was set to 50 members, that is, 50 different possible solutions. The `maximum number of generations`, was set to 100.

The `initial population` was chosen by a stochastic process with respect to the design variable's bounds. Regarding the `selection`, the `Tournament Selection` method was used, with the parameter q for the selection set to 2 members of the population. For the genetic operators of crossover and mutation, `the random crossover B` and the `random non-uniform mutation` were chosen with probabilities of 0.8 and 0.1 respectively.

The results of the optimization process for the fuzzy inputs, that is, the electric potential and the electric current are presented in Figure 99 and Figure 100 respectively.
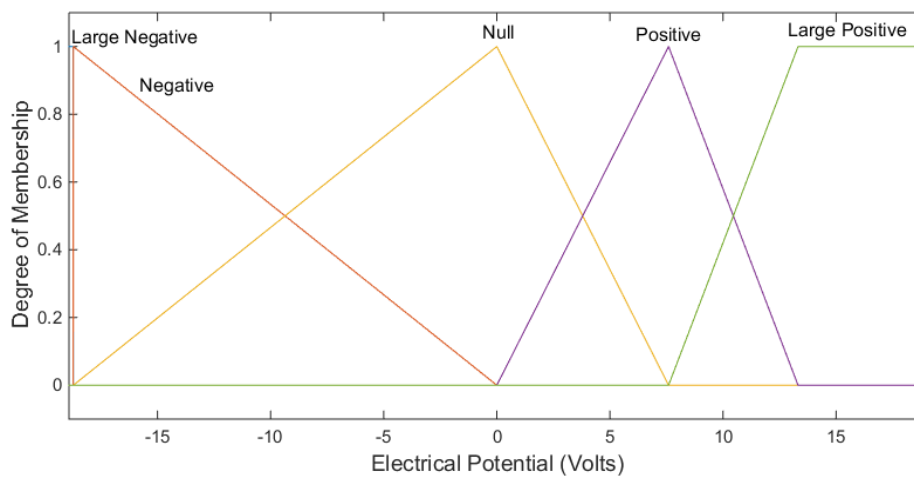
Figure 99: Optimized membership function of the electric potential
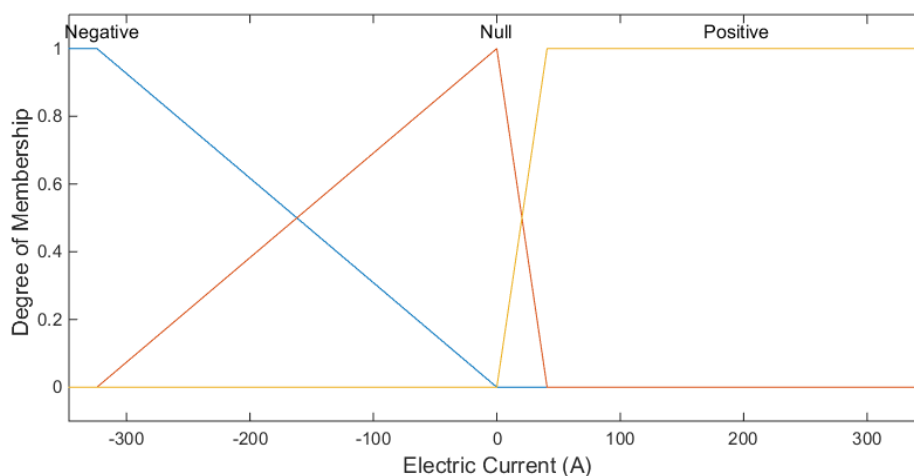
Figure 100: Optimized membership function of the electric current

The results of the application of the optimized controller to the system without delamination are shown in Figure 101 and Table 17. The blue color denotes the vibration before the application of control, while with red color is denoted the response after the application of the fuzzy control. As for the forces, with blue color is denoted the external loading, while the control force is shown with red color.
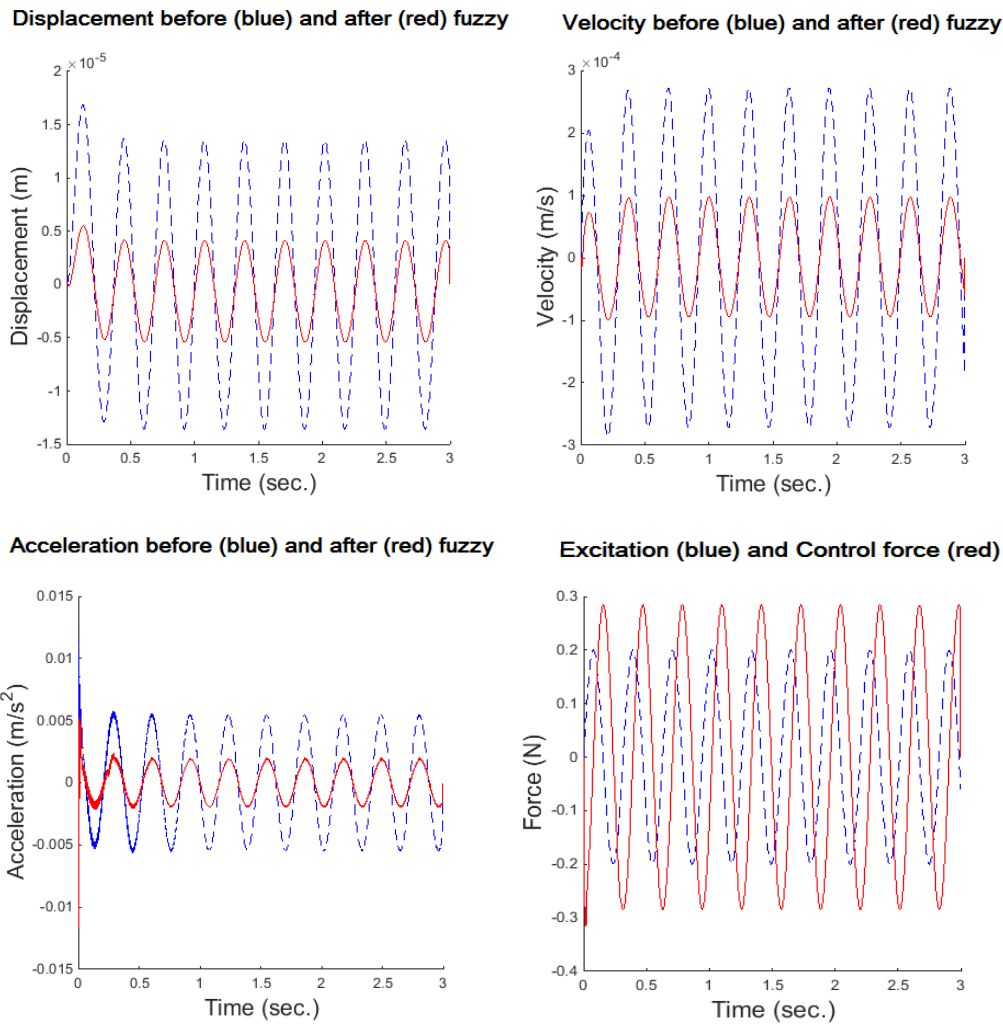
Figure 101: Displacement, velocity, acceleration and forces for the system without delamination and optimized membership functions (coupled electromechanical model)

From the results above, a slight improvement of the suppression in terms of displacement, velocity and acceleration is noticed. In addition, the vibrations are smoother.

This optimized controller is used for the reduction of the oscillations of the structure (considering the coupled electromechanical model) in presence of delamination as shown in the following paragraph.

6.2.2.2.3 Fuzzy control on the delaminated, coupled electromechanical model

A relatively significant partial delamination of 50% of the actuator is presented in this paragraph. The results are shown in Figure 102 and Table 17. The vibration prior and after the application of fuzzy control is denoted with blue and red color respectively.
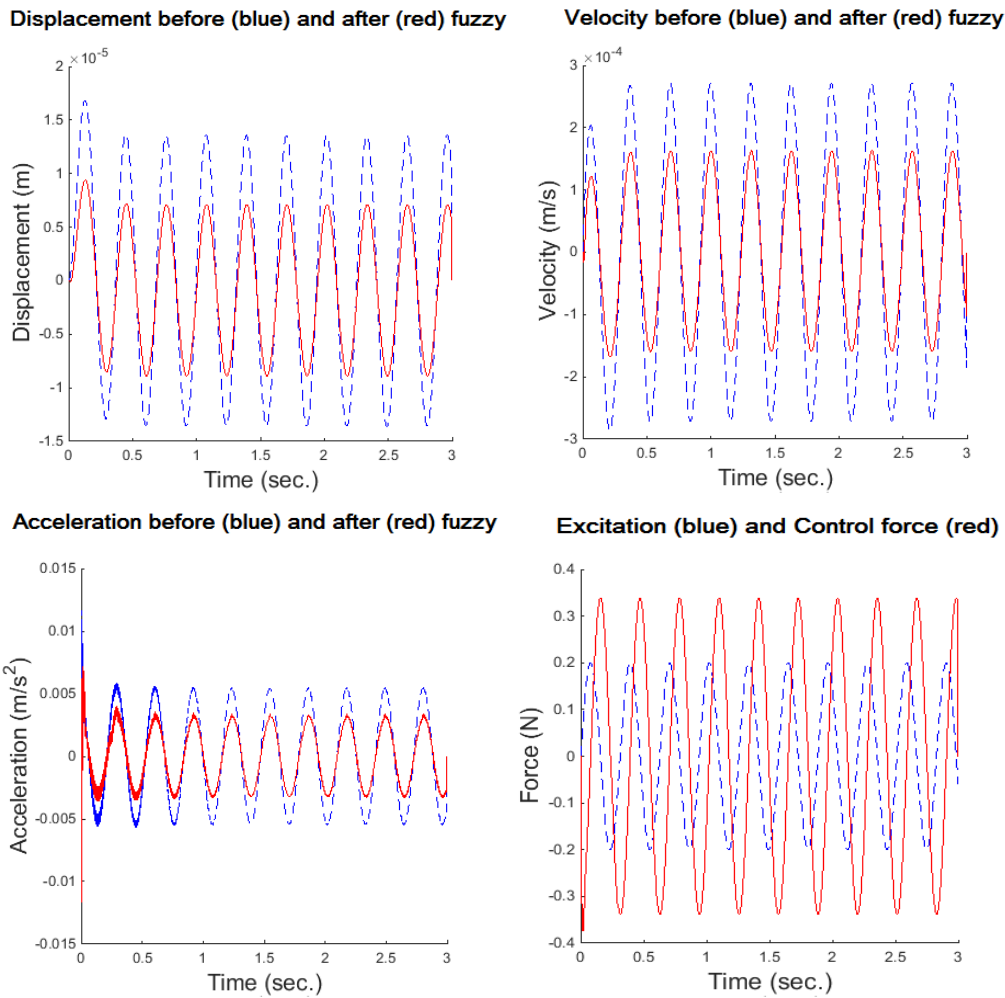
Figure 102: Displacement, velocity, acceleration and forces for the system with 50% delamination and optimized MF of fuzzy variables (coupled electromechanical model)

In this case, one can observe that the response of the control in terms of displacement, velocity and acceleration is noticeably worse compared to the ones of the non-delaminated case, however the reduction achieved remains satisfactory. This fact is very important for the robustness of control, as it proves that the fuzzy controller remains quite efficient, even under quite large amounts of delamination.

In Table 17, the percentage of the reduction of displacement, velocity and acceleration for the investigations of the electrical model are presented in detail.

Table 17: Percentages of reduction of displacement, velocity and acceleration

Percentage of reduction	0% delamination		50% delamination
	No optimization	Memb. Fcn. optimization	Memb. Fcn. optimization
Displacement	62.97%	69.09%	39.88%
Velocity	62.94%	64.62%	40.61%
Acceleration	53.77%	60.10%	33.71%

The same controller was also tested for the case of 10% delamination of the actuator patch, as well as for the occurrence of delamination at the collocated patch. These investigations can be found in (Koutsianitis, et al., 2016b).

It is noteworthy that, if the delamination appears exactly at the position of the sensor or the collocated actuator (see Figure 96), the effectiveness of the control scheme drastically deteriorates.

6.3 Adaptive neuro-fuzzy control of a cantilever beam

This last numerical example deals with the application of an optimized neuro-fuzzy controller for the vibration suppression of a cantilever beam model (see section 3.3). For this investigation, the Sugeno controller (controller 3) which described in subsection 4.5.3 is used.

The beam is made of aluminium. For demonstration purposes the smart beam is assumed to be of rectangular cross section with cross-sectional area equal to 0.004 m^2, length 0.8 m, width 0.02 m and height 0.005 m. The material properties of the host structure and of the piezoceramic are given in detail in the following Table 18 (see also (Foutsitzi, et al., 2002), (Stavroulakis, et al., 2005), (Tairidis, et al., 2009).

Table 18: Material properties of the composite plate with piezoelectric sensors and actuators

Property	Aluminium	Piezoceramic
E_1 **(GPa)**	73	69
ϱ **(kg/m^3)**	2700	7600
d_{31}**(m/V)**	-	$210 \cdot 10^{-12}$
g_{31}**(Vm/N)**	-	$11.5 \cdot 10^{-3}$

The structure is divided into 4 rectangular finite elements yielding to a system with 8 degrees of freedom as shown in Figure 103.
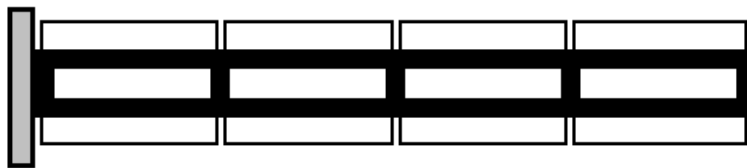

Figure 103: Cantilever beam with piezoelectric patches acting as sensors and actuators discretized into 4 finite elements

Sinusoidal external excitation concentrated at the free end of the cantilever is chosen. The loading is of the form:

$$P = P_0 sin\omega t \tag{139}$$

The amplitude of the loading is chosen to be equal to 1 N and the frequency ω has been set to 20 rad/s. The structure has been discretized with four finite elements resulting in a model with eight degrees of freedom. The purpose of the use of the adaptive Sugeno-type neuro-fuzzy controller is the oscillation reduction. The model is first simulated under the sinusoidal loading without any control in order to collect the necessary vibration data. Hereupon, these data are used for the training of the controller.

In fact, vibration suppression of a sinusoidal loading on the beam can be achieved using Mamdani-type fuzzy controllers without fine tuning of the involved parameters. Such results were presented in (Tairidis, et al., 2007), (Tairidis, et al., 2009) (Papachristou, et al., 2011), (Stavroulakis, et al., 2011). The results were very satisfactory for displacements, while velocities and accelerations were not acceptable. On the other hand, adaptive controllers can provide significantly better results. For instance, a suitably tuned Sugeno controller can provide smooth results and, the most, important, comparable with the ones obtained by classical controllers. For this reason, a LQR model was used for comparison.

The parameters of the LQR controller are chosen from the literature as follows:

$$q = 1 \ \text{ and } \ r = 0.00001$$

while the matrices Q and R are given as:

$$Q = q \times I \ \text{ and } \ R = r \times I$$

where I is the identity matrix.

The results of the Sugeno controller (controller 3) compared to the ones of a classical LQR controller are presented in Figure 104.

In the first three diagrams of Figure 104 one can observe that the reduction of displacements, velocities and accelerations respectively, is significant and comparable to the one that a classical LQR control provides. Note that with black color is denoted the vibration of the beam without control, while with blue and red color are the results of LQR and of the Sugeno controller, respectively. In the last segment of Figure 104 one can see the loadings of the system. The excitation is presented with black color, the LQR output force is denoted with blue color and with red color is indicated the Sugeno control force.

In comparison to a tested fuzzy controller (Tairidis, et al., 2007), (Tairidis, et al., 2009), the neuro-fuzzy controller provides a slight improvement of displacements. In fact, the vibration suppression which is achieved using a simple fuzzy controller can be also similar to the one obtained with LQR. However, the improvement of the results in terms of velocities and accelerations, with the Sugeno controller is impressive. As shown in Figure 105, the amplitude of the vibration using the neuro-fuzzy controller (right) is significantly lower compared to the corresponding given by the fuzzy controller. In addition, the results are smoother and comparable to the LQR ones.
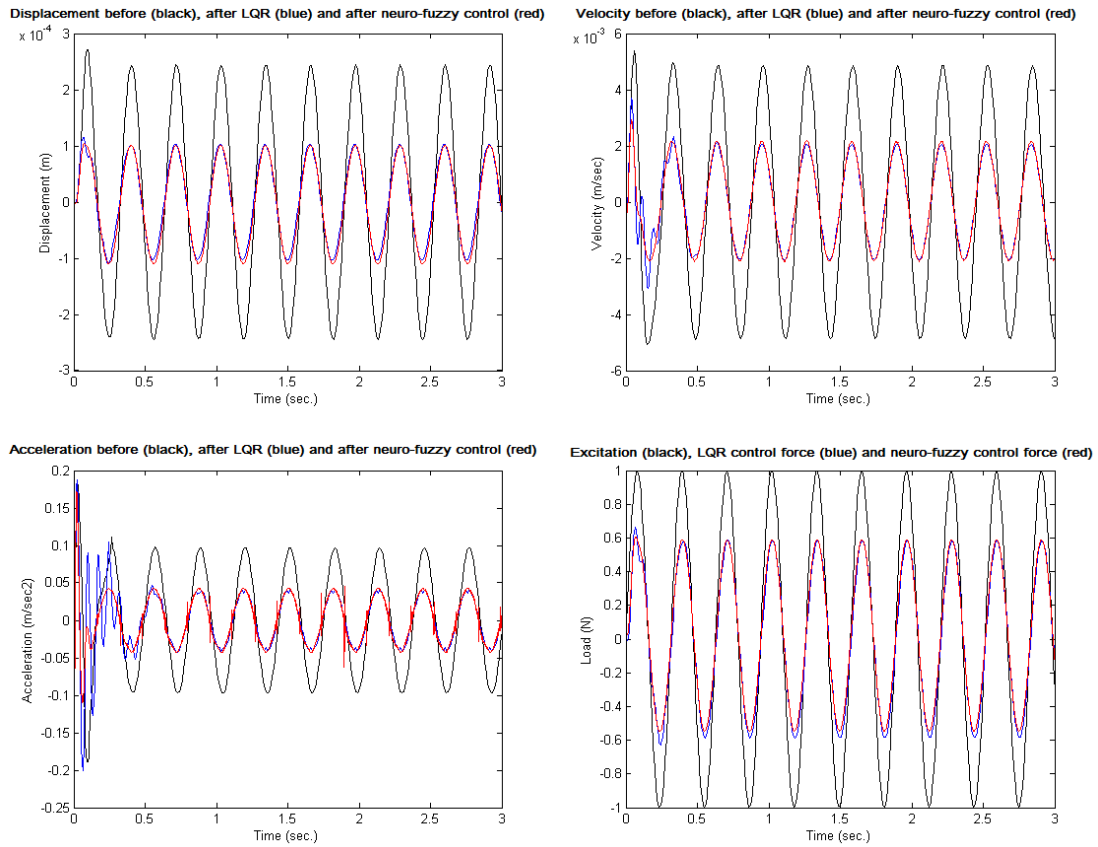
Figure 104: Vibration suppression achieved by the Sugeno controller compared to the one given by a classic LQR controller
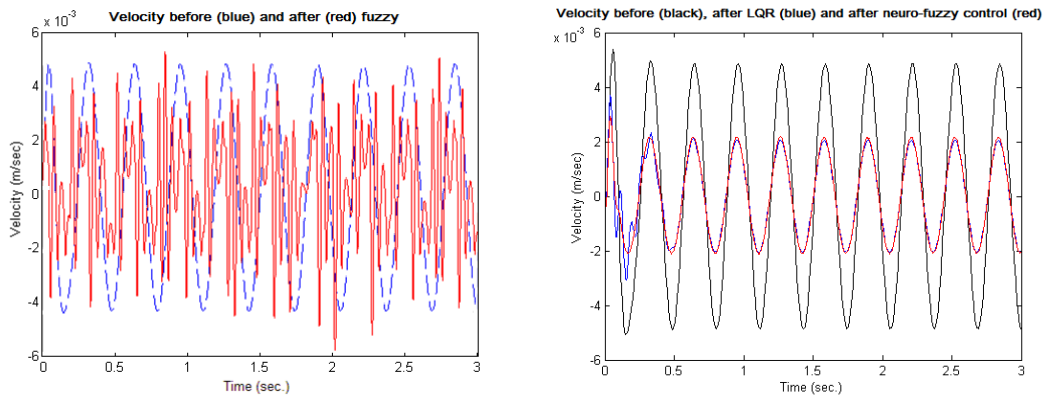
Figure 105: Comparison between fuzzy and neuro-fuzzy control

From the presented results one concludes that adaptive fuzzy controllers can be very effective in the construction of useful and smooth controllers. In addition, adaptive neuro-fuzzy controllers can lead to satisfactory vibration suppression without knowledge of the full state-space of the problem and without use of any classical optimization method.

7 Energy harvesting

As mentioned above, piezoelectric materials have the ability to produce electric charge when subjected to mechanical stresses or vibration. It was also stated that these materials can be both natural and synthetic, usually ceramics, and are widely used for the formation of sensors and actuators in smart composite structures for static and dynamic analysis and control (Tairidis, et al., 2014), (Tairidis, et al., 2009), (Tairidis, et al., 2007), (Foutsitzi, et al., 2013), (Foutsitzi, et al., 2013b) as well as for mechanical energy harvesting from vibrations (Liao & Sodano, 2012), (Park, et al., 2008), (Anton & Sodano, 2007), (Liu, et al., 2012).

Composite materials are becoming the material of choice in structural applications today and for the future. Composite smart structures (see chapter 3) consist of the laminated composite layer as the host structure, the embedded smart materials which serve as sensors and/or actuators, and the control mechanism as described at chapter 4.

These novel structures combine the advantage of classical composite laminated structures, such as high strength-to-weight ratio, with the self-monitoring capability of smart structures.

On smart composite structures that excited by various external loadings, piezoelectric components can be placed in selected positions in order to harvest the maximum amount of energy produced by the vibrations of the structure. Of course this procedure can be extended in order to include harvesting from pyroelectric materials, from ferroelectrics, from thermal energy through temperature fluctuation, and so on.

The behavior of the interface between the different layers of a laminate composite structure in order to transfer energy from the structure body to the energy harvester is an object of study.

The design of the harvester, which is based on the usage of piezoelectric elements, is performed in such a way as to be able to obtain the maximum amount of energy. For the same reason, the piezoelectric elements are placed in locations which present the maximum strain for given vibrations. It is obvious that the position of the harvesters play a significant role in the final result, due to the avoidance of critical points, such as bonds and/or other points with absence of information i.e. eigenvector intersections, *etc*.

Moreover, the geometric characteristic of the harvesters, which is the shape and the dimensions of the components, affects not only the geometry and topology of the smart structure, but the efficiency of the energy harvesting process as well.

The harvesting criteria come from the recent literature and include the location, the shape, the mass and the size of the piezoelectric components (Liu, et al., 2012), (Galchev, et al., 2011), (Shen, et al., 2008), (Kumar, et al., 2012), (Tairidis, et al., 2015c).

A short review of vibration-based microelectromechanical systems (MEMS) piezoelectric energy harvesters can be found in (Saadon & Sidek, 2011). A review of power harvesting using piezoelectric materials is made in (Anton & Sodano, 2007).

7.1   The energy harvester

In the present chapter, the smart cantilever beam, which is described in detail in section 3.3 is used for energy harvesting, through the surface bonded piezoelectric patches.

The model is tested with respect to the maximum amount of energy that can be produced, using modal analysis tools. The amount of energy that can be produced is estimated using structural dynamics. The actual amount that can be harvested depends on the available technology.

The objective of the present study is to harvest energy from a smart structure, and namely a cantilever beam as described in previous sections. In order to achieve this, a single piezoelectric patch can be placed in various positions of the beam as shown in Figure 106.
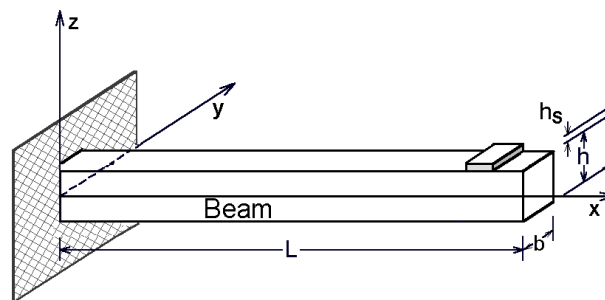
Figure 106: A beam model used for energy harvesting

The total beam length (L) is 0.8 m with cross-sectional area (A) of the beam 0.02x0.02 m². The host structure is made of aluminum. The elastic modulus (E) of structure is 73x10⁹ N/m² and the mass density (ρ) of the beam is 2700 kg/m³. For further details see also (Foutsitzi, et al., 2002), (Stavroulakis, et al., 2005), (Tairidis, et al., 2009).

In the present investigation a larger amount of elements is chosen, thus the beam is discretized into 32 finite elements with 2 degrees of freedom per node, yielding to a system with 64 degrees of freedom. The beam is a cantilever, which means that it is fixed at the left end.

In order to maximize the amount of energy produced and/or to transfer it from the fixed end to other parts of the structure, we placed an extra mass, equal to the whole mass of the structure, at every finite element of the structure. This leads to 32 different scenarios for each eigenvector. In the present paper we study the first three eigenvectors of the structure.

The justification behind this choice is that an analogous change of mass and density does not significantly change the resulting modal characteristics, while a drastic change of mass distribution like the one tried here has this ability. Change of the shape of the beam would be another possibility to modify the results (Liu, et al., 2012). Further investigation will certainly require structural optimization techniques.

7.1.1 Modal analysis

The governing system dynamics of the beam are given by equation (22):

$$[M]\{\ddot{X}\} + [K_{uu}]\{X\} = \{F_m\} + \{F_{el}\} \tag{22}$$

Equation (22) can be expressed in modal space by introducing new variables derived by modal transformation as follows:

$$\{X\} = \sum_{i=1}^{N} \Phi_i \eta_i(t) = [\Phi]\{\eta\} \tag{140}$$

where $[\Phi]$ is the modal matrix and $\{\eta\}$ is the modal coordinate vector. Substituting equations (140) into equations (22), leads to:

$$\{\ddot{\eta}\} + [\Omega^2]\{\eta\} = [\Phi]^T \{F_m\} - [\Phi]^T [K_{u\phi}] V \tag{141}$$

Also using the modal approach, structural damping can be easily introduced as:

$$\{\ddot{\eta}\} + [\Lambda]\{\dot{\eta}\} + [\Omega]\{\eta\} = [\Phi]^T \{F_m\} - [\Phi]^T [K_{u\phi}] V \tag{142}$$

where $[\Lambda]$ is a diagonal modal damping matrix with the generic term $2\xi_i \omega_i$, where ξ_i is the modal damping ratio and ω_i the undamped natural frequency of the i-th mode.

The first two eigenvectors of a cantilever beam are shown in the following Figure 107.
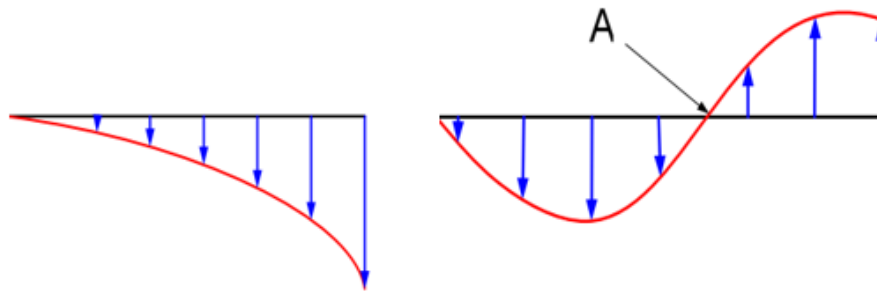
Figure 107: The first and the second eigenvectors of a cantilever beam

7.1.2   Estimate of energy production

The amount of energy produced from every piezoelectric element in each eigenvector is given by the following expression:

$$E = \frac{1}{2} G \left(\frac{\Delta u}{L} \right) V_{vol} \tag{143}$$

where G is the elastic modulus, L is the total length of the beam and V_{vol} is the volume of the beam.

The quantity Δu is given by the following equation:

$$\Delta u = \left(\varphi_i^j - \varphi_{i+1}^j \right) \frac{h}{2} \tag{144}$$

where φ_i^j is the ith element of the jth eigenvector and h is the height of the beam.

Depending on the electronic equipment for the electric energy harvesting or storage, one can obtain more precise estimates.

7.2   Numerical results of the energy harvesting

In the following sections, the total amount of energy produced at each element and the elements that present the maximum amount of energy are being discussed.

7.2.1   Numerical results for the first eigenvector

In the following Table 19 is shown the finite element where the extra mass is placed, along with the amount of the maximum energy produced and the node where this amount is produced. Note that node 1 is the fixed (left) end of the cantilever, while node 32 denotes the free end. The energy is given in Joules. The value of the maximum energy that produced by the structure without the extra mass is 1562.6 J and it appeared at the fixed end of the beam.

From the results of Table 19, one can observe that the total energy is not transferred to other elements of the structure when the extra mass is placed. This means that in any case the maximum energy is given at the fixed end of the beam. As for the amount of the maximum energy that produced, we observe a slight increase when the extra mass is placed at the 9th node. Namely, this amount is 1640.8 J, instead of 1562.6 J, which means that a 5% increase was achieved.

Table 19: Numerical results for the 1ˢᵗ eigenvector

Element of extra mass	Node of max energy	Amount of max energy (J)	Element of extra mass	Node of max energy	Amount of max energy (J)
1	1	1562.80	17	1	1149.20
2	1	1562.80	18	1	1052.10
3	1	1571.60	19	1	957.84
4	1	1582.10	20	1	868.25
5	1	1596.20	21	1	784.51
6	1	1612.30	22	1	707.24
7	1	1627.50	23	1	636.60
8	1	1638.40	24	1	572.49
9	1	1640.80	25	1	514.61
10	1	1630.80	26	1	462.56
11	1	1605.00	27	1	415.89
12	1	1561.90	28	1	374.10
13	1	1501.80	29	1	336.75
14	1	1426.70	30	1	303.39
15	1	1340.20	31	1	273.59
16	1	1246.40	32	1	246.98

In Figure 108 and Figure 109, the fluctuation of energy at each element before (blue line) and after (red line) the adding of the extra mass are shown.
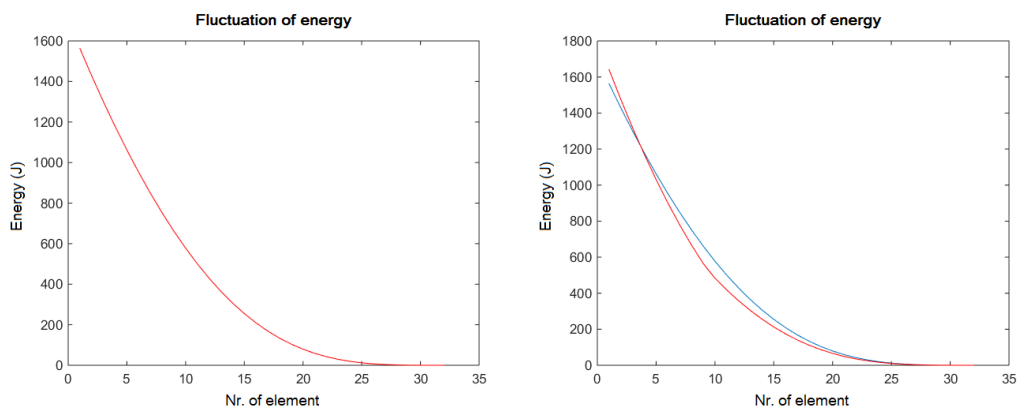
Figure 108: Total energy (J) at each node when extra mass placed at elements 1 and 9
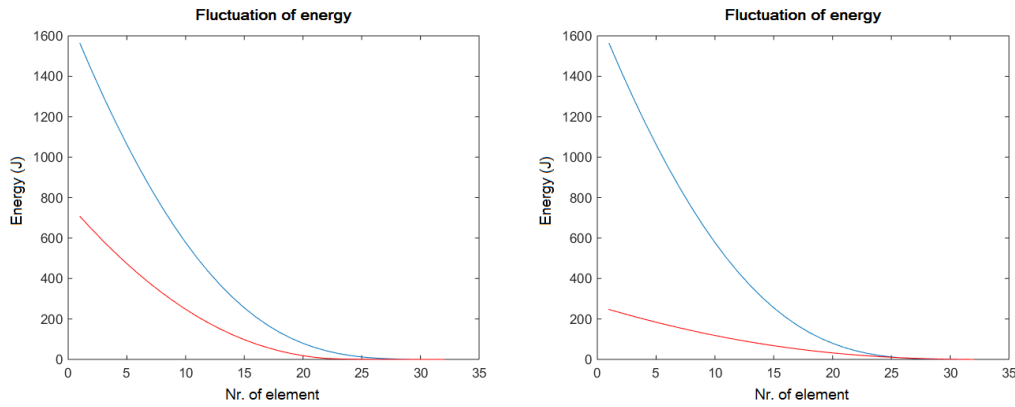
Figure 109: Total energy (J) at each node when extra mass placed at elements 22 and 32

7.2.2   Numerical results for the second eigenvector

In the Table 20 below, the finite element where the extra mass is placed, along with the amount of the maximum energy and the node where this amount is produced, is shown. The amount of total energy is given in Joules. The maximum energy without the extra mass is 54879 J and appeared again at the fixed end.

Table 20: Numerical results for the 2nd eigenvector

Element of extra mass	Node of max energy	Amount of max energy (J)	Element of extra mass	Node of max energy	Amount of max energy (J)
1	1	55185.00	17	17	22472.00
2	1	58067.00	18	18	24676.00
3	1	64564.00	19	19	26942.00
4	1	72566.00	20	20	28925.00
5	1	76196.00	21	21	29908.00
6	1	71248.00	22	1	29732.00
7	1	60539.00	23	1	38164.00
8	1	49000.00	24	1	47454.00
9	1	39156.00	25	1	54540.00
10	1	31520.00	26	1	57099.00
11	1	25833.00	27	1	55394.00
12	1	21687.00	28	1	51057.00
13	1	18726.00	29	1	45588.00
14	15	18344.00	30	1	39941.00
15	16	19526.00	31	1	34631.00
16	17	20878.00	32	1	29895.00

One can observe that if the extra mass is placed in the first 14 finite elements, the maximum amount of energy is given at the fixed end of the beam. Then, at the next 7 finite elements the maximum amount of energy is given near or exactly at the node where the mass is placed. It is also observed that if the extra mass is placed at the last 11 finite elements, the maximum amount of energy is produced again at the fixed end of the beam. The maximum energy that produced with the extra mass, was achieved at the fixed end of the beam, when the mass placed at the fifth element, and was 76196 J. This means that an increase of 38.84% was achieved. When the extra mass is placed at the last elements of the structure the amount of maximum energy decreases.
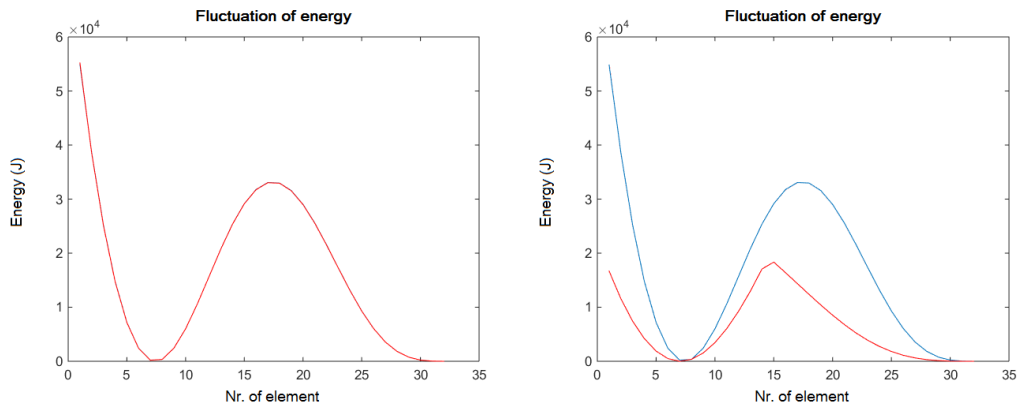

Figure 110: Total energy (J) at each node when extra mass placed at elements 1 and 14
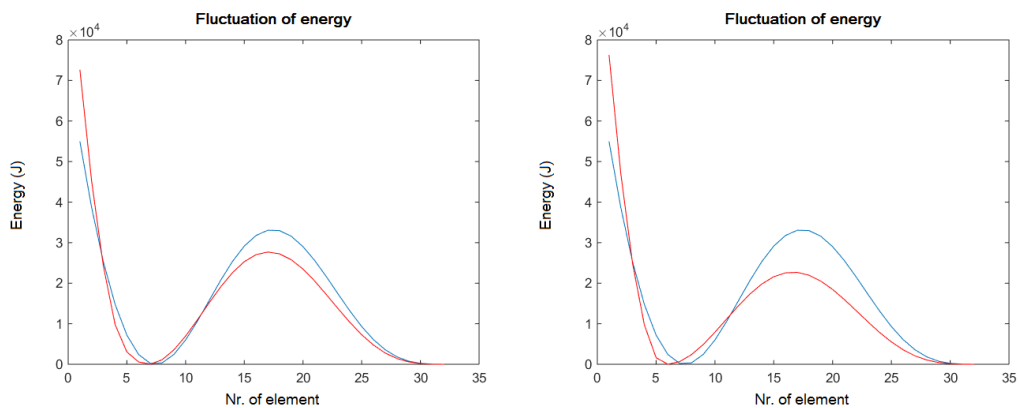
*Figure 111: Total energy (J) at each node when extra mass placed at elements 4 and 5*
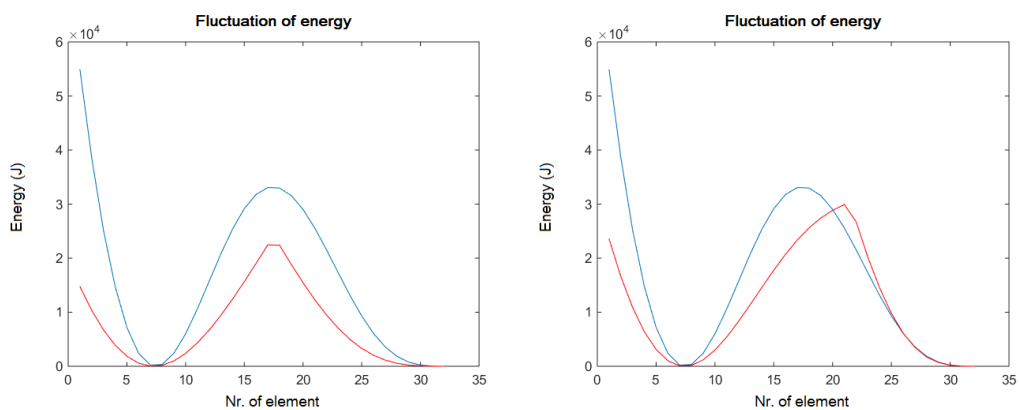

Figure 112: Total energy (J) at each node when extra mass placed at elements 17 and 21

In Figure 110, Figure 111 and Figure 112, one can observe the fluctuation of energy at each element before (blue line) and after (red line) the adding of the extra mass.

7.2.3 Numerical results for the third eigenvector

In this case, Table 21 shows the element where the extra mass is placed, the amount of the maximum energy produced, as well as the node where this energy appears. The energy is given in Joules. In this case, the maximum energy of the structure before the application of the extra mass, appeared at the fixed end of the beam and it is 386860 J.

Table 21: Numerical results for the 3rd eigenvector

Element of extra mass	Node of max energy	Amount of max energy (J)	Element of extra mass	Node of max energy	Amount of max energy (J)
1	1	402640.00	17	1	466430.00
2	1	553580.00	18	1	470060.00
3	1	736930.00	19	1	423390.00
4	1	568320.00	20	1	364810.00
5	1	342740.00	21	1	309580.00
6	1	207230.00	22	1	262230.00
7	8	154570.00	23	24	259290.00
8	9	144610.00	24	24	302840.00
9	22	146800.00	25	25	344380.00
10	22	174010.00	26	26	320620.00
11	22	206640.00	27	1	338280.00
12	22	243790.00	28	1	393680.00
13	23	288190.00	29	1	388190.00
14	23	329390.00	30	1	352750.00
15	23	341650.00	31	1	309430.00
16	1	372280.00	32	1	267720.00

In this case, from the results of the Table 21, one can observe that there are many variations regarding the node that the maximum amount of energy appears. Namely, when the extra mass is placed in the first 6 finite elements, the maximum amount of energy is given at the fixed end of the beam. If the mass is placed at the finite elements 7 and 8 the maximum amount of energy is given at elements 8 and 9 respectively. Then we observe that if the extra mass is applied to the elements 10 to 15 the maximum energy appears far from the element of application. Also, if we place the extra mass at element 15, the maximum amount of energy approaches the value of maximum energy

without the extra mass. In case that this extra mass is applied to the nodes from 16 to 22 and from 27 to the free end of the beam, the maximum energy appeared at the fixed end of the structure, that is, at the first element. Lastly, if the mass is placed at elements 23 to 26, the maximum energy appears near the element of application.

It is notable that in case that we place the extra mass at element 25 the maximum amount of energy is not only transferred to this element, but it approaches the value of maximum energy without the extra mass, as well. In addition, for mass placement at element 28 one can observe that the energy curve approaches the initial curve.

The maximum energy, was achieved at the fixed end of the beam when the mass placed at the third element and was 736930 J. The maximum energy of the structure before the application of the extra mass is 386860 J which means that an increase of 90.49% was achieved. In Figure 113, Figure 114, Figure 115 and Figure 116, one can observe the amount of energy that is produced at each element before (blue line) and after (red line) the adding of the extra mass.
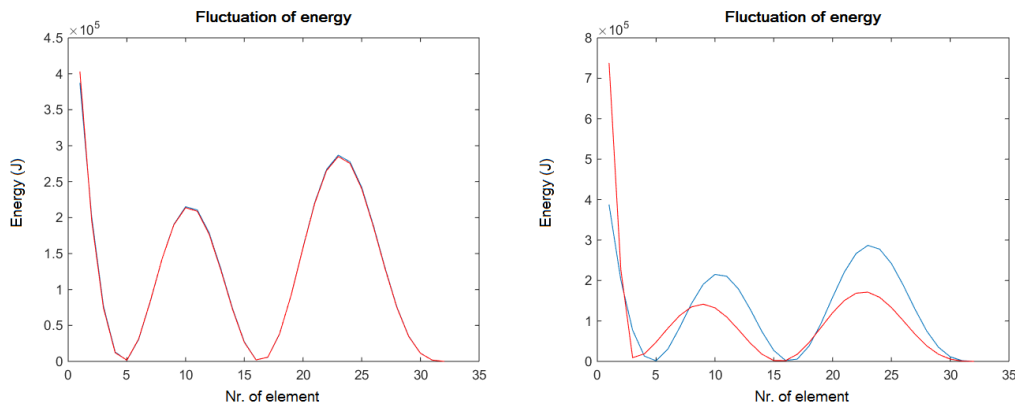
Figure 113: Total energy (J) at each node when extra mass placed at elements 1 and 3
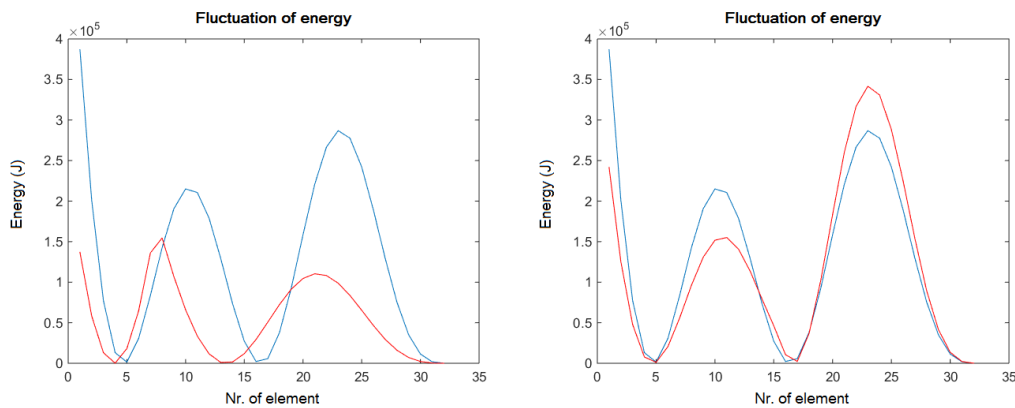
Figure 114: Total energy (J) at each node when extra mass placed at elements 7 and 15
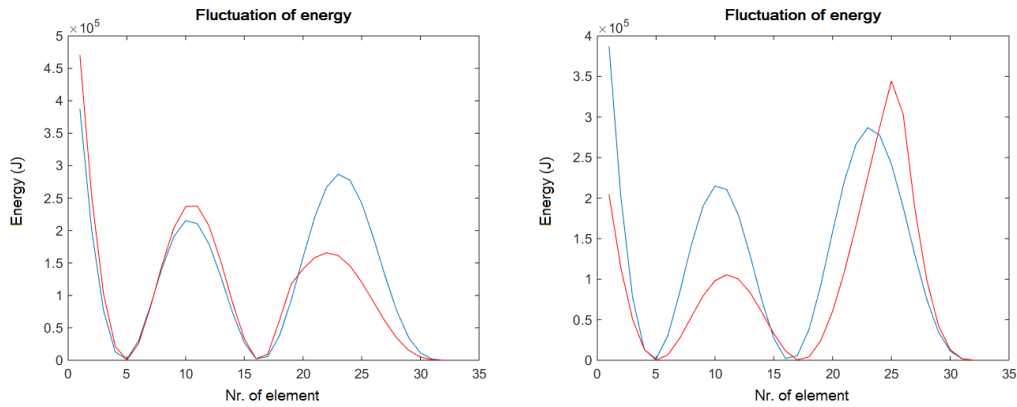
Figure 115: Total energy (J) at each node when extra mass placed at elements 18 and 25
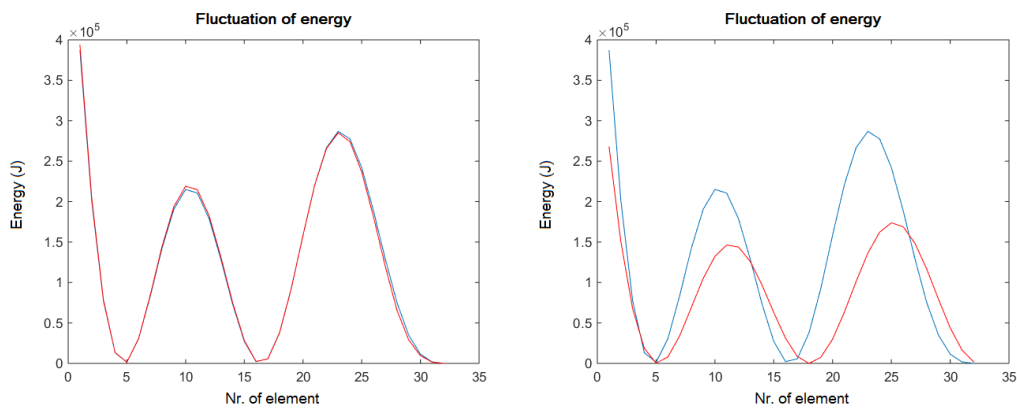
Figure 116: Total energy (J) at each node when extra mass placed at elements 28 and 32

To conclude, the criteria of the harvester, that is, the location, the shape and the size of the piezoelectric components, could be properly quantified within an optimization process for the fine tuning of the properties of the harvesters. Structural optimization for dynamic problems, involving modal characteristics, is a challenging task. Optimization algorithms inspired by nature and especially Evolutionary Algorithms (EAs) can provide very powerful tools for this purpose. Moreover, the ability of the proposed model to provide satisfactory results for a large width of different frequencies that described various phenomena i.e. wind excitations, random vibrations, ocean waves, *etc*. may be part of future investigations.

8 Conclusions and future work

The main objective of this dissertation was the implementation and testing of fuzzy, and adaptive neuro-fuzzy control mechanisms to smart composite structures, i.e. smart beams and plates with embodied sensors and actuators.

More specifically the incorporation of fuzzy control with global optimization techniques for the fine tuning of the characteristics of control, i.e. of the membership functions and/or the ranges of the fuzzy variables was implemented.

The modification of the control parameters was achieved through the use of suitably defined adaptive neuro-fuzzy inference systems (ANFIS), genetic algorithms and the particle swarm optimization method. The outcome of this procedure was the establishment of vigorous and robust optimized control schemes.

The impressive results of this procedure can be concluded to two different points:

a. The ANFIS method was proved to be very efficient for smoothing down the vibration results in terms of velocity and acceleration, even if such a measure was not directly requested.
b. The optimized controllers worked satisfactorily, not only for the undelaminated structures, but even for the case of relatively extensive delamination between the elastic core and the piezoelectric patches.

The conclusions of this dissertation are discussed in detail in the next section. Moreover, some possible next steps of further research are briefly presented in section 8.2.

8.1 Conclusions of this work

From the application of fuzzy control on plates one can observe that while the applied control strategy was quite efficient and smooth in terms of displacement and velocity, the results in terms of acceleration were very disappointing and a burden for the material and/or the sensors and actuators. It is worth to mention that similar problems were encountered while testing fuzzy control on beams.

These problems were addressed using genetic algorithms and particle swarm optimization for the fine tuning of the parameters of the fuzzy control, as well as adaptive neuro fuzzy control (ANFIS).

The results of fuzzy control, prior optimization, fine tuning or training, were proven to be very satisfactory in terms of displacement for different smart structures. However, the suppression of velocity and acceleration was not satisfactory.

Due to this situation, the need of optimization of some of the parameters of the fuzzy controller arose. This fine tuning is a really exacting process, thus a simple, effective and well known procedure has to be chosen. Among the plethora of optimization methods and algorithms, genetic algorithms and particle swarm optimization were selected due to their simplicity and smooth behavior in such problems. Namely, the algorithms were used in order to optimize the membership functions of the variables of the fuzzy controllers.

From the investigations presented, it is more than clear that genetic algorithms is a very powerful optimization tool that can be used in order to optimize and fine-tune fuzzy controllers. The oscillations of the smart plate were significantly reduced, not only in terms of displacement and velocity, but in terms of acceleration as well, which is a very important achievement. Moreover, the results were not only successful in terms of oscillations reduction, but smooth as well.

Moreover, it was shown that the use of particle swarm optimization combined with other fine tuning options, such as the alteration of the defuzzification methods, was very beneficiary. More specifically it was shown that the vibration suppression achieved by the tuned controller was exceedingly satisfactory and the results were very smooth, not only for displacement and velocity, but for acceleration as well.

The tuned fuzzy controllers, which resulted from the optimization through genetic optimization and particle swarm method, were proved to be robust for a wide range of different external loadings (Tairidis, et al., 2016), (Tairidis, et al., 2015) or frequencies (Tairidis, et al., 2016).

From the presented numerical results, it can also be concluded that adaptive fuzzy techniques can be very effective in the construction of smooth controllers. One systematic approach of adaptive fuzzy control constitutes the hybrid neuro-fuzzy Sugeno controller, where the optimization of the system parameters is achieved via a training process of a suitable neural network. In addition, one can assert that adaptive neuro-fuzzy controllers can lead to satisfactory vibration suppression, equivalent to classic control, without the need of knowledge of the full state-space of the problem or any other information, except of a set of data, which is necessary in order to define and train the controller.

In addition, in this dissertation a multilayer formulation of a piezocomposite plate accounting for adhesive flexibility was also considered, allowing the investigation of delamination effects and the preparation of models for the study of controlled structures including partial delamination near to reality.

Delamination between the layers (both sensors and actuators) may appear and influences the effectiveness of active vibration control. Moreover, delamination phenomenon leads to structural changes. Namely, it is responsible for the weakening and/or ageing of the materials of a smart structure, as well as it modifies, in some extend, the characteristics of the mechanical system, mainly its stiffness. This fact affects the effectiveness of the control methods proposed. For this reason, robust control schemes are necessary, in order to work with the presence of these deviations.

From numerical experiments the applicability of fine-tuned fuzzy controllers, even in the case of partial delamination had been shown. The parameters of fuzzy controllers can be optimized, using genetic algorithms. Numerical results demonstrate that a suitably designed and optimized fuzzy controller works effectively in both initial and partially delaminated structure. Supplementary tuning, after the appearance of delamination, was proved to make the system adaptive and extend the applicability of the proposed fuzzy controllers. Even if the results are satisfactory, further adaptation may become necessary for severely delaminated structures.

8.2 Future work

It should be mentioned, that in this dissertation, exclusively collocated sensor-actuator pairs have been considered. Moreover, the controllers were MISO (multiple inputs – single output), which means that pendulum-like rules are applicable.

Non-collocated configurations as well as MIMO (multiple inputs – multiple outputs) control schemes require a global optimization method for the implementation and tuning of fuzzy linguistic rules as well. This is due to the fact that the complexity dramatically increases and the manual setting of such rules becomes unrealizable. This task has been left open for future investigation.

Another topic of future research is the extension of the fuzzy and neuro-fuzzy control techniques to non-linear problems of smart civil structures, such as beams, plates and shells.

Furthermore, the studying of structural health monitoring and vibration control with energy harvesting and self-repairing also attracts interest and has been left open for further research, since similar methods can be used. In that case, the objective could be the optimal function of a dynamical system under extreme events, such as strong winds, severe earthquakes, *etc*.

The proposed control strategies can be extended to other technologies of smart structures, such as shape-memory alloy, which is a material with the ability to remember its original shape and thus to return to its pre-deformed condition.

Last but not least, the effect of incomplete information (measurements) of the investigated system or the presence of delay in the application of control and their impact to

the efficiency of the proposed methods can also be part of further investigation in the future.

9 Bibliography

Abdeljaber, O., Avcia, O. & Inman, D. J., 2016. Active vibration control of flexible cantilever plates using piezoelectric materials and artificial neural networks. *J Sound Vibration*, Volume 363, pp. 33-53.

Akbarov, S. D., Yahnioglu, N. & Karatas, E. E., 2014. A 3D FEM Analysis of Buckling Delamination of a Rectangular Plate with an Inner Rectangular Crack under a Biaxial Compressive Force. *Mech Compos Mater*, 49(6), pp. 585-594.

Alonso, C., Andradel, C., Rodriguez, J. & Diez, J. M., 1998. Factors controlling cracking of concrete affected by nreinforcement corrosion. *Mat Struct*, Volume 31, pp. 435-441.

Anderson, B. & Moore, J., 1989. *Optimal Control: Linear Quadratic Methods.* s.l.:Prentice-Hall.

Anton, S. & Sodano, H., 2007. A review of power harvesting using piezoelectric materials (2003–2006). *Smart Mater Struct*, 16(3), pp. R1-R21.

Antsaklis, P., 1990. Neural Networks for Control Systems. *IEEE T Neural Networ*, 1(2), pp. 242-244.

Banks, A., Vincent, J. & Anyakoha, C., 2007. A Review of Particle Swarm Optimization. Part I: Background and Development. *Natural Computing*, 6(4), pp. 467-484.

Banks, A., Vincent, J. & Anyakoha, C., 2008. A Review of Particle Swarm Optimization. Part II: Hybridisation, Combinatorial, Multicriteria and Constrained Optimization, and Indicative Applications. *Natural Computing*, Volume 7, pp. 109-124.

Benjeddou, A., 2000. Advances in piezoelectric finite element modeling of adaptive structural elements: a survey. *Computers and Structures*, Volume 76, pp. 347-363.

Benvenuti, E., Orlando, N., Ferretti, D. & Tralli, A., 2016. A new 3D experimentally consistent XFEM to simulate delamination in FRP-reinforced concrete. *Compos Part B-Eng*, Volume 91, pp. 346-360.

Berenji, H., 1990. *Neural Networks and Fuzzy Logic in Intelligent Control.* Philadelphia, 5th IEEE International Symposium on Intelligent Control Proceedings, pp. 916-920.

Blickle, T. & Thiele, L., 1996. A comparison of selection schemes used in evolutionary algorithms. *Evol Comput*, 4(4), pp. 361-394.

Bruno, D., Greco, F. & Lonetti, P., 2005. A 3D delamination modeling technique based on plate and interface theories for laminated structures. *Eur J Mech A-Solid*, 24(1), pp. 127-149.

Bui, H. L., Nguyen, C. H. & Vu, N. L., 2015. General design method of hedge-algebras-based fuzzy controllers and an application for structural active control. *Appl Intell*, 43(2), pp. 251-275.

Cantwell, W. J. & Morton, J., 1991. The impact resistance of composite materials - a review. *Composites*, 22(5), pp. 347-362.

Caporale, A., Luciano, R. & Sacco, E., 2006. Micromechanical analysis of interfacial debonding in unidirectional fiber-reinforced composites. *Comp Struct*, Volume 84, pp. 2200-2211.

Carrera, E. & Fagiano, C., 2007. Mixed piezoelectric plate elements with continuous transverse electric displacements. *J Mech Mater Struct* , 2(3), pp. 421-438.

Chiu, S., 1994. Fuzzy Model Identification Based on Cluster Estimation. *J Intell Fuzzy Syst*, 2(3), pp. 267-278.

Clerc, M. & Kennedy, J., 2002. The Particle Swarm: Explosion, Stability and Convergence in a Multi-dimensional Complex Space. *IEEE Trans Evol Comput*, Volume 6, pp. 58-73.

Cohen, K., Weller, T. & Ben-Asher, J. Z., 2002. Active control of flexible structures using a fuzzy logic algorithm. *Smart Mater Struct*, 11(4), p. 541–552.

Cook-Chennault, K. A., Thambiand, N. & Sastry, A. M., 2008. Powering MEMS portable devices - a review of non-regenerative andregenerative power supply systems with special emphasis on piezoelectric energy harvesting systems. *Smart Mater Struct*, Volume 17, p. 043001.

Cox, B. N., 1994. Delamination and buckling in 3D Composites. *J Compos Mater*, Volume 28, pp. 1114-1126.

Crassidis, J. L., Baz, A. & Wereley, N., 2000. H∞ Control of Active Constrained Layer Damping. *J Vib Control*, 6(1), p. 113–136.

Curie, J. & Curie, P., 1880. Développement par compression de l'électricité polaire dans les cristaux hémièdres à faces inclinées (Development, via compression, of electric polarization in hemihedral crystals with inclined faces). *Bulletin de la Société minérologique de France*, Volume 3, p. 90 – 93.

Damle, R., Lashlee, R., Rao, V. & Kern, F., 1994. Identification and robust control of smart structures using artificial neural networks. *Smart Mater Struct*, Volume 3, pp. 35-46.

Dávila, C. G., Camanho, P. P. & Rose, C. A., 2005. Failure criteria for FRP laminates. J Compos Mater. *J Compos Mater,* Volume 39, pp. 323-345.

Driankov, D., Hellendoorn, H. & Reinfrak, M., 1996. *An introduction to fuzzy control.* 2nd ed. Munchen: Springer.

Drosopoulos, G. A., Wriggers, P. & Stavroulakis, G. E., 2014. A Multi-scale computational method including contact for the analysis of damage in composite materials. *Comp Mater Sci,* Volume 95, p. 522–535.

Elshafei, M. A. & Alraiess, F., 2013. Modeling and analysis of smart piezoelectric beams using simple higher order shear deformation theory. *Smart Mater. Struct.,* 22(3), p. 035006 (14pp).

Erturk, C. L. & Tekinalp, O., 2005. A layer wise approach to piezoelectric plates accounting for adhesive and delaminated regions. *Comp Struct ,* Volume 83, pp. 279-296.

Foutsitzi, G., Marinova, D., Hadjigeorgiou, E. & Stavroulakis, G. E., 2002. *Finite Element Modelling of Optimally Controlled Smart Beams.* Sozopol, Bulgaria, 28th Summer School: Applications of Mathematics in Engineering and Economics.

Foutsitzi, G. A., Hadjigeorgiou, E. P., Gogos, C. G. & Stavroulakis, G. E., 2013. *Modal shape control of smart composite beams using piezoelectric actuators.* Chania, Crete, Proceedings of 10th HSTAM International Congress on Mechanics.

Foutsitzi, G. A., Gogos, C. G., Hadjigeorgiou, E. P. & Stavroulakis, G. E., 2013b. Actuator Location and Voltages Optimization for Shape Control of Smart Beams Using Genetic Algorithms. *Actuators,* 2(4), pp. 111-128.

Fremond, M., 2002. *Non-smooth thermomechanics.* Berlin Heidelberg: Springer.

Galchev, T., Kim, H. & Najafi, K., 2011. Micro Power Generator for Harvesting Low-Frequency and Nonperiodic Vibrations. *J Microelectromech Syst,* 20(4), pp. 852-866.

Garcia Lage, R., Mota Soares, C. M., Mota Soares, C. A. & Reddy, J. N., 2004. Modelling of piezolaminated plates using layerwise mixed finite elements. *Comp Struct ,* Volume 82, pp. 1849-1863.

Goldberg, D., 1989. *Genetic Algorithms in Search, Optimization, and Machine Learning.* MA: Addison-Wesley, Reading.

Greco, F., Leonetti, L. & Lonetti, P., 2015. A novel approach based on ALE and delamination fracture mechanics for multilayered composite beams. *Compos Part B-Eng ,* Volume 78, pp. 447-458.

Hadjigeorgiou, E. P., Stavroulakis, G. E. & Massalas, C. V., 2006. Shape control and damage identification of beams using piezoelectric actuation and genetic optimization. *Int J Eng Sci,* Volume 44, pp. 409-421.

Hakim, S. J. S. & Razak, H. A., 2013. Adaptive Neuro Fuzzy Inference System (ANFIS) and Artificial Neural Networks (ANNs) for structural damage identification. *Struct Eng Mech*, 45(6), pp. 779-802.

Han, J. H. & Lee, I., 1998. Analysis of composite plates with piezoelectric actuators for vibration control using layerwise displacement theory. *Composites Part B*, 29(5), pp. 621-632.

Han, J. H. & Lee, I., 1999. Optimal placement of piezoelectric sensors and actuators for vibration control of a composite plate using genetic algorithms. *Smart Mater Struct*, Volume 8, pp. 257-267.

Holland, J. H., 1975. *Adaptation in natural and artificial systems.* University of Michigan Press.

Ho, S. L., Joshi, S. P. & Tay, A. A. O., 2012. *Cohesive zone modeling of 3D delamination in encapsulated silicon devices.* San Diego, IEEE 62nd Proceedings.

Hsueh, C. H., 1995. Criteria for Progressive Interfacial Debonding with Friction in Fiber-Reinforced Ceramic Composites. *MRS Proceedings*, Volume 409, p. 205.

Icardi, U. & Di Sciuva, M., 1996. Large-deflection and stress analysis of multilayered plates with induced-strain actuators. *Smart Mater Struct*, Volume 5, pp. 140-164.

Iorga, L., Baruh, H. & Ursu, I., 2008. A Review of H∞ Robust Control of Piezoelectric Smart Structures. *Appl Mech Rev*, 61(4), pp. 040802-1-040802-15.

Irschik, H., 2002. A review of static and dynamic shape control of structures using piezoelectricactuation. *Eng Struct*, 24(1), pp. 5-11.

Jang, J.-S. R., 1991. *Fuzzy modeling using generalized neural networks and Kalman filter algorithm*, AAAI, pp. 762-767.

Jang, J.-S. R., 1993. ANFIS: Adaptive-Network-based Fuzzy Inference Systems. *IEEE Transactions on Systems, Man, and Cybernetics*, 23(3), pp. 665-685.

Jang, J.-S. R. & Sun, C.-T., 1995. Neuro-fuzzy modeling and control. *Proceedings of the IEEE,* 83(3), pp. 378-406.

Kapuria, S., Ahmed, A. & Dumir, P. C., 2005. An efficient coupled zigzag theory for dynamic analysis of piezoelectric composite and sandwich beams with damping. *J Sound Vib,* Volume 279, pp. 345-371.

Kapuria, S. & Alam, N., 2006. Efficient layerwise finite element model for dynamic analysis of laminated piezoelectric beams. *Comput Methods Appl Mech Engrg ,* Volume 195, pp. 2742-2760.

Kennedy, J. & Eberhart, R., 1995. *Particle Swarm Optimization.* s.l., Proceedings of 1995 IEEE International Conference on Neural Networks, pp. 1942-1948.

Kim, S. J. & Jones, J. D., 1996. Effects of Piezo-Actuator Delamination on the Performance of Active Noise and Vibration Control Systems. *J Intell Mater Syst Struct,* Volume 7, pp. 668-676.

Klug, J. C. & Sun, C. T., 1996. Large deflection effects of cracked aluminum plates repaired with bonded composite patches. *Comp Struct ,* Volume 35, pp. 423-433.

Koutsianitis, P., Drosopoulos, G., Tairidis, G. K. & Stavroulakis, G. E., 2015. *Optimally tuned fuzzy control for smart, possibly damaged piezocomposites.* Gdansk, 3rd Polish Congress of Mechanics & 21st Computer Methods in Mechanics.

Koutsianitis, P., Moutsopoulou, A., Drosopoulos, G. A., Tairidis, G. K., Foutsitzi, G. & Stavroulakis, G. E., 2016. *Optimal control tuning in smart structures with delaminations.* Crete, ECCOMAS VII European Congress on Computational Methods in Applied Sciences and Engineering.

Koutsianitis, P., Tairidis, G. K., Drosopoulos, G., Foutsitzi, G. & Stavroulakis, G. E. 2016b. Effectiveness of optimized fuzzy controllers on partially delaminated piezocomposites. *Acta Mechanica,* Issue Submitted for publication.

Kumar, D. N., Raja, S. & Ikeda, T., 2007. Active vibration control of smart plates with partially debonded multilayered PZT actuators. *Smart Mater Struct,* 16(5), pp. 1584-1594.

Kumar, M. C. B., Prabhu, D. B., Akila, R., Gupta, A. & Alagappan, M., 2012. *Design and Simulation of MEMS Based Piezoelectric Vibration Energy Harvesting System.* Bangalore, Proceedings of the 2012 COMSOL Conference.

Kuo, A. S., 1984. A Two-Dimensional Shear Spring Element. *AIAA J ,* 22(10), pp. 1460-1464.

Kushch, V. I., Shmegera, S. V., Brøndsted, P. & Mishnaevsky, L. J., 2011. Numerical simulation of progressive debonding in fiber reinforced composite under transverse loading. *Int J Eng Sci,* Volume 49, p. 17–29.

Lam, K. Y., Peng, X. Q., Liu, G. R. & Reddy, J. N., 1997. A finite-element model for piezoelectric composite laminates. *Smart Mater Struct,* Volume 6, pp. 583-591.

Latha, B. & Senthilkumar, V. S., 2009. Fuzzy Rule Based Modeling of Drilling Parameters for Delamination in Drilling GFRP Composites. *J Reinf Plast Compos,* 28(8), pp. 951-964.

Liao, Y. & Sodano, H. A., 2012. Optimal placement of piezoelectric material on a cantilever beam for maximum piezoelectric damping and power harvesting efficiency. *Smart Mater Struct,* Volume 21, p. 105014.

Li, C. Q., Zheng, J. J., Lawanwisut, W. & Melchers, R. E., 2007. Concrete Delamination Caused by Steel Reinforcement Corrosion. *J Mater Civ Eng,* Volume 19, pp. 591-600.

Lin, C. C., Hsu, C. Y. & Huang, H. N., 1996. Finite element analysis on deflection control of plates with piezoelectric actuators. *Comp Struct*, Volume 35, pp. 423-433.

Lin, C. C. & Ko, T. C., 1993. Adhesive interface element for bonding of laminated plates. *Comp Struct*, Volume 25, pp. 217-225.

Liu, H., Lee, C., Kobayashi, T., Tay, C. J. & Quan, C., 2012. A new S-shaped MEMS PZT cantilever for energy harvesting from low frequency vibrations below 30 Hz. *Microsyst Technol*, Volume 18, p. 497–506.

Liu, P., Groves, R. M. & Benedictus, R., 2014. 3D monitoring of delamination growth in a wind turbine blade composite using optical coherence tomography. *NDT & E Int*, Volume 64, pp. 52-58.

Luo, Q. & Tong, L., 2004. An adhesively laminated plate element for PZT smart plates. *Comput Mech*, 34(3), pp. 224-236.

Lu, Q., Peng, Z., F, C. & Huang, J., 2003. Design of fuzzy controller for smart structures using genetic algorithms. *Smart Mater Struct*, 12(6), p. 979–986.

Mahieddine, A., Pouget, J. & Ouali, M., 2010. Modeling and analysis of delaminated beams with integrated piezoelectric actuators. *C R Mecanique*, Volume 338, pp. 283-289.

Mahmoodabadi, M. J. & Jahanshahi, H., 2016. Multi-objective optimized fuzzy-PID controllers for fourth order nonlinear systems. *Int J Eng Sci Technol*, 19(2), pp. 1084-1098.

Mahmoodabadi, M. J., Mottaghi, M. B. S. & Mahmodinejad, A., 2016. Optimum design of fuzzy controllers for nonlinear systems using multi-objective particle swarm optimization. *J Vib Control*, 22(3), pp. 769-783.

Mamdani, E. H. & Assilian, S., 1975. An experiment in linguistic synthesis with a fuzzy logic controller. *Int J Man Mach Stud*, 7(1), pp. 1-13.

Marinaki, M., Marinakis, Y. & Stavroulakis, G. E., 2011. Vibration control of beams with piezoelectric sensors and actuators using particle swarm optimization. *Expert Syst Appl*, 38(6), p. 6872–6883.

Marinaki, M., Marinakis, Y. & Stavroulakis, G. E., 2011b. Fuzzy control optimized by a Multi-Objective Particle Swarm Optimization algorithm for vibration suppression of smart structures. *Struct Multidisc Optim*, Volume 43, p. 29–42.

Marinaki, M., Marinakis, Y. & Stavroulakis, G. E., 2015. Fuzzy control optimized by a Multi-Objective Differential Evolution algorithm for vibration suppression of smart structures. *Comp Struct*, Volume 147, pp. 126-137.

Marinova, D. G., Stavroulakis, G. E. & Zacharenakis, E. C., 2005. *Robust control of smart beams in the presence of damage-induced structural uncertainties.* International Conference PhysCon 2005, Saint Petersburg, IEEE.

Maslehuddin, M. et al., 1990. Effect of rusting of reinforcing steel on its mechanical properties and bond with concrete. *ACI Mater J*, pp. 496-502.

Mayhan, P. & Washington, G., 1998. Fuzzy model reference learning control: a new control paradigm for smart structures. *Smart Mater Struct*, Volume 7, pp. 874-884.

McCulloch, W. S. & Pitts, W. H., 1942. A logical Calculus of Ideas Immanent in Nervous Activity. *Bull Math Biophys*, Volume 5, pp. 115-133.

Michalewicz, Z., 1996. *Genetic Algorithms + Data Structures = Evolution Programs.* 3rd ed. Berlin, Heidelberg, New York: Springer-Verlag.

Mindlin, R. D., 1951. Influence of rotatory inertia and shear on flexural motions of isotropic, elastic plates. *J Appl Mech*, 18(1), pp. 31-38.

Mistakidis, E. S. & Stavroulakis, G. E., 1998. *Nonconvex optimization in Mechanics.* Berlin: Springer.

Mitchell, J. A. & Reddy, J. N., 1995. A refined hybrid plate theory for composite laminates with piezoelectric laminae. *Int J Solids Structures*, 32(16), pp. 2345-2367.

Moutsopoulou, A. J., Stavroulakis, G. E. & Pouliezos, A. T., 2014. Active Control in Smart Beams. *J CSSE*, 2(2), pp. 1-8.

Muradova, A. D. & Stavroulakis, G. E., 2013. Fuzzy Vibration Control of a Smart Plate. *Int J Comput Meth Eng Sci Mech*, Volume 14, pp. 212-220.

Muradova, A. D. & Stavroulakis, G. E., 2015. Hybrid control of vibrations of a smart von Kármán plate. *Acta Mechanica*, 226(10), pp. 3463-3475.

Neduncheliyan, S., Umapathy, M. & Ezhilarasi, D., 2009. Simultaneous periodic output feedback control for piezoelectric actuated structures using interval methods. *Int J Smart Sensing Intell Syst*, 2(3), pp. 417-431.

Nestorovic, T., Durrani, N. & Trajkov, M., 2012. Experimental model identification and vibration control of a smart cantilever beam using piezoelectric actuators and sensors. *J Electroceram*, 29(1), pp. 42-55.

Nestorovic, T., Trajkov, M. & Garmabi, S., 2015. Optimal placement of piezoelectric actuators and sensors on a smart beam and a smart plate using multi-objective genetic algorithm. *Smart Struct Syst*, 15(4), pp. 1041-1062.

Nguyen, D. H. & Didrow, B., 1990. Neural Networks for Self-Learning Control Systems. *IEEE Contr Syst Mag*, 10(3), pp. 18-23.

Nikishkov, Y., Seon, G., Makeev, A. & Shonkwiler, B., 2016. In-situ measurements of fracture toughness properties in composite laminates. *Mater Des*, Volume 94, pp. 303-313.

Nyongesa, H. O., Otieno, A. W. & Rosin, P. L., 2001. Neural fuzzy analysis of delaminated composites from shearography imaging. *Compos Struct*, 54(2-3), pp. 313-318.

Okafor, A. C., Chandrashekhara, K. & Jiang, Y. P., 1996. Delamination prediction in composite beams with built-in piezoelectric devices using modal analysis and neural network. *Smart Mater Struct*, Volume 5, pp. 338-347.

Oveisi, A. & Gudarzi, M., 2012. Robust Active Vibration Control of Smart Structures; a Comparison between Two Approaches: μ-Synthesis & LMI-Based Design. *IJAS*, 1(5), pp. 116-127.

Papachristou, I., Salonikidis, S., Tairidis, G. K. & Stavroulakis, G. E., 2011. *Adaptive fuzzy control of smart structures - ANFIS.* Athens, 7th International Congress on Computational Mechanics (GRACM).

París, F., Correa, E. & Cañas, J., 2003. Micromechanical view of failure of the matrix in fibrous composite materials. *Compos Sci Technol*, 63(7), pp. 1041-1052.

Park, G. et al., 2008. Energy Harvesting for Structural Health Monitoring Sensor Networks. *J Infrastruct Syst*, 14(Special issue), pp. 64-79.

Perez, R. E. & Behdinan, K., 2007. Particle swarm approach for structural design optimization. *Comput Struct*, Volume 85, p. 579–1588.

Piezel, B. et al., 2012. Bending effect on the risk for delamination at the reinforcement/matrix interface of 3D woven fabric composite using a shell-like RVE. *Compos Struct*, 94(8), pp. 2343-2357.

Plagianakos, T. S. & Saravanos, D. A., 2005. Coupled High-Order Shear Layerwise Analysis of Adaptive Sandwich Piezoelectric Composite Beams. *AIAA J*, 43(4), pp. 885-894.

Plagianakos, T. S. & Saravanos, D. A., 2005b. Higher-order layerwise laminate theory for the prediction of interlaminar shear stresses in thick composite and sandwich composite plates. *Compos Struct*, Volume 87, pp. 23-35.

Pons, R., Jauberthie, C., Travé-Massuyès, L. & Goupil, P., 2008. Interval analysis based learning for fault model identification. Application to control surfaces oscillatory failures. *AAAI.*

Pradhan, A. K. & Parida, S. K., 2013. 3D FE delamination induced damage analyses of adhesive bonded lap shear joints made with curved laminated FRP composite panels. *J Adhes Sci Technol*, 27(10), pp. 1104-1121.

Preumont, A., 2006. *Mechatronics: Dynamics of Electromechanical and Piezoelectric Systems.* Dordrecht: Springer.

Priya, S. & Inman, D. J., 2009. *Energy harvesting technologies.* Berlin: Springer.

Qu, L., Huang, Y. & Ling, L., 2008. *Design of Intelligent PID Controller Based on Adaptive Genetic Algorithm and Implementation of FPGA.* Berlin, Springer.

Rao, S. S. & Sunar, M., 1994. Piezoelectricity and its use in disturbance sensing and control of flexible structures: a survey. *Appl Mech Rev,* 47(4), pp. 113-123.

Reddy, J. N., 1997. *Mechanics of laminated composite plates: theory and analysis.* CRC press.

Reddy, J. N., 1999. On laminated composite plates with integrated sensors and actuators. *Eng Struct,* Volume 21, p. 568–593.

Reddy, J. N., 2004. *Mechanics of Laminated Composite Plates and Shells, Theory and Analysis.* 2nd ed. Boca Raton, FL: CRC Press.

Reissner, E., 1945. The effect of transverse shear deformation on the bending of elastic plates. *J Appl Mech,* 12(2), pp. 69-72.

Rosenblatt, F., 1957. *The Perceptron - a perceiving and recognizing automaton,* Cornell Aeronautical Laboratory.

Rumelhart, D. E., Hinton, G. E. & Williams, R. J., 1986. Learning representations by back-propagating errors. *Nature ,* 323(9), pp. 533-536.

Saadon, S. & Sidek, O., 2011. A review of vibration-based MEMS piezoelectric energy harvesters. *Energ Convers Manage,* 52(1), pp. 500-504.

Sawyer, J. P. & Rao, S. S., 2000. Structural Damage Detection and Identification Using Fuzzy Logic. *AIAA J,* 38(12), pp. 2328-2335.

Seshu, P. & Naganathan, N. G., 1997. Finite-element analysis of strain transfer in an induced strain actuator. *Smart Mater Struct,* Volume 6, pp. 76-88.

Sharma, M., Singh, S. P. & Sachdeva, B. L., 2005. Fuzzy logic based modal space control of a cantilevered beam instrumented with piezoelectric patches. *Smart Mater Struct,* 14(5), pp. 1017-1024.

Shen, D., Park, J. H., Ajitsara, J., Choe, S. Y., Wikle III, H.C. & Kim, D. J., 2008. The design, fabrication and evaluation of a MEMS PZT cantilever with an integrated Si proof mass for vibration energy harvesting. *J Micromech Microeng,* Volume 18, p. 055017.

Shirane, G., Sawaguchi, E. & Takagi, Y., 1951. Dielectric Properties of Lead Zirconate. *Phys. Rev.,* Volume 84, p. 476.

Shirazi, A. H. N., Owji, H. R. & Rafeeyan, M., 2011. Active Vibration Control of an FGM Rectangular Plate using Fuzzy Logic Controllers. *Procedia Eng,* Volume 14, pp. 3019-3026.

Shi, Y. & Eberhart, R., 1998. *A Modified Particle Swarm Optimizer.* Evolutionary Computation Proceedings, pp. 69-73 DOI: 10.1109/ICEC.1998.699146.

Sodano, H. A., Park, G. & Inman, D. J., 2004. Estimation of electric charge output for piezoelectric energy harvesting. *Strain*, 40(2), pp. 49-58.

Song, G., Sethi, V. & Li, H. N., 2006. Vibration control of civil structures using piezoceramic smart materials: A review. *Eng Struct*, Volume 28, pp. 1513-1524.

Sprenger, W., Gruttmann, F. & Wagner, W., 2000. Delamination growth analysis in laminated structures with continuum-based 3D-shell elements and a viscoplastic softening model. *Comput Methods Appl Mech Engrg*, 185(2-4), pp. 123-139.

Stavroulakis, G. E., Foutsitzi, G., Hadjigeorgiou, V., Marinova, D. G., Baniotopoulos, C. C., 2005. Design and Robust Optimal Control of Smart Beams with Application on Vibrations Suppression. *Adv Eng Software*, Volume 36, pp. 806-813.

Stavroulakis, G. E., Papachristou, I., Salonikidis, S., Papalaios, I. & Tairidis, G. K., 2011. Neurofuzzy Control for Smart Structures. In: Y. Tsompanakis & B. Topping, eds. *Soft Computing Methods for Civil and Structural Engineering*. Stirlingshire: Saxe-Coburg Publications, pp. 149-172.

Sugeno, M., 1985. An Introductory Survey of Fuzzy Control. *Inform Sciences*, Volume 36, pp. 59-83.

Suleman, A. & Venkayya, V. B., 1995. A Simple Finite Element Formulation for a Laminated Composite Plate with Piezoelectric Layers. *J Intell Mater Syst Struct*, Volume 6, pp. 776-782.

Tairidis, G. K., Stavroulakis, G. E., Marinova, D. G. & Zacharenakis, E. C., 2007. *Classical and soft robust active control of smart beams.* Rethymno, Crete, ECCOMAS Thematic Conference on Computational Methods in Structural Dynamics and Earthquake Engineering.

Tairidis, G. K., Stavroulakis, G. E., Marinova, D. G. & Zacharenakis, E. C., 2009. Classical and soft robust active control of smart beams. In: M. Papadrakaikis, D. C. Charmpis, Y. Tsompanakis & N. D. Lagaros, eds. *Computational Structural Dynamics and Earthquake Engineering.* London: CRC Press, pp. 165 - 177.

Tairidis, G. K., Foutsitzi, G., Tsagkaris, A. & Stavroulakis, G. E., 2014. *Fuzzy Control for Vibration Suppression of Smart Plates.* Stirlingshire, Civil-Comp Press.

Tairidis, G. K., Foutsitzi, G., Koutsianitis, P. & Stavroulakis, G. E., 2015. *Fine tuning of Fuzzy Controllers for Vibration Suppression of Smart Plates using Particle Swarm Optimization.* Volos, 8th GRACM International Congress on Computational Mechanics proceedings.

Tairidis, G. K., Foutsitzi, G. A., Koutsianitis, P., Drosopoulos, G. & Stavroulakis, G. E., 2015b. *Design and testing of fuzzy controllers on smart structures in the presence of delamination.* Prague, Proceedings of the Fourth International Conference on Soft Computing Technology in Civil, Structural and Environmental Engineering.

Tairidis, G. K., Foutsitzi, G. A., Koutsianitis, P. & Stavroulakis, G. E., 2015c. *Energy Harvesting using Piezoelectric Materials on Smart Composite Structures.* Prague, Proceedings of the Fifteenth International Conference on Civil, Structural and Environmental Engineering Computing

Tairidis, G. K., Foutsitzi, G., Koutsianitis, P. & Stavroulakis, G. E., 2016. Fine tuning of a Fuzzy Controller for Vibration Suppression of Smart Plates using Genetic Algorithms. *Adv Eng Softw,* doi:10.1016/j.advengsoft.2016.01.019.

Tairidis, G. K. et al., 2016b. Delamination and control on multi-layered structures: A review. In: M. Kuczma, J. Schröder & G. E. Stavroulakis, eds. *Smart Material Systems and Structures - Modeling and Simulation.* in press.

Takagi, T. & Sugeno, M., 1985. Fuzzy identification of systems and its applications to modeling and control. *IEEE Trans Syst Man Cybern,* 15(1), p. 116–132.

Thai, H.-T. & Choi, D.-H., 2013. A simple first-order shear deformation theory for laminated composite plates. *Compos Struct,* Volume 106, pp. 754-763.

Tong, L. & Sun, X., 2003. Adhesive elements for stress analysis of bonded patch to curved thin-walled structures. *Comput Mech,* Volume 30, pp. 143-154.

Trajov, M. & Nestorovic, T., 2012. *Optimal placement of piezoelectric actuators and sensors for smart structures.* Porto, ICEM15 - 15th International Conference on Experimental Mechanics .

Trindade, M. A., Benjeddou, A. & Ohayon, R., 2001. Finite element modelling of hybrid active–passive vibration damping of multilayer piezoelectric sandwich beams-part I: Formulation. *Int J Numer Meth Engng ,* Volume 51, pp. 835-854.

Tsou, P. & Shen, H. M. H., 1994. Structural Damage Detection and Identification Using Neural Networks. *AIAA J,* 32(1), pp. 176-183.

Tylikowski, A., 2001. Effects of piezoactuator delamination on the transfer functions of vibration control systems. *Int J Solids Struct,* Volume 38, pp. 2189-2202.

Wang, L. X., 1994. *Adaptive fuzzy systems and control: design and stability analysis.* Upper Saddle River: Prentice Hall.

Whitney, J. M., 1969. The Effect of Transverse Shear Deformation on the Bending of Laminated Plates. *J Compos Mater,* Volume 3, pp. 534-547.

Widrow, B. & Lehr, M. A., 1990. 30 years of adaptive neural networks: Perceptron, madline, and backpropagation. *Proc IEEE,* Volume 78, pp. 1415-1442.

Wriggers, P., Zavarise, G. & Zohdi, T. I., 1998. A computational study of interfacial debonding damage in fibrous composite materials",. *Comput Mater Sci,* Volume 12, pp. 39-56.

Youn, S. H., Han, J. H. & Lee, I., 2000. Neuro-adaptive vibration control of composite beams subject to sudden delamination. *J Sound Vib,* 238(2), pp. 215-231.

Zabihollah, A., Sedagahti, R. & Ganesan, R., 2007. Active vibration suppression of smart laminated beams using layerwise theory and an optimal control strategy. *Smart Mater Struct,* Volume 16, pp. 2190-2201.

Zadeh, L. A., 1965. Fuzzy sets. *Inform Control,* Volume 8, pp. 338-353.